Neutrino and Dark Matter Properties from Cosmological Observations

PAR

Benjamin AUDREN

ÉCOLE POLYTECHNIQUE
FÉDÉRALE DE LAUSANNE

Suisse
2014

To Ann-Kathrin,

Habe nun, ach! Philosophie,
Juristerei und Medizin,
Und leider auch Theologie
Durchaus studiert, mit heißem Bemühn.
Da steh ich nun, ich armer Tor!
Und bin so klug als wie zuvor;

— Johann Wolfgang von Goethe

Acknowledgements

As a result of more than four years of work, this document is not so much a testimony of my abilities, but rather the product of fruitful interaction with many people. I would like to take the occasion to thank them individually here for bringing me where I stand today.

First of all, I would like to thank my advisor, Julien Lesgourgues, for guiding me skillfully in my first steps in the world of academic research. His friendly presence, and constant advice were a great source of support at the beginning of my PhD. Thanks to his patience, I built the foundation of my knowledge in this field. Despite all the problems, and the not functioning codes, and the last-minute debugging, and the oh so very last-second preparations, I am very grateful to have had this opportunity to study cosmology with him, meet so many nice people, and travel the world.

I would also like to thank Thomas Tram, that provided me with a much needed support during the two years of his presence. Our like-mindedness on many scientific topics helped me a lot to strengthen my confidence in my own capacities.

It was an incredible luck for me to be in this particular floor of this particular building, because I got to know, if not work with, two extremely knowledgeable, friendly and brilliant professors, Mikhail Shaposhnikov and Riccardo Rattazzi. Their incredibly sane approach to science, each in their own specific style, was a constant inspiration for me during these four years.

Most importantly, I would like to thank my wife, Ann-Kathrin, for being this indispensable presence during every single day of my work. She was always listening to my little and big problems, to my ramblings against the world, never failing to support me and cheer me up. Thank you for having provided me with so much happiness day after day, year after year.

But the day-to-day research work was fuelled by many other people, and it is them that I would like to thank now, even though half a page will never do justice to their friendliness. In random order, from the bottom of my heart.

Acknowledgements

vi

Abstract

We apply the principles of Bayesian statistics to the main probes of cosmology, in order to refine our knowledge of the Standard Model and possibly extend it. Notably, we investigate the basic elements of the model in detail in order to reinforce this basic foundation of the field, and lay down a systematic way of obtaining model-independent constraints on parts of the Standard Model.

We further try to constrain some of the unknown properties of Dark Matter, namely its decay or annihilation rates, to help reducing the range of possibilities for model builders. By using recent cosmological probes and making as little assumptions as possible, we are able to meaningfully constrain these properties in the prospect of narrowing down a particle physics search.

Eventually, we show how future experiments will be able to put strong bounds on the neutrino total mass, as long as the theoretical uncertainty is handled carefully. Despite being cautiously pessimistic, we prove how EUCLID will be able to detect even the lowest possible allowed neutrino mass, by simply using properly the linear scales. We also show the target precision for the theoretical prediction in order to make full use of the forthcoming wealth of data at mildly non-linear scales.

Key words: cosmology, neutrino, dark matter, parameter extraction, CMB physics

Résumé

Il est difficile d'expliquer en quoi consiste la cosmologie à des non physiciens. Il y a pourtant une analogie qui parle en général suffisamment aux gens : celle de l'archéologie. En effet, la cosmologie consiste à regarder loin dans le passé pour comprendre comment était l'univers, comprendre d'où l'on vient, mais aussi où l'on va. Le jeu est d'autant plus intéressant qu'il ne s'agit pas uniquement d'un simple exercice d'observation et de déductions – il est en effet possible de construire des modèles prédisant ce qui s'est passé avant. Notamment, en sachant quelles sont les particules élémentaires de la nature, il est possible de dérouler de façon consistante l'évolution de l'univers.

Dans cette dissertation, il sera question principalement de comprendre comment, à l'inverse, l'observation précise de l'univers primordial va nous permettre de contraindre les propriétés manquantes de la physique des particules. Les bases du modèle cosmologique seront aussi interrogées afin de consolider nos connaissances à leur sujet.

Nous appliquons les principes de statistique Bayésienne aux observations cosmologiques, dans le but de raffiner notre compréhension du Modèle Standard et potentiellement aussi de le compléter. Notamment, nous étudions en détail les bases de ce modèle pour les consolider, en présentant une façon systématique d'obtenir des contraintes sur une partie du Modèle Standard, indépendamment du reste.

Nous présentons ensuite une étude tentant de contraindre certaines des propriétés inconnues de la matière noire, à savoir ses taux de désintégration et d'annihilation, pour aider à réduire l'éventail des possibilités pour la construction de modèles. En utilisant les données d'expériences récentes, et en ne faisant qu'un nombre minimal d'hypothèses, il est de fait possible de contraindre de façon significative ces propriétés et par conséquent concentrer l'effort de leur recherche du côté de la physique des particules.

Enfin, nous montrons comment les expériences à venir seront à même d'encadrer la masse totale des neutrinos, pour autant que les incertitudes théoriques reliées aux prédictions soient pris en compte avec attention. En dépit d'un pessimisme prudent, nous montrons comment EUCLID sera capable de détecter même la plus petite masse des neutrinos permise, et cela en utilisant seulement l'information venant des échelles linéaires. Nous montrons également la précision à atteindre dans nos prédictions théoriques pour pouvoir réellement exploiter l'abondance de donnée qui sera disponibles aux échelles faiblement non linéaires.

Mots clefs : cosmologie, neutrino, matière noire, estimation de paramètres, CMB

Zusammenfassung

Es ist schwierig, einem Nicht-Physiker zu erklären, was Kosmologie ist. Es gibt dennoch eine Analogie, die normalerweise vielen Leuten einsichtig ist. Man kann Kosmologie als die Archäologie des Universums ansehen. Tatsächlich, besteht die Kosmologie darin, in die ferne Vergangenheit zu schauen, um zu verstehen, wie das Universum einmal war, woher es kommt, aber auch wohin es sich entwickelt. Es ist umso interessanter da es sich nicht nur um eine Aufgabe von Beobachtungen und Folgeschlüssen handelt, sondern es ist in der Tat möglich, Modele zu bauen, die vorhersagen, was davor passiert ist. Genau gesagt ist es möglich die Evolution des Universums konsistent zu beschreiben, indem man die Elementarteilchen in der Natur kennt.

Diese Dissertation beschäftigt sich hauptsächlich mit der Fragestellung, wie man andersherum durch präziese Beobachtungen des primordialen Universums die fehlenden Eigenschaften der Teilchenphysik eingrenzen kann. Die Grundlagen des kosmologischen Models werden unter die Lupe genommen, um unser Vertrauen in das Model zu verstärken. Wir wenden die Prinzipien der Bayessche Statistik auf die Haupt-Experimente der Kosmologie an, um unser Wissen über das Standardmodell zu vertiefen und es eventuell zu erweitern. Wir präsentieren einen systematischen Weg, modellunabhängige Einschränkungen in Teilen des Standardmodells zu erhalten.

Des Weiteren versuchen wir unbekannte Eigenschaft der Dunklen Materie zu beschränken, im Speziellen die Zerfallsrate und die Paarvernichtungsrate, um die vielfältigen Möglichkeiten für Modellbauer einzuschränken. Indem man aktuelle kosmologische Experimente verwendet und indem man möglichst wenige Hypothesen macht, ist es möglich, starke Beschränkungen der Parameter zu finden, um die Suche nach neuen Teilchen zu einzugrenzen.

Zum Schluss zeigen wir wie zukünftige Experimente sinnvolle Grenzen der gesamten Neutrinomasse aufstellen können, solange theoretische Unsicherheiten sorgfältig behandelt werden. Trotz einer verhalten pessimistischen Haltung zeigen wir, dass EUCLID bei alleiniger Benutzung der linearen Ordnung fähig sein wird, selbst die niedrigst mögliche Neutrinomasse nachzuweisen. Wir berechnen die Zielpräzision theoretischer Vorhersagen, um die zukünftigen grossen Datenmengen von leicht nicht-linearer Ordnung nutzen zu können.

Stichwörter: Kosmologie, Neutrino, Dunkle Materie, Parameterextraktion, Physik der kosmologischen Hintergrund-Strahlung

Contents

Contents

Contents

1 Introduction

1.1 Focus of the thesis

It is a fascinating period for cosmology, where the Standard Model of Cosmology is being refined, with its properties carefully measured, but where hints about novelties, upcoming experiments and conclusions from Particle Physics stir some excitement. So far, this field of study stands out as promising to shed light on the mysterious Dark Matter component, an important component of the model. Already, strong constraints are put on the nature of this component through cosmology, that are complementary to the push from Particle Physics.

It is crucially important in a time like this to be completely sure of the foundations of the model. The two first articles [1, 2] presented in chapters 2 and 3 of this dissertation address this issue by questioning the way the Standard Model is usually thought of. Only by thoroughly understanding how the reference model works can we gain understanding about potential hints of new physics. As cosmology is based on many different aspects of physics, it is important to keep the relative merit of each part well in mind: the physics related to early-time on one side and to the late-time evolution on the other. These two studies are a first step in putting strong, model independent constraints on the early-time part of the Standard Model, and present a novel way of shedding light on the late-time part as well.

In chapters 4 and 5, we present a study [3, 4] in which we used cosmology, and in particular the less known reionization era, but also the temperature anisotropies and the large scale structures, in order to constrain the nature of Dark Matter. As our understanding of this elusive particle is very weak, lacking any confirmed direct or indirect detection, the ability to constrain some of its properties is very appealing. It turns out that one can provide stringent constraints on its stability, both as a decaying particle or as an annihilating, that are on par with Particle Physics measurements. This would help with the effort to build a model for a complete description of Dark Matter.

In chapter 6, the focus is set on a future mission, EUCLID, and its potential predictive power to constrain the total neutrino mass [5]. The mission will embark several probes of the large scale structures, but we focus here on the two main ones, the galaxy power spectrum, and the weak lensing. We show how the detection of even the lowest possible total neutrino mass can be observed by the satellite, even when taking conservative assumptions about our theoretical understanding of the non-linear evolution.

Finally, in chapter 7, we will discuss about software development and its role in science in general, and in cosmology in particular. Complex, extensive and intricate codes provide the basis of most of the papers published daily in this field, and yet proper development practice is still lacking. By having developed a code from scratch during my PhD, MONTE PYTHON,[1] I became aware of this issue, and I will argue why I believe that we should, as a community, pay more attention to this field as a topic of its own.

The rest of this introductive chapter will be devoted to explain the basic physics behind the research work presented in the other chapters, with a particular emphasis on Bayesian parameter extraction.

1.2 Standard Model of Cosmology

Cosmology as a scientific description of the universe is a young field, regardless of the fact that it was introduced shortly after the formulation of General Relativity, almost one hundred years ago. The Standard Model (SM) of cosmology evolved massively during the last three decades, narrowing down on a unified, if not still polemical, view of the Universe. The goal of this short section is by no means to provide a complete historical overview of the building of this theory, but instead to give a brief summary of its current status.

The model relies on a fundamental assumption: the Cosmological Principle. It states that, when looked at sufficiently large scales, the Universe is homogeneous and isotropic, wherever the observer might be located inside it. It includes in a sense the older Copernican Principle, simply stating that our planet Earth does not hold any particular place in the Universe. This principle has been confirmed by the observation of the acceleration of the Universe, the homogeneity of the early Universe, the uniform distribution of galaxies. It is still under scrutiny by large scale experiments, but it held up so far.

In addition to this assumption, cosmology is based on the theory of General Relativity to compute the evolution of matter and radiation in the Universe, which describes the interplay between space-time and matter. The gravitational force is understood as a deformation of space-time, created by matter particles. In turn, the matter feels the deformations and move in space-time.

---

[1]https://github.com/baudren/montepython_public

1.2.1 General Relativity and Homogeneous Cosmology

A point in space-time is defined by the 4-dimensional space-time coordinate $x^\mu = (ct, x^i)$, simply composed by the time t multiplied by the constant speed of light c, and of the 3-dimensional space vector. We follow the convention of choosing natural units in the following, where $c = \hbar = k_B = 1$. The field equation of Einstein's theory are:

$$G_{\mu\nu} + \Lambda g_{\mu\nu} = 8\pi G T_{\mu\nu}, \tag{1.1}$$

with $g_{\mu\nu}$ the space-time metric, G the Newton Gravitational constant, Λ the Cosmological Constant. The other tensorial quantity that appears on the left hand side, $G_{\mu\nu}$, is the Einstein tensor, defined as $G_{\mu\nu} = R_{\mu\nu} - \frac{1}{2}Rg_{\mu\nu}$, with $R_{\mu\nu}$ the Ricci tensor. The latter is a contraction of the Riemann tensor, and can be expressed in terms of the Christoffel symbols Γ:

$$R_{\mu\nu} = R^a_{\mu a\nu} = \partial_a \Gamma^a_{\mu\nu} - \partial_\nu \Gamma^a_{\mu a} + \Gamma^a_{ab}\Gamma^b_{\mu\nu} - \Gamma^a_{\nu b}\Gamma^b_{a\mu}, \tag{1.2}$$

$$\Gamma^i_{kl} = \frac{1}{2}g^{ij}\left(\partial_l g_{jk} + \partial_k g_{jl} - \partial_j g_{kl}\right). \tag{1.3}$$

The Einstein convention is used for repeated indices being summed over. On the right hand side of eq. (1.1), $T_{\mu\nu}$ stands for the Energy-Momentum tensor of the matter content of the universe, as opposed to the geometrical content.

The unknown in eq. (1.1) is the metric $g_{\mu\nu}$, and it appears non-linearly in the equation. Hence, searching for a general solution to this equation is a complicated problem that cosmology does not tackle. Instead, we focus on finding a solution to this equation that would describes the geometry of our universe. For this, we restrain our choice for $g_{\mu\nu}$: it should be homogeneous and isotropic. The most general form of such a metric is called the Friedmann-Lemaître-Robertson-Walker (FLRW) metric, and is expressed by:

$$g_{\mu\nu}\,\mathrm{d}x^\mu\mathrm{d}x^\nu = \mathrm{d}s^2 = -\mathrm{d}t^2 + a(t)\left(\frac{\mathrm{d}r^2}{1-kr^2} + r^2\mathrm{d}\Omega^2\right), \tag{1.4}$$

$$= a(\tau)\left(-\mathrm{d}\tau^2 + \frac{\mathrm{d}r^2}{1-kr^2} + r^2\mathrm{d}\Omega^2\right), \tag{1.5}$$

where a is a function of time. This ensures that all the spatial part can be rescaled, with a change in a, without selecting a particular point in the metric. Within the parenthesis, it is a simple metric corresponding to a positively, negatively curved or flat space, with $k = -1, 1, 0$ respectively, r the radius and $d\Omega^2$ the solid angle. Note that r, θ and φ are called *comoving coordinates*, since they move with the expanding universe: they only get globally rescaled by the scale factor. τ is the comoving time, which also gets rescaled by the scale factor, whereas t stands for proper time.

To further simplify the equation, we will assume that the constituents of the universe can be described as perfect fluids, *i.e.* that their Energy-Momentum tensor can be written as $T_{\mu\nu} = \text{diag}(-\rho, p_i)$ with ρ the density, and p_i the pressure in the i-th spatial direction.

With all these assumptions, one can write the 00 term and the trace of eq. (1.1), giving the Friedmann equations:

$$\frac{\dot{a}^2}{a^2} + \frac{k}{a^2} = \frac{8\pi G}{3}\rho + \frac{\Lambda}{3}, \tag{1.6}$$

$$\frac{\ddot{a}}{a} = -\frac{4\pi G}{3}(\rho + 3p) + \frac{\Lambda}{3}, \tag{1.7}$$

where we introduced the $\dot{}$ notation as the derivative with respect to proper time. These two equations relate the expansion of the universe (the rate of variation of the scale factor a as a function of time) to the behaviour of the matter content. We usually define the Hubble parameter, $H \equiv \frac{\dot{a}}{a}$. We denote by H_0 the value of this parameter at present time. This number is still not completely fixed, as will be discussed in chapter 3, so it is usual to parametrise it this way: $H_0 = 100 \times h\,\text{km/s/Mpc}$, where h is called the reduced Hubble constant, whose numerical value is around 0.7. H_0 is readily interpreted as the speed of an object sitting at a distance of $1\,\text{Mpc}$ from us, comoving with the universe expansion.

By measuring the speed of galaxies in our vicinity, Hubble was the first to make a measurement of this quantity [6], and observed the behaviour that the further the galaxy is away from us, the faster it recedes from us. This is sometimes referred to as the Hubble flow, but is nothing more than the manifestation that our universe is expanding.

Another important quantity to define is the redshift z such that $1 + z = \frac{a_0}{a}$ where a_0 is simply the scale factor today. In a flat universe where $k = 0$, we can set this normalising quantity to 1. The redshift is thus a quantity varying from 0, today, to large values as we go further in the past. This scale is usually confusing, as it is very far from a linear scale in proper time. Indeed, for our standard model, there is 7.7 billion years between today and redshift 1 (more than half the age of our universe), while there is only 5.7 billion years between redshift 1 and 1000. It is however a good scale to understand the growth of the universe. At a redshift of 999, it was 1000 times smaller than it is today.

We finally introduce the critical density $\rho_c = \frac{3H^2}{8\pi G}$, and define the total energy density in units of ρ_c, $\Omega = \rho/\rho_c$, to recast eq. (1.6) to:

$$\frac{k}{a^2 H^2} = \Omega(a) - 1, \tag{1.8}$$

where we have inserted into Ω the contribution from the cosmological constant. We introduce Λ as the source of the late homogeneous accelerated expansion of our universe [7,

8]. Despite the major concerns about the huge fine tuning required to have Λ become dominant only around a redshift of 1, there are currently no alternative explanations that come close to the simplicity of this proposition.[2]

We see from this equation that the curvature of the universe is directly linked to the total amount of energy in it, compared to the critical density. The geometry of our universe is very close to flat, as measured by both Large Scale Structure experiments [10] and the analysis of the Cosmic Microwave Background [11]. It means that at all times, the total energy density is very close to the critical one, a fact that will be explained in section 1.3.3. It is interesting to compute the critical density of the universe today, $\rho_c^0 = 3H_0^2/8\pi G = 1.88 \times 10^{-29}\ h^2\,\mathrm{g.cm}^{-3}$, as it is less dense than the intergalactic medium, suggesting the domination of voids in the matter distribution.

Until now, the actual components adding up to the total energy budget of the universe were left unspecified. Nonetheless, it is useful to note that, for any component which can be described as a perfect fluid, it is possible to actually relate the pressure p to the density ρ of this component through a simple equation, called the equation of state.

$$p = w\rho. \tag{1.9}$$

Generally, w will be a constant, though one can envision particular species with a non-constant w, as we will be discussing in section 1.2.2. For the remainder of this chapter, though, we will consider w to be a constant. With eqs. (1.6), (1.7) and (1.9), we can now describe the time evolution of a simple universe.

1.2.2 Content of the Universe

Now that we have all the basic equation, we can try and understand what are exactly the components of the universe, and identify the phases through which it passed. To start with, one can reformulate eq. (1.7) by using eq. (1.6) into:

$$\dot\rho + 3\frac{\dot a}{a}(\rho + p) = 0. \tag{1.10}$$

Given eq. (1.9), one can easily solve this differential equation and obtain:

$$\rho(a) = \rho_0 \left(\frac{a}{a_0}\right)^{-3(1+w)}. \tag{1.11}$$

For matter, radiation, or the cosmological constant Λ, the w are respectively equal to 0, $\frac{1}{3}$ and -1, which translate into ρ being (resp.) proportional to a^{-3}, a^{-4} and const.

---

[2]See [9] for an attempt at an alternative explanation.

So as the universe grows, a becomes bigger, pressureless matter dilutes as the volume, radiation dilutes even faster, while the cosmological constant stays the same. From this observation, it is clear that these different components will dominate at some stage in the universe, depending on their initial quantity. A figure helps in representing this knowledge, and a sketch of the situation in our universe is presented in fig. 1.1.
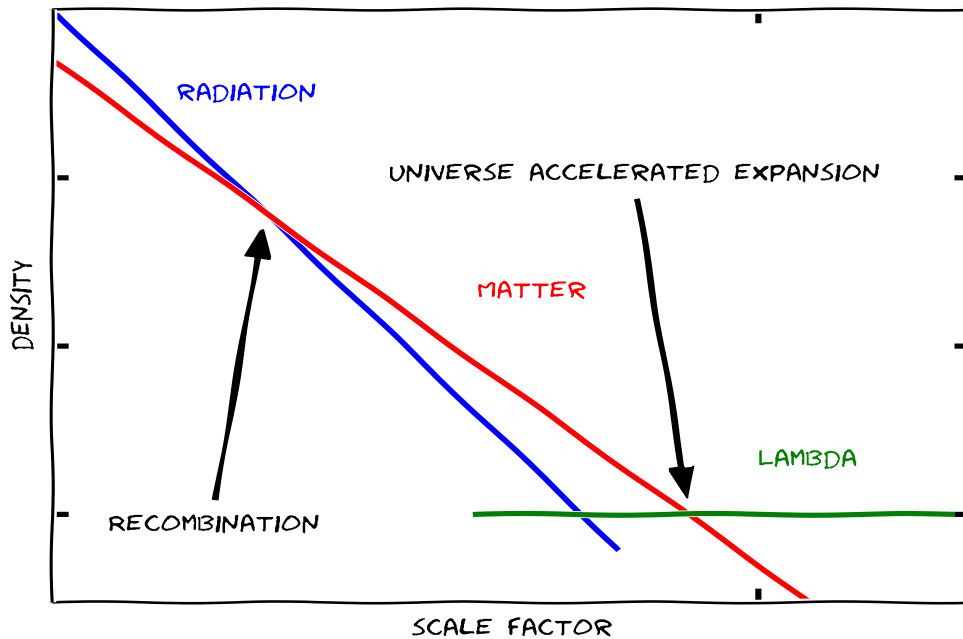
Figure 1.1 – Sketch of the evolution of densities of species in our universe as a function of the scale factor. We live somewhere inside the Λ-dominated epoch.

In the very early universe, radiation was driving the expansion (Radiation Domination, RD), which was followed by a matter dominated (MD) era, where structures formed. The final stage, which has been taking place for roughly half the age of the universe, is dominated by the cosmological constant (ΛD). Indeed, as the only density which is not diluted with the expansion of the universe, this term will always end up dominating the evolution in an expanding universe.

The whole fate of the universe, whether it expands or collapse, is readily computed from eq. (1.6), and by using eq. (1.11):

$$a(t) = \begin{cases} t^{\frac{2}{3(1+w)}} \text{ for } w \neq -1 \\ e^{\bar{H}t} \text{ else} \end{cases} \tag{1.12}$$

Evidently, this result holds for the time where a particular species dominates the energy density of the universe. For instance, we switched from a decelerated expansion under the matter-dominated era to an accelerated one with the Λ dominated era. If the cosmological constant is indeed the explanation for dark energy, then it seems likely that our universe will continue to expand faster and faster.

1.3 Perturbed Cosmology

In section 1.2, we have discussed about the homogeneous cosmological evolution. It provides an important insight in the nature of the components of our universe, and can be probed by measuring the redshift of distant galaxies. It gives us the age of our universe, and tells us about the ultimate fate of the universe. However, it does little to tackle in any sense what happens at small scales. It should be clear, however, that this part is of the highest importance, for several reasons. First of all, we are ourselves the products of the collapse of matter - all our environment is constituted by highly inhomogeneous media. It is therefore of crucial importance to understand how collapsed objects came to be. Moreover, the theoretical challenge to understand how such a homogeneous universe at large scale (variation of 10^{-5} in density at the largest scale observable) can generate such an inhomogeneous one at short scale (compare the density inside a neutron star, around $10^{17}\,\mathrm{kg/m^3}$, with the density of the intergalactic medium, around $10^{-27}\,\mathrm{kg/m^3}$) leads to fascinating developments. The goal of cosmology is however limited in this direction - it does not plan and explain how to form stars, or planets, which are rather the domain of Astrophysics. But the non-linear description of the structure collapse is part of cosmology, even though I will not describe it in details in this introduction.

1.3.1 Perturbed Friedmann equations

Considering the above arguments, it is clear that our universe is not only constituted by a homogeneous fluid, but also by perturbations on this background field. To describe this now perturbed universe, we also need to introduce a perturbed metric. However we know from observations of the early universe that these perturbations must be small, making it unnecessary to restart from the Einstein field eq. (1.1). At zeroth order in perturbation, the Friedmann eqs. (1.6) and (1.7) will still be valid, and we will have new equations to describe the perturbations on top of the expanding background. The new metric $g_{\mu\nu}$ is now simply the sum of the FLRW metric plus a perturbed metric: $\mathrm{d}s^2 = (\bar{g}_{\mu\nu} + \delta g_{\mu\nu})\mathrm{d}x^\mu \mathrm{d}x^\nu$.

This new tensor is also symmetric, so has only 10 degrees of freedom (d.o.f.). It is convenient to separate them under the spatial rotations [12] into three sectors: 4 scalar d.o.f., 4 vector d.o.f. and 2 tensor d.o.f. The advantage of such a classification is that these components separate at first order in perturbations, such that it is possible to

study their evolution independently. The total metric can be cast in the following way:

$$\mathrm{d}s^2 = a^2(\tau) \left[(1+2\psi)\mathrm{d}\tau^2 + B_i \mathrm{d}x^i \mathrm{d}\tau - \{(1-2\phi)\delta_{ij} + H_{ij}\} \, \mathrm{d}x^i \mathrm{d}x^j \right] \tag{1.13}$$

Where ϕ and ψ are scalar modes. The other two scalars are constituted by b, defined by the decomposition of $\vec{B}$, $B_i = \partial_i b + \epsilon_{ijk}\partial_j b_k$ and μ, defined by the decomposition of H_{ij} into $H_{ij} = 2(\partial_i \partial_j - 1/3\delta_{ij}\Delta)\mu + (\partial_i A_j + \partial_j A_i) + H_{ij}^T$. The four vector modes are composed by the rest of the vector $\vec{B}$ as well as the transverse divergence part of H_{ij}, while the remaining two tensor modes are constituted by the other components of the symmetric matrix H_{ij}. However, this separation between background and perturbation is slightly arbitrary, and it is possible to perform a change of gauge, *i.e.* a change of the background plus perturbations to recover the same physical deformation of the metric. By keeping gauge invariant quantities, it is possible to continue the reasoning, because each of these d.o.f. have a physical meaning. However, any physical observation is independent of the gauge, it can thus be consistently fixed, to simplify as a consequence the equations. There are two common choices for the gauge, the Newtonian and the synchronous one, as discussed in the following

As a further simplification in the following, we will set the vector and tensor modes to zero. For the vector part, this is justified, at least in the linearized theory, because there are no sources for these modes in the SM. Even if they were initially excited, they would rapidly decay to zero with the expansion of the universe. Note, nonetheless, that this is only true at linear order, since already at second order, vector modes are generated through gravitational collapse [13]. The situation is also entirely different if there is an active source of vector modes, for example cosmic defects, such as cosmic strings. It could then produce significant observable quantities [14].

Concerning the tensor modes, it is also meaningful to set them to zero, as there is so far no evidence of them being relevant today.[3]

The expression of the perturbed metric in the Newtonian gauge, with both vector and tensor modes fixed to zero, is the following:

$$\mathrm{d}s^2 = a^2(\tau) \left[-(1+2\psi)\mathrm{d}\tau^2 + (1-2\phi)\mathrm{d}\vec{x}^2 \right] \ \text{Newtonian} \tag{1.14}$$

The synchronous gauge is instead defined as a gauge in which all the perturbations lie in the spatial part of the metric. We can therefore see that its expression is the following:

$$\mathrm{d}s^2 = a^2(\tau) \left[-\mathrm{d}\tau^2 + ((1-2\phi)\delta_{ij} + H_{ij}) \, \mathrm{d}x^i \mathrm{d}x^j \right] \ \text{Synchronous} \tag{1.15}$$

---

[3]Apart from the recent claim from the BICEP2 collaboration [15] to have observed primordial gravitational waves, but in the light of independent analysis [16, 17, 18], it seems very unlikely that it is indeed the case.

Note however that this does not completely fix the gauge, as there is a remaining degree of freedom [19]. It is arbitrarily removed by setting the velocity divergence of the dark matter component to zero – a point that will be discussed in the context of decaying dark matter in chapter 5.

The Newtonian gauge is slightly easier to understand physically, because in the Newtonian limit, $\phi = \psi = \Phi$, where Φ designates the Newtonian potential. Notice however that this result does not hold if there is a species with a non vanishing traceless and longitudinal part in its energy momentum tensor (such as massive neutrinos). As all the results inside the Hubble radius are gauge independent, the choice of gauge for computing the physical observables is not important. Notice that it is possible to extend this formalism described here for flat universes to non-flat ones, as described in [20].

Now that we decided for a shape of the metric perturbation, we can describe the energy-momentum tensor perturbations. Following the convention in [19], we will write:

$$T_0^0 = \bar{T}_0^0 + \delta T_0^0 = -(\bar{\rho}(\tau) + \delta\rho(\tau, \vec{x})), \tag{1.16}$$

$$T_i^0 = \bar{T}_i^0 + \delta T_i^0 = (\bar{\rho}(\tau) + \bar{p}(\tau))\, v_i(\tau, \vec{x}), \tag{1.17}$$

$$T_j^i = \bar{T}_j^i + \delta T_j^i = (\bar{p}(\tau) + \delta p(\tau, \vec{x}))\delta_j^i + \Sigma_j^i(\tau, \vec{x}), \tag{1.18}$$

with $\bar{\rho}$ and $\bar{p}$ designating the average density and pressure, only time-dependent. Σ_j^i is a traceless tensor, $v_i = \frac{\mathrm{d}x_i}{\mathrm{d}\tau}$ the comoving velocity, and we usually define θ as the divergence of the velocity. We introduce δ as the relative density contrast, such that $\delta = \frac{\delta\rho}{\rho}$. We also define the scalar σ as the anisotropic stress, defined, in Fourier space, as $(\bar{\rho} + \bar{p})\sigma = -\left(\hat{k}_i\hat{k}_j - \frac{1}{3}\delta_{ij}\right)\Sigma_j^i$.

The fully non-linear equation to solve for the species is the collisionless Boltzmann equation, as explained in [21]. To find a solution to this fully non-linear equation of the phase space constitutes a branch of cosmology in itself, and will not be discussed here. It is however possible to linearize this equation, assuming that the velocity has only a divergence part. This gives the continuity and Euler equation for each species, in Fourier space:

$$\dot{\delta} = -(1 + w)\left(\theta - 3\dot{\phi}\right) - 3\frac{\dot{a}}{a}\left(\frac{\delta p}{\delta\rho} - w\right)\delta, \tag{1.19}$$

$$\dot{\theta} = -\frac{\dot{a}}{a}(1 - 3w)\theta - \frac{\dot{w}}{1 + w}\theta + \frac{\delta p/\delta\rho}{1 + w}k^2\delta - k^2\sigma^2 + k^2\psi. \tag{1.20}$$

There are two main motivations for going to Fourier space. One is that a linear system in real space has independent mode evolution in Fourier space. Another motivation is that, if the source of these perturbations is random, we will not learn much by observing in detail the exact placement of each over and under density. Instead, it would be interesting

to determine the properties of the random process that sourced these seeds. To this end, it is customary to use Fourier space, as the quantities defined there are more readily interrelated. It exists of course a one to one correspondence between the two, and it is therefore irrelevant which one is studied. Considering a random variable $\delta(\vec{x})$, all its properties are encoded in its Fourier transform: [4] $\delta(\vec{k}) \propto \int \mathrm{d}^3 x e^{-i\vec{k}\vec{x}} \delta(\vec{x})$.

If the species we follow are perfect fluids, then eqs. (1.19) and (1.20) are sufficient in a first approximation to solve their entire evolution. This is the case for baryons after decoupling from the photon-baryon fluid, or for cold dark matter. For more complicated species, like photons or neutrinos, it is however needed to solve the Boltzmann equation.

1.3.2 Boltzmann Equation

To follow the classical (as opposed to quantum) evolution of photons, we use the Boltzmann equation. It is expressed in its simplest form as:

$$\frac{\mathrm{D}f}{\mathrm{D}t} = C[f], \tag{1.21}$$

where f is the distribution function of the particles, and D stands for the total derivative. The distribution function is a generic function of time τ, space x_i and conjugate momenta P_i, which simply defines the amount of particle per unit space and momentum. Note that the conjugate momenta P_i are related to the proper momenta (the ones measured by an observer at rest) by the following equations in the Newtonian gauge: $P_i = a(1 - \phi)p_i$.

To avoid having to deal with metric perturbations in the definition of the momenta, we introduce, following the common practice, the variable $q_i = ap_i$, decomposed in its norm q and direction unit vector $\hat{n}$. The distribution function is split between background and perturbations, in the following way:

$$f(\tau, x_i, q, \hat{n}) = f_0(q) \left[1 + \Psi\left(\tau, x_i, q, \hat{n}\right)\right]. \tag{1.22}$$

f_0 refers to the background distribution. This function depends on the way the species was produced initially. For a thermally produced species, this background distribution is actually the Bose-Einstein (resp. Fermi-Dirac) distribution for bosons (resp. fermions):

$$f_0(\epsilon) = \frac{g_s}{(2\pi)^3} \frac{1}{e^{\epsilon/T_0} \pm 1}, \tag{1.23}$$

with the $-$ sign for bosons, and the $+$ sign for fermions, $\epsilon = a(q^2 + m^2)^{1/2}$ the energy,

---

[4]Where we take the usual physicist notation when calling both function and Fourier transform with the same letter.

T_0 the species' temperature today, and g_s the number of degrees of freedom. It means that the background distribution function evolves with time, albeit slowly. Moreover, for a relativistic species, where the mass m is negligible, there is no more time dependence – this is the case for photons, and for most of the time evolution of neutrinos. From this definition, and by recalling the link between the phase-space distribution and the energy-momentum tensor:

$$T_{\mu\nu} = \int \mathrm{d}P_1 \mathrm{d}P_2 \mathrm{d}P_3 (-g)^{-1/2} \frac{P_\mu P_\nu}{P^0} f(x_i, P_j, \tau), \tag{1.24}$$

one can infer the expression of the Boltzmann equation in the Newtonian gauge:

$$\frac{\partial \Psi}{\partial \tau} + i\frac{q}{\epsilon}(\vec{k} \cdot \hat{n})\Psi + \frac{\mathrm{d}\log f_0}{\mathrm{d}\log q}\left[\dot{\phi} - i\frac{\epsilon}{q}(\vec{k}\cdot\hat{n})\psi\right] = \frac{1}{f_0}C[f]. \tag{1.25}$$

As a reminder, this equation needs to be solved for relativistic species (photons and neutrinos), [5] where simply tracking the density and velocity dispersion is not enough, as it was the case for baryons and CDM. The actual principles behind the solving of this equation would be too lengthy to cover in this introduction. In practice, the code CLASS[6] was developed to solve it efficiently [23, 24].

1.3.3 Inflation

With the concepts previously introduced, it is possible to realise that a key issue is the source of the perturbations. The theory of cosmology would not be complete without a way to explain the origin of the seeds of perturbations. The theory of inflation proposes a mechanism to generate these initial conditions. We will see that it addresses also several puzzling facts about our universe.

We already know that the universe expands - at different rates depending on which species dominate the evolution. By looking at one point in the sky, the furthest we can reach, we receive photons that were emitted around 300.000 years after the Big Bang – almost nothing compared to the 13.7 billion years of the universe. On the other side of the sky, we can also look at these photons, that travelled from the other end of the universe. We can then ask the following question: were these photons ever in causal contact? They are meeting here, on Earth, after having travelled towards each other for almost 14 billion years. If they were never in contact before, should we really expect that they have almost the same temperature?

It is possible to determine the size of the sky, on the last scattering surface, where photons could influence each other (in terms of GR, being in the past light-cone of each

---

[5] Though the latter require a different set of approximations [22].

[6] Standing for Cosmic Linear Anisotropy solving system.

other), as will be described in section 1.4.1. Roughly, it corresponds to one degree of separation in the sky. It means that all the points separated by more than one degree should never have been in thermal equilibrium. How to explain, under these conditions, that the universe is so homogeneous? Indeed, all around us, the sky, the distributions of galaxies, the CMB, all these quantities are very uniformly distributed.

A very natural way of solving this issue is to speculate the existence of a new field, the inflaton, which will drive an early period of accelerated expansion of the universe. By having an accelerated expansion, the universe can actually expand so fast that modes will exit the Hubble horizon. When this period of *inflation* finally ends, the modes will slowly reenter the horizon and be in causal contact again.

Of course, introducing a new field in the SM requires careful consideration. Since it can be a scalar field, a simple proposition is that this could actually be the recently discovered Higgs boson [25, 26]. This model, called Higgs inflation, extends the quartic interaction of the Higgs particle at high energy to provide for the inflation (see [27] and references therein for a complete review). More generally, a review of the currently allowed models in the light of Planck data can be found in [28].

Regardless of the exact model, it is possible with this mechanism to have a physical process responsible for fluctuations (quantum fluctuations), that are afterwards causally separated by the accelerated expansion of the universe. In a sense, it is only a reformulation of the problem: instead of having to explain why different patches of the sky have the same overall fluctuations, it is now needed to understand how a particle can generate a sufficiently long period of inflation, then stop.

The basic idea that inflation can be realised by a scalar-field is easily understood. Consider a scalar-field φ, with a generic potential $V(\varphi)$. Its Lagrangian is $\mathcal{L}_\varphi = \frac{1}{2}g^{\mu\nu}\partial_\mu\varphi\partial_\nu\varphi - V(\varphi)$. Assuming that it is homogeneous in space, *i.e.* that $\varphi(\vec{x}, t) = \bar{\varphi}(t)$, the energy momentum tensor of this field is composed by:

$$\rho = \frac{1}{2}\dot{\bar{\varphi}}^2 + V(\bar{\varphi}) \tag{1.26}$$

$$p = \frac{1}{2}\dot{\bar{\varphi}}^2 - V(\bar{\varphi}) \tag{1.27}$$

The condition $p < -\frac{1}{3}\rho$ to obtain accelerated expansion, as seen in eq. (1.7), translates into a relation between the kinetic energy of the field, $\dot{\bar{\varphi}}$ and its potential energy $V(\varphi)$, namely: $\dot{\bar{\varphi}} < V(\varphi)$. This is the first Slow-Roll Condition (SRC). To be sure that this condition is enforced for a sufficiently long time, we impose as well that the time derivative of this condition is fulfilled – which is then the second SRC.

The name comes from the fact that the kinetic energy of the field is related to the derivative of the potential – it is therefore clear that, to have inflation, the potential

needs to be flat enough.

The exact details on the generation of the fluctuations, as well as the decay of the inflaton to SM particles via (p)reheating[7] is not the focus here. It is enough to understand that the exact details are model dependent. There is however a way to gather all possible predictions in terms of their statistical properties. Each model will generate fluctuations according to some probability distribution, as a stochastic process of generating the seeds of over and under densities. What is significant here is not the particular place of each trough and peak, but rather their statistical distribution. Therefore, by switching to Fourier space, one can define the power spectrum (two-points correlator) at a wave-number k of the original fluctuations as a generic function of k. It is traditionally parametrized in the following way:

$$\mathcal{P}_s(k) = A_s \left(\frac{k}{k_\star}\right)^{n_s - 1 + \frac{1}{2}\alpha_s \log\left(\frac{k}{k_\star}\right)}. \tag{1.28}$$

The subscript s stands for scalar perturbations. A_s is the initial amplitude of fluctuations at the (arbitrary) pivot scale $k_\star$, n_s the tilt, α_s the running of the tilt. It is of course possible to further refine this modelling by introducing a running of the running, and so on and so forth.

Different theories will predict different preferred value for A_s, n_s and α_s. All inflation models predict nearly scale invariant power spectrum for scalars, that is to say that the total exponent should be close to 0: n_s is therefore a number very close to 1.

The overall amplitude is parametrized by a single value, A_s which will hence control the global amplitude of fluctuations. Considering that the over-densities grow during the RD epoch, the initial amplitude has to be fairly low for the fluctuations to be of the order of 10^{-5} at the time of recombination (see section 1.4.1) – in the SM, the best-fit value of A_s lies indeed around 2.4×10^{-9}).

It is also possible to apply the same formalism to the tensor perturbations, defining the primordial power spectrum as:

$$\mathcal{P}_t(k) = A_t \left(\frac{k}{k_\star}\right)^{n_t + \frac{1}{2}\alpha_t \log\left(\frac{k}{k_\star}\right)}. \tag{1.29}$$

---

[7]Preheating designates a non-perturbative effect that can produce SM particles, while reheating takes place later in most scenarios, and supposes that the decay rate of the inflaton is bigger than the Hubble expansion, allowing for the decay to take place.

It is customary to introduce the parameter r as the tensor-to-scalar ratio, defined by:

$$r = \frac{\mathcal{P}_t(k = k_\star)}{\mathcal{P}_s(k = k_\star)}, \tag{1.30}$$

as an alternative parametrisation for the tensor amplitude. Generically, r is expected to be small, although with the recent attention given to the BICEP2 result, most models have been shown to possibly accommodate larger r values (see for instance [29] for an example in the context of Higgs inflation).

1.4   Cosmological probes

In order to understand the work presented in chapters 2 to 6, it is crucial to understand the main observables of cosmology. Now that the basic equations and principles have been laid down, it is possible to explain the principles behind these experiments.

The observations roughly fall in two main categories. One concerns the observation of the primordial radiation emitted at decoupling, and the other the description of large scale structures of our universe (namely galaxies, and cluster of galaxies). Both provide interesting insight in the constitution of our universe.

1.4.1   Cosmic Microwave Background

As the universe expanded, at a time roughly coinciding with the end of the radiation dominated era, the electrons and protons recombined into hydrogen atoms. This stage is called the recombination, and is the event that lead to photon decoupling. The temperature and polarization fluctuations present at this stage in the plasma get imprinted in the distribution of photon as they decouple. By travelling through the universe until reaching us, the photons get lensed by the structures in between, and their properties are slightly altered. By observing these patterns of fluctuation on the sphere around us (see on fig. 1.2 for the observation of these fluctuations by the Planck satellite, it is possible to extract information on the composition of the plasma, the amplitude of the primordial fluctuation, and also some information on the large scale structures in our universe through the lensing effect.

In this section, we will focus in explaining the main characteristics of the photon decoupling, and therefore the properties of the CMB, as it stands out as one of the most important probes for cosmology. We will focus on the temperature anisotropies for clarity, and refer to [30] for an in-depth explanation of polarization effects.

Before starting to describe the physical process powering this particular moment in the cosmological history, it is important to notice that the CMB is usually described
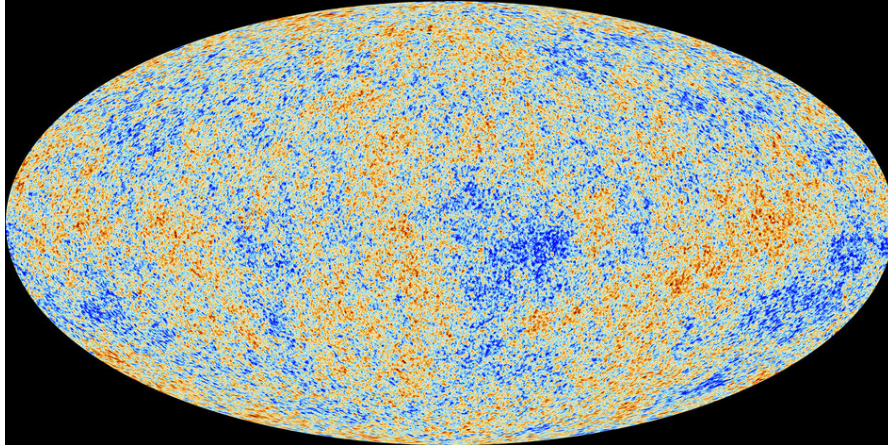
Figure 1.2 – The anisotropies of the CMB as observed by Planck. *Credits: ESA and the Planck Collaboration*

in multipole space, as it is observed on a sphere. Just like the Fourier transform is adapted for describing statistical properties in a flat space, this harmonic transformation is designed to analyze the statistical properties of a function on a sphere. The spatial variables x_i are replaced by the multipoles $\ell \in [0, \infty[$. The multipole $\ell = 0$ is called a monopole, and simply corresponds to the average temperature on the sphere, $\ell = 1$ is the dipole, and so on.

During the radiation dominated era, and inside the Hubble radius, the baryon-photon plasma presents oscillations, due to the nature of its components. The gravitational force tends to collapse the plasma, while the pressure from the photons resists against it. It leads to the propagation of sound waves in the fluid, which get imprinted in the statistical properties of the fluctuations in temperature, as the main scale present in the fluid. This phenomenon, referred to as Baryon Acoustic Oscillation (BAO), will therefore be present in the CMB, and its imprint will be present in the statistical distribution of LSS as well, since the CDM component follows the evolution of density of the fluid during the radiation dominated period.

A peak of correlation in real space translates to a series of oscillations in harmonic space. The position of these peaks depends on the sound horizon of the plasma at decoupling, but also on the apparent size on the last-scattering surface. It is also clear that the amount of matter will have an impact on the amplitude of the peaks. For an in-depth description of all the effects of the SM parameters on the CMB, see section 2.2.

This series of peaks and troughs, as measured with extreme precision by the Planck satellite, is one of the most convincing proof of the presence of DM. It is very difficult to explain the contrast between the odd and even peaks without an additional pressureless particle, that mostly interact through gravitation with the other SM particles.

It is also important to realise that the six parameters of the ΛCDM model induce a variety of effects on the CMB temperature spectrum which are not exactly degenerate with each other. Hence the CMB alone allows to constrain all the parameters of ΛCDM. When adding new ingredients in the model, it can happen that there are no new effects, leading to parameter degeneracies; or on the contrary, that the new ingredients introduce new physical effects, and remain measurable. Hence the CMB can provide a lot of independent information on different aspects of the cosmological model. This is why it is possible to constrain additional parameters with cosmological data, as it is done in chapters 4 and 5 with non-minimal properties of the DM particle.

1.4.2 Large Scale Structures

The second main cosmological observable (or rather, group of observables) is the Large Scale Structure (LSS) of the universe. It consists in recovering the statistical distribution of gravitationally collapsed objects, mostly composed of DM, but also of baryons.

The origin of the seed from which the collapsed objects evolved was explained in the previous section. After decoupling, the universe entered a phase of Matter Domination, where the perturbations of CDM and baryon grow faster than the universe expands. For the baryonic matter, pressure complicates the evolution, as it prevents the collapse through gravitation. Through the emission of radiation, however, dust can cool down and eventually collapse into stars. The description of the entire process of forming galaxies, stars and planets lies beyond the scope of cosmology, and therefore the interesting objects to study for us are mostly clusters of galaxies, but can go down to galactic scales (around the kpc).

The basic equations have already been introduced. Once baryons and DM are free, they each obey eqs. (1.19) and (1.20), as long as the perturbations remain small. Obviously, by solving only the linearized equation, we are effectively restricting ourselves to very low wavenumbers, *i.e.* very large scales, where objects are barely collapsed. In real space, this would correspond to above galaxy cluster size, meaning around $10\,\text{Mpc}$. In Fourier space, knowing that the reduced Hubble constant h is around 0.7, it corresponds to a wavenumber of $k = 0.14\,h/\text{Mpc}$. All the scales with higher wave-numbers correspond to collapsed objects – deeply non-linear –, whereas scales above this are still more or less linear today [21]. The major problem with this perturbative expansion is that it appears to be not convergent, as discussed in a recent study [31], and will therefore not be presented here.

Even when restricting the study range to large scales, and treating the CDM evolution linearly, there are several remaining caveats to look out for when dealing with LSS. The first is obviously to be sure to stay well within the linear regime, where predictions are robust, at the expense of losing constraining power from smaller scales. When trying to
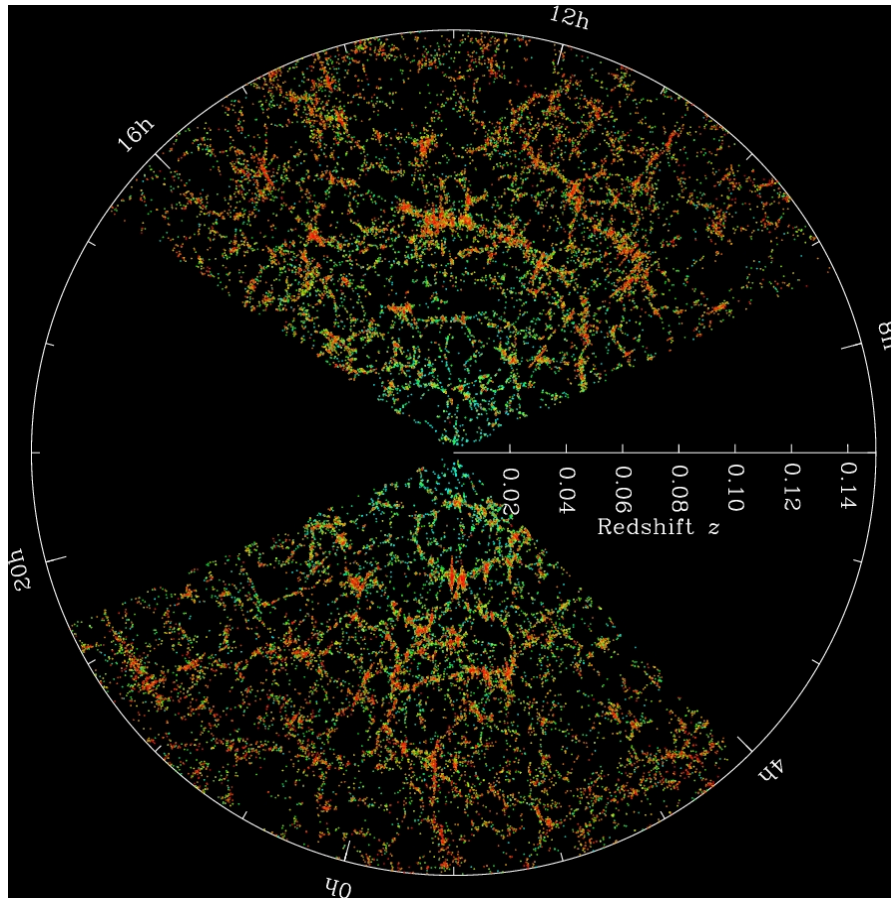
Figure 1.3 – Slices through the SDSS 3-dimensional map of the distribution of galaxies. Earth is at the center, and each point represents a galaxy. Galaxies are colored according to the ages of their stars, with the redder, more strongly clustered points showing galaxies that are made of older stars. The outer circle is at a distance of two billion light years. The region between the wedges was not mapped by the SDSS because dust in our own Galaxy obscures the view of the distant universe in these directions. Both slices contain all galaxies within -1.25 and 1.25 degrees declination. *Credit: M. Blanton and the Sloan Digital Sky Survey.*

predict the power spectrum at larger wavenumbers, it is then crucial to keep in mind the uncertainty of the prediction, whether it depends on the accuracy of a fitting formula or on a partial solution of the fully non-linear evolution. As will be discussed in chapter 6, this uncertainty will play a central role in the interpretation of future experiments.

The second issue is related to the method of observation. One way of measuring the distribution of matter in the nearby universe is to observe luminous galaxies, as seen in fig. 1.3. Baryons being not the dominant matter component, their perturbations should follow the ones of CDM. Galaxies being collapsed objects, we commonly assume that they lie in the bottom of the CDM density wells. Therefore, they do not show anything

of the actual shape of the well they are sitting in – we can qualify them as *biased tracers* of the underlying distribution. When inferring the total matter power spectrum from the galaxy power spectrum, it is therefore compulsory to take into account this bias parameter [21].

One promising way of sidestepping this difficulty is to use another probe of the matter density, which is directly sensitive to the total matter density: weak lensing. It is based on the principle of the deflection of light by the presence of mass along the line of sight, between the source of the light and the observer. With GR, it is possible to compute how much the light will get deflected. This overcomes completely the issue of bias, but is however still plagued, although not as strongly, from the issue of non-linearities.

Finally, another drawback of these methods is the uncertainty associated to the measurement of the radial position of galaxies. Indeed, while the two angular positions are measured as accurately as possible, the radial coordinate is measured via its redshift, as a tracer for its distance from the observer. However, the redshift is a function of the scale factor a, which in turns depends on the composition of the universe. Moreover, it is assumed to be linked to the coherent velocity (the Hubble flow), but the effect coming from the peculiar velocity can also influence it. Consider two galaxies, A and B, with B being further away from the observer than A. Both experience a certain Hubble flow, but B should have a higher redshift, because it is further away. If now B has its peculiar movement towards A and the observer, while A moves away from the observer, then their redshift measurement could indicate that they sit in the same position, degrading the precision of the analysis.

As a last remark on the topic of the LSS, it can be noticed that the CMB is not observed independently of them. Indeed, as the light from the CMB travels towards the observer, it gets lensed. This has the effect of smoothing out the contrast between the peaks. The evidence for slightly too strong lensing in the Planck results will be discussed in chapters 2 and 3.

1.4.3   Experimental confirmation of the Standard Model

As a summary of this section, it is interesting to remind all the experimental proofs that led to our SM of cosmology.

- The precise observation of the CMB from Planck has nailed down a universe composed of baryons, DM, currently dominated by Dark Energy (DE, of which the simplest model is the cosmological constant).
- The apparent homogeneity and near flatness of the universe can be explained by an unspecified scalar field, the inflaton, which is responsible for the seeds of perturbations.
- The observation of the LSS confirmed the presence of DM and DE, and established

that the universe is currently experiencing an accelerated stage of expansion.
- The observation of the reionization of our universe, through the decrease of temperature anisotropies on small scales, and the Gunn-Peterson effect, introduced in the model a parameter, z_{reio}, to determine the time of reionization.
- The abundance of primordial element abundances, confronted with the predictions from standard Big Bang Nucleosythesis, confirmed that the universe was radiation dominated when the temperature of the universe was of the order of 10 to 100 keV, with a radiation density close to that of thermalised photons and neutrinos, and a baryon density compatible with that inferred from CMB observations.

All these observations led to the construction of the Big Bang scenario, with the following six parameters. A_s and n_s for the initial amplitude and tilt of the scalar perturbations. ω_{b}, ω_{cdm} for the current amplitude of baryons and CDM. Ω_Λ is introduced to parametrize the importance of the late-time acceleration of the universe, and z_{reio} controls the reionization effect. Technically, the amplitude of radiation today, ω_{r} should be a free parameter, but the temperature of the CMB photons has been so well measured by the experiments that it is considered a fixed quantity.

Even though the nature of DM has not been explained, the fact that it is an important block for the whole cosmological theory is not disputable anymore. Concerning DE, the cosmological constant Λ constitutes a simple, if not completely satisfactory, explanation. It stands today as the seemingly simplest candidate. As far as DM is concerned, there is unfortunately no such simple situation. There exist simple DM candidates, but none of them have been so far observed or pinned down by other mean than its cosmological influence.

Nonetheless, the following section will be devoted to present the current status of DM from the particle physics side, and explain how cosmology can help constraining its nature.

1.5 Dark Matter

From the previous sections, we arrived at the conclusion that a special kind of matter was filling our universe: Dark Matter. We know it has to behave as pressureless matter (*i.e.* it has to dilute as $\rho \propto a^{-3}$), and it must emit very little light, or it would have been seen already. It also should be extremely long-lived in order to be stable on cosmological time-scales.

The other piece of information which we did not discuss so far is that the DM has to be *cold*, that is to say that it should have very little thermal velocity. It can not be, for instance, made only of the SM neutrinos, which still have a large thermal velocity today (a neutrino with $m = 0.05$ eV, for instance, would have a thermal velocity of the

order of 3000 km/s at redshift 0 [32]). Indeed, with large proper velocities, the particles would stream outside of the potential well, effectively dampening them, and forming less structures. A dominant Hot DM component is therefore excluded. However, Warm DM (WDM) is still in agreement with observations.

By assuming further that there is only one particle responsible for the DM, we also know the total energy density that this particle should have. Note however that this is not enough to pinpoint the mass. It can be realised that a particle with a mass of order GeV, interacting weakly with the rest of the SM particles, would be produced thermally with approximately the right abundance. This has been referred to as the "WIMP" miracle, for Weakly Interacting Massive Particle, and is one among the many possible candidates for DM.

1.5.1   Particle Physics

The first fact to realise is that there is no candidate in the SM of particle physics that could act as CDM. As discussed already, neutrinos are too hot to be the only DM particle. The two other particles which would be sufficiently long lived, the proton and the electron, are respectively a baryon and a lepton. Both interact with photons, and are therefore not *dark*.

Neutrinos are weakly interacting neutral species, and would therefore satisfy most of the constraints. They are, however, too light, giving them a high peculiar velocity. This would in turn prevent clustering because of the particles leaving their potential wells. Their special case will be reviewed in section 1.5.2.

A candidate for DM thus belongs to Beyond the Standard Model (BSM). One such possibility, which was very compelling for a long time, was the Lightest Supersymmetric Particle, (LSP), in the supersymmetry (SUSY) theory. [8] It provides an example of a WIMP, stable on cosmological scales. Indeed, in such a scenario, the introduced R-parity guarantees the proton stability, which also ensures the LSP stability. This does not prevent however a possible annihilation between a supersymmetric particle and its antiparticle. To have the proper relic abundance through thermal production, such SUSY particles would typically lie in the TeV range (see [33] for a model independent study). Currently, though, the most stringent lower bound from collider searches is of the order of 50 GeV for a neutralino as LSP, and 90 GeV for charginos (LEP data). Surprisingly enough, the LHC data did not improve this bound, illustrating the fact that SUSY has a wide range of predictions, and it is particularly hard to make a single truly model-independent statement.

If such a particle were found in a collider experiment, it would be possible to assess

---

[8]Note that this theory was not introduced to solve the DM problem, but rather to provide a natural explanation for the lightness of the Higgs mass.

its contribution to the DM energy density. However, despite the continuous efforts in searching for SUSY particles in colliders, nothing has been discovered yet. Notice as well that collider experiments are also performing Missing Energy searches, which are harder to do, but are also more model independent.

As previously pointed out, the WIMP is but one of many possible form for a DM candidate, and this absence of result should therefore not hinder cosmology in trying to characterize in more details the properties of the unknown particle. This is the approach followed in chapters 4 and 5, respectively with the annihilation rate and the decaying rate of these particles.

It is important to note that another viable alternative for DM has been proposed in the neutrino Minimal Standard Model (νMSM) under the form of sterile neutrinos [34]. It proposes a simple extension of the SM with three right-handed neutrinos, one of which could play the role of a WDM component. Two recent studies [35, 36] detected a promising decay line in the keV range, which would be a smoking gun signal for such a candidate. Although more statistics have to be gathered on other galaxies in order to make a more statistically robust claim, it is an encouraging signal nonetheless.

With these two examples, we already covered six orders of magnitude in terms of mass. It is however but a small portion of candidates, ranging from the μeV (axions) to 10^{50} GeV (primordial black holes), passing by very heavy particles of 10^{16} GeV (wimpzillas). From this point of view, the need for a cosmological study being as model-independent as possible is even more striking.

1.5.2 Neutrinos

Neutrinos have a somehow peculiar place in the SM of particle physics: they are assumed to be massless. Oscillation experiments, initially prompted by the missing solar neutrino puzzle, have on the other hand led to the theory of the flavor eigenstates being different than the mass eigenstates – and related through the Pontecorvo-Maki-Nakagawa-Sakata matrix (PMNS) matrix. This theory however stipulates that the mass states must be non-degenerate, leading to at least two massive neutrinos. Indeed, the rate of oscillation is proportional to the mass difference.

This observation leads to a lower bound on the total neutrino mass of 0.05 eV. On the other hand, the relative density Ω_ν of the neutrino can be computed to be [32]:

$$\Omega_\nu = \frac{\sum_i m_i}{93.14 \, h^2 \text{eV}} \tag{1.31}$$

By imposing simply that the neutrinos should not contribute more than the DM component ($\Omega_{\text{cdm}} \simeq 0.3$), we find, for three degenerate masses and a reduced Hubble constant

h of 0.7, that $m_i < 5$ eV. Therefore, we know, even before looking in details at how neutrinos affect the cosmological evolution, that cosmology is very sensitive to their total mass, and that most probably future experiments will be able to reduce the upper bound to levels close to the lower one.

Since they have a very small mass, these particles were relativistic in the past. It is important to notice that they might not be the only relativistic species present in the early universe. As discussed in section 1.5.1, the presence of sterile neutrinos would also play a similar role. In order to quantify these relativistic degrees of freedom in the early universe, we follow the convention of counting them under the variable N_{eff} in the following way:

$$\rho_{\text{relativistic}} = \left(1 + \frac{7}{8} \left(\frac{4}{11} \right)^{4/3} N_{\text{eff}} \right) \rho_\gamma, \tag{1.32}$$

where ρ_γ is the density of photons, which is observationally fixed by measuring the temperature of the CMB. The SM prediction of N_{eff} is a number close to 3 (for the three neutrinos): $N_{\text{eff}} = 3.046$. The small deviation from 3 comes from considering a refined decoupling model, instead of the usual instantaneous decoupling limit.

Thus an increase by one unit to this number will not necessarily mean that another relativistic degree of freedom has been found in the data. This relation is for instance also altered if the neutrinos do not follow a standard Fermi-Dirac statistic, or if there is additional late-time cooling of the photons [37]. In general, though, an increase to N_{eff} indicates a departure from the SM [38]. Such an excess was reported by one ground-based telescope, the South Pole Telescope, and triggered the research presented in chapter 2.

The last effect that will be discussed in this section is the impact of neutrinos on the matter power spectrum. As massive particles, they undergo a transition from relativistic to non-relativistic during the evolution of the universe. The smaller their mass, the later they entered the non-relativistic regime. Since they usually enter it rather late, they still possess large thermal velocities, and will therefore not collapse on small scales – they will stream out of the potential wells, essentially smoothing out the perturbations below their free-streaming scale at the time of the transition [32]. The free-streaming wavenumber k_{FS} is proportional to the mass of the neutrino with the following dependence:

$$k_{\text{FS}}(\tau) \simeq 0.82 \frac{\sqrt{\Omega_\Lambda + \Omega_{\text{m}}(1+z)^3}}{(1+z)^2} \left(\frac{m}{1\text{eV}} \right) \; h\text{Mpc}^{-1}. \tag{1.33}$$

It means that at redshift $z = 0$, and for a minimal neutrino mass of $0.05\,\text{eV}$, the scale at which the loss of power due to neutrino streaming out of the potential well is $k \simeq 0.04\,h/\text{Mpc}$ – as discussed in section 1.4.2, this is well within what is considered to be the linear regime of LSS.

The fact that such large scales are influenced for very light neutrinos is what drives the surprisingly good detection power of a future LSS experiment like EUCLID, as discussed in chapter 6. Indeed, the precision of our prediction on linear scales is very good, and the effect of neutrinos is already present. Note that the entire discussion here is at the linear level – it has been shown [39] that the non-linear effect is a further suppression of the power spectrum, at slightly smaller scales.

Notice finally that this last fact is what allows the bound on the neutrino mass to be really competitive, even compared to direct detection experiments, like the KATRIN experiment. Since their impact can be largely felt in the structure formation, corresponding to a suppression of power on small scales, we know that they can not constitute the entire DM – there would be a significant lack of structures on low scales. It drives the previous estimate of $5\,\mathrm{eV}$ down by a factor of a few, which significantly closes the allowed mass range.

1.6 Bayesian Statistics and Parameter Extraction

As discussed previously, cosmology is a stochastic theory. Therefore, observables need to be statistical ones, and this is why we only described the two-points correlators of density, whether in Fourier space or in harmonic space. But the problem with cosmology goes even further in the sense that we observe the universe today, and want to infer information on its initial conditions.

In Mathematics, this is called a boundary condition problem. You want to infer the initial condition, given the universe observable quantities today. You then need to utilize a shooting method, where you essentially "shoot in the dark", *i.e.* you start from random initial conditions, and compare the resulting observable to the experiment. You then shoot a second bullet, *i.e.* you start from different initial conditions, and see if you moved away or closer to the goal. By iterating this process, you can converge to a set of initial values for your parameter that reproduce the experiment you made.

One should keep in mind that any observation has uncertainties linked to it, whether they are instrumental noise or foreground coming from different sources. All this should reflect in the way we infer the values of our parameters. There is an entire framework to deal with these issues, the Bayesian framework, which is used widely in the scientific community when dealing with uncertain measurements, which I will introduce briefly, and explain how it is used in cosmology. The notation used here follows the book by Hobson et.al, Bayesian Methods in Cosmology [40].

1.6.1 Bayesian vocabulary

The very first concept to comprehend is that all our knowledge depends on the data we have at our disposition. What is true today, given the results from Planck, SDSS, and all the current experiments, can become not accurate anymore when EUCLID will come. In this sense, truth is really a moving target, modified by each new piece of evidence. The Bayesian word used to describe the ensemble of our knowledge is the *data*, $\mathcal{D}$.

Given the data $\mathcal{D}$, one can assume a model to describe these experiments. This is referred to as the *context*, $\mathcal{I}$. Having in mind the previous warning, the goal of the framework is to answer two fundamental questions: *i)* is this model $\mathcal{I}$ better than another one and *ii)* in this model, what are the *credible intervals* for the parameters.

Both questions, once answered, provide very valuable pieces of information, but one has to notice two things. First, this framework can not answer the question: "is this model true?" It will always be a comparison between two models, and as such, the only question it can answer is: "given the current data, is this model better than the others?" Second, the answer to *ii)* does not provide an absolute credible interval of the parameter value. Indeed, in another model, it might be that another parameter is degenerate with the former, thus enlarging its credible interval. It is important to keep in mind that all credible intervals are thus model-dependent.

Inside the context $\mathcal{I}$, we regroup the values of the parameters in a vector $\theta \in \mathbb{R}^N$, where N is the number of free parameters in the context. The Standard Model holds only six free cosmological parameters, but this number is greatly increased when analyzing some experiments, due to the addition of *nuisance parameters*. They parametrize our ignorance, be it of the exact amplitude of a foreground signal, or of the intrinsic configuration of the experiment.

We will also consider probabilities associated with the vector of parameters θ. For a function "pr" to be a probability, it must satisfy $\mathrm{pr}(\theta) \geq 0$. Its sum over the whole parameter space must also be normalized to 1, $\int \mathrm{pr}(\theta)\mathrm{d}\theta = 1$. The integral runs on the entire *prior volume*, which is a restriction of $\mathbb{R}^N$ in the sense that some parameters can be left to vary only within a closed range, instead of the whole real axis. The probabilities must also satisfy the product rule, $\mathrm{pr}(\varphi, \theta) = \mathrm{pr}(\varphi|\theta)\mathrm{pr}(\theta)$, where the joint probability of having φ and θ is expressed in terms of the conditional probability of having φ knowing we have already θ, times the probability of having θ.

1.6.2 Bayes Theorem

With all these definitions laid out, we come to the formulation of the Bayes Theorem. Given a context $\mathcal{I}$, it links our input knowledge (the model and the data) to an output

knowledge (the credible intervals of the parameters, and the relative merit of the model).

$$\text{pr}(\theta)\text{pr}(\mathcal{D}|\theta) = \text{pr}(\theta, \mathcal{D}) = \text{pr}(\mathcal{D})\text{pr}(\theta|\mathcal{D}) \tag{1.34}$$
$$\pi(\theta)\mathcal{L}(\theta) = \cdots \qquad = \mathcal{E}\mathcal{P}(\theta)$$

It is more widely known under the name of its terms: Prior π times Likelihood $\mathcal{L}$ equals Evidence $\mathcal{E}$ times Posterior $\mathcal{P}$.

The prior $\pi(\theta)$ is a probability that has to be assigned before-hand, which corresponds to the knowledge preceding experimental data. Whether it comes from a previous experiment or from a theoretical preference (this number should be Gaussian distributed around this value), it will impact significantly the credible interval. Its choice is a non-trivial matter, and not the point of this brief introduction, but we can note that it can be conveniently chosen to be a flat distribution - thus, by not preselecting a particular region in the prior volume, the result of the Bayesian framework will truly reflect the results of the data $\mathcal{D}$.

The likelihood $\mathcal{L}(\theta)$ is a function of the parameter vector. It is the probability of measuring the data $\mathcal{D}$, given that a theoretical model θ is responsible for the universe. This term is better understood when thinking about a simple experiment. When performing a measurement of any sort, you always have to make sure that the machine performs as expected on a known input: you calibrate it. You can then be confident that, if you observe a given output, it corresponds reliably to a certain input - up to the precision of your machine. The likelihood is exactly a formulation of this concept of calibration through a probabilistic statement: to observe $\mathcal{D}$ knowing that θ was the input.

For a complicated experiment, this function might be arbitrarily complicated to come up with. It requires an excellent knowledge about the actual sensors, and all the electronics and optics. It can be numerically expensive to compute, and can also be a non-analytical function of the vector θ. The importance of this fact will be highlighted in section 1.6.3.

On the right hand side of eq. (1.34), the output of the procedure is composed of the *Bayesian evidence* $\mathcal{E}$, which gives a relative number describing how likely it is that the model $\mathcal{I}$ produce the universe observed by the data $\mathcal{D}$. By taking ratios of this quantity computed for several models, one can compare the merits of the two models and decide which one is favored by the data. According to the Kass and Raftery scale [41], any number between 1 and 3 is not an indication of anything, while more than 150 would be a decisive proof. Note that it does not depend at all of a particular value of θ, since it truly is the merit of the model as a whole to explain the data.

Finally, the posterior distribution $\mathcal{P}(\theta)$ represents the credible interval where we are confident that the parameters of the underlying theory live. It is an *a posteriori* knowledge, since it takes into account the data. It is also a probability, so it also sums to 1. After having described all the terms, and by taking into account their properties, one can

express the two terms in the output as a function of the input:

$$\mathcal{E} = \int \mathcal{L}(\theta)\pi(\theta)\mathrm{d}\theta \tag{1.35}$$

$$\mathcal{P}(\theta) = \frac{\mathcal{L}(\theta)\pi(\theta)}{\mathcal{E}} \tag{1.36}$$

There are two things to note in these equations. The first one is that the evidence appears as an N-dimensional integral of a (potentially) non-analytical function of the vector of parameters θ. Even if the prior distribution, $\pi(\theta)$ is flat, and thus does not complicate the computation further, this is possibly a tough integral to compute numerically. However, we can also notice that $\mathcal{E}$ only appears at the denominator in the expression of the posterior distribution: it acts as a normalization constant. If one would be interested only in the posterior distribution, then the integral could be ignored completely. It is indeed what is being done in the Metropolis-Hastings method described in section 1.6.4.

1.6.3 Parameter Extraction

The application of the Bayesian Framework to cosmology is straightforward. Whenever a new experiment gives a result, we want to test whether we still believe in the Standard Model or not (*computing the evidence*). If we still do, we want to know what are the preferred values of the parameters according to the experiment, and which values are allowed (*computing the credible intervals for each parameter*). In any case, it will require an exploration of the parameter space constituted of the six standard cosmological parameters, in addition to any other parameter needed to describe the experiment. For instance, the Planck experiment requires the exploration of 14 nuisance parameters, which model the remaining uncertainty on the astrophysical foregrounds.

When considering cosmological applications, it is important to realise that computing the likelihood is a two-step process, one of which being very time-consuming. As described in the previous part, the likelihood relates the probability to observe the data given the input. However, it is not possible to go directly from the values of the parameters, θ, to what the experiment should observe: the step in between consists in computing how should the universe look like, given the value of θ.

This first step is the resolution of the Boltzmann Equation 1.25, by using a program such as CLASS or CAMB, to compute the CMB temperature anisotropies, polarization, and/or the matter power spectrum. The execution of the code, depending on the model and the desired precision, can take up to a few seconds.

Once this is done, the second step consists only in comparing the output of the Boltzmann code with the observation of the experiment. This is typically a much faster operation.

Exploring an unknown function (the likelihood) over such a high number of dimensions in the parameter space (20 for the Standard Model and Planck data) requires a better method than brute-force sampling. As one does not know beforehand what the likelihood looks like, it would be indeed very time-consuming to systematically scan the parameter space with an arbitrary sampling. Indeed, even when knowing the position of the maximum of likelihood, sampling the likelihood on a regular grid of m values around this maximum would require m^N evaluations of the likelihood. For as little as 10 values in each dimension, and considering an evaluation time of 5 seconds for each point, this would require a computing time slightly below 16 trillion years, on one core.

An alternative solution is to rely on a random sampling of the parameter space. In the context of cosmology, this idea has been introduced in [42], and many techniques are currently using it. Instead of deciding on an *a priori* exploration of the parameter space, the idea is instead to explore randomly the space, starting from a random position. There are several ways of choosing exactly how to move in the space, but they are all based on somehow selecting a new point, comparing the likelihood between the current one and the proposed one, and deciding to move there or not. If a point is accepted, it is appended to the chain, and the process restarts. If rejected, then a new proposition is made, while the weight associated to the current point is increased by one. As long as the jumping process only depends on the previous point in the chain, and on no other, the resulting chain of points is called a *Markov Chain.*

It is then clear that, if a point is accepted only when the likelihood is higher, the chain will quickly converge to the maximum of likelihood, and stay there. If instead the goal is to explore the space and find the entire posterior distribution, then one needs to also accept points which have a smaller likelihood. The chain should then trace the underlying distribution, with more weight given to more likely points.

1.6.4 Metropolis Hastings

The Metropolis-Hastings (MH) algorithm is one illustration of a Markov Chain process. It is very simply described by the following list of steps for the $n-$th iteration:

1. Propose a random point in the parameter space, following an arbitrary Gaussian distribution (the *proposal density*) around the last point in the chain $n-1$.
2. Compute the likelihood at this point n, $\mathcal{L}(n)$, and the ratio $a = \mathcal{L}(n)/\mathcal{L}(n-1)$
3. If $a > 1$, append this point to the chain
4. Else:
   - with probability a: append this point to the chain
   - with probability $1-a$: increase the multiplicity of the $n-1$ by one.

In fig. 1.4, this process is illustrated. The underlying probability distribution is shown in orange. Obviously, this precise shape and contours is precisely what is meant to be

The consequence of these facts is that the MH algorithm, though able to converge on the target distribution in principle, can in practice be inconveniently slow to do so. Alternative techniques have to be employed, such as Nested Sampling (see [45] for a numerical implementation with MultiNest).

As a final note on this technique, it is important to remark that a peculiarity of cosmology, particularly in recent experiments, can be used to improve the convergence speed of the algorithm: numerous *nuisance parameters*. These parameters represent the remaining uncertainty on certain phenomena, such as the amplitude of a foreground effect, or an instrumental noise. They have a different role than the other cosmological parameters for two reasons: *i)* they correspond to an information we are generally not interested in and *ii)* they are much cheaper to vary. Indeed, if we were to vary during one step only the value of a nuisance parameter, the entire Boltzmann hierarchy would not need to be recomputed, since the cosmological parameter retained their values. To compute the likelihood of this new point would therefore only consist in comparing the result of the Boltzmann code to the observation, a task typically much shorter.

By taking advantage of this fact, is is possible to devise a scheme in which these fast directions in parameter space are exploited. From time to time, several fast steps will be taken in these directions where the update of the likelihood will be almost immediate. It is based on the Cholesky decomposition, and has been introduced in the context of cosmology in [46].

1.6.5   Structure of Monte Python

After having presented the basic concepts behind Bayesian parameter estimation, we will describe hereafter the structure of Monte Python, the code that I developed during my PhD to perform cosmological parameter extraction. In appendix A, the motivations and goals of the code are being presented, and we instead focus here on understanding the different parts of the code, and how they work together. This section focuses on two goals. It should first serve as an introduction to my existing slides on the topic[9], that can be consulted for a more thorough explanation. But it is also a mean of illustrating the content of the previous section into the concrete example of cosmology. As advocated in chapter 7, the code is obviously under version control, and its main branch is publicly available on Github.[10]

Modules

The main folder contains all the modules (`.py` files), as well as the `likelihoods` folder, which contains the separate code for the likelihood computations. The first set of modules

---

[9]http://lesgourg.web.cern.ch/lesgourg/class-tour/class-tour.html
[10]https://github.com/baudren/montepython_public

only handle basic behaviour:

MontePython.py: Main file. It currently only checks for MPI support, and launches the corresponding `run` function (either `run` or `run_mpi`).

parser_mp.py Handles the parsing of the command-line arguments, and the display of the help.

io_mp.py Deals with all the input-output, display on the terminal, and writing to files.

The modules that follow are instead handling all the Monte Carlo process. The one part that will not be described here is the link with the Boltzmann solver, CLASS. This interface was built using Cython, a language allowing to build a Python library out of a C code. It is enough to understand that it will feed the parameters' value to CLASS, which will return whatever observables needed by the experiments to compute the likelihood, such as the CMB anisotropies or the matter power spectrum.

data.py: Defines the `Data` class that will hold information on the parameters, the prior volume, the list of experiments tested.

likelihood_class.py: Defines the generic `Likelihood` class of which all other specialized likelihoods should inherit from. It sets up the handling of likelihood data in a unified way in order to reduce the time spent in developing new likelihoods.

run.py: Initialises all the quantities needed according to the input file, a file with extension `.param`. It then launches the sampler.

sampler.py: Generic sampling file, with a direct call to the specialized sampling methods (Metropolis Hastings, Nested Sampling, Importance Sampling). It also contains the definition of a few functions of general interest across the samplers, such as `compute_lkl`. This function returns the log-likelihood at the `current` point in the chain, which is then used by the sampling method to determine where to go next in the chain.

The last module, `analyze.py`, is used to extract the posterior distribution from the samples of the distribution stored in the Markov chains produced by the algorithm.

Extensions

The modular structure makes it easy to implement another sampling algorithm. It is enough to add a new Python module, and refer to it from the file `sampler.py`.

In order to add a new likelihood, it is enough to add a new folder in the existing `montepython/likelihoods/`, for instance: `montepython/likelihoods/Euclid`. This new folder should contain *a minima* two files: `__init__.py` and `Euclid.data`. The `.data` file should contain information on the path of the data provided by the experiment, and other important settings. The Python file will contain the definition of a new class, called `Euclid`, inheriting from `Likelihood`. Apart from the initialisation, it should also

contain the redefinition of the `loglkl` function, returning the log likelihood at the current point in parameter space.

Another possible thing to do for the end user is to introduce non-standard parameters. By default, any parameters understood by CLASS can be asked to be marginalized over in the Monte Carlo process. Indeed, MONTE PYTHON does not interpret by itself the meaning of the cosmological parameters, they are simply transfered to CLASS. There is however a method of the class `Data` where the parameters can be altered before being send to the Boltzmann code: `update_cosmo_arguments`. The purpose of such a modification can have several sources. One common instance is to define combinations of parameters, such as $e^{-2\tau}A_s$ (see section 2.2). This parameter is unknown to CLASS, but the known ones are readily computed from it. Another reason would be to marginalize over custom parameters, for example $\log(10^{10}A_s)$ instead of A_s.

The rest of the documentation is available online,[11] and was automatically generated from the source code via the program Sphinx.

1.7 Additional open issues in Cosmology

The previous sections have but brushed the surface of the current status of the field, in order to provide the reader with the basic knowledge needed to understand the following chapters. From this concise presentation, it could be wrongly inferred that there are very little open questions in the field apart from the nature of dark matter. This section is here to discuss some of the main other outstanding problems in the domain that are closely related to the other topics that I tackled during my PhD, but did not present in this dissertation. This, in turn, covers only a very small fraction of all the open problems in the field.

The Dark Energy question is also a central topic, and since the simplest explanation (a non-zero cosmological constant Λ) suffers from a naturality point of view, there are many attempts to try and propose an alternative mechanism for expansion which will be natural. Unfortunately, as it is the case for instance in [9], the approach is always to set first the cosmological constant to zero. After doing so, it is sometimes possible to find a more natural candidate for the large-scale acceleration of the universe, but it comes at the cost of arbitrarily setting Λ to zero – an assumption arguably even more contrived than having it very small.

Another important question concerns the non-linear evolution of perturbations. As discussed in chapter 6, non-linear effects will be crucially relevant in order to understand properly the upcoming generation of LSS experiments. This includes: *i)* predicting accurately the DM perturbations on mildly non-linear scales [31, 47, 48], *ii)* having a

---

[11]http://baudren.web.cern.ch/baudren/documentation/index.html

good handle on the non-linear and non-local bias, and *iii)* understanding in details the redshift-space distortions. All these three items are currently being studied from the analytical and numerical points of view, and there has been promising developments (see for instance [49] for including massive neutrinos within the halo bias), but it is still very much an open field. We showed for instance in an early paper [50] how the Time Renormalization Group method proposed in [51] was not performing numerically as expected. The previously found agreement was shown to be the result of wrongly set initial conditions.

Finally, the recent excitement over the BICEP2 prompted us to verify some claims presented in the original paper [15]. We pointed out in a brief arXiv note [17] several misleading points in their analysis. Notably, we highlighted their omission of the pivot scale, rendering the comparison with Planck data very slippery. We also pointed out that the code they publicly released was not reproducing the best-fit to their data.

2 Agnostic Study

Foreword

At the time of writing of this paper, the cosmological community was buzzing with excitement over the high value of N_{eff} reported by WMAP [52] (3.84 ± 0.40) and the South Pole Telescope [53] (3.91 ± 0.42), a ground-based experiment. The Atacama Cosmology Telescope [54] (ACT), however, did not observe such an excess. As presented in section 1.5.2, this adimensional variable characterizes the effective number of relativistic species. If the Standard Model of Particle Physics is correct, we expect this number to be equal to 3.046 [32] - but these two experiments were hinting at a value much closer to 4.

In order to have such an excess, it would be needed to have extra relativistic particles at early times. It can be accomplished for instance by introducing an extra species of neutrinos, that do not interact with the rest of the SM particles - a *sterile* neutrino.[1]

As these particles form by themselves an interesting branch of particle physics and cosmology, it was very tempting for the community to find in this small excess a hint of detection. Even though the excess was never more than 2 or 3σ away from the Standard Model value, this measurement understandably prompted a lot of activity in the field.

The approach taken in this paper is instead in the exact opposite direction. Instead of assuming that the high value of N_{eff} was pointing towards the need of introducing new physics, we wondered if this excess could be caused by our assumptions on the late-time evolution of the universe, contaminating our measurement of this early quantity? Assuming that this is not the result of a measurement error, or a calibration problem, our point is simply to ensure that this excess can not be explained by the weakest part of our model being slightly different than expected.

To understand more clearly the proposition, let us recall that the Standard Model of

---

[1]Though it should be noted that increasing N_{eff} is not a strong prediction of this model in general.

cosmology can be described with 6 free parameters. There is some freedom in choosing which ones are set to be explored, *i.e.* which ones will have a flat prior. A customary choice of parametrisation is the following set:

$$\{\omega_{\rm b}, \omega_{\rm cdm}, d_A^{\rm rec}, \tau_{\rm reio}, A_s, n_s\}. \tag{2.1}$$

As cosmology explores a wide range of scale and epoch, some parameters in this list correspond to the early universe (the amplitude and tilt of the primordial scalar perturbations, A_s and n_s, and the initial amount of baryonic and cold dark matter), whereas the others refer to the late universe ($\tau_{\rm reio}$ and $d_A^{\rm rec}$). The distinction between early and late is set after recombination, when the structures start to form. Whereas the early cosmology is very well understood, the late part is less under control. The parameters entering the Standard Model are based on several assumptions that are not yet tested at the same level than the early cosmology ones. The study presented here addresses two very simple questions: *i)*: can our (mostly untested) assumptions about the late cosmology contaminate our knowledge of the early part, and if yes, *ii)* is it possible to design a way to analyze data that constrains the early parameters only, while being model-independent concerning the late-time evolution?

If the answer to the first question is yes, then it can be that, after answering the second one, we find that this excess of $N_{\rm eff}$ can be explained away by our uncertainties on the rest of our Standard Model, instead of introducing new physics. It is by no way because of strong feelings against sterile neutrinos that the study was designed, on the contrary. If one wants to properly build an extension to the Standard Model, one has to make sure that it stands on a firm basis. This paper addresses the firmness of this basis, and in particular, shows that when extracting constraints on the entire model, our uncertainties on the late time universe is spoiling some of our understanding about the early universe.

The questions is timely, as CMB experiments keep pushing the precision of the measurement of the temperature anisotropies. Every assumption making up our Standard Model needs to be assessed, as independently as possible, in order to reinforce our trust in its structure. It is a very similar situation than the one in particle physics, where the current uncertainty on the mass of the top quark is affecting other predictions of the SM. To beat down this uncertainty, and make a more precise determination of the mass will, among other things, tighten the predictions of the Higgs inflation model [55].

Note that this study was done before the release of Planck results, and therefore only uses WMAP7 data. It was updated, as well as expanded, in the work presented in chapter 3.

Conservative Constraints on Early Cosmology with MONTE PYTHON

Benjamin Audren, Julien Lesgourgues, Karim Benabed and Simon Prunet

Abstract: Models for the latest stages of the cosmological evolution rely on a less solid theoretical and observational ground than the description of earlier stages like BBN and recombination. As suggested in a previous work by Vonlanthen et al., it is possible to tweak the analysis of CMB data in such way to avoid making assumptions on the late evolution, and obtain robust constraints on "early cosmology parameters". We extend this method in order to marginalise the results over CMB lensing contamination, and present updated results based on recent CMB data. Our constraints on the minimal early cosmology model are weaker than in a standard ΛCDM analysis, but do not conflict with this model. Besides, we obtain conservative bounds on the effective neutrino number and neutrino mass, showing no hints for extra relativistic degrees of freedom, and proving in a robust way that neutrinos experienced their non-relativistic transition after the time of photon decoupling. This analysis is also an occasion to describe the main features of the new parameter inference code MONTE PYTHON, that we release together with this paper. MONTE PYTHON is a user-friendly alternative to other public codes like COSMOMC, interfaced with the Boltzmann code CLASS.

2.1 Introduction

Models for the evolution of the early universe between a redshift of a few millions and a few hundreds have shown to be very predictive and successful: the self-consistency of Big Bang Nucleosynthesis (BBN) model could be tested by comparing the abundance of light elements and the result of Cosmic Microwave Background (CMB) observations concerning the composition of the early universe; the shape of CMB acoustic peaks matches accurately the prediction of cosmological perturbation theory in a Friedmann-Lemaître Universe described by general relativity, with a thermal history described by standard recombination. The late cosmological evolution is more problematic. Models for the acceleration of the universe, based on a cosmological constant, or a dark energy component, or departures from general relativity, or finally departure from the Friedmann-Lemaître model at late times, have shown no predictive power so far. The late thermal history, featuring reionization from stars, is difficult to test with precision. Overall, it is fair to say that "late cosmology" relies on less solid theoretical or observational ground than "early cosmology".

When fitting the spectrum of temperature and polarisation CMB anisotropies, we make simultaneously some assumptions on early and late cosmology, and obtain intricate

constraints on the two stages. However, Vonlanthen et al. [56] suggested a way to carry the analysis leading to constraints only on the early cosmology part. This is certainly interesting since such an analysis leads to more robust and model-indepent bounds than a traditional analysis affected by priors on the stages which are most poorly understood. The approach of [56] avoids making assumptions on most relevant "late cosmology-related effects": projection effects due to the background evolution, photon rescattering during reionization, and the late Integrated Sachs Wolfe (ISW) effect.

In this work, we carry a similar analysis, pushed to a higher precision level since we also avoid making assumptions on the contamination of primary CMB anisotropies by weak lensing. We use the most recent available data from the Wilkinson Microwave Anisotropy Probe (WMAP) and South Pole Telescope (SPT) data[2], and consider the case of a minimal "early cosmology" model, as well as extended models with free density of ultra-relativistic relics or massive neutrinos.

This analysis is an occasion to present a new cosmological parameter inference code. This Monte Carlo code written in Python, called MONTE PYTHON[3], offers a convenient alternative to COSMOMC [58]. It is interfaced with the Boltzmann code CLASS[4] [23, 24]. MONTE PYTHON is released publicly together with this work.

In section 2, we explain the method allowing to get constraints only on the early cosmological evolution. We present our result for the minimal early cosmology model in section 3, and for two extended models in section 4. Our conclusions are highlighted in section 5. Finally, in appendix A, we briefly summarize some of the advantages of MONTE PYHTON, without entering into technical details (presented anyway in the code documentation).

2.2 How to test early cosmology only?

The spectrum of primary (unlensed) CMB temperature anisotropies is sensitive to various physical effects:

- (C1) the location of the acoustic peaks in multipole space depends on the sound horizon at decoupling $d_s(\eta_{rec})$ (an "early cosmology"-dependent parameter) divided by the angular diameter distance to decoupling $d_A(\eta_{rec})$ (a "late cosmology"-dependent parameter, sensitive to the recent background evolution: acceleration, spatial curvature, etc.)
- (C2) the contrast between odd and even peaks depends on ω_b/ω_γ, i.e. on "early cosmology".

---

[2]after the submission of this work to arXiv, further data was published by the SPT collaboration in Ref [57]

[3]http://montepython.net

[4]http://class-code.net

- (C3) the amplitude of all peaks further depends on the amount of expansion between radiation-to-matter equality and decoupling, governing the amount of perturbation damping at the beginning of matter domination, and on the amount of early integrated Sachs-Wolfe effect enhancing the first peak just after decoupling. These are again "early cosmology" effects (in the minimal ΛCDM model, they are both regulated by the redshift of radiation-to-matter equality, i.e by ω_m/ω_r).

- (C4) the envelope of high-ℓ peaks depends on the diffusion damping scale at decoupling $\lambda_d(\eta_{rec})$ (an "early cosmology" parameter) divided again by the angular diameter distance to decoupling $d_A(\eta_{rec})$ (a "late cosmology" parameter).

- (C5-C6) the global shape depends on initial conditions through the primordial spectrum amplitude A_s (C5) and tilt n_s (C6), which are both "early cosmology" parameters.

- (C7) the slope of the temperature spectrum at low ℓ is affected by the late integrated Sachs Wolfe effect, i.e. by "late cosmology". This effect could actually be considered as a contamination of the primary spectrum by secondary anisotropies, which are not being discussed in this list.

- (C8) the global amplitude of the spectrum at $\ell \gg 40$ is reduced by the late reionization of the universe, another "late cosmology" effect. The amplitude of this suppression is given by $e^{-2\tau}$, where τ is the reionization optical depth.

In summary, primary CMB temperature anisotropies are affected by late cosmology only through: (i) projection effects from real space to harmonic space, controlled by $d_A(\eta_{rec})$; (ii) the late ISW effect, affecting only small ℓ's; and (iii) reionization, suppressing equally all multipoles at $\ell \gg 40$. These are actually the sectors of the cosmological model which are the most poorly constrained and understood. But we see that the shape of the power spectrum at $\ell \gg 40$, interpreted modulo an arbitrary scaling in amplitude ($C_\ell \to \alpha C_\ell$) and in position ($C_\ell \to C_{\beta\ell}$), contains information on early cosmology only. This statement is very general and valid for extended cosmological models. In the case of the ΛCDM models, it is illustrated by figure 2.1, in which we took two different ΛCDM models (with different late-time geometry and reionization history), and rescaled one of them with a shift in amplitude given by $e^{-2\tau-\tau'}$ and in scale given by d_A/d'_A. At $\ell \gg 40$, the two spectra are identical. For more complicated cosmological models sharing the same physical evolution until approximately $z \sim 100$, a similar rescaling and matching would work equally well.

If polarization is taken into account, the same statement remains valid. The late time evolution affects the polarization spectrum through the angular diameter distance to decoupling $d_A(\eta_{rec})$ and through the impact of reionization, which also suppresses the global amplitude at $\ell \gg 40$, and generates an additional feature at low ℓ's, due to photon re-scatering by the ionized inter-galactic medium. The shape of the primary temperature and polarization spectrum at $\ell \gg 40$, interpreted modulo a global scaling in amplitude and in position, only contains information on the early cosmology.
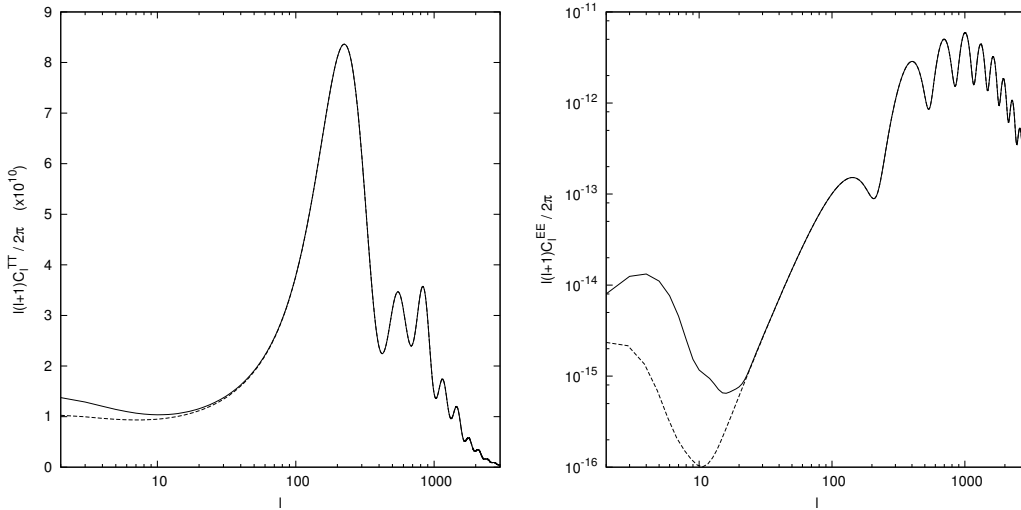
Figure 2.1 – Dimensionless temperature (left) and E-polarization (right) unlensed spectra of two ΛCDM models with the same value of "early cosmology" parameters (ω_b, ω_{cdm}, A_s, n_s) (fixed to WMAP best-fitting values), and different values of "late cosmology" parameters: (Ω_Λ, z_{reio}) = (0.720,10) (solid curves) or (0.619, 5) (dashed curve). The dashed curves have been rescaled vertically by the ratio of $e^{-2\tau}$ and horizontally by the ratio of $d_A(\eta_{rec})$ in each model, using the values of τ and $d_A(\eta_{rec})$ calculated by CLASS for each model. At $\ell = 40$, the difference between the dashed and solid line in the temperature plot is under $2\,\mu\text{K}^2$. At $\ell = 80$, it is already below $1\,\mu\text{K}^2$.

However, the CMB spectrum that we observe today gets a contribution from secondary anisotropies and foregrounds. In particular, the observed CMB spectra are significantly affected by CMB lensing caused by large scale structures. This effect depends on the small scale matter power spectrum, and therefore on late cosmology (acceleration, curvature, neutrinos becoming non-relativistic at late time, possible dark energy perturbations, possible departures from Einstein gravity on very large scales, etc.). In the work of [56], this effect was mentioned but not dealt with, because of the limited precision of WMAP5 and ACBAR data compared to the amplitude of lensing effects, at least within the multipole range studied in that paper ($40 \leq \ell \leq 800$). The results that we will present later confirm that this simplification was sufficient and did not introduce a significant "late cosmology bias". However, with the full WMAP7+SPT data (that we wish to use up to the high multipoles), it is not possible to ignore lensing, and in order to probe only early cosmology, we are forced to marginalize over the lensing contamination, in the sense of the method described below. By doing so, we will effectively get rid of the major two sources of secondary (CMB) anisotropies, the late ISW effect and CMB lensing. We neglect the impact of other secondary effects like the Rees-Sciama effect. As far as foregrounds are concerned, the approach of WMAP and SPT consists in eliminating them with a spectral analysis, apart from residual foregrounds which can be fitted to the data, using some nuisance parameters which are marginalized over. By following this

approach, we also avoid to introduce a "late cosmology bias" at the level of foregrounds.

Let us now discuss how one can marginalize over lensing corrections. Ideally, we should lens the primary CMB spectrum with all possible lensing patterns, and marginalize over the parameters describing these patterns. But the lensing of the CMB depends on the lensing potential spectrum $C_\ell^{\phi\phi}$, that can be inferred from the matter power spectrum at small redshift, $P(k, z)$. In principle, we should marginalize over all possible shapes for $C_\ell^{\phi\phi}$, i.e. over an infinity of degrees of freedom. We need to find a simpler approach.

One can start by noticing that modifications of the late-time background evolution caused by a cosmological constant, a spatial curvature, or even some inhomogeneous cosmology models, tend to affect matter density fluctuations in a democratic way: all Fourier modes being inside the Hubble radius and on linear scales are multiplied by the same redshift-dependent growth factor. CMB lensing is precisely caused by such modes. Hence, for this category of models, differences in the late-time background evolution lead to a different amplitude for $C_\ell^{\phi\phi}$, and also a small tilt since different ℓ's probe the matter power spectrum at different redshifts. Hence, if we fit the temperature and polarization spectrum at $\ell \gg 40$ modulo a global scaling in amplitude, a global shift in position, and additionally an arbitrary scaling and tilting of the lensing potential that one would infer assuming ΛCDM, we still avoid making assumption about the late-time evolution.

There are also models introducing a scale-dependent growth factor, i.e. distortions in the shape of the matter power spectrum. This is the case in the presence of massive neutrinos or another hot dark matter component, of dark energy with unusually large perturbations contributing to the total perturbed energy-momentum tensor, or in modified gravity models. In principle, these effects could lead to arbitrary distortions of $C_\ell^{\phi\phi}$ as a function of ℓ. Fortunately, CMB lensing only depends on the matter power spectrum $P(k, z)$ integrated over a small range of redshifts and wave numbers. Hence it makes sense to stick to an expansion scheme: at first order we can account for the effects of a scale-dependent growth factor by writing the power spectrum as the one predicted by ΛCDM cosmology, multiplied by arbitrary rescaling and tilting factors; and at the next order, one should introduce a running of the tilt, then a running of the running, etc. By marginalizing over the rescaling factor, tilting factor, running, etc., one can still fit the CMB spectra without making explicit assumptions about the late-time cosmology. In the result section, we will check that the information on early cosmology parameters varies very little when we omit to marginalize over the lensing amplitude, or when we include this effect, or when we also marginalize over a tilting factor. Hence we will not push the analysis to the level of an arbitrary lensing running factor.

We could have followed a slightly different approach based on principal components. Ref [59] showed that the lensed T and E modes depend on very few degrees of freedom in $C_\ell^{\phi\phi}$, since only the first two principal components are well constrained by the data. Hence we could have marginalized over the coefficients of these two components. Our

method with arbitrary amplitude and tilt has the same number of degrees of freedom and should be roughly equivalent.

2.3 Results assuming a minimal early cosmology model

We assume a "minimal early cosmology" model described by four parameters (ω_b, ω_{cdm}, A_s, n_s). In order to extract constraints independent of the late cosmological evolution, we need to fit the CMB temperature/polarisation spectrum measured by WMAP (seven year data [60]) and SPT [61] only above a given value of ℓ (typically $\ell \sim 40$), and to marginalize over two factors accounting for vertical and a horizontal scaling. In practice, there are several ways in which this could be implemented.

For the amplitude, we could fix the reionization history and simply marginalize over the amplitude parameter A_s. By fitting the data at $\ell \gg 40$, we actually constrain the product $e^{-2\tau}A_s$, i.e. the primordial amplitude rescaled by the reionization optical depth τ, independently of the details of reionization. In our runs, we fix τ to an arbitrary value, and we vary A_s; but in the Markov chains, we keep memory of the value of the derived parameter $e^{-2\tau}A_s$. By quoting bounds on $e^{-2\tau}A_s$ rather than A_s, we avoid making explicit assumptions concerning the reionization history.

For the horizontal scaling, we could modify CLASS in such way to use directly $d_A(\eta_{rec})$ as an input parameter. For input values of (ω_b, ω_{cdm}, $d_A(\eta_{rec})$), CLASS could in principle find the correct spectrum at $\ell \gg 40$. It is however much simpler to use the unmodified code and pass values of the five parameters (ω_b, ω_{cdm}, A_s, n_s, h). In our case, h should not be interpreted as the reduced Hubble rate, but simply as a parameter controlling the value of the physical quantity $d_A(\eta_{rec})$. For any given set of parameters, the code computes the value that $d_A(\eta_{rec})$ would take in a ΛCDM model with the same early cosmology and with a Hubble rate $H_0 = 100h$km/s/Mpc. It then fits the theoretical spectrum to the data. The resulting likelihood should be associated to the inferred value of $d_A(\eta_{rec})$ rather than to h. The only difference between this simplified approach and that in which $d_A(\eta_{rec})$ would be passed as an input parameter is that in one case, one assumes a flat prior on $d_A(\eta_{rec})$, and in the other case a flat prior on h. But given that the data allows $d_A(\eta_{rec})$ to vary only within a very small range where it is almost a linear function of h, the prior difference has a negligible impact.

To summarize, in order to get constraints on "minimal early cosmology", it is sufficient to run Markov Chains in the same way as for a minimal ΛCDM model with parameters (ω_b, ω_{cdm}, A_s, n_s, τ, h), excepted that:

- we do not fit the lowest temperature/polarization multipoles to the data;
- we fix τ or z_{reio} to an arbitrary value;
- we do not plot nor interpret the posterior probability of the parameters A_s and h.

	$100\,\omega_b$	ω_{cdm}	n_s	$d_A^{rec}(\text{Mpc})$	$10^9 e^{-2\tau} A_s$	A_{lp}	n_{lp}
	ΛCDM						
	$2.241^{+0.043}_{-0.044}$	$0.1114^{+0.0048}_{-0.0048}$	$0.960^{+0.011}_{-0.011}$	$12.93^{+0.11}_{-0.12}$	$2.069^{+0.085}_{-0.092}$		
	same lensing potential as in ΛCDM						
$\ell \geq 40$	$2.204^{+0.048}_{-0.047}$	$0.1160^{+0.0056}_{-0.0059}$	$0.946^{+0.014}_{-0.014}$	$12.85^{+0.13}_{-0.13}$	$2.20^{+0.12}_{-0.13}$		
$\ell \geq 60$	$2.203^{+0.050}_{-0.053}$	$0.1163^{+0.0063}_{-0.0065}$	$0.945^{+0.016}_{-0.016}$	$12.84^{+0.14}_{-0.14}$	$2.20^{+0.13}_{-0.15}$		
$\ell \geq 80$	$2.190^{+0.053}_{-0.057}$	$0.1180^{+0.0067}_{-0.0073}$	$0.940^{+0.019}_{-0.018}$	$12.81^{+0.15}_{-0.15}$	$2.26^{+0.15}_{-0.18}$		
$\ell \geq 100$	$2.184^{+0.054}_{-0.056}$	$0.1187^{+0.0067}_{-0.0079}$	$0.935^{+0.020}_{-0.019}$	$12.80^{+0.16}_{-0.15}$	$2.29^{+0.16}_{-0.20}$		
	marginalization over lensing potential amplitude						
$\ell \geq 100$	$2.159^{+0.060}_{-0.064}$	$0.1227^{+0.0083}_{-0.0088}$	$0.926^{+0.022}_{-0.022}$	$12.73^{+0.18}_{-0.17}$	$2.39^{+0.20}_{-0.23}$	$0.88^{+0.12}_{-0.13}$	
	marginalization over lensing potential amplitude and tilt						
$\ell \geq 100$	$2.160^{+0.064}_{-0.068}$	$0.1222^{+0.0088}_{-0.0094}$	$0.927^{+0.024}_{-0.024}$	$12.74^{+0.18}_{-0.18}$	$2.38^{+0.20}_{-0.25}$	$0.78^{+0.20}_{-0.15}$	$-0.16^{+0.55}_{-0.33}$

Table 2.1 – Limits at the 68% confidence level of the minimum credible interval of model parameters. The ΛCDM model of the first line has a sixth independent parameter (z_{reio}) that we do not show. We do not show either the limits on the three nuisance parameters associated to the SPT likelihood.

> We only pay attention to the posterior probability of the two derived parameters $e^{-2\tau} A_s$ and $d_A(\eta_{rec})$, which play the role of the vertical and horizontal scaling factors, and which are marginalized over when quoting bounds on the remaining three "early cosmology parameters" (ω_b, ω_{cdm}, n_s).

Hence, for a parameter inference code, this is just a trivial matter of defining and storing two "derived parameters". For clarity, we will refer to the runs performed in this way as the "agnostic" runs.

In the second line of Table 2.1, we show the bounds obtained with such an agnostic run, for a cut-off value $\ell = 40$. These results can be compared with those of a minimal ΛCDM model, obtained through the same machinery but with all multipoles $\ell \geq 2$. Since the agnostic bounds rely on less theoretical assumptions, they are slightly wider. Interestingly, the central value of ω_b and n_s are smaller in absence of late-cosmology priors, and larger for ω_{cdm}. Still the ΛCDM results are compatible with the agnostic results, which means that on the basis of this test, we cannot say that ΛCDM is a bad model. Our agnostic bounds on (ω_b, ω_{cdm}, n_s) are simply more model-independent and
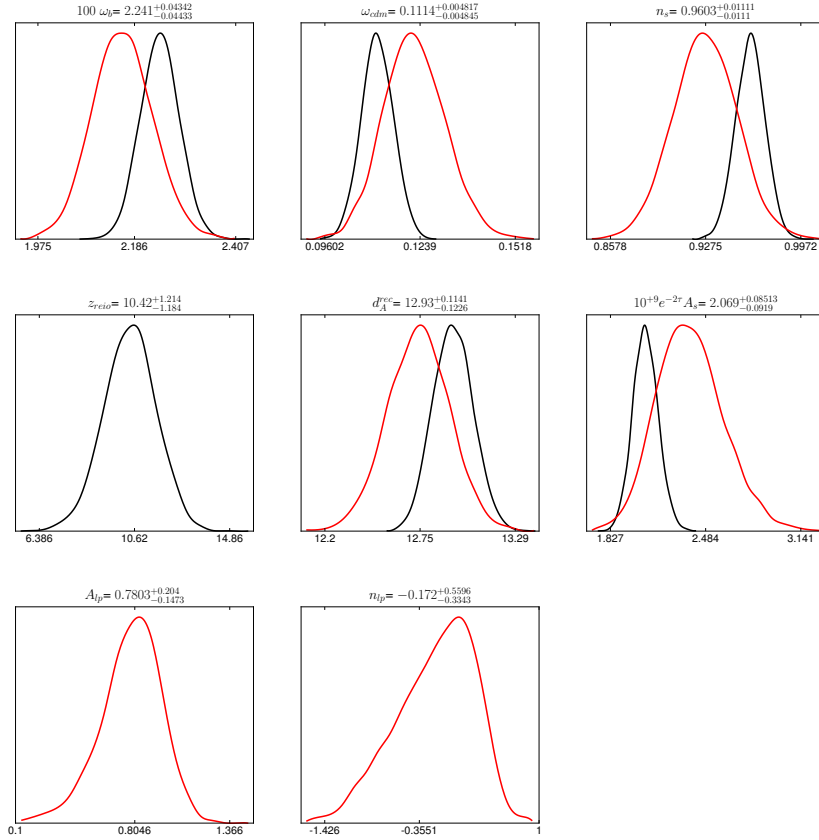
Figure 2.2 – Constraints on the five parameters of the minimal early cosmology model (red), compared to usual constraints on the minimal ΛCDM model (black). The ΛCDM has a sixth independent parameter, the reionization optical depth. The constraints on early cosmology (called "agnostic constraints" in the text) includes a marginalization over the amplitude and tilt of the matter power spectrum leading to CMB lensing, and takes only data for $\ell \geq 100$. We do not show here the posterior of the three nuisance parameter used to fit SPT data.

robust, and one could argue that when using CMB bounds in the study of BBN, in CDM relic density calculations or for inflationary model building, one should better use those bounds in order to avoid relying on the most uncertain assumptions of the minimal cosmological model, namely Λ domination and standard reionization.

The decision to cut the likelihood at $\ell \geq 40$ was somewhat arbitrary. Figure 2.1 shows that two rescaled temperature spectra with different late-time cosmology tend only gradually towards each other above $\ell \sim 40$. We should remove enough low multipoles in order to be sure that late time cosmology has a negligible impact given the data error bars. We tested this dependence by cutting the likelihood at $\ell \geq 60$, $\ell \geq 80$ or $\ell \geq 100$. When increasing the cut-off from 40 to 100, we observe variations in the mean value

that are less important than from 2 to 40. To have the more robust constraints, we will then take systematically the cut-off of $\ell = 100$, which is the one more likely to avoid any contamination from "late time cosmology".

Until now, our analysis is not completely "agnostic", because we did not marginalize over lensing. We fitted the data with a lensed power spectrum, relying on the same lensing potential as an equivalent ΛCDM model with the same values of $(\omega_b, \omega_{cdm}, n_s, A_s, d_A(\eta_{rec}))$. To deal with lensing, we introduce three new parameters (A_{lp}, n_{lp}, k_{lp}) in CLASS. Given the traditional input parameters $(\omega_b, \omega_{cdm}, A_s, n_s, h)$, the code first computes the Newtonian potential $\phi(k, z)$. This potential is then rescaled as

$$\phi(k, z) \longrightarrow A_{lp} \left(\frac{k}{k_{lp}} \right)^{n_{lp}} \phi(k, z) \ . \tag{2.2}$$

Hence, the choice $(A_{lp}, n_{lp}) = (1,0)$ corresponds to the standard lensing potential predicted in the ΛCDM model (if z_{reio} is the same as the fixed arbitrary value of the agnostic analysis, here $z_{reio} = 10$). Different values correspond to an arbitrary rescaling or tilting of the lensing potential, which can be propagated consistently to the lensed CMB temperature/polarization spectrum.

The sixth run shown in Table 2.1 corresponds to $n_{lp} = 0$ and a free parameter A_{lp}. The minimum credible interval for this rescaling parameter is $A_{lp} = 0.88^{+0.12}_{-0.13}$ at the 68% Confidence Level (CL), and is compatible with one. This shows that WMAP7+SPT data alone are sensitive to lensing, and well compatible with the lensing signal predicted by the minimal ΛCDM model. We note that the error bars on other cosmological parameters increase more from ΛCDM to the previous agnostic run ($\approx 30\%$) than from the latter to this run ($\approx 10\%$), showing that "agnostic bounds" are robust.

In the seventh line of Table 2.1, we also marginalize over the tilting parameter n_{lp} (with unbounded flat prior). A priori, this introduces a lot of freedom in the model. Nicely, this parameter is still well constrained by the data ($n_{lp} = -0.16^{+0.55}_{-0.33}$ at 68%CL), and compatible with the ΛCDM prediction $n_{lp} = 0$. Bounds on other parameters vary this time by a completely negligible amount: this motivates us to stop the expansion at the level of n_{lp}, and not to test the impact of running. The credible interval for A_{lp} is the only one varying significantly when n_{lp} is left free, but this result depends on the pivot scale k_{lp}, that we choose to be equal to $k_{lp} = 0.1/\text{Mpc}$, so that the amplitude of the lensing spectrum $C_\ell^{\phi\phi}$ is nearly fixed at $\ell \sim 100$. By tuning the pivot scale, we could have obtained bounds on A_s nearly equal for the case with/without free n_{lp}. The posterior probability of each parameter marginalized over other parameters is shown in Figure 2.2, and compared with the results of the standard ΛCDM analysis.

Our results nicely agree with those of [56]. These authors found a more pronounced drift of the parameters $(\omega_b, \omega_{cdm}, n_s)$ with the cut-off multipole than in the first part of our analysis, but this is because we use data on a wider multipole range and have a larger

lever arm. Indeed, Ref. [56] limited their analysis of WMAP5 plus ACBAR data to $\ell \leq 800$, arguing that above this value, lensing would start playing an important role. In our analysis, we include WMAP7 plus 47 SPT band powers probing up to $\ell \sim 3000$, but for consistency we must simultaneously marginalize over lensing. Indeed, the results of Ref. [56] are closer to our results with lensing marginalization (the fully "agnostic" ones) that without. Keeping only one digit in the error bar, we find ($100\omega_b = 2.16 \pm 0.07$, $\omega_{cdm} = 0.122 \pm 0.009$, $n_s = 0.93 \pm 0.02$), when this reference found ($100\omega_b = 2.13 \pm 0.05$, $\omega_{cdm} = 0.124 \pm 0.007$, $n_s = 0.93 \pm 0.02$). The two sets of results are very close to each other, but our central values for ω_b and ω_{cdm} are slightly closer to the ΛCDM one. The fact that we get slightly larger error bars in spite of using better data in a wider multipole range is related to our lensing marginalization: we see that by fixing lensing, this previous analysis was implicitly affected by a partial "late cosmology prior", but only at a very small level.

Our results from the last run can be seen as robust "agnostic" bounds on (ω_b, ω_{cdm}, n_s), only based on the "minimal early cosmology" assumption. They are approximately twice less constraining than ordinary ΛCDM models, and should be used in conservative studies of the physics of BBN, CDM decoupling and inflation.

2.4 Effective neutrino number and neutrino mass

We can try to generalize our analysis to extended cosmological models. It would make no sense to look at models with spatial curvature, varying dark energy or late departures from Einstein gravity, since all these assumptions would alter only the late time evolution, and our method is designed precisely in such way that the results would remain identical[5]. However, we can explore models with less trivial assumptions concerning the early cosmological evolution. This includes for instance models with:

- a free primordial helium fraction Y_{He}. So far, we assumed Y_{He} to be a function of ω_b, as predicted by standard BBN (this is implemented in CLASS following the lines of Ref. [63]). Promoting Y_{He} as a free parameter would be equivalent to relax the assumption of standard BBN. Given the relatively small sensitivity of current CMB data to Y_{He} [60], we do not perform such an analysis here, but this could be done in the future using e.g. Planck data.
- a free density of relativistic species, parametrized by a free effective neutrino number N_{eff}, differing from its value of 3.046 in the minimal ΛCDM model [64]. This parameter affects the time of equality between matter and radiation, but this effect can be cancelled at least at the level of "early cosmology" by tuning

---

[5]In the case with spatial curvature, the result would remain identical only in first approximation. As explained in Ref. [62], section II-B-2, the finite thickness of the last-scattering surface projects slightly differently depending on curvature, such that the geometrical degeneracy is not exact. This is however an effect of the order of 10^{-3}, for $\Omega_k = 0.02$, so that the results of the previous section still extend to curved models in very good approximation.

$100\,\omega_b$	ω_{cdm}	n_s	N_{eff}	$d_A^{rec}(\text{Mpc})$	$10^9 e^{-2\tau} A_s$	A_{lp}	n_{lp}
			ΛCDM				
$2.279^{+0.053}_{-0.056}$	$0.124^{+0.011}_{-0.013}$	$0.979^{+0.019}_{-0.019}$	$3.77^{+0.58}_{-0.66}$	$12.35^{+0.46}_{-0.53}$	$2.01^{+0.10}_{-0.10}$		
		$\ell \geq 100$, marginalization over lensing potential amplitude and tilt					
$2.03^{+0.13}_{-0.16}$	$0.113^{+0.011}_{-0.015}$	$0.862^{+0.065}_{-0.077}$	$2.04^{+0.78}_{-1.26}$	$13.59^{+0.96}_{-0.87}$	$2.84^{+0.49}_{-0.59}$	$0.69^{+0.21}_{-0.18}$	$-0.23^{+0.57}_{-0.43}$

Table 2.2 – Limits at the 68% confidence level of the minimum credible interval of model parameters. The ΛCDM+N_{eff} model of the first line has a seventh independent parameter (z_{reio}) that we do not show. We do not show either the limits on the three nuisance parameters associated to the SPT likelihood.

appropriately the density of baryons and CDM. Even in that case, relativistic species will leave a signature on the CMB spectrum, first through a change in the diffusion damping scale $\lambda_d(\eta_{rec})$, and second through direct effects at the level of perturbations, since they induce a gravitational damping and phase shifting of the photon fluctuation [65, 66]. It is not obvious to anticipate up to which level these effects are degenerate with those of other parameters. Hence it is interesting to run Markov chains and search for "agnostic bounds" on N_{eff}.

- neutrino masses (or for simplicity, three degenerate masses m_ν summing up to $M_\nu = 3m_\nu$). Here we are not interested in the fact that massive neutrinos affect the background evolution and change the ratio between the redshift of radiation-to-matter equality, and that of matter-to-Λ equality. This is a "late cosmology" effect that we cannot probe with our method, since we are not sensitive to the second equality. However, for masses of the order of $m_\nu \sim 0.60$ eV, neutrinos become non-relativistic at the time of photon decoupling. Even below this value, the mass leaves a signature on the CMB spectrum coming from the fact that, first, they are not yet ultra-relativistic at decoupling, and second, the transition to the non-relativistic regime takes place when the CMB is still probing metric perturbations through the early integrated Sachs-Wolfe effect. Published bounds on M_ν from CMB data alone probe all these intricate effects [60], and it would be instructive to obtain robust bounds based only on the mass impact on "early cosmology".

For the effective neutrino number, we performed two runs similar to our previous ΛCDM and "fully agnostic" run (with marginalization over lensing amplitude and tilt), in presence of one additional free parameter N_{eff}. Our results are summarized in Table 2.2 and Figure 2.3. In the ΛCDM+N_{eff} case, we get $N_{\text{eff}} = 3.77^{+0.58}_{-0.66}$ (68% CL), very close to the result of [67], $N_{\text{eff}} = 3.85 \pm 0.62$ (differences in the priors can explain this insignificant difference). It is well-known by now that the combination of WMAP and small-scale
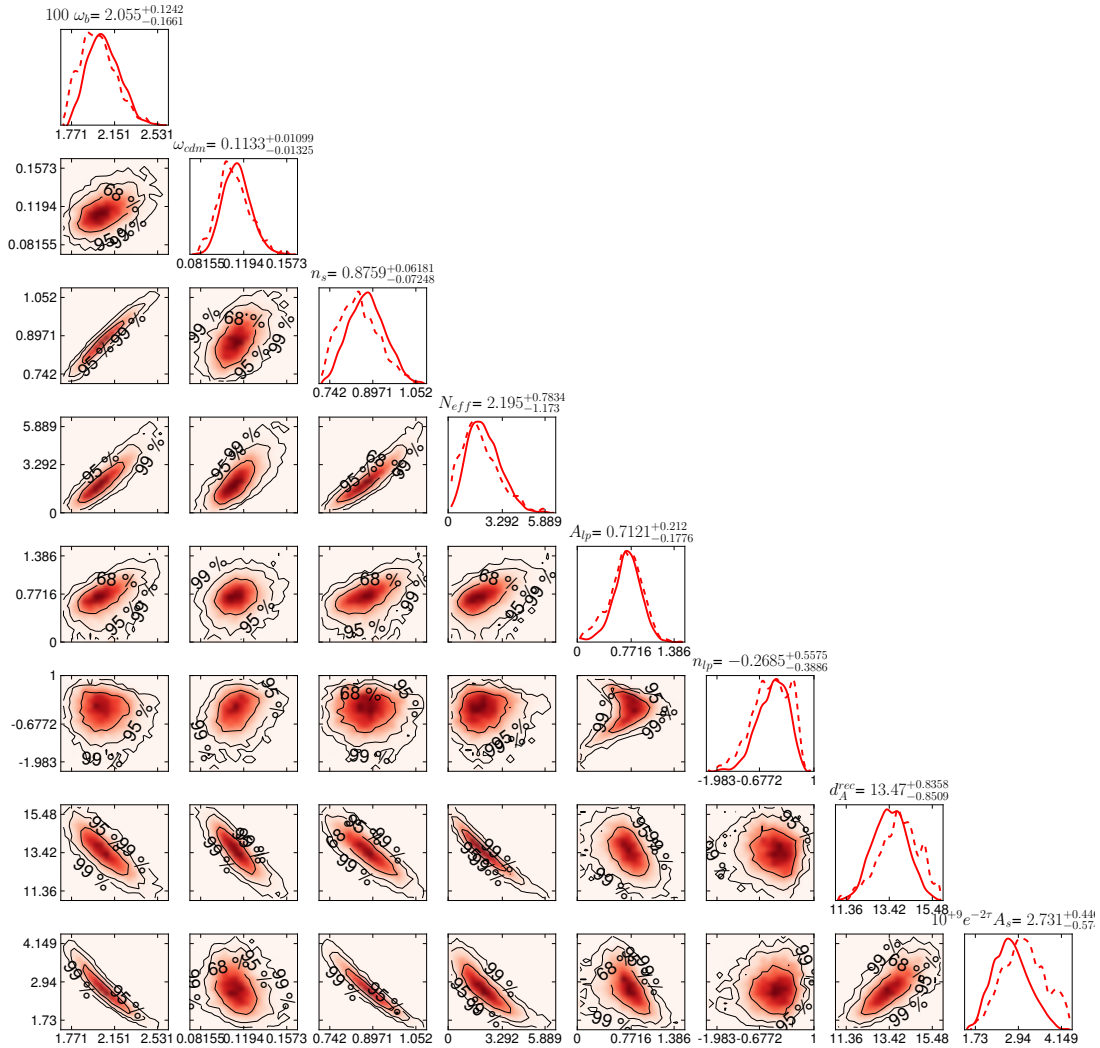
Figure 2.3 – One and two-dimensional posterior distribution (solid line) of the parameters of the "agnostic" run with a free effective neutrino number. The dashed line stands for the average likelihood distribution. The concentric contour lines in the two-dimensional posteriors stand for 68, 95 and 99% CL.

CMB data shows a marginal preference for extra relativistic degrees of freedom in the seven-parameter model. The surprise comes from our "agnostic" bound on this number, $N_{\text{eff}} = 2.04^{+0.78}_{-1.26}$ (68% CL). As explained before, this bound cannot come from a change in the time of equality, nor in the scale of the first peak, nor in the late integrated Sachs-Wolfe effect; it can only result from the measurement of the the sound horizon $d_s(\eta_{rec})$ *relatively* to the diffusion damping scale $\lambda_d(\eta_{rec})$, and from the direct effects of extra relativistic degrees of freedom on photon perturbations. Hence it is normal that N_{eff} is much less constrained in the agnostic runs, but the interesting conclusion is that

without assuming ΛCDM at late time, the CMB does not favor high values of N_{eff}. It is compatible with the standard value $N_{\text{eff}} = 3.046$ roughly at the one-σ level, with even a marginal preference for smaller values. This shows that recent hints for extra relativistic relics in the universe disappear completely if we discard any information on the late time cosmological evolution. It is well-known that N_{eff} is very correlated with H_0 and affected by the inclusion of late cosmology data sets, like direct measurement of H_0 or of the BAO scale. Our new result shows that even at the level of CMB data only, the marginal hint for large N_{eff} is driven by physical effects related to late cosmology (and in particular by the angular diameter distance to last scattering as predicted in ΛCDM).

The triangle plot in Figure 2.3 shows that in the agnostic run, N_{eff} is still very correlated with other parameters such as ω_b, ω_{cdm} and n_s. These degeneracies are easily explained. Increasing N_{eff} increases the damping scale $\lambda_d(\eta_{rec})$ *relatively* to the sound horizon $d_s(\eta_{rec})$. So, in terms of angles, it increases the damping angular scale θ_D *relatively* to the peak angular scale θ_s. Increasing n_s can compensate this enhanced damping by tilting the whole spectrum, so there is a positive correlation between N_{eff} and n_s. Increasing $\omega_b + \omega_{cdm}$ together with N_{eff} can preserve the redshift of matter-radiation equality, so there is also a positive correlation between N_{eff} and ω_b, and between N_{eff} and ω_{cdm}. The correlation with ω_b is stronger, because increasing ω_b also has the effect of decreasing θ_D relatively to θ_s (as shown in Ref. [68]), which counteracts the effect of increasing N_{eff}. Low values of N_{eff} (significantly smaller than the standard value 3.046) are only compatible with a very small ω_b, ω_{cdm} and n_s. Note that in this work, we assume standard BBN in order to predict Y_{He} as a function of ω_b (and of N_{eff} when this parameter is also left free), but we do not incorporate data on light element abundances. By doing so, we would favor the highest values of ω_b in the range allowed by the current analysis ($\omega_b \sim 0.022$), and because of parameter correlations we would also favor the highest values of ω_{cdm}, n_s and N_{eff}, getting close to the best-fitting values in the minimal early cosmology model with $N_{\text{eff}} \sim 3.046$.

For neutrino masses, we performed two similar runs (summarised in Table 2.3 and Figure 2.4), with now M_ν being the additional parameter (assuming three degenerate neutrino species). In the ΛCDM case, our result $M_\nu < 1.4$ eV (95%CL) is consistent with the rest of the literature, and close to the WMAP-only bound of [60]: measuring the CMB spectrum does not bring significant additional information on the neutrino mass. In the agnostic run, this constraint only degrades to $M_\nu < 1.8$ eV (95%CL). This limit is consistent with the idea that for sufficiently large m_ν, the CMB can set a limit on the neutrino mass not just through its impact on the background evolution at late time (and its contribution to ω_m today), but also through direct effects occurring at the time of recombination and soon after. It is remarkable that this is true even for neutrinos of individual mass $m_\nu \sim 0.6$ eV, becoming non-relativistic precisely at the time of photon decoupling. The conclusion that the CMB is not compatible with neutrinos becoming non-relativistic before z_{rec} appears to be very robust, and independent of any constraint on the late cosmological evolution.

$100\,\omega_b$	ω_{cdm}	n_s	M_ν (eV)	d_A^{rec}(Mpc)	$10^9 e^{-2\tau} A_s$	A_{lp}	n_{lp}
			ΛCDM				
$2.205^{+0.046}_{-0.049}$	$0.114^{+0.0052}_{-0.0050}$	$0.949^{+0.014}_{-0.013}$	< 1.4	$12.86^{+0.13}_{-0.13}$	$2.16^{+0.10}_{-0.12}$		
		$\ell \geq 100$, marginalization over lensing potential amplitude and tilt					
$2.136^{+0.065}_{-0.072}$	$0.123^{+0.009}_{-0.010}$	$0.920^{+0.025}_{-0.025}$	< 1.8	$12.69^{+0.19}_{-0.19}$	$2.43^{+0.21}_{-0.28}$	$0.81^{+0.22}_{-0.16}$	$-0.11^{+0.58}_{-0.32}$

Table 2.3 – Limits at the 68% confidence level of the minimum credible interval of model parameters (excepted for M_ν, for which we show the 95% CL upper limit). The ΛCDM+M_ν model of the first line has a seventh independent parameter (z_{reio}) that we do not show. We do not show either the limits on the three nuisance parameters associated to the SPT likelihood.

2.5 Conclusions

Models for the latest stages of the cosmological evolution rely on a less solid theoretical and observational ground than the description of earlier stages, like BBN and recombination. Reference [56] suggested a way to infer parameters from CMB data under some assumptions about early cosmology, but without priors on late cosmology. By standard assumption on early cosmology, we understand essentially the standard model of recombination in a flat Friedmann-Lemaître universe, assuming Einstein gravity, and using a consistency relation between the baryon and Helium abundance inferred from standard BBN. The priors on late cosmology that we wish to avoid are models for the acceleration of the universe at small redshift, a possible curvature dominated stage, possible deviations from Einstein gravity on very large scale showing up only at late times, and reionization models.

We explained how to carry such an analysis very simply, pushing the method of [56] to a higher precision level by introducing a marginalization over the amplitude and tilt of the CMB lensing potential. We analyzed the most recent available WMAP and SPT data in this fashion, that we called "agnostic" throughout the paper. Our agnostic bounds on the minimal "early cosmology" model are about twice as weak than in a standard ΛCDM analysis, but perfectly compatible with ΛCDM results: there is no evidence that the modeling of the late-time evolution of the background evolution, thermal history and perturbation growth in the ΛCDM is a bad model, otherwise it would tilt the constraints on ω_b, ω_{cdm} and n_s away from the "agnostic" results. It is interesting that WMAP and SPT alone favor a level of CMB lensing different from zero and compatible with ΛCDM predictions.

We extended the analysis to two non-minimal models changing the "early cosmology",
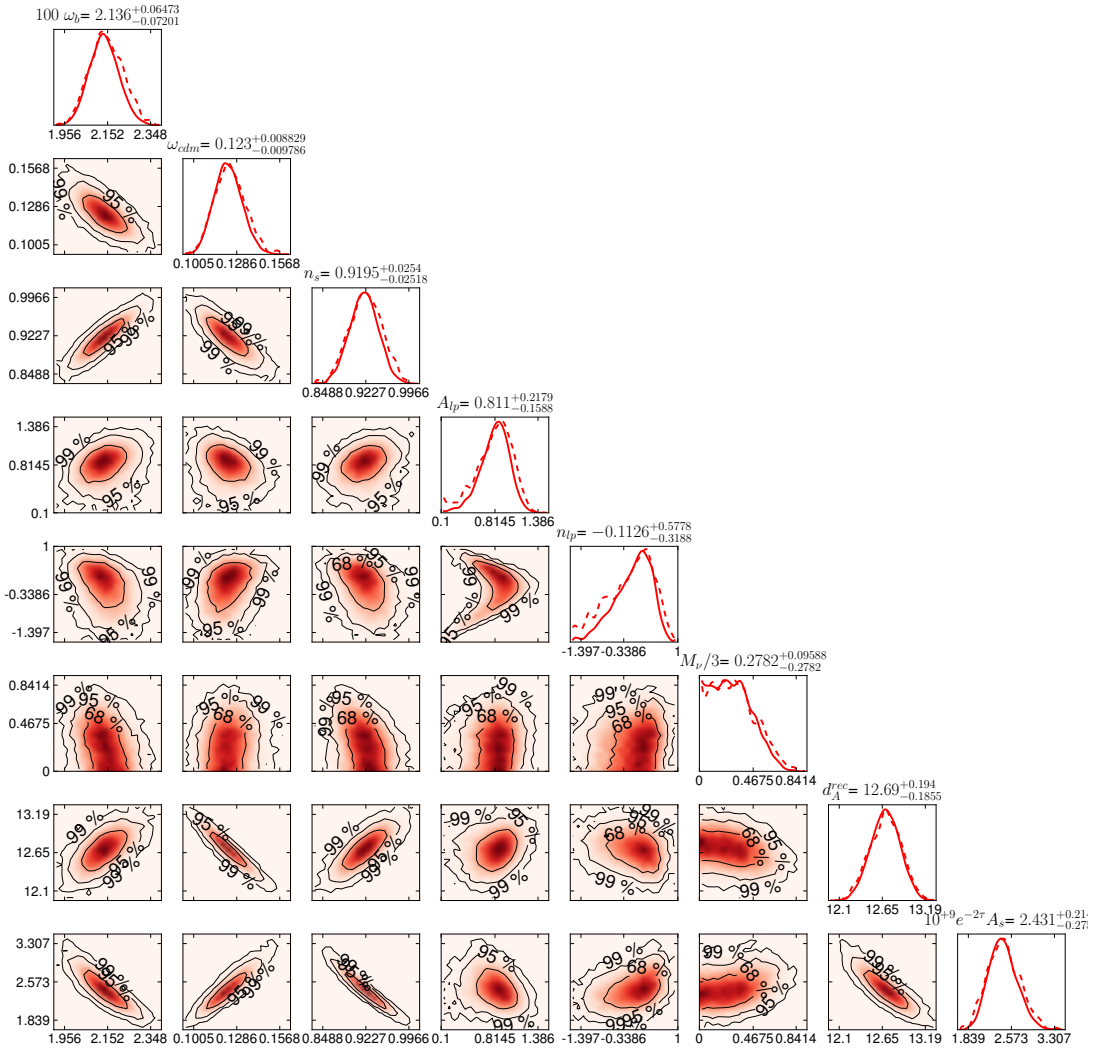
Figure 2.4 – One and two-dimensional posterior distribution (solid line) of the parameters of the "agnostic" run with a total neutrino mass M_ν (assuming three degenerate neutrinos of individual mass m_ν). Again, dashed line stands for average likelihood distribution, contour lines indicate the 68, 95 and 99% CL.

with either a free density of ultra-relativistic relics, or some massive neutrinos that could become non-relativistic before or around photon decoupling. In the case of free N_{eff}, it is striking that the "agnostic" analysis removes any hint in favor of extra relics. The allowed range is compatible with the standard value $N_{\text{eff}} = 3.046$ roughly at the one-sigma level, with a mean smaller than three. In the case with free total neutrino mass M_ν, it is remarkable that the "agnostic" analysis remains sensitive to this mass: the two-sigma bound coincides almost exactly with the value of individual masses corresponding to a non-relativistic transition taking place at the time of photon decoupling.

The derivation of these robust bounds was also for us an occasion to describe the main feature of the new parameter inference code MONTE PYTHON, that we release together with this paper. MONTE PYTHON is an alternative to COSMOMC, interfaced with the Boltzmann code CLASS. It relies on the same basic algorithm as COSMOMC, but offers a variety of user-friendly function, that make it suitable for a wide range of cosmological parameter inference analyses.

3 Separate constraints on Early and Late Cosmology

Foreword

The study presented in chapter 2 only focuses on disentangling the early and late cosmology, in order to obtain model independent bounds for the early parameters. In this study, the goal is to push the reasoning one step further and utilize this knowledge on the early cosmology in order to assess, separately, the merit of different assumptions about the late universe.

Indeed, after having obtained constraints independently of any assumptions, it is in principle possible to add back, one by one, the hypothesis that were removed. This way, you can test separately how good one part of the model works, independently of another one. Here, we focus on addressing the single question: can a simple cosmological constant, Λ, be responsible for the late homogeneous evolution of our universe. Indeed, this assumption is often reassessed, and alternatives are proposed.

By introducing only this hypothesis, and still maintaining an agnostic attitude towards the reionization history and on the clustering of matter, we can check whether or not Λ provides a valid model for this part of the cosmological history. It will therefore only address this specific question, centered on the homogeneous evolution.

The motivation for this works lies in the measurement by Planck [11], which found a value of the Hubble rate close to $H_0 = 67\,\mathrm{km/s/Mpc}$, whereas other homogeneous probes found a value closer to $H_0 = 73\,\mathrm{km/s/Mpc}$. Even though being only of the order of 2σ, this observed small tension raised some questions. Since the two measurements are actually probing H_0 at different scales (the CMB measures it globally, while the homogeneous measurements are essentially probing the value only locally), it might be an indication of the small scale inhomogeneity of our universe. Since this explanation was proven to be not sufficient [69], the need to somehow reconcile the two measurements stayed. Some favored explanations were revolving around replacing the cosmological constant by a

more refined explanation for the late-time acceleration of the universe. It was therefore interesting to test the hypothesis of Λ using our framework.

It is important to keep in mind that, as explained in section 3.2, in order to render the study agnostic, the information concerning the lower multipoles has been discarded. Thus, no matter how much we manage to relax the hypothesis about Λ, we will still be using less information than what we started with. This would in turn widen the constraints on H_0, and potentially resolve by itself the observed tension. It is not a trivial point to resolve, however, because it is impossible to perform a standard analysis with only the large multipoles. Indeed, as it can be realized by looking at section 2.2, the low multipoles are the only one constraining the global amplitude of the initial curvature power spectrum, A_s, leaving effectively this direction unconstrained - a difficult problem for any parameter exploration. This fact is irrelevant for the agnostic analysis because this amplitude appears only in the product $e^{-2\tau}A_s$. There is therefore not much that can be done to alleviate this potential problem, except to remember this as being a limiting factor of the analysis.

Separate Constraints on Early and Late Cosmology

Benjamin Audren

Abstract: Since the public release of Planck data, several attempts have been made to explain the observed small tensions with other data-sets, most of them involving an extension of the ΛCDM Model. We try here an alternative approach to the data analysis, based on separating the constraints coming from the different epochs in cosmology, in order to assess which part of the Standard Model generates the tension with the data. To this end, we perform a particular analysis of Planck data probing only the early cosmological evolution, until the time of photon decoupling. Then, we utilize this result to see if the ΛCDM model can fit all observational constraints probing only the late cosmological background evolution, discarding any information concerning the late perturbation evolution. We find that all tensions between the data-sets are removed, suggesting that our standard assumptions on the perturbed late-time history, as well as on reionization, could sufficiently bias our parameter extraction and be the source of the alleged tensions.

3.1 Introduction

It is a well established fact that early cosmology history until photon recombination is well understood. What happens after this epoch relies however on a less solid ground. The nature of dark energy, the details of reionization, the collapse of structures, all this is based on priors that are not well tested, or non-linear physics, and thus might bias our analysis.

As was done originally in [56], it is possible to devise an analysis of the early cosmology parameters that is independent of assumptions concerning the late universe, providing so-called "agnostic" constraints, *i.e.* constraints without believing in any late-time cosmology model. In [1], this analysis was done with the data sets available at the time, and improved in order to be also independent of the CMB lensing contamination. It provided a consistency check of our current standard model of early-cosmology.

The purpose of this paper is two-fold. On the one hand, we refine the "agnostic" analysis with a better treatment of the lensing marginalization, and update it to the current Planck data. On the other hand, we propose to utilize this newly acquired knowledge about the early universe and treat it as a measurement of early quantities, in the sense that it gives posterior distribution on a set of cosmological parameters. From there, one can assume a model for the homogeneous late-time evolution, and test the implications of the previous measurement on this model, as well as the constraints coming from other

probes. The goal would then be to exclusively test the merit of the cosmological constant as an explanation for the late time acceleration, without any contamination from other assumptions. This second point could be extended in the future to more general models for late cosmology, involving *e.g.* neutrino masses or dynamical dark energy.

The main idea behind this approach is to be able to separate the effects of different assumptions on parameter extraction. In order to say that the ΛCDM model is in tension with current measurements, one must be sure that this tension is a failure of the model to describe the late-time acceleration, and is not due to some of our assumptions about structure formation, or about reionization, for instance. We will therefore adopt a simple ΛCDM model for the late homogeneous cosmology.

With the recent release of Planck temperature anisotropies map, it is possible to apply these ideas and see how it affects the analysis. Indeed, there are some tensions between the current Planck analysis [11, 70] and the results of other cosmological probes: as it has for instance been pointed out in [71], current existing constraints on the value of H_0 disagree with each other. One example is the discrepancy between the Planck result of the Hubble parameter: $H_0 = 67.3 \pm 1.2$ km s^{-1} Mpc^{-1}, and the Hubble Space telescope measurement: $H_0 = 73.8 \pm 2.4$ km s^{-1} Mpc^{-1}, at 1σ. Although only a 2σ tension, it could be seen as a sign of something wrong in the theoretical assumptions. It has been proposed in [69] that this tension could be partially lifted by taking into account the local gravitational potential at the position of the observer in the HST measurement, but this effect is not enough to sufficiently relieve the tension. Another mismatch exists between the value of σ_8 as probed by the weak lensing of the CMB or through the Sunyaev-Zel'dovich cluster count identified with Planck - it may advocate for neutrino mass although this is not favored by Planck temperature anisotropies spectrum alone. A recent proposition states that these anomalies are alleviated when analysing in a different way the 217 GHz map [72]. We are assuming here that the standard, publicly available likelihood is correct.

The idea of the paper is to see if one can reduce the observed tensions, by assuming only a minimal number of hypotheses. It is interesting to check whether one can make all current experiments agree with each other, by performing first an "agnostic" early universe analysis, and then assuming ΛCDM for the late-time homogeneous evolution. At the very least, it would show the importance of the missing assumptions, especially in the case of studying extended standard models.

In section 3.2, we will present an improved "agnostic" analysis method, and discuss its similarities and differences with the standard analyses. In section 3.3, we will show how to take one further step and derive constraints on a standard ΛCDM model coming from different homogeneous probes. We will show and discuss the results in section 3.4 and conclude in section 3.5.

3.2 Agnostic Study

The main idea on which the so-called "agnostic" study [1] relies on is the realisation that, at the level of the primary (unlensed) power spectrum, the late-time cosmological parameters of some standard scenarios have a clear effect. They simply globally rescale in amplitude ($C_\ell \rightarrow \alpha C_\ell$), or shift the position of the peaks through a rescaling of the multipoles ($C_\ell \rightarrow C_{\beta\ell}$). In the Standard Model, the amplitude is controlled by a combination of the initial amplitude of perturbations A_s and the optical depth at reionization τ_{reio}, while the rescaling of the multipoles is affected by the angular diameter distance at decoupling d_A^{rec} - as far as large multipoles (*i.e.* $\ell \geq 50$) are concerned. Thus, by removing the low-multipole from the analysis, and marginalizing over these two quantities, one should in principle be able to extract constraints on early cosmology parameters, independently on our assumptions for the late evolution.

By contrast, a standard analysis of the Standard Model would constrain the following set of parameters:

$$\{\omega_{\mathrm{b}}, \omega_{\mathrm{cdm}}, A_s, n_s, \tau_{\mathrm{reio}}, d_A^{\mathrm{rec}}\}$$

Where ω_{b} and ω_{cdm} designate respectively the physical baryon and cold dark matter density, A_s and n_s the amplitude and tilt of the initial scalar perturbations, and d_A^{rec} the angular diameter distance at recombination. On the other hand, by performing an "agnostic" analysis, hence removing low multipoles and marginalizing over the parameters controlling the rescaling in amplitude and multipole, one would actually constrain:

$$\{\omega_{\mathrm{b}}, \omega_{\mathrm{cdm}}, e^{-2\tau_{\mathrm{reio}}} A_s, n_s, d_A^{\mathrm{rec}}\}$$

The relevant extracted information would then lie in the marginalized posterior distribution of the remaining, early parameters: $\omega_{\mathrm{b}}, \omega_{\mathrm{cdm}}$ and n_s.

Note that this discussion is also valid for extensions of the Standard Model where only the late evolution is different (*e.g.* with spatial curvature, non-zero neutrino mass, dynamical Dark Energy, but not for models with free N_{eff}, varying constants, or Lorentz-violating dark energy).

Since one observes in reality lensed anisotropies, it is crucial to treat the effect of lensing on the CMB photons in the same agnostic way. In the standard analysis, the lensing potential is generated by the same initial power spectrum amplitude and tilt than the one generating the perturbations. However, this assumes that ΛCDM is valid for the

late-homogeneous evolution, and this assumption should not be used here.

If one wants to be as general as possible, the lensing power spectrum can have any shape and amplitude, and should not be the same as the one generated by A_s and n_s. In [1], two parameters A_{lp} and n_{lp} were introduced for the lensing potential, that simply modified the shape of the original spectrum. Hence, $A_{\mathrm{lp}} = 1$ and $n_{\mathrm{lp}} = 0$ correspond there to the standard amount of lensing generated by the underlying power spectrum in a ΛCDM universe. In this parametrisation, the meaning of these value changes from one point in parameter space to the other, because they are defined with respect to the initial power spectrum.

Instead, in this paper, we reformulate the approach, and we use these two parameters A_{lp} and n_{lp} to define, on their own, respectively the amplitude and the tilt of the lensing potential, and allow to marginalise over them. In this way, if they are equal to A_s and n_s, respectively, it will mean that the lensing is caused by a late-time ΛCDM universe. By allowing them to vary freely, we do not impose this prior knowledge. We moreover set the pivot scale of this lensing potential to coincide with the maximum of the lensing potential, which is roughly $k = 0.012/\mathrm{Mpc}$ from Planck data.

Finally, we set the effective number of relativistic species N_{eff} to 2.03351, and we take one massive neutrino of a total mass of 0.06 eV, as specified in the base analysis of the Planck study. These values impact the prediction of H_0 by 0.6 km s^{-1} Mpc^{-1} - a significant change considering Planck error bars on the Hubble rate.

We run the Markov Chain Monte Carlo code Monte Python[1] on Planck data, in which we only take the high-ℓ likelihood (starting at $\ell = 50$). We discard the information coming from the WMAP polarisation data, and from the low-ℓ likelihood. We also discard the lensing reconstruction likelihood to avoid making hypotheses on structure formation.

Note also that, due to the way the Planck likelihood is coded, it was not possible to use only the multipoles above 100, as was advocated in [1]. The error introduced by not taking the same starting multipole is readily estimated from the previous analysis. Indeed, Planck and WMAP have the same sensitivity around these multipoles, so one expects the contamination from the late-time cosmology to be of the same order than for WMAP. From table 1 in this reference, one can estimate the similarity between the distributions A (starting at $\ell = 100$), B (starting at $\ell = 60$) and C (taking all multipoles), for each parameter. In average, we see that the distributions B overlap with 85% of A, whereas the distributions C overlap with 60% of A. It is then clear that starting the analysis at $\ell = 50$, while not removing the entire contamination from the late-time cosmology, manages nonetheless to suppress a significant part of it.

---

[1]http://montepython.net

The final set of varied parameters is then

$$\{\omega_{\mathrm{b}}, \omega_{\mathrm{cdm}}, e^{-2\tau_{\mathrm{reio}}} A_s, n_s, d_A^{\mathrm{rec}}, A_{\mathrm{lp}}, n_{\mathrm{lp}}\}.$$

Through this analysis, one can obtain model-independent information on the values of $\omega_{\mathrm{b}}, \omega_{\mathrm{cdm}}$ and n_s.

It has to be noted that a similar approach was performed in the standard analysis [11], with only the lensing amplitude being varied (parameter A_{l} in this paper), but not the lensing tilt. This was simply done to highlight the fact that the CMB alone preferred a value slightly higher than 1 for this parameter. The test was done both with A_{l} defined with respect to the initial power spectrum, and with A_{l} defined on its own[2]. These results were however not further investigated.

3.3 Constraining the late time homogeneous evolution

We have seen in the previous section how to obtain in principle a constraint on early cosmological parameters, with their posterior distribution and correlations, in a model-independent way. We want now to push the analysis further, and utilize this knowledge to determine whether or not ΛCDM is a good model to explain the homogeneous evolution of the late-time universe.

The idea is to choose a model for the late-time evolution, namely the cosmological constant, and test its merit to explain the accelerated expansion. By basing our analysis on the "agnostic" study, we have indeed the possibility to test this single assumption, without involving any other one. This approach thus differs from the standard one by the fact that we test separately the hypotheses of the standard model, instead of evaluating the general merit of all of them considered at the same time.

We will restrict ourselves to a flat universe. Therefore, since we only look at the background evolution, the only relevant parameters are:

$$\{h, \Omega_\Lambda\} \tag{3.1}$$

or other ones related to these two through the budget equation, such as Ω_m and H_0. We then test this cosmological set of parameters against the following existing data on homogeneous cosmology:

1. *Direct Measurement*: In [73], the authors provide an updated measurement of

---

[2]http://www.sciops.esa.int/wikiSI/planckpla/index.php?title=File:Grid_limit68.pdf&instance=Planck_Public_PLA

supernovae, as well as its spectroscopic redshift. One can then ask the angular diameter distance from the cosmological code, compute the luminosity distance with the relation $d_L = (1+z)^2 d_A$, and compare it with the observed one. Recalling that

$$d_L(z_i) = (1+z_i) \int_0^{z_i} \frac{dz}{H(z)} = (1+z_i) \int_0^{z_i} \frac{dz}{H_0\sqrt{\Omega_m(1+z)^3 + \Omega_\Lambda}}, \qquad (3.2)$$

one would expect this probe to be sensitive both to the values of h and Ω_Λ. However, the likelihood formula uses a simple χ^2 formula for each data point, with non zero correlations between them, as well as a marginalized nuisance parameter accounting for the absolute magnitude of the measurement. This leads that only the information on Ω_Λ is extracted from this experiment. We used the data from [74] (Union2 data) in this study.

3. *BAO*: The observed Baryonic Acoustic Oscillation scale at a given redshift is given by the following ratio:

$$r_s^{\text{BAO}} = \frac{r_s^{\text{drag}}}{\left((d_A)^{2/3}(d_R)^{1/3}\right)} \qquad (3.3)$$

where r_s^{drag} is the baryon drag scale (photon and baryon are usually considered to decouple at the same time, but since there are much less baryons, they actually decouple slightly later than the photons (around $z = 1000$). This period where they are still in equilibrium with the remaining photons is called the drag epoch, and the drag scale thus marks the end of this epoch). The baryon drag scale is determined by the agnostic analysis (it is followed as a derived parameter), with an accuracy better than 1%.

$d_A(z_{\text{survey}})$ and $d_R(z_{\text{survey}}) = z_{\text{survey}}/h(z_{\text{survey}})$ are respectively the angular diameter and radial distances, measured at the redshfit of each galaxy. The denominator consists of the geometric mean of these two quantities, that both vary strongly with h and Ω_Λ. The BAO likelihood is then simply built as a χ^2 formula on every measured point. The data used comes from 6dFGRS [75], SDSS-II [76] (Data Release 7),and BOSS [77] (Data Release DR9).

The standard analysis of the BAO data relies on computing the baryon drag scale, as well as angular and radial distances at a given redshift, for each point in the parameter space during the parameter extraction. We adapted this method to consider the baryon drag scale as a measured quantity, coming from the agnostic study, with a best-fit and an error. We add both the measurement error from the BAO data and this measurement error from the agnostic study in quadrature, and keep the simple χ^2 formula. It has to be noted that the baryon drag scale is measured with a precision of 0.5%, so the error is dominated by the BAO error.

4. *Time Delay*: Quasar Time-Delay measurements probe cosmological parameters

through the time delay between different images of gravitationally strongly lensed quasars. The chosen quasars have a highly intrinsic variable light curve, which is then observed coming from separate positions, and thus having travelled through different path. The time-delay between the different images accounts for differences in the path, but also from the different Shapiro delays induced by the lensing galaxy (for an in-depth explanation of the measurement, see [78]). This time-delay distance $D_{\Delta t}$ is defined as follows:

$$D_{\Delta t} = (1 + z_d)\frac{D_d D_s}{D_{ds}}, \tag{3.4}$$

where D_d is the angular diameter distance to the lens, z_d the redshift of the lens, D_s the angular diameter distance to the source and D_{ds} the angular diameter distance between source and lens. The data we used for this study is taken from [79] and [80], with a shifted log normal distribution.

Finally, we have to take into account the information coming from the early parameter analysis. To do this, we can realise that this first analysis gives the posterior distribution for ω_b, ω_{cdm} and d_A^{rec}. As seen previously, d_A^{rec} is a function of $\{h, \Omega_\Lambda\}$, and $\omega_b + \omega_{cdm} = \omega_m = \frac{1 - \Omega_\Lambda}{h^2}$, for a flat universe. As mentioned previously, since ω_b is measured to a much greater precision than ω_{cdm}, and since only the sum of the two is involved in the late-time evolution, we fixed ω_b to its best-fit value.

We thus use the 2-dimensional posterior distribution of d_A^{rec} and ω_{cdm} found with an "agnostic" analysis to define a multi-Gaussian likelihood, which seems a reasonable choice considering Fig 3.1. As these two parameters are found to be correlated in this first study, it is crucial that our likelihood takes into account this degeneracy. If one did not take into account this correlation, one would have lost a factor of two in the marginalised error bars. In the next section, this last experiment will be referred to as *Planck (this work)*. It corresponds then to the constraint coming from Planck data alone, which will be compared with the aforementioned probes of homogeneous cosmology.

3.4 Results

3.4.1 "Agnostic" early universe results

We used for this study the public Boltzmann code CLASS [24]. After running MCMC chains with MONTE PYTHON[3], with a modified Metropolis-Hastings algorithm [46], we obtain the best-fit, mean and one-sigma constraints for our "agnostic" parameters, as shown in table 3.1. In this table, we compare with the standard results based on the high-ℓ, low-ℓ Planck likelihoods as well as the WMAP polarisation. As we can see there,

---

[3]http://montepython.net

Parameters	This work	Planck Standard
$100\ \omega_b$	$2.243^{+0.038}_{-0.042}$	2.205 ± 0.028
ω_{cdm}	$0.1165^{+0.0036}_{-0.0038}$	0.1199 ± 0.0027
n_s	$0.966^{+0.011}_{-0.011}$	0.9603 ± 0.0073
d_A^{rec}	$12.8^{+0.071}_{-0.065}$	/
$10^{+9}e^{-2\tau}A_s$	$2.032^{+0.086}_{-0.093}$	/
$10^{+9}A_{lp}$	$3.513^{+0.95}_{-0.42}$	/
n_{lp}	$-0.338^{+0.74}_{-0.66}$	/

Table 3.1 – The "agnostic" analysis gives a value for $-\ln\mathcal{L}_{\min} = 3895.34$, and a minimum $\chi^2 = 7791$, to compare with $\chi^2 = 7797.91$ from the standard analysis - an expected improvement considering the two additional parameters. Note that the 1σ interval of "this work" has always an overlap with the 1σ interval of "Planck", even though the central value falls outside for both $\omega_{\rm b}$ and $\omega_{\rm cdm}$.

there are only minor shifts in central values for most of the parameters. The error bars are however degraded by around 40%.

Note that it was not possible to perform a comparison of the posterior distribution of the cosmological parameters between the agnostic approach and a standard analysis using only the high-ℓ likelihood. Indeed, this data set alone leaves unconstrained a degeneracy between A_s and $z_{\rm reio}$, leading to extremely poor convergence. It is only with the inclusion of the low-ℓ likelihood and the WMAP polarisation that convergence is reached.

Notice as well that it is not possible to compare the distribution of the parameter $10^{+9}e^{-2\tau}A_s$, even though the Planck analysis provides the distribution for the parameters that appear in this combination. This is due to the fact that there is a flat prior on this specific combination of parameters, whereas in Planck analysis, the flat prior is set on τ and $\ln(10^{10}A_s)$.

3.4.2 Late time universe results

The most important differences with respect to the standard analysis start to appear when analysing the late-time universe with minimal assumptions.

The mean values for the H_0 parameter, for all the different experiments, are summarised in table 3.2. One can notice on the first hand that, in addition to a wider error bar on the Hubble parameter, the central value is significantly different than the one from the published Planck analysis. The central value and marginalised posterior distribution at 1σ are $H_0 = 69.8 \pm 1.9 {\rm km\ s^{-1}\ Mpc^{-1}}$, to contrast with $H_0 = 67.3 \pm 1.2 {\rm km\ s^{-1}\ Mpc^{-1}}$. Note first that the two values are in agreement at the level of 1σ, and that the discrepancy in both central value and marginalised width can be attributed to *i)* the contaminating

eters. We then utilized this knowledge to constrain the parameter space of $\{H_0, \Omega_m\}$, and compared this analysis with other experimental probes of the homogeneous late-time universe.

We showed that, in contrast with the standard analysis, this study reconciles the local measurement of H_0 and Planck data, without sacrificing the agreement with the other data-sets.

Our analysis demonstrated that some of the less often tested assumptions behind the Standard Model of Cosmology, like the reionization history and the growth of structures, can play an important role in the determination of the posterior distribution of its parameters. It seems striking that the effects described here are on par with existing propositions for evidence for new physics in Planck data.

It is at the best of our knowledge not possible to further refine and pinpoint which assumption in particular is biasing the most the standard analysis in the direction of lower H_0 values. Indeed, to achieve this goal, one would need to compare this "agnostic" analysis of the high-ℓ likelihood with a standard analysis of the same. However, as discussed above, the presence of a large degeneracy between A_s and z_{reio} prevents the convergence of the parameter extraction in this case.

It is not our point to suggest that this method is a better way to reconcile the data-sets than any other proposition, but rather to highlight the importance of testing as thoroughly as possible every underlying assumptions of our standard model of cosmology.

This only further illustrates the fact that the Planck satellite opened the doors of a precision era in our field. Such effects were previously considered unimportant, because of the lack of resolution of past experiments. With access to such a high sensitivity experiment, a better understanding of the underlying assumptions behind our Standard Model, notably the role of reionization and structure formation, seems to be in order.

4 Annihilating Dark Matter

Foreword

The two following chapters are focused on constraining the nature of DM from cosmology. It has to be seen as a complementary approach from the usual three competitors: direct detection, indirect detection, and collider searches.

In a sense, this approach is closer to indirect detection, since it merely consists in trying to find any unusual signature on cosmological probes that would indicate a non-standard property of DM. The distinct advantage of this approach over collider searches or direct detection is that it can be more model-independent.

The study presented in this chapter addresses a simple question: could a DM candidate annihilating into SM particles produce a sufficiently strong emission to account for the entire reionization of the universe? This would effectively solve two problems at once. On the one hand, reionization is one of the less understood aspects of the SM of cosmology: it corresponds to a period where stars are supposed to reionize the Inter-Galactic Medium (IGM), but is modelled by a simple empirical formula. On the other hand, many models of DM from particle physics predict a non-zero annihilation rate to SM particles. It could then be possible to explain reionization completely or partially as a signal of annihilating DM, and derive as a consequence some constraints on the nature of the DM candidate.

Knowing that DM clusters and forms halos, our attempt was to verify whether the bounds inferred from halo emission are stronger or not than the diffuse signal coming from background emission. By letting the halo parameters vary freely, we checked that except for very sharp halo profiles, the effect from the annihilation from within halos is less strong than the one from the mean background density. It is worth mentioning that the halo profiles are still an open question in the field, and that there are two orders of magnitude difference in the predicted density in the center of the halos, depending on the model. Sharp profiles are therefore not excluded so far by the data.

The reionization computation was implemented numerically by modifying two existing codes, RECFAST and HYREC. Assuming that all reionization is performed by DM annihilation, we performed a parameter extraction against WMAP and SPT data. The resulting reionization is however very smooth in redshift, which is in tension with the Gunn-Peterson observation, stating that the level of gas ionization changed abruptly around a redshift of six. This represents also an obstacle for the standard reionization scenario, but by deciding for a hybrid reionization process, it was possible to accommodate for both observations. We show in fig. 4.11 the three different models, and highlight in fig. 4.14 the consequence of this extraction on the mass/cross-section plane. It covers the three different profiles that we considered in this study, which characterise our uncertainty. The horizontal blue line represents the thermal cross-section for the WIMP to have the proper abundance. If we assume a realistic prior on the IGM temperature (green lines), we notice that cosmology excludes DM masses below $10\,\mathrm{GeV}$ to $1\,\mathrm{TeV}$, depending on the halo model.

Finally, it is worth mentioning that the annihilation presented here is assumed to have no impact on the gravitational behaviour of CDM. As will be discussed in further details in chapter 5, where only the gravitational effect will be taken into account, it is subdominant compared to the effect on reionization.

CMB photons shedding light on dark matter

Gaëlle Giesen, Julien Lesgourgues, Benjamin Audren, Yacine Ali-Haïmoud

Abstract: The annihilation or decay of Dark Matter (DM) particles could affect the thermal history of the universe and leave an observable signature in Cosmic Microwave Background (CMB) anisotropies. We update constraints on the annihilation rate of DM particles in the smooth cosmological background, using WMAP7 and recent small-scale CMB data. With a systematic analysis based on the Press-Schechter formalism, we also show that DM annihilation in halos at small redshift may explain entirely the reionization patterns observed in the CMB, under reasonable assumptions concerning the concentration and formation redshift of halos. We find that a mixed reionization model based on DM annihilation in halos as well as star formation at a redshift z $\simeq$ 6.5 could simultaneously account for CMB observations and satisfy constraints inferred from the Gunn-Peterson effect. However, these models tend to reheat the inter-galactic medium (IGM) well above observational bounds: by including a realistic prior on the IGM temperature at low redshift, we find stronger cosmological bounds on the annihilation cross-section than with the CMB alone.

4.1 Introduction

In the minimal ΛCDM model, the CMB has very little to say about Dark Matter (DM), apart from a measurement of the relic abundance parameter $\Omega_{DM}h^2$. However, there is a chance that DM could leave another signature in the CMB. In the case of annihilating DM, if the ratio of the annihilation cross section over the mass is not too small, annihilation products could contribute to the ionization of the thermal bath, and affect the history of recombination and reionization. This has already been discussed in detail in several references including [81, 82, 83, 84, 85, 86, 87, 88, 89, 90, 91, 92]. In the case of decaying dark matter, similar effects could take place if the particle lifetime is not too large [93, 94, 95, 96, 97].

In a detailed study of these mechanisms, assumptions concerning the nature of dark matter are of course crucial. Different DM particles may annihilate or decay in different channels (into hadrons, leptons, gauge bosons, etc.). The produced particles can themselves decay in several steps, until only stable particles like electrons, photons and neutrinos remain. While the energy contained in neutrinos is lost for the cosmic plasma, other decay products can contribute to the ionization and heating of this plasma. The authors of [87] computed $f(z)$, the redshift-dependent fraction of the energy produced by annihilations that contributes to the ionization and heating of the plasma, for several WIMP models. Similar calculations could be carried on any type of annihilating or

decaying DM particles. In a cosmological analysis like that presented in this paper, we don't need to refer specifically to a given DM particle, and we may incorporate all model-dependent particle physics assumptions in the unknown fraction $f(z)$.

In this work, we revisit the impact on the CMB of annihilating DM. We will not introduce any new physical ingredients, neither from the point of view of particle physics, nor from that of structure formation models. However, we will present some new generic parametrizations of the relevant phenomena, in order to perform a systematic comparison of various models to recent CMB data sets. This will allow us to tighten some of the bounds presented previously in the literature.

In section 2, we summarize the impact of DM annihilation on recombination, and explain how we took it into account by modifying the public Boltzmann code CLASS. This code can simulate recombination with either of the two public codes RECFAST and HYREC. We double-checked our results by modifying the two algorithms. We show that they give the same results, but for non-trivial models like those assumed in section 4, only HYREC remains numerically stable.

In section 3, we focus on the effects of annihilation in the smooth DM background distribution. We find similar but slightly stronger bounds than in recent studies, thanks to our updated CMB data set. With a generic parametrization of the redshift-dependence of the function accounting for the fraction of energy released to the gas, we confirm that current CMB data is not sensitive to this dependence.

In section 4, we consider the additional effect of enhanced DM annihilation in halos at small redshifts. This effect has been previously discussed in several references including [83, 84, 85, 88, 91, 92]. Some of these works suggest that it could account for a significant fraction (if not the totality) of the reionization of the universe at low redshift. We derive an approximate but rather generic parametrization of this effect, and carry on the first systematic parameter inference using current CMB data in a model with reionization from annihilation. We also confront to the data a mixed model, with reionization explained both by DM annihilation and star formation, and discuss the relevance of this model for explaining simultaneously CMB data and Gunn-Peterson bounds. Finally, we show that these models tend to reheat the inter-galactic medium (IGM) well above observational bounds; by including a realistic prior on the IGM temperature at low redshift and allowing most of the reionization to be due to star formation, we find stronger cosmological bounds on the annihilation cross-section than with the CMB alone.

Our general conclusions and future directions of research are outlined in section 5.

4.2 Equations of recombination with Dark Matter annihilation

4.2.1 Standard recombination

Before discussing the impact of DM annihilation (or alternatively dark matter decay) on the recombination history, we first briefly review the standard recombination model. We start by describing the simple three-level atom model of Peebles [98, 99] and then discuss the subsequent improvements of this model.

In what follows we shall assume that helium has entirely recombined (which is indeed the case for all redshifts of interest) and only deal with hydrogen recombination. We denote n_e the number density of free electrons, n_H the total number density of hydrogen (in ionized and atomic forms), $x_e = \frac{n_e}{n_H}$ the free electron fraction and T_M (resp. T_r) the matter (resp. photon) temperature.

The effective three-level atom (TLA) model

It is well known that direct recombinations to the ground state are highly inefficient: if a hydrogen atom forms directly in its ground state, it emits a photon which is going to immediately ionize an other atom, leaving the overall free electron fraction unchanged. The basic idea of Peebles' "case B recombination" is that efficient recombination only takes place when the electron gets first captured into an excited state $n \geq 2$, from which it cascades down to $n = 2$. The newly formed atom may then eventually reach the ground state, either by emitting a Lyman-α photon from $2p$, or by the $2s \to 1s$ two-photon process. The Lyman-α line being very optically thick, the net rate of $2p \to 1s$ transitions is, to a first approximation, the rate at which Lyman-α photons redshift across the resonance. At early times ($z \gtrsim 900$), the net rate of transitions from the $n = 2$ state to the ground state is much smaller than the rate at which excited atoms are photoionized by CMB photons, and the slow $2 \to 1$ transitions constitute the bottleneck of the recombination process. At late times ($z \lesssim 900$), the intensity of the radiation field drops, and atoms that do recombine to an excited state almost certainly reach the ground state; during this period the new bottleneck is the rate at which free electrons and protons can encounter each other and recombine.

To correctly describe recombination, accounting for the effects mentioned above, Peebles introduced the pre-factor C defined as

$$C = \frac{1 + K_H \Lambda_H n_H (1 - x_e)}{1 + K_H (\Lambda_H + \beta_H) n_H (1 - x_e)}, \tag{4.1}$$

where $\Lambda_H = 8.22458 \text{ s}^{-1}$ is the decay rate of the $2s$ level, $K_H = \frac{\lambda_{\text{Ly}\alpha}^3}{8\pi H(z)}$ accounts for the

cosmological redshifting of Lyman-α photons[1], and β_H is the effective photoionization rate from $n = 2$ (per atom in the $2s$ state). C represents the probability for an electron in the $n = 2$ state to get to the ground state before being ionized. The evolution equation for the free-electron fraction is then given by

$$\frac{dx_e}{dz} = \frac{1}{(1+z)H}C\left[\alpha_H x_e^2 n_H - \beta_H(1-x_e)e^{-\frac{h\nu_\alpha}{k_b T_r}}\right],\tag{4.2}$$

where α_H is the case-B recombination coefficient and ν_α is the Lyman-α frequency. Because the effective recombination rate per free electron $C\alpha_H x_e n_H$ is always much smaller than the Hubble rate (due to the two bottlenecks mentioned above), primordial recombination proceeds much slower than in Saha equilibrium.

In addition, the matter temperature is determined from the Compton evolution equation:

$$\frac{dT_M}{dz} = \frac{1}{(1+z)H}\frac{8\sigma_T a_r T_r^4}{3m_e c}\frac{x_e}{1+f_{He}+x_e}(T_M - T_r) + \frac{2T_M}{1+z}.\tag{4.3}$$

$$= \frac{1}{(1+z)}\left[2T_M + \gamma(T_M - T_r)\right],\tag{4.4}$$

where we have defined the dimensionless parameter

$$\gamma \equiv \frac{8\sigma_T a_r T_r^4}{3Hm_e c}\frac{x_e}{1+f_{He}+x_e},$$

where σ_T is the Thomson cross-section, a_r the radiation constant, m_e the electron mass, c the speed of light and f_{He} the fraction of helium by number of nuclei. When $\gamma \gg 1$, the matter temperature is locked to the radiation temperature by Compton heating, $T_M \approx T_r \propto (1+z)$; it decays adiabatically as $T_M \propto (1+z)^2$ when $\gamma \ll 1$.

Beyond the TLA model

With the prospect of upcoming high-precision data from the Planck satellite, several groups have revisited the simple TLA model presented above and introduced important corrections. Here we use the codes RECFAST [100] and HYREC [101] which implement these corrections, approximately for the former and exactly for the latter. The corrections are of two types:

• Highly excited states of hydrogen are not in Boltzmann equilibrium with each other, and one must account for all bound-bound and bound-free transitions involving them, including stimulated transitions. The original RECFAST code accounted for these transitions approximately by multiplying the case-B recombination coefficient (and effective photoionization rate) by a "fudge factor" $F = 1.14$, fitted to reproduce multilevel computations [100]. The original computation of Seager et al assumed that angular momentum

---

[1] $[K_H n_H (1 - x_e)]^{-1}$ is the rate of escape of Lyman-α per atom in the $2s$ state

substates were in statistical equilibrium. This approximation, however, was shown not to be accurate enough [102, 103]. The latest version of RECFAST[2] attempts to account for these more detailed high-n computations approximately by using a new fudge factor $F = 1.125$.

It turns out that the effect of highly-excited states can be <u>exactly</u> and efficiently accounted for by generalizing the case-B coefficient to a non-zero CMB temperature [104, 105]. The code HYREC is using precomputed effective recombination coefficients in an effective few-level atom model, at virtually no speed cost compared to the TLA model, and with the advantage of being exact.

• Being the recombination bottleneck at early times, the Lyman-α escape and two-photon $2s \to 1s$ decays need to be modeled very precisely. Several radiative transfer effects were shown to be important for high-accuracy predictions of CMB anisotropies (see for example Refs. [106, 107, 108, 109, 103] and references therein). Detailed codes such as HYREC and COSMOREC [103] account for all important radiative transfer effects exactly, by evolving the radiation field numerically. This part of the calculation is heavier computationally, but efficient implementations render the runtime for the recombination calculation comparable with the runtime of the Boltzmann code itself. RECFAST accounts for radiative transfer effects by adding a correction function to the recombination rate $\dot{x}_e|_{\mathrm{corr}}$, fitted to reproduce the detailed codes for cosmologies close to the current best-fit value.

4.2.2 Parametrization of Dark Matter annihilation

We wish to express the rate at which the energy released by DM annihilations is injected in the thermal bath. In the next subsection, we will summarize how this energy is used and in which proportions.

We can write the energy injected into the plasma per unit of volume and time as the product of the number of DM particle pairs n_{pairs}, the annihilation probability per unit of time P_{ann}, the released energy per annihilation E_{ann}, and the redshift-dependent fraction of released energy $f(z)$ absorbed by the gas

$$\frac{dE}{dV dt}\bigg|_{\mathrm{DM}}(z) = n_{pairs} \cdot P_{\mathrm{ann}} \cdot E_{\mathrm{ann}} \cdot f(z) = \frac{n_{\mathrm{DM}}}{2} \cdot \langle \sigma v \rangle \cdot n_{\mathrm{DM}} \cdot 2 m_{\mathrm{DM}} c^2 \cdot f(z)$$

$$= \rho_{\mathrm{c}}^2 c^2 \Omega_{\mathrm{DM}}^2 (1+z)^6 f(z) \frac{\langle \sigma v \rangle}{m_{\mathrm{DM}}}. \tag{4.5}$$

In Eq. (4.5), σ is the annihilation cross-section, v is the relative velocity of DM particles, $\langle \sigma v \rangle$ is the average of $\sigma \times v$ over the velocity distribution, m_{DM} the mass of the DM

---

[2]This work was completed using RECFAST v1.5.1. The next version 1.5.2, including new fudge factors leading to very good agreement with HyRec, was released after the submission of this paper.

particle, $\rho_{\rm c} = \frac{3H_0^2}{8\pi G}$ the critical density of the universe today (with H_0 the Hubble constant today), and $\Omega_{\rm DM}$ the Dark Matter abundance today relative to the critical density. In the case where DM consists of Dirac Fermions, there should be an extra factor $1/2$ in the last two equalities (since only half of the pairs are made of one particle and one anti-particle). If this is the case, we can decide to absorb this factor in a redefinition of $f(z)$. Then, for a given cosmological evolution, all the model-dependent part of the energy injection rate can be parametrized by the following function of redshift,

$$p_{\rm ann}(z) = f(z)\frac{\langle \sigma v \rangle}{m_{\rm DM}}. \tag{4.6}$$

The authors of [87] computed $f(z)$ for several WIMP models. They found that $f(z)$ is a smoothly decreasing function, lying in the range from 0.2 to 0.9 at redshift 2500 (depending on the WIMP mass and dominant annihilation channel), and decreasing by a factor 2 to 5 at small redshift. Similar calculations could be carried for any type of annihilating or decaying DM particles.

4.2.3 Effects of Dark Matter annihilation on the thermal history of the universe

The energy injected by DM annihilation has three effects: ionizing the plasma, exciting hydrogen atoms , and heating the plasma [110, 86]. A fraction of the atoms excited by the second mechanism will be subsequently ionized by CMB photons. Hence, the first two effects (illustrated in Figure 4.1) have a direct impact on the free electron fraction, and the last one on the matter temperature.
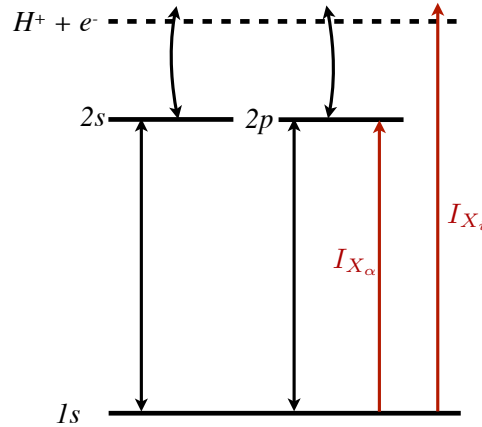
Figure 4.1 – Illustration of the impact of DM annihilation on Peeble's "case B recombination" model. The upper dashed line correspond to the ionized state, with separate proton and electron. The two red arrows correspond to the two cases considered in this paper for the DM energy injection. I_{X_i} is the rate of direct ionization per redshift interval, while I_{X_α} is the transition rate from the ground state, both due to DM annihilation only.

For simplicity, let us introduce the basic equations describing the three effects of DM annihilation using the on-the-spot approximation, which supposes that all interactions between the decay products of DM annihilation and the plasma take place locally, on a time scale negligible with respect to the expansion time scale.

Ionization of the plasma. In the on-the-spot approximation, if $\chi_i(z)$ denotes the fraction of the injected energy going into ionization, and E_i the average ionization energy per baryon, the number of direct ionizations per interval of redshift dz reads

$$I_{X_i}(z) = -\frac{\chi_i(z)}{(1+z)\,H(z)\,n_H(z)\,E_i}\,\frac{dE}{dV dt}\bigg|_{\text{DM}}, \tag{4.7}$$

where we used $dz/dt = -(1+z)H$. Shull and Van Steenberg found that for a neutral gas, approximately $1/3$ of the energy goes into ionization [111]. For an ionized gas, none of the energy can be used for ionization. Thus, for a partially ionized gas, Chen and Kamionkowski proposed to approximate χ_i by $(1-x_e)/3$ [93]. The fact that $\chi_i \propto (1-x_e)$ makes physical sense, since the ionization rate must be proportional to the abundance of neutral hydrogen.

Excitation of hydrogen. The rate of collisional excitation of hydrogen (1s→2p and 1s→2s transitions, etc.) due to DM annihilation is similar to that of direct ionization, with E_i replaced by the Lyman-α energy E_α and $\chi_i(z)$ by the fraction $\chi_\alpha(z)$ of the injected energy going into excitations. Once a given atom is in the $n = 2$ state, it has a probability $(1 - C(z))$ to be ionized by CMB photons. Thus, the net ionization rate per redshift interval dz due to collisional excitations by DM annihilation products reads

$$I_{X_\alpha}(z) = -\frac{(1 - C(z))\,\chi_\alpha(z)}{(1+z)\,H(z)\,n_H(z)\,E_\alpha}\,\frac{dE}{dV dt}\bigg|_{\text{DM}}. \tag{4.8}$$

Chen and Kamionkowski showed that in first approximation one may assume $\chi_i = \chi_\alpha = (1 - x_e)/3$. Note that this process is subdominant with respect to the direct ionization of the plasma.

Heating of the plasma. Finally, DM matter annihilation heats the plasma at a rate (per unit of time)

$$\frac{dT_{\text{M}}}{dt}\bigg|_{\text{DM}} = \frac{2\chi_{\text{h}}}{3k_b n_H(1 + f_{He} + x_e)}\,\frac{dE}{dV dt}\bigg|_{\text{DM}}, \tag{4.9}$$

with $\chi_{\text{h}} = 1 - \chi_i - \chi_\alpha = (1 + 2x_e)/3$ the remaining fraction of the total injected energy.

The range of validity of these equations extends beyond the on-the-spot approximation, provided that the ratio $\frac{dE}{dV dt}\big|_{\text{DM}}$ stands for the effective injection rate at redshift z coming

from DM annihilation at all redhsifts $z' \geq z$, taking into account energy transfer and absorption processes between z' and z. The function $f(z)$ was actually computed by [87, 112, 91] beyond the on-the-spot approximation.

4.2.4   Recombination equations with DM annihilation

We can now write the modifications needed for each of the two recombination codes RECFAST and HYREC, both implemented in the Boltzmann code CLASS[3] [23, 24] used throughout this work. The point of using two different codes is to compare the results and check that our approach for including annihilation effects is robust and consistent. In addition, we will see that in some of the cases discussed below, the second code is more stable numerically and allows to explore more general models.

Given equations (4.5 – 4.9), implementing DM annihilation in the two codes only requires to add two new terms proportional to $p_{\text{ann}}(z)$ in the basic equations for hydrogen recombination and matter temperature:

$$\frac{dx_e}{dz} = \frac{dx_e}{dz}\bigg|_{\text{st}} - \frac{\rho_c^2 c^2 \Omega_{\text{DM}}^2 (1+z)^5}{H(z)} \left[\frac{1 - x_e(z)}{3\,n_H(z)} p_{\text{ann}}(z) \left(\frac{1}{E_i} + \frac{1 - C(z)}{E_\alpha} \right) \right], \quad (4.10)$$

$$\frac{dT_{\text{M}}}{dz} = \frac{dT_{\text{M}}}{dz}\bigg|_{\text{st}} - \frac{\rho_c^2 c^2 \Omega_{\text{DM}}^2 (1+z)^5}{H(z)} \left[\frac{2}{3k_b} \frac{1 + 2x_e(z)}{3\,n_H(z)} \frac{1}{1 + f_{He} + x_e(z)} p_{\text{ann}}(z) \right], \quad (4.11)$$

where the subscript "st" stands for the standard rates, given by eqs (4.2,4.3) for case B recombination. These equations neglect the possibility that a fraction of the energy released by DM annihilation would serve for helium ionization. As in ref. [89], we checked that such a refinement would have a negligible impact on the CMB spectra.

In HYREC, it is also necessary to write separately the impact of DM annihilation in the equations accounting for approximation schemes, like the steady-state approximation for the matter temperature at early times. In appendix B, we write explicitly our modified HYREC equations.

In section 4.4, we will introduce extra modifications allowing to account for DM annihilation at small redshift beyond the on-the-spot approximation. Our modification to CLASS, including those in RECFAST and HYREC, will be part of the next public distribution 1.5 of the code.

---

[3]http://class-code.net

4.3 Dark Matter annihilation before structure formation and reionization

In this section, we wish to better understand the impact of DM annihilation on the CMB at relatively high redshift, i.e. roughly for $z \gtrsim 100$. At lower redshift, enhanced DM annihilation in non-linear structures might be responsible for additional effects that we will study separately in the next section. Since the two regimes have a rather different impact on the CMB spectra, it is legitimate to split the discussion in this way. DM annihilation effects on the CMB at high redshift have been thoroughly investigated by Galli et al. [86, 89, 90]. In this section, we will only update previous results, before exploring new models including halo effects in the next section.

For simplicity, we first assume in subsections 4.3.1, 4.3.2, 4.3.3 that the annihilation parameter p_{ann} is independent of redshift, as in [86, 89]. We will relax this assumption in subsection 4.3.4.

4.3.1 Annihilation effects on x_e and T_{M}

In fig. 4.2, we show the evolution of $x_e(z)$ and $T_{\mathrm{M}}(z)$ computed with either RECFAST or HYREC for four values of the annihilation parameter. We tested RECFAST and HYREC
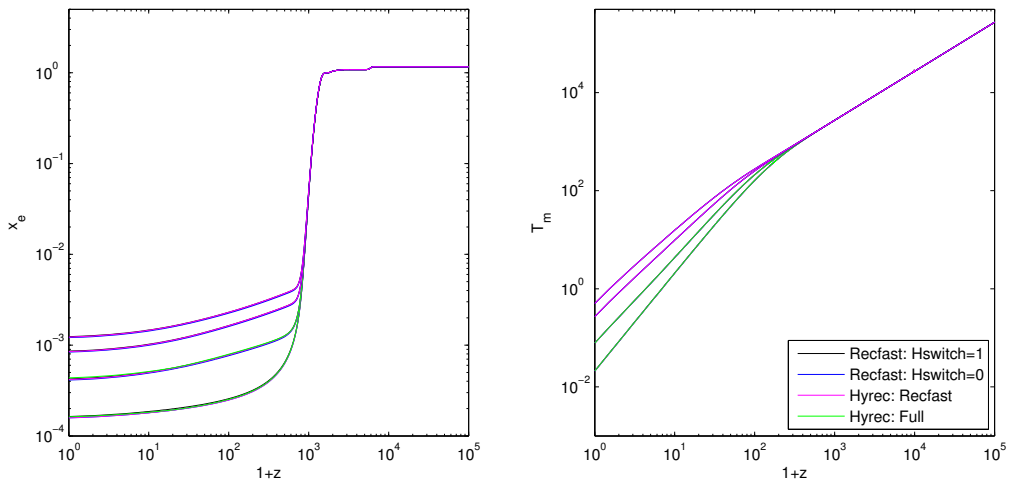
Figure 4.2 – Free electron fraction and matter temperature as a function of the redshift with, from bottom to top, $p_{\mathrm{ann}} = 0, 10^{-6}, 5 \cdot 10^{-6}$ or 10^{-5} m^{3}s^{-1}kg^{-1}. For each value of p_{ann}, we used either RECFAST or HYREC, and two different options for each of the two codes; the four results agree to better than a few percent, and the difference would be indistinguishable on the plots.

in two modes: for RECFAST, with or without taking into account the hydrogen physics effects described in [113] (using the switch `Hswitch`), and for HYREC, using the mode

RECFAST (mimicking a simplified version of RECFAST) and FULL (including a state-of-the art description of an effective multi-level hydrogen atom as well as radiative transfer near the Lyman lines). The FULL mode uses interpolation tables requiring $T_\mathrm{M} < T_r$. This is the case at all times provided that the annihilation parameter does not exceed $p_\mathrm{ann} \leq 3 \cdot 10^{-6}$ m^{3}s^{-1}kg^{-1}. In order to test HYREC/FULL above this value, we removed the condition $T_\mathrm{M} < T_r$ from the code, letting it extrapolate from the table. For all used values of p_ann, T_M never exceeds T_r by a large fraction and the extrapolation is therefore accurate.

In the results presented in fig. 4.2, we assumed a ΛCDM model without reionization. The first two small steps seen on the electron fraction curve correspond to the two helium recombinations, and bring the ratio $x_e = n_e/n_H$ down to one. The third and biggest step accounts for hydrogen recombination. As expected, the energy injected by DM annihilation inhibits recombination, and the free electron fraction freezes out at a larger value. Moreover, the matter temperature decreases more slowly after photon decoupling due to energy injection in the gas resulting from DM annihilation.

For each value of p_ann, the difference between the four algorithms is extremely small[4]. We checked that the shifts induced in the CMB power spectra are well below the sensitivity level of current CMB data sets, and lead to the same observational bounds on p_ann. This means that the four approaches can be used indifferently in the rest of this analysis. Whenever we could, we sticked to RECFAST with Hswitch on, in order to speed up the computation. We will mention below that for some models, we had to use instead HYREC with the RECFAST or FULL mode, found to be the more stable numerically. In these cases, the increase in computing time in the full parameter extraction process was less than a factor of two.

4.3.2 Effects on the CMB Power spectrum

We could expect the effect of DM annihilation to be degenerate with that of reionization, since both mechanisms increase the ionization fraction after photon decoupling, and therefore the optical depth to last scattering $\tau(z_\mathrm{dec})$. Indeed, a high ionization fraction at $z < z_\mathrm{dec}$ implies that more photons interact along the line of sight, which tends to damp temperature and polarization anisotropies on sub-Hubble scale, and to regenerate extra polarization around the Hubble scale at the time of re-scattering.

In fig. 4.3, we compare the effect of varying p_ann with that of changing the redshift of reionization, under the usual simplifying assumption of a single reionization step, such that $x_e(z)$ follows a hyperbolic tangent centered on z_reio. The two effects turn out to be rather different for reasons that are easy to understand.

---

[4]It would be even smaller using the fudge factor values of version 1.5.2 of RECFAST, that was released after the submission of this work.
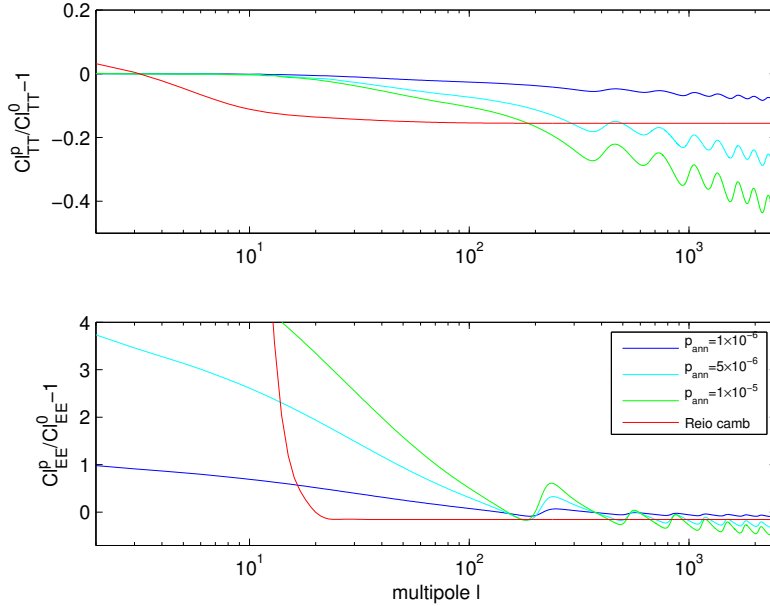
Figure 4.3 – Temperature and polarization power spectra for several models with DM annihilation or reionization, rescaled by a reference model with none of them. The curves with oscillatory patterns correspond to different values of p_{ann} (expressed in the key in $\mathrm{m^3 s^{-1} kg^{-1}}$) and no reionization. The last curve was obtained with $p_{\mathrm{ann}} = 0$ and with reionization at $z_{\mathrm{reio}} = 11$.

First, the annihilation effect is already present around $z = z_{\mathrm{dec}}$, and results in a small delay in the decoupling time (defined as the maximum of the visibility function $-\tau' e^{-\tau}$). Hence, the sound horizon at decoupling has the time to grow, while the diffusion damping scale has sufficient time to reach larger scales. The increased sound horizon results in peaks visible under larger angles or smaller l's: this shifting of the peak explains the oscillatory patterns clearly visible in fig. 4.3. The increased diffusion damping scale enhances Silk damping at large $l's$, leading to the negative high-l slope in fig. 4.3.

Second, DM annihilation increases the ionization fraction and the optical depth at all redshifts in the range $0 < z < z_{\mathrm{dec}}$. This means that some power is removed from the temperature and polarization spectrum on all scales, with a maximum suppression for $l > 200$, corresponding to modes being always inside the Hubble radius in the range $0 < z < z_{\mathrm{dec}}$. In the temperature spectrum, multipoles with $l < 200$ are less and less affected when l decreases. In the polarization spectrum, the rescattering of the photons generate extra polarization on all scales in the range $2 < l < 200$ corresponding to the variation of the Hubble scale between decoupling and today.

In contrast, reionization enhances $x_e(z)$ only at small redshift, $z \leq 10$ in our example. It does not affect recombination and does not shift the peaks: the reionization curve in

fig. 4.3 has no oscillatory patterns. Power is maximally suppressed for all scales being inside the Hubble radius at reionization, i.e. all multipoles $l > 20$. The regeneration of power in the polarization spectrum is limited to $l < 20$ for the same reason (but is very strong, since reionization enhances $x_e(z)$ much more than DM annihilation).

Hence, DM annihilation effects are clearly not degenerate with reionization effects. In order to check that the impact of p_{ann} cannot be mimicked by other parameters in the ΛCDM model, we should however run a parameter extraction code and marginalize the posterior distribution of p_{ann} over other cosmological parameters.

4.3.3 Analysis with WMAP and SPT data

We compared to observations a model described by the six free parameters of the vanilla ΛCDM model, the annihilation parameter p_{ann}, and the effective neutrino number N_{eff}, accounting *e.g.* for extra relativistic degrees of freedom. Since the South Pole Telescope (SPT) collaboration reported an intriguingly high best-fit value of N_{eff} [67], we wish to check whether p_{ann} and N_{eff} are correlated in some way, such that the effect of one parameter could be confused with that of the other. A priori, this is not impossible, because both parameters impact the amplitude of the high-l damping tail of the temperature spectrum, relatively to the amplitude of the first acoustic peaks.

We compared this model to WMAP 7-year data [60] and SPT data [67], using the code MONTE PYTHON [1], based on Monte Carlo Markhov Chains and on the Metropolis-Hastings algorithm (like COSMOMC [58], but MONTE PYTHON is interfaced with CLASS instead of CAMB [114], written in PYTHON, and has extra functionalities; this software will soon be released publicly). On top of the cosmological parameters, we vary three nuisance parameters related to the foreground contamination of the SPT data and constrained by gaussian priors, following strictly the recommendations and the software released by the SPT collaboration. All results on cosmological parameters are marginalized over these three nuisance parameters. We took flat priors on all parameters and just imposed $p_{ann} > 0$.

Our results, summarized in the first column of Table 4.1 and in the triangle plot of figure 4.4, are in excellent agreement with those of the SPT collaboration for the first seven parameters (last column of Table 3 in ref. [67]). For DM annihilation, we obtain a bound

$$p_{ann} < 0.89 \times 10^{-6} \text{m}^3/\text{s/kg} \qquad (\text{WMAP7} + \text{SPT, } 95\%\text{C.L}). \qquad (4.12)$$

We observe no correlation between p_{ann} and any other parameter in the analysis (in particular, we checked that there is no correlation at all with N_{eff}). The marginalized posterior probability for p_{ann} is displayed on figure 4.4, and shows no evidence for DM annihilation in current data. Our bound is stronger than the most recent one, presented

in ref. [89],

$$p_{\mathrm{ann}} < 2.09 \times 10^{-27} \mathrm{cm}^3/\mathrm{s}/[\mathrm{GeV}/c^2] = 1.17 \times 10^{-6} \mathrm{m}^3/\mathrm{s}/\mathrm{kg} \qquad (\mathrm{WMAP7} + \mathrm{ACT}, \ 95\% \mathrm{C.L}),$$

(4.13)

due to the inclusion of the SPT dataset. It is also stronger than that from ref. [91]. We refer the reader to ref. [89] for a discussion of derived limits on the DM annihilation cross-section, given various ansatz for the mass and released energy fraction f.
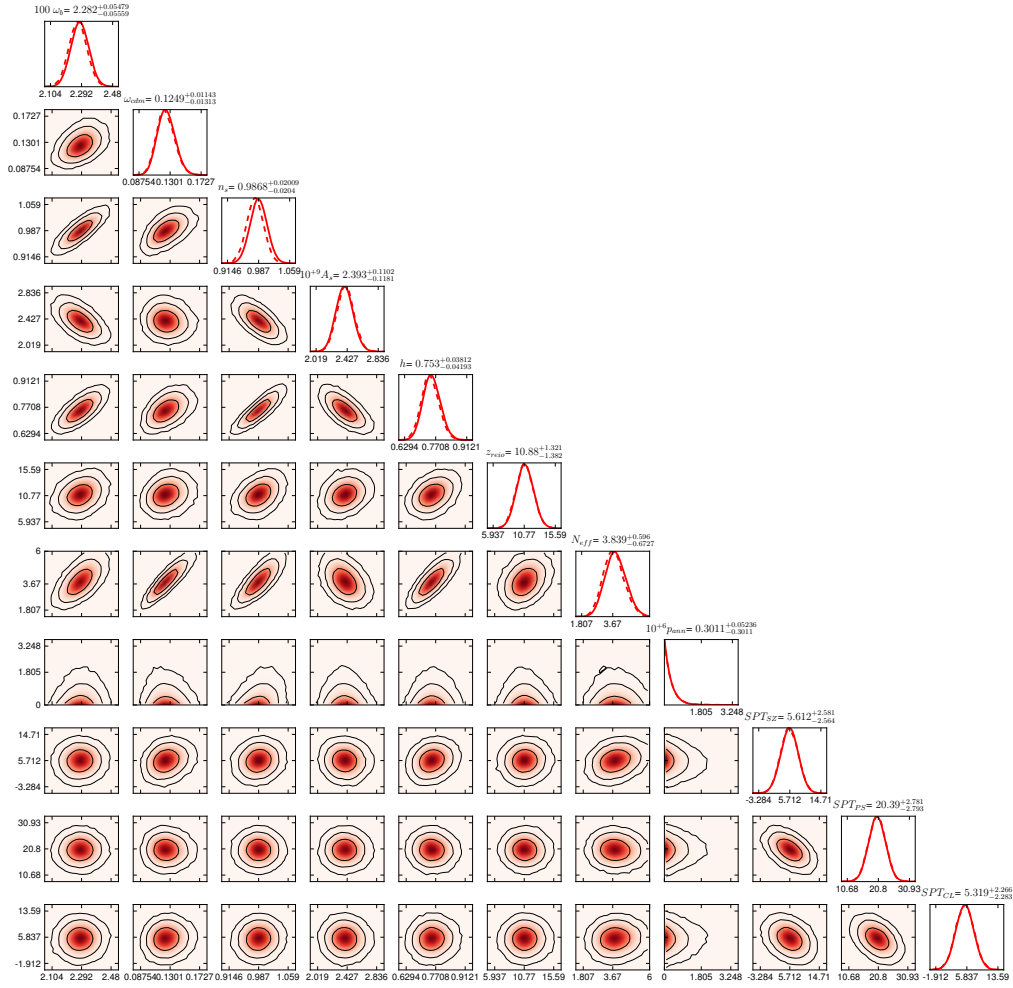
Figure 4.4 – One and two-dimensional marginalized posterior probabilities for the free parameters of a ΛCDM model with a free effective neutrino number N_{eff} and time-independent annihilation parameter p_{ann}, compared to WMAP7 + SPT data. For the two-dimensional posterior, we show the contours corresponding to the 68.3%, 95.4% and 99.7% credible regions. The last three parameters are nuisance parameters accounting for foregrounds contributions to the SPT data set.

annihilation in halos:	neglected	neglected	yes	yes	yes
reionization from stars:	yes	yes	neglected	yes	yes
data:	CMB	CMB	CMB	CMB + Gunn-Pet.	CMB + T_M prior
section:	3.3	3.4	4.4	4.4.5	4.4.6
$100\,\omega_b$	$2.282^{+0.055}_{-0.055}$	$2.281^{+0.054}_{-0.057}$	$2.267^{+0.052}_{-0.052}$	$2.267^{+0.052}_{-0.053}$	$2.280^{+0.055}_{-0.055}$
ω_{cdm}	$0.125^{+0.011}_{-0.013}$	$0.125^{+0.011}_{-0.013}$	$0.126^{+0.011}_{-0.013}$	$0.126^{+0.011}_{-0.013}$	$0.126^{+0.011}_{-0.013}$
n_s	$0.987^{+0.020}_{-0.020}$	$0.987^{+0.020}_{-0.020}$	$0.980^{+0.019}_{-0.019}$	$0.980^{+0.019}_{-0.018}$	$0.985^{+0.019}_{-0.021}$
$10^9 A_s$	$2.39^{+0.11}_{-0.12}$	$2.39^{+0.11}_{-0.12}$	$2.44^{+0.11}_{-0.13}$	$2.42^{+0.11}_{-0.12}$	$2.38^{+0.11}_{-0.12}$
h	$0.753^{+0.038}_{-0.042}$	$0.753^{+0.038}_{-0.042}$	$0.750^{+0.036}_{-0.040}$	$0.751^{+0.037}_{-0.039}$	$0.760^{+0.039}_{-0.043}$
$N_{\rm eff}$	$3.84^{+0.60}_{-0.67}$	$3.85^{+0.66}_{-0.60}$	$3.89^{+0.59}_{-0.64}$	$3.88^{+0.59}_{-0.65}$	$3.96^{+0.58}_{-0.67}$
$z_{\rm reio}$	$10.9^{+1.3}_{-1.4}$	$10.9^{+1.3}_{-1.4}$	-	$6.58^{+0.10}_{-0.09}$	$12.2^{+1.6}_{-1.6}$
$\frac{10^6 p_{\rm ann}}{\rm m^3/s/kg}$	< 0.89	< 0.91	< 0.78	< 0.75	< 0.78
α	-	flat	-	-	-
$\frac{f_{\rm h}}{\rm m^3/s/kg}$	-	-	12600^{+4100}_{-8800}	13000^{+3100}_{-8400}	< 1400
$z_{\rm h}$	-	-	$23.4^{+2.7}_{-8.4}$	$20.7^{+3.7}_{-5.2}$	flat
$[-2\ln\mathcal{L}]_{\rm min}$	3752.7×2	3752.7×2	3753.1×2	3753.2×2	3752.7×2

Table 4.1 – Mean and edges of the 68% Minimum Credible Interval (MCI) for the cosmological parameters of the five models that we compared to WMAP7 and SPT data. We don't show results for the nuisance parameters associated to SPT data, that have been marginalized over. The second model differs from the first one by the inclusion of a z-dependent annihilation function parametrized by α. All parameters have been assigned top-hat priors, and never reach prior edges except $p_{\rm ann}$ (limited to positive values), α (limited to the range $-0.2 < \alpha < 0$) and $z_{\rm h}$ (on which we imposed a prior $20 \leq z_{\rm h} \leq 30$ only in the last column). For $p_{\rm ann}$ (and $f_{\rm h}$ in the last column), we indicate the 95% Confidence Level (C.L.) upper bound.

4.3.4 Redshift dependent annihilation parameter

In any realistic model, the fraction of energy absorbed by the overall gas is a function of the redshift $f = f(z)$, as shown in Figure 4 of Slatyer et al. [87] for several examples.

The shape of $f(z)$ depends on the DM annihilation channel(s). The impact of the redshift-dependence of $f(z)$ on current/future CMB constraints on DM annihilation has been questioned with different methods in various papers [91, 89, 90]. Here we will check this issue with yet another approach, and confirm the results of other references showing that taking this dependence into account is of very little relevance.

All examples for $f(z)$ shown in [87] have strong similarities: $f(z)$ is always a smooth step-like function, with plateaux at $z > 2500$ and $z < 30$. In view of performing a model-independent comparison to the data, it is tempting to approximate $f(z)$ with a family of simple analytic functions, capturing the essential behavior of $f(z)$ in all cases. The CMB is marginally affected by the behavior of $f(z)$ at low z even in the case of a constant p_{ann}, and even more if $f(z)$ decreases; moreover, the effect of DM annihilation at low z is superseded by that of reionization. Hence, a given approximation scheme doesn't need to be accurate at low z, but should capture the essential behavior for $z > 100$. Figure 4 in [87] suggests that $f(z)$ could be chosen to be constant at $z > 2500$, to decrease like a parabola in log-log space for $30 < z < 2500$, and to remain again constant at $z < 30$, as displayed in figure 4.5.
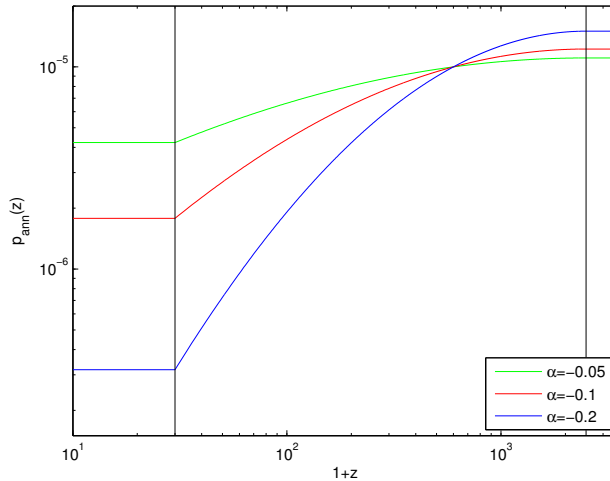
Figure 4.5 – Redshift dependent $p_{ann}(z)$, approximated as a two-parameter family of functions as described in the text, with $\bar{p}_{ann} \equiv p_{ann}(z = 600) = 1 \cdot 10^{-5}$ m^{3}s^{-1}kg^{-1} and $\alpha = -0.05, -0.1, -0.2$.

The work of [90] analyzed the amount of information that one can extract from current and future CMB data on $f(z)$ or $p_{ann}(z)$ (we recall that these two functions are simply related to each other by a time-independent factor, as long as we assume that the annihilation cross section does not vary with temperature). A model-independent analysis, based on the expansion of $p_{ann}(z)$ in principal components, reveals that the CMB is mainly sensitive to the first principal component, peaking around $z = 600$, and at the next order

to the second principal component, accounting for the redshift variation of $f(z)$ around this same value.

The goal of this section is to check these results with a simpler approach than a full principal component analysis. We will stick to the simple approximation for $p_{\mathrm{ann}}(z)$ suggested above, involving two plateaus and one parabola. This family of functions has two free parameters, one amplitude and one curvature. We can choose to define the amplitude parameter $\bar{p}_{\mathrm{ann}}$ at $z = 600$:

$$
p_{\mathrm{ann}}(z) = \begin{cases} \bar{p}_{\mathrm{ann}} \exp\left[-\alpha \log^2\left(\dfrac{601}{2501}\right)\right] & \text{for } z > 2500, \\[2ex] \bar{p}_{\mathrm{ann}} \exp\left[\alpha \left(\log^2\left(\dfrac{1+z}{2501}\right) - \log^2\left(\dfrac{601}{2501}\right)\right)\right] & \text{for } 30 < z < 2500, \quad (4.14) \\[2ex] \bar{p}_{\mathrm{ann}} \exp\left[\alpha \left(\log^2\left(\dfrac{31}{2501}\right) - \log^2\left(\dfrac{601}{2501}\right)\right)\right] & \text{for } z < 30, \end{cases}
$$

with $\bar{p}_{\mathrm{ann}} \equiv f(z = 600)\langle\sigma v\rangle/m_{\mathrm{DM}}$ and $\alpha < 0$. With respect to the previous section, we now have a new dimensionless parameter α, that expresses the redshift dependence of $p_{\mathrm{ann}}(z)$. The question is whether this new parameter can be detected with current data: if not, the analysis of the previous section captures all the information that we can extract, with p_{ann} standing for the value of the annihilation parameter near $z \sim 600$.

We show in figure 4.6 the evolution of x_e and T_{M} for fixed $\bar{p}_{\mathrm{ann}}$ and several values of α. As long as α remains small in absolute value ($|\alpha| \ll 1$), its impact is mainly on the slope of $x_e(z)$ in the region $z \ll z_{\mathrm{dec}}$. We expect this slope to be difficult to probe experimentally, since the CMB is mainly sensitive to the optical depth, which is an integrated quantity over redshift.

When the redshift dependance of $p_{\mathrm{ann}}(z)$ increases with a fixed normalization at $z = 600$, the annihilation rate at high redshift increases. We expect to reach such large values that the decoupling time is not just slightly affected by DM annihilation, but radically postponed to a later time, because the massive energy injection from DM annihilation forbids hydrogen recombination. This happens for $\alpha < -4$, as illustrated in figure 4.6. In this regime, the sound horizon at recombination is dramatically increased, and the CMB data will enforce a similar increase in the angular diameter distance to last scattering, in order to keep the same peak scale in multipole space. This will generate a correlation between α and parameters such as the Hubble rate. However, the scale of the acoustic peaks and of Silk damping react differently to such a transformation, so we expect that α cannot be pushed to arbitrary negative values. This "extreme" regime could not be reached in the previous subsection: as long as we assumed a constant p_{ann}, observational bounds on p_{ann} prevented the annihilation rate to be too high around $z \sim 1000$. When comparing this model with CMB data, we first imposed no prior on α (apart from $\alpha < 0$). We obtained a bound $\alpha > -5.3$ (95% C.L.) and some non-trivial correlation between very negative values of α and other parameters.
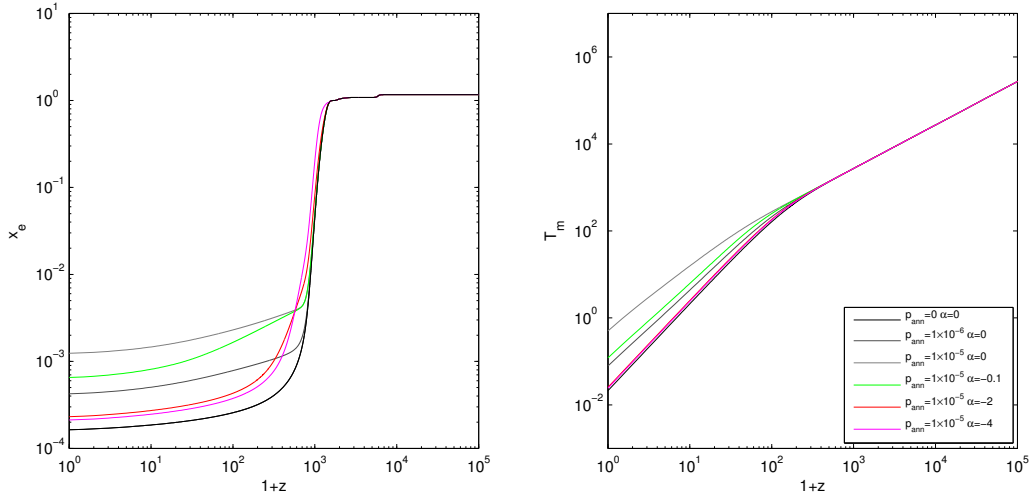
Figure 4.6 – Free electron fraction x_e and matter temperature $T_{\rm M}$ as a function of redshift for a constant $p_{\rm ann} = 0$, $1 \cdot 10^{-6}$ and $1 \cdot 10^{-5}$ m^{3}s^{-1}kg^{-1}(black and gray curves) and a redshift dependent $p_{\rm ann}(z)$ with $\bar{p}_{\rm ann} = 1 \cdot 10^{-5}$ m^{3}s^{-1}kg^{-1} and $\alpha = -0.1, -2$ and 4, using RECFAST and assuming no reionization.

However, this region in parameter space should not be taken seriously, because the realistic examples provided in [87] correspond to values of $|\alpha|$ at most of the order of 0.1 or 0.2. We performed a more "realistic" run with a top-hat prior $-0.2 < \alpha < 0$. The results are summarized in the second column of Table 4.1. The data still gives no indication in favor of DM annihilation. The posterior probability of α is flat throughout the prior range, and the bounds on other parameters are essentially unchanged with respect to the run with a constant annihilation parameter, i.e. with $\alpha = 0$. Even the two-dimensional probability contours in the space $(\bar{p}_{\rm ann}, \alpha)$ show no significant correlation between these parameters.

These results are fully consistent with those of [90], showing that the first principal component peaks near $z \sim 600$. They also prove that current data is not sensitive to the second principal component, unless it has an unreasonably large amplitude like in the run with no prior on α. We could have defined our parameter $\bar{p}_{\rm ann}$ at a different redshift: in that case, we would have expected to find a correlation between $\bar{p}_{\rm ann}$ and α. The maximum of the first principal component can be seen as the "decorrelation redshift" between $\bar{p}_{\rm ann}$ and α.

In conclusion of this section, it appears that the moderate variation of $f(z)$ (or equivalently $p_{\rm ann}(z)$) in the range $40 < z < 1000$ suggested by the realistic examples of [87] is far from being detectable with WMAP7+SPT data. Ref. [89, 91] reached a similar conclusion by comparing bounds on $p_{\rm ann}$ for some particular cases out of the possible $f(z)$ functions presented in [87]. In the next section, it will be legitimate to neglect any variation of

$p_{\text{ann}}(z)$ at least until the redshift of halo formation.

4.4 Annihilation in Dark Matter halos and Reionization

Until now we considered that Dark Matter is uniformly distributed in the universe. It is well-known that structure formation generates a concentration of DM in halos that is likely to enhance DM annihilation. This issue has been widely discussed in the context of dark matter indirect detection in cosmic rays. It has also been pointed out that enhanced DM annihilation could be relevant for the reionization of the universe, and therefore for CMB physics [83, 84, 85, 88, 91, 92]. In this section, we wish to propose a systematic investigation of such effects, based on a generic parameterization of DM annihilation in halos, and a full parameter extraction from CMB data.

4.4.1 Energy density release in DM halos

The energy released by Dark Matter annihilation in halos can be written as (see e.g. [84, 92])

$$\left. \frac{dE}{dV dt} \right|_{\text{halos}} = \rho_\chi^2(z) c^2 p_{\text{ann}}, \tag{4.15}$$

where ρ_χ^2 is the squared dark matter density averaged over space, that exceeds the square of the average dark matter density in presence of non-linear structures. In the halo model, this quantity is given by:

$$\rho_\chi^2(z) = (1+z)^3 \int_{M_{\text{min}}}^\infty dM \frac{dn}{dM} \left(\int_0^{r_{200}} dr 4\pi r^2 \rho_{\text{h}}^2(r) \right). \tag{4.16}$$

Here M_{min} is the minimal mass of DM halos, $\frac{dn}{dM}$ the differential comoving number density of DM halos of mass M, r_{200} the radius of a sphere enclosing a mean density equal to 200 times the background density, and ρ_{h} the spherical DM halo density profile. The shape of density profiles is still a subject of controversy. If we consider for instance a Navarro-Frenk-White (NFW) profile [115], we can express the last integral as

$$\int_0^{r_{200}} dr 4\pi r^2 \rho_{\text{h}}^2(r) = \frac{M\bar{\rho}(z_{\text{F}})}{3} \left(\frac{\Omega_{\text{DM}}}{\Omega_M} \right)^2 f_{\text{NFW}}(c_{\text{h}}), \tag{4.17}$$

where z_{F} is the redshift of halo formation, $\bar{\rho}(z_{\text{F}}) = 200\rho_{\text{c}}\Omega_{\text{M}}(1+z_{\text{F}})^3$ the average matter density within a radius r_{200}, and f_{NFW} a function of the so-called halo concentration parameter c_{h}. We recall that the critical density ρ_{c} and density fraction parameters Ω_i are defined today. In order to get an analytic approximation to dn/dM, one can use the

Press-Schechter formalism [116], leading to

$$\frac{dn}{dM}(M, z) = \frac{\rho_{\rm M}}{M} \frac{d\ln\sigma^{-1}}{dM} f(\sigma),$$ (4.18)

where $\rho_{\rm M} = \rho_{\rm c}\Omega_{\rm M}$ is the average matter density today, and $f(\sigma)$ the differential mass function. The variance of the linear density field $\sigma(M, z)$ is given as usual by

$$\sigma^2(M, z) = \int_0^\infty P(k, z) W^2(k, M) k^2 dk,$$ (4.19)

with $P(k, z)$ the linear power spectrum at redshift z, and $W(k, M)$ the window function. Assuming that the collapse of the high density regions can be described by a spherical model, one can use a top-hat filter for W [117]. For the differential mass function, we could rely on the original function of Press and Schechter

$$f_{PS}(\sigma) = \sqrt{\frac{2}{\pi}} \frac{\delta_{sc}}{\sigma} \exp\left(-\frac{\delta_{sc}^2}{2\sigma^2}\right)$$ (4.20)

with $\delta_{sc} = 1.28$, or the more accurate function proposed by Seth and Thormen [118]. We could compute these terms exactly within the Boltzmann code, but the CMB spectra are not highly sensitive to the details of the halo model: they can only provide constraints on integrated quantities. Hence, it is irrelevant to search for high accuracy in this context. Instead, it would be very useful for the purpose of fitting CMB data to derive a simple, approximate parametric form for the energy injection function. To start with, we can use the fact that in a universe dominated by matter (i.e. any time between decoupling and $z \sim 1$), the redshift dependence of the variance σ is somewhat trivial:

$$\sigma(M, z) = \sigma(M, 1)\frac{2}{1+z}.$$ (4.21)

If we recollect all terms, we get the following contribution to the energy rate due to Dark Matter halos

$$\left.\frac{dE}{dVdt}\right|_{\rm halos} = \rho_{\rm c}^2 \, \Omega_{\rm DM}^2 \, c^2 \, p_{\rm ann}(z) \, (1+z)^3 \, \frac{200}{3}(1+z_{\rm F})^3 f_{\rm NFW}(c_{\rm h})$$
$$\times \int_{M_{\rm min}}^\infty dM \left\{ \frac{d\ln\sigma^{-1}(M, 1)}{dM} \frac{2}{\sqrt{\pi}} \frac{\delta_{sc}\,(1+z)}{2\sqrt{2}\,\sigma(M, 1)} \exp\left(-\frac{\delta_{sc}^2\,(1+z)^2}{8\,\sigma^2(M, 1)}\right) \right\},$$ (4.22)

where we used the original Press-Schechter differential mass function for simplicity. The redshift-dependent integral simplifies with the change of variable $u = \frac{\delta_{sc}(1+z)}{2\sqrt{2}\sigma(M,1)}$. If we

define $u_{\min}(z) = \frac{\delta_{sc}(1+z)}{2\sqrt{2}\sigma(M_{\min},1)}$, it reduces to

$$\int_{u_{\min}(z)}^{\infty} du \frac{2}{\sqrt{\pi}} \exp\left(-u^2\right) = \text{erfc}(u_{\min}(z)) \ , \tag{4.23}$$

where $\text{erfc}(x)$ is the complementary error function. It is suppressed at high redshift, before halo formation, i.e. as long as $u_{\min}(z) \gg 1$. At low redshift, we do not expect the function $p_{\text{ann}}(z)$ to vary significantly, as can be seen in figure 4 of [87] for several examples. Hence, we can replace it by a nearly constant value $p_{\text{ann}}(0)$. In this case, the energy rate from annihilation in halos can be expressed as a function of only two parameters (beyond $\rho_c \Omega_{\text{DM}}$),

$$\left.\frac{dE}{dV dt}\right|_{\text{halos}} \simeq \rho_c^2 \Omega_{\text{DM}}^2 c^2 (1+z)^3 f_{\text{h}} \ \text{erfc}\left(\frac{1+z}{1+z_{\text{h}}}\right) \ , \tag{4.24}$$

where z_{h} is the characteristic redshift at which halos start to contribute[5],

$$z_{\text{h}} \equiv \frac{2\sqrt{2}}{\delta_{sc}} \sigma(M_{\min}, 1) - 1 \ , \tag{4.25}$$

and f_{h} is a parameter related to the formation redshift and concentration of halos, and to the DM annihilation function at low redshift,

$$f_{\text{h}} \equiv \frac{200}{3} (1+z_{\text{F}})^3 f_{\text{NFW}}(c_{\text{h}}) \, p_{\text{ann}}(0) \ . \tag{4.26}$$

The parameter f_{h} shares the same units as p_{ann}. In principle, z_{h} and the ratio $f_{\text{h}}/p_{\text{ann}}(0)$ should be inferred from a fit of the Press-Schechter formalism to detailed simulations of structure formation. However, there is no full consensus yet on the dynamics of halo formation and on halo density profiles. Moreover, these parameters should have a strong dependence on cosmological parameters, and also on the matter power spectrum at large k, which is poorly constrained by observations. Hence we will treat z_{h} and f_{h} as free parameters in our analysis.

4.4.2 Beyond the on-the-spot approximation

Sticking to the on-the-spot approximation, we could express the net ionization rate per interval of redshift $I_{X_i} + I_{X_\alpha}$ using eqs. (4.7,4.8). The equation of evolution for x_e and T_{M} would receive extra contributions

$$\left.\frac{dx_e}{dz}\right|_{\text{ann}} = -\frac{1}{(1+z)H(z)n_H(z)} \frac{dE}{dV dt}(z) \left[\frac{1-x_e(z)}{3}\left(\frac{1}{E_i} + \frac{1-C(z)}{E_\alpha}\right)\right], \tag{4.27}$$

$$\left.\frac{dT_{\text{M}}}{dz}\right|_{\text{ann}} = -\frac{1}{(1+z)H(z)n_H(z)} \frac{dE}{dV dt}(z) \left[\frac{2}{3k_b}\frac{1+2x_e(z)}{3}\frac{1}{1+f_{He}+x_e(z)}\right], \tag{4.28}$$

---

[5]In fact, the functions $\text{erfc}(x)$ starts to raise at $x \leq 2$, so halos contribute below $z \leq 2z_{\text{h}}$.

with $\frac{dE}{dVdt}(z)$ given by the sum of the smooth density and halo density contributions. However, this approximation becomes inaccurate at low redshift, as we shall see below. Well after recombination, the energy injection responsible for ionization and heating at a given redshift z comes from the decay products of DM annihilation at all redshifts $z' \geq z$, taking into account the fact that particle energies are redshifted between z' and z, and that a fraction of the particles created at z' interact along the line-of-sight and do not play a role at z. Moreover, in general, the interaction cross-section between z' and z depends on the energy of each particle. Hence, the ionization rate obeys a rather complicated equation involving two integrals: one over dz', and one over the energy of the particles created at z', and interacting with the plasma at intermediate redshift.

However, ref. [84] found that at low redshift, most of the ionization and heating is caused by photons produced by the inverse Compton scattering (ICS) of charged particles resulting from DM annihilation over CMB photons. It was shown by the authors of [88] that taking mainly this process into account leads to the simplified expression:

$$\left. \frac{dx_e}{dz} \right|_{\text{ann}} = -\frac{c\sigma_T\,\gamma(z)}{(1+z)H(z)} \int_z^\infty \frac{dz'}{(1+z')H(z')} \left(\frac{1+z}{1+z'} \right)^3 e^{\kappa(z,z')} \frac{dE}{dVdt}(z'), \quad (4.29)$$

where $e^{\kappa(z,z')}$ is an absorption factor: it represents the fraction of photons produced around z' by ICS that already interacted with the inter-galactic medium and deposited their energy before z. Hence κ can be approximated as

$$\kappa(z,z') = c\sigma_T \int_z^{z'} \frac{-dz''}{(1+z'')H(z'')} n_H(z'') \,, \quad (4.30)$$

not to be confused with the optical depth of CMB photons, featuring an extra factor $x_e(z'')$. Finally, $\gamma(z)$ is a short-cut notation for

$$\gamma(z) \equiv \left[\frac{1 - x_e(z)}{3} \left(\frac{1}{E_i} + \frac{1 - C(z)}{E_\alpha} \right) \right]. \quad (4.31)$$

The integral in $\kappa(z,z')$ can be performed analytically:

$$\kappa(z,z') = \frac{2}{3} c\sigma_T \frac{n_H(0)}{H_0\sqrt{\Omega_M}} \left[(1+z)^{3/2} - (1+z')^{3/2} \right] = \frac{2}{3} c\sigma_T \left[\frac{n_H(z)}{H(z)} - \frac{n_H(z')}{H(z')} \right] . \quad (4.32)$$

Let us define $\alpha \equiv c\sigma_T \frac{n_H(0)}{H_0\sqrt{\Omega_M}}$. We notice that

$$\int_z^\infty dz'\, \alpha\, \sqrt{1+z'}\, e^{\kappa(z,z')} = 1 \,. \quad (4.33)$$

Hence, the function $\Delta(z,z') \equiv \alpha\,\sqrt{1+z'}\,e^{\kappa(z,z')}$ peaking in $z' = z$ can be approximated with the Dirac function $\delta(z - z')$ in the limit in which it decreases with z' much faster

than any other function in the integrand of equation (4.29). Writing (4.29) as

$$\left.\frac{dx_e}{dz}\right|_{\text{ann}} = -\frac{\gamma(z)}{(1+z)H(z)} \int_z^\infty dz'\, \Delta(z,z')\, n_H(z')^{-1} \left(\frac{1+z}{1+z'}\right)^3 \frac{dE}{dVdt}(z')\,, \quad (4.34)$$

we see that in the approximation mentioned above, one recovers exactly the on-the-spot expression of eq. (4.27). But in the general case, we have to deal with the full integral. This is mathematically equivalent to keeping expression (4.27), with the on-the-spot energy rate replaced by an effective one, defined as

$$\left.\frac{dE}{dVdt}\right|_{\text{eff}}(z) \equiv \int_z^\infty dz'\, \Delta(z,z')\, \frac{n_H(z)}{n_H(z')} \left(\frac{1+z}{1+z'}\right)^3 \frac{dE}{dVdt}(z')$$
$$= \int_z^\infty dz' \Delta(z,z') \left(\frac{1+z}{1+z'}\right)^6 \frac{dE}{dVdt}(z')\,. \qquad (4.35)$$

Similarly, this effective energy rate should be used in equation (4.28) to get the correct temperature evolution.
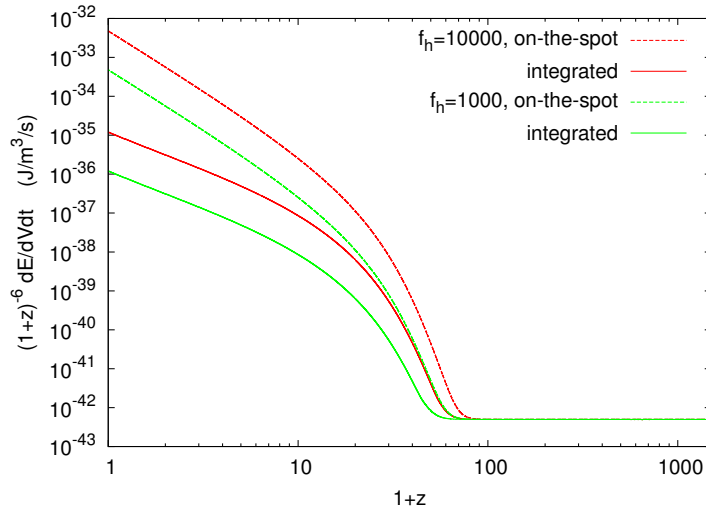
Figure 4.7 – Effective energy injection rate rescaled by $(1+z)^6$, computed with or without the on-the-spot approximation, for either $f_\text{h} = 10000$ or 1000. Other annihilation parameters are fixed to $p_\text{ann} = 10^{-6}$ and $z_\text{h} = 20$.

4.4.3 Effects on x_e, T_M and the CMB spectra

In figure 4.8, we compare the effect of DM annihilation in halos with that of the default reionization model implemented in CLASS and CAMB, based on a hyperbolic tangent centered in z_reio. The effect of DM annihilation on the ionization fraction is found to be very similar, except that it induces a slower reionization. The parameter z_h controls the

onset of reionization from halos, while f_h controls its amplitude. For large enough values of f_h, DM annihilation in halos can entirely reionize the universe before the current epoch, as shown previously in [84, 88, 92]. With the default reionization model, the ionization fraction x_e is larger than one at low redshift, because Helium reionization is also taken into account. In our model for DM annihilation in halos, we neglect helium reionization for simplicity, so that x_e is smaller or equal to one by definition.
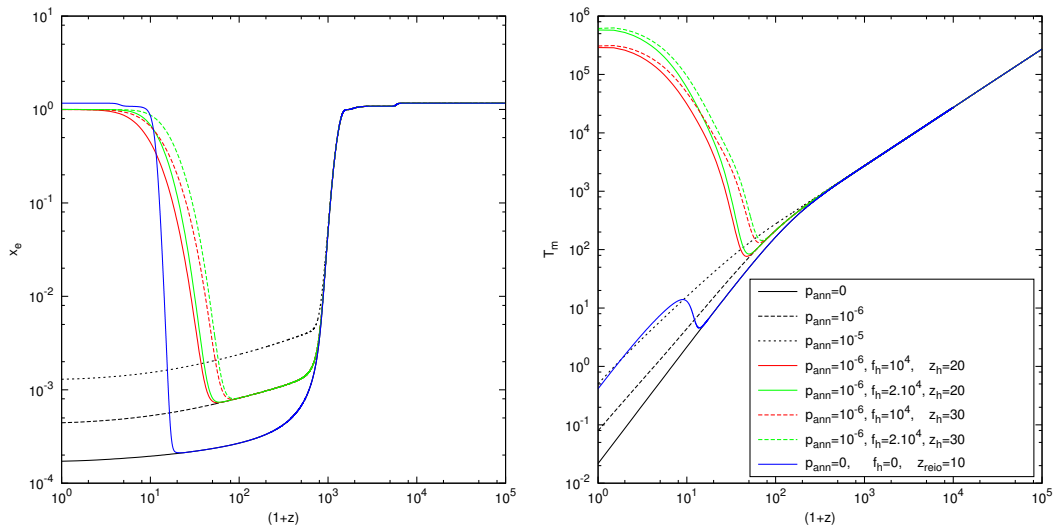
Figure 4.8 – Free electron fraction and matter temperature for $p_{\mathrm{ann}} = 0, 10^{-6}$ and 10^{-5} m^{3}s^{-1}kg^{-1} (from bottom to top) and different values of f_h and z_h, compared to the usual results for $p_{\mathrm{ann}} = 0$ and a single-step model for reionization from stars. All curves were obtained using HYREC in mode RECFAST.

When including the effect of DM annihilation in halos, we work with the RECFAST mode of HYREC. Indeed, with RECFAST, we experienced numerical instability issues: the free electron fraction explodes and oscillates very rapidly already for small value of our parameters f_h and z_h. With HYREC in FULL modes, the only problem is that for large values of z_h and f_h, the ratio T_M/T_r may exceed one, falling outside the range of one interpolation tables. The RECFAST mode of HYREC is always well behaved.

The right plot in figure 4.8 shows that the matter temperature increases a lot due DM annihilation in halos. Note also that for extreme values of the temperature $T_M > 2 \times 10^4$ K, using RECFAST's case-B recombination coefficient becomes inaccurate [119]. We will see anyway in section 4.4.6 that such large values are in contradiction with constraints on the temperature of the inter-galactic medium at $z \leq 4$, as inferred from Lyman-α observations: this will provide an addition constraint on the DM annihilation rate.

The signature of DM annihilation on the primary CMB anisotropy spectrum is found to be very similar to that of reionization. In addition to the peak shifting and damping due to a non-zero p_{ann} parameter, the halo effect controlled mainly by f_h leads to an

overall suppression of temperature/polarization power for $l > 30$, and an enhancement of polarization for $l < 30$. We can anticipate that the CMB alone can hardly discriminate between the contribution of reionization from stars and from halos, since the CMB spectra probe mainly the optical depth, i.e. the integral of x_e over time. However, the fact that DM induces a slow reionization process starting at high redshift[6] implies that the step-like suppression of temperature and the low-l polarization bump are smoother and wider than with the default reionization model. To illustrate this, we compare in figure 4.9 the low-l polarization spectrum for two models with the same optical depth. Accurate CMB polarization data limited only by cosmic variance on large angular scale may probe such a difference.
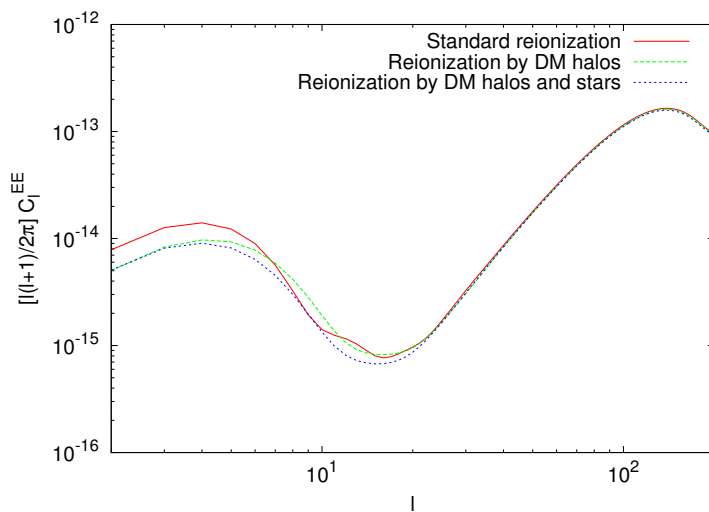
Figure 4.9 – Low-l polarization spectrum for the three best-fitting models assuming reionization from stars (with the usual single step parameterization), from DM annihilation in halos, or from both with an additional Gunn-Peterson prior.

4.4.4   Can Dark Matter annihilation alone explain reionization?

We wish to check whether WMAP7 and SPT data are compatible with the assumption that the reionization of the universe can be explained entirely by DM annihilation in halos, as suggested in [84, 88, 92]. It is rather obvious that the free parameters z_h and f_h of our model can be adjusted in such way that the reionization optical depth is be compatible with the WMAP7 best-fitting value. However, we have seen that DM annihilation can only induce slow reionization starting at high redshift, and induce a wider step (resp. bump) in the low-l temperature (resp. polarization) spectrum. A priori, this may lead to a value of the maximum likelihood significantly lower for the annihilation

---

[6]In the CMB analysis of the next subsections, z_h is found in the range from 20 to 30, implying that halos start contributing between 40 and 60, well before star formation.

model. In addition, an analysis with free z_h and f_h could lead to preferred values in strong contradiction with expectations from structure formation and halo models.

The results of our MONTEPYTHON run with WMAP and SPT data are summarized in the third column of Table 4.1 and in the triangle plot of figure 4.10. The new free parameters z_h and f_h are not degenerate with other parameters, so the credible interval for the usual ΛCDM parameters and N_{eff} are unchanged with respect to the standard model without annihilation. There is instead a significant correlation between z_h and f_h: if halos form very late, a very large amplitude parameter f_h is needed in order to get the same optical depth. The effective chi square $\chi^2_{\text{eff}} \equiv -2 \ln \mathcal{L}$ is higher for DM reionization than single-step star reionization, but only by 0.8, showing that the data shows no strong preference for one model against the other.

The characteristic redshift z_h is found in the range $12 < z_h < 40$ (95%C. L.). This parameter has a strongly non-gaussian posterior probability, with a mean value of 23, but a best-fit value of 19. The shape of the $\text{erfc}(x)$ function is such that the halo contribution starts raising around $z \sim 2z_h$. Values of z_h close to 20 imply a raise in the range 40-50, which is plausible from the point of view of structure formation.

To see whether the required value of halo concentration is sensible, we need to make an assumption about the DM annihilation amplitude, since the data is sensitive to f_h, i.e. to the product $f_{\text{NFW}}(c_h) \times p_{\text{ann}}(0)$. If we first assume a value of p_{ann} at $z \sim 600$ saturating our CMB bound, $p_{\text{ann}}(600) \sim 9 \times 10^{-7}$, we expect that at low redshift this parameter will fall to approximately $p_{\text{ann}}(0) = \sim 2 \times 10^{-7}$. Then the best-fitting value $f_h \sim 12600 \, \text{m}^3/\text{s/kg}$ requires

$$f_{\text{NFW}}(c_h) \sim \frac{3 f_h}{200(1 + z_F)^3 p_{\text{ann}}(0)} \sim 4200 \;, \tag{4.36}$$

where we also assumed $z_F \sim 60$. The quantity $f_{\text{NFW}}(c_h)$ is poorly constrained, but models of halo formation suggest an order of magnitude ranging from 10^3 to 10^5. Hence the "reionization from DM annihilation" model points towards a reasonable value of the concentration parameter. If $f_{\text{NFW}}(c_h)$ is of the order of 4×10^3, then constraints on DM annihilation from the smooth background and from halos are comparable. If $f_{\text{NFW}}(c_h)$ is of the order of 10^3 (resp. 10^4 or 10^5), then constraints from annihilation in the smooth background (resp. in halos) are stronger. Indeed, the bound on p_{ann} coming from annihilation from halos can be found using the relation

$$p_{\text{ann}}(z = 600) = 3.3 \times 10^{-11} \frac{p_{\text{ann}}(600)/p_{\text{ann}}(0)}{0.5} \frac{61^3}{(1 + z_F)^3} \frac{10^4}{f_{\text{NFW}}(c_h)} f_h \;. \tag{4.37}$$

Taking $f_h^{\text{max}} = 25600 \, \text{m}^3/\text{s/kg}$ (95% C.L.) from our analysis, this implies

$$p_{\text{ann}}(z = 600) < 0.84 \times 10^{-6} \left[\frac{p_{\text{ann}}(600)}{0.5 p_{\text{ann}}(0)} \frac{61^3}{(1 + z_F)^3} \frac{10^4}{f_{\text{NFW}}(c_h)} \right] \text{m}^3/\text{s/kg} \; (95\% \text{C.L.}) \tag{4.38}$$
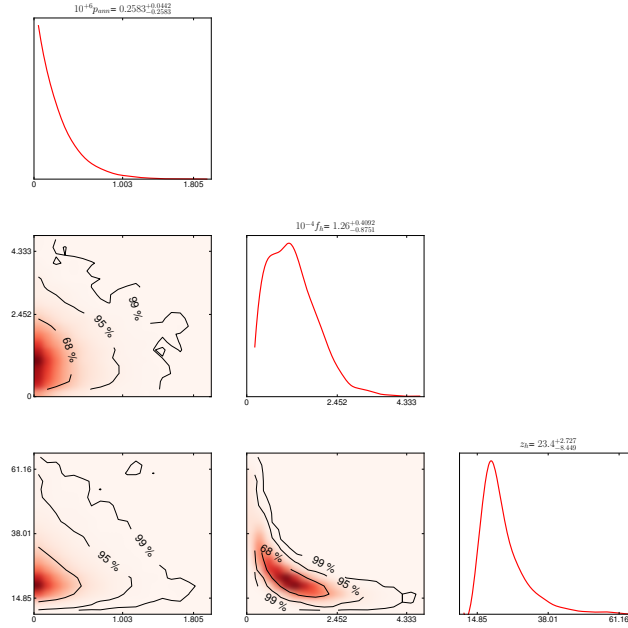
Figure 4.10 – Assuming a ΛCDM model with free electron fraction, dark matter annihilation (background and halos) and no extra reionization from stars, marginalized probability distribution of the annihilation parameters p_{ann}, f_{h} and z_{h} given WMAP7 and SPT data.

The low-l polarization spectrum for the best fitting model is shown on figure 4.9. Given its distinct shape due to an early and slow reionization process (with respect to star reionization), we expect future small-scale polarized measurements by Planck and other CMB experiments to improve the bound on f_{h}.

4.4.5 The Gunn-Peterson effect

It was realized in 1965 by Gunn and Peterson [120] that the observation of redshifted Lyman-α absorption lines in quasar spectra was a very sensitive probe of the presence of neutral hydrogen along the line of sight, and hence of the ionization fraction of the universe at different redshifts. Since even a small fraction of neutral hydrogen leads to a clear signature, we have some evidence that the universe was almost fully ionized until $z \sim 6$, since quasars at such a redshift show a very small level of Lyman-α absorption. More precisely, according to [121], the fraction of neutral hydrogen x_{HI} has to satisfy:

- for $z \geq 6$, $x_{\mathrm{HI}} \geq 10^{-3}$ (x_{HI} might even be equal to 10^{-1}),
- for $z \leq 5.5$, $x_{\mathrm{HI}} \leq 10^{-4}$,

(see also [122] for a recent constraint at $z \simeq 7$). Thus there seems to be an abrupt transition between $z = 5.5$ and $z = 6$. This raises some tension with the simplest model

of single-step reionization from stars, in which the ionization fraction is assumed to evolve roughly like a hyperbolic tangent centered on a reionization redshift $z_{\rm reio}$. The problem is not related so much to the precise shape of the step, but to the fact that any abrupt step should be centered near $z = 6$ or 7 to comply with Gunn-Peterson observations, instead of $z_{\rm reio} = 10.6 \pm 2.4$ (95%C.L.) to explain the optical depth $\tau_{\rm reio} = 0.088 \pm 0.015$ measured by WMAP [60][7]. A single-step reionization at $z \sim 10$ or even 8 would lead to $x_{\rm HI} < 10^{-3}$ at $z = 6$.

The model of the previous subsection, in which reionization is caused entirely by DM annihilation in halos, also fails to explain Gunn-Peterson observations for the opposite reason: reionization is then so slow that all allowed models have $x_{\rm HI} > 10^{-4}$ at $z = 5.5$.

There could be several solutions to this problem:

- the Gunn-Peterson bounds may be wrong or not correctly interpreted. These bounds are in fact model-dependent and controversial, since they rely on assumptions concerning the density and temperature of the inter-galactic medium, and the ultra-violet background. Observations at $z \sim 6$ could be explained with alternative models for the IGM and UV background, instead of incomplete reionization [123]. The evidence that the universe is fully ionized below $z \sim 5.5$ could also disappear with different assumptions, for instance in the context of inhomogeneous reionization [124].
- the cosmological model describing our universe may have extra ingredients (not necessarily related to reionization) such that a good fit to WMAP data can be obtained with single-step reionization at $z_{\rm reio} \sim 6$ or 7.
- reionization may be caused by different population of stars forming at different redshifts. The single-step model is too naive and should be replaced by a model with at least two steps. The late one should take place around $z \sim 6$ or 7 to account for Gunn-Peterson observations. The early one, possibly related to the generation of massive, metal-free stars [125, 126], should partially reionize the universe and enhance the optical depth.
- reionization may be caused both by star and by the decay or annihilation of some particles. The possibility of enhancing reionization with sterile neutrino decay has been proposed by [127]. In the case of annihilating DM, ref. [88] suggested that DM annihilation in halos may start to slowly reionize the universe. At a redshift close to six, star formation processes take over and quickly ionize the remaining hydrogen atoms.

In this subsection, we wish to test the last paradigm. It is a priori not obvious that any model of this type can work, because in order to explain the observed optical depth, DM annihilation may need to be so large that in any case $x_{\rm HI} < 10^{-3}$ at $z = 6$. Fortunately, we

---

[7]To be more precise, the CMB constraint is dominated by the measurement of low-l E-type polarization by WMAP, and depends on the assumed cosmological model

will see that this mixed model nicely complies with Gunn-Peterson and CMB constraints, and points to plausible halo parameter values.

We added a Gunn-Peterson prior to WMAP7 and SPT data and ran MONTEPYTHON again. More precisely, we impose two top-hat priors $10^{-3} \leq x_{\mathrm{HI}}(6) \leq 1$ and $0 \leq x_{\mathrm{HI}}(5.5) \leq 10^{-4}$. We neglect Helium reionization for simplicity. In this approximation, x_e just represents the fraction of ionized hydrogen, and we have $x_{\mathrm{HI}} = 1 - x_e$. Our Boltzmann code CLASS simulates mixed reionization in the following way. For each model, the ionization fraction is first computed down to $z = 0$ neglecting reionization from stars, using HYREC (in `RECFAST` mode) in order to avoid numerical instability. The effect of stars is then implemented "by hand": below some arbitrary redshift z_{reio}, $x_e(z)$ is cut and matched continuously to a half-hyperbolic tangent centered on z_{reio}, reaching an asymptotic value of one for $z \to 0$ (see one example of such models in figure 4.11). The precise shape of this function is in fact identical to that for ordinary single-step reionization in CLASS and CAMB, except that only the side $z \leq z_{\mathrm{reio}}$ of the step-like function is used, and that the transition width parameter is decreased to $\delta z = 0.2$ in order to model a very fast reionization process.
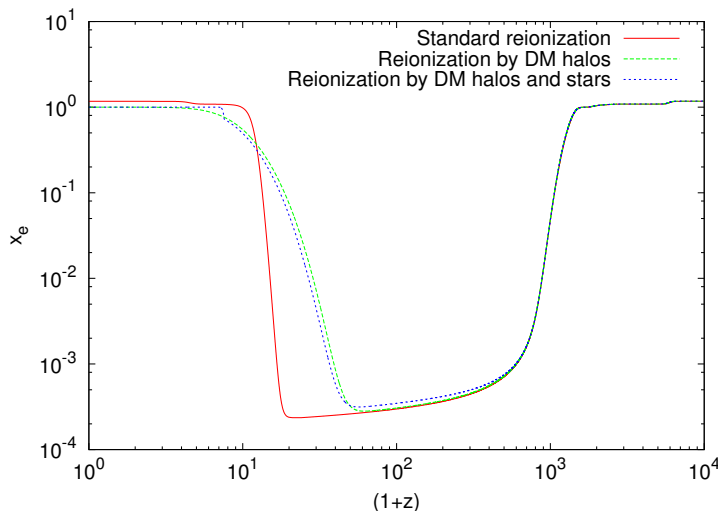
Figure 4.11 – Free electron fraction for the three best-fitting models assuming reionization from stars (with the usual single step parameterization), from DM annihilation in halos, or from both with an additional Gunn-Peterson prior. All curves were obtained using HYREC in mode `RECFAST`.

Our results are summarized in the second-last column of Table 4.1 and in the triangle plot of figure 4.12. With respect to the previous model of section 4.4.4, we have one more parameter z_{reio}, that is very well constrained by the Gunn-Peterson prior: it can only fluctuate in the range $6.4 < z_{\mathrm{reio}} < 6.8$ (95% C.L.). The posterior probability of f_{h} and z_{h} are shifted to slightly smaller values, since DM annihilation in halos is only expected to contribute to a fraction of the optical depth. For all other parameters, the results are

Figure 4.12 – Assuming a ΛCDM model with free effective neutrino number, dark matter annihilation (background and halos) and single-step reionization from stars, marginalized probability distribution of the annihilation parameters p_{ann}, f_{h}, z_{h} and z_{reio} given WMAP7 and SPT data and an additional Gunn-Peterson prior.

essentially identical to those of the previous case. The minimum effective chi square is also unchanged. The discussion of section 4.4.4 concerning f_{h} and z_{h} still applies: z_{h} is fixed to a range that coincides with expectations from structure formation, and values of $f_{\mathrm{NFW}}(c_{\mathrm{h}})$ in the range from 10^3 to 10^5 could be accommodated provided that p_{ann} and $f_{\mathrm{NFW}}(c_{\mathrm{h}})$ fulfill the relation (4.37) with f_{h} in the range $2100 < f_{\mathrm{h}} < 28600$ (95% C.L.).

In conclusion of this subsection, we see that this mixed model for reionization is interesting: DM annihilation in halos could explain the value of the optical depth probed by CMB data, while reionization from star formation at $z \simeq 6.5$ would complete the reionization process and explain Gunn-Peterson observations.

4.4.6 Including an upper bound on the IGM temperature

The best-fitting models of sections 4.4.4 and 4.4.5 have a halo parameter f_h of the order of $10^4\,\mathrm{m^3/s/kg}$, leading to a matter temperature of the order of 10^5K at low redshift (see figure 4.8). This estimate of the average matter temperature in the universe should be taken with a grain of salt, since we did not account for inhomogeneities in the matter distribution, nor for the thermodynamical evolution of the inter-galactic medium (IGM) during structure and star formation.

However, Lyman-α observations suggest that the IGM temperature is of the order of a few times 10^4K in the redshift range $2 \leq z \leq 4.5$. Reference [85] pointed out that these measurements should provide at least an upper bound on the average temperature enhancement due to DM annihilation.

In other words, the results of the previous two subsections are compatible with Lyman-α observations only if we are modelling the temperature evolution incorrectly. The ansatz that a fraction $(1 + 2x_e)/3$ of the energy injected into the gas by DM annihilation goes into heating might be incorrect at low redshift; or the IGM temperature growth might be limited by some temperature regulation mechanisms not described by our simplistic set of equations (such as, for instance, line cooling or Bremsstrahlung effects). If instead our temperature evolution law is realistic, then DM annihilation cannot explain the reionization of the universe alone, and cannot even contribute sufficiently to reionization at $z \sim 6$ in order to explain Gunn-Peterson bounds with a mixed reionization model, based on annihilation plus a single-step star formation process.

It is still interesting to perform a parameter extraction with a prior on T_{M}, while assuming a mixed reionization from halos and stars, in order to check whether IGM temperature estimates provide a stronger bound on p_{ann} than the CMB alone. In this section, we will repeat our analysis with a conservative upper bound on the IGM temperature at low redshift, inspired from figure 6 (left) in [128]:

$$T_{\mathrm{M}}(z = 2) \leq 3.2 \times 10^4 \mathrm{K}. \tag{4.39}$$

We implemented this constraint in the form of a top-hat prior in MONTEPYTHON. We checked in the presence of such a prior, the model of section 4.4.4 in which reionization is caused entirely by DM annihilation requires unrealistically high values of $z_h \sim 100$, totally incompatible with structure formation models.

Like in the previous subsection, we implemented star reionization into CLASS "by hand": below some arbitrary redshift z_{reio}, $x_e(z)$ is cut and matched continuously to a half-hyperbolic tangent centered on z_{reio}, reaching an asymptotic value of one for $z \to 0$. We kept the transition width parameter at its default value: $\delta z = 1.5$. We also imposed a top-hat prior $20 \leq z_{\mathrm{h}} \leq 30$ in order to ensure that halos form at a realistic redshift, compatible with simulations of structure formation.
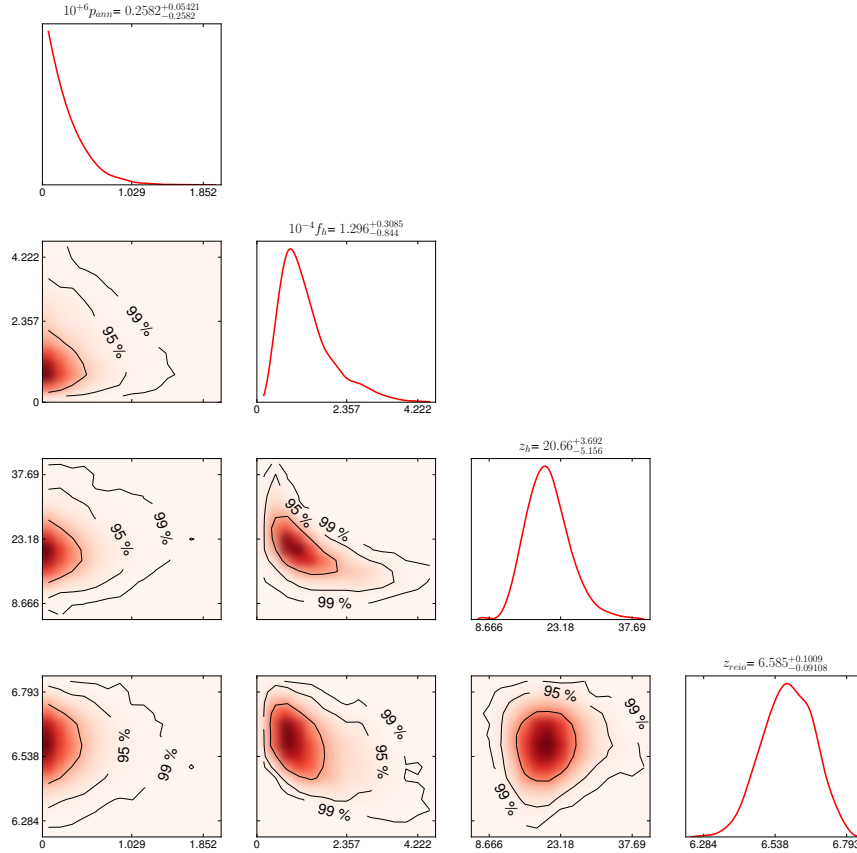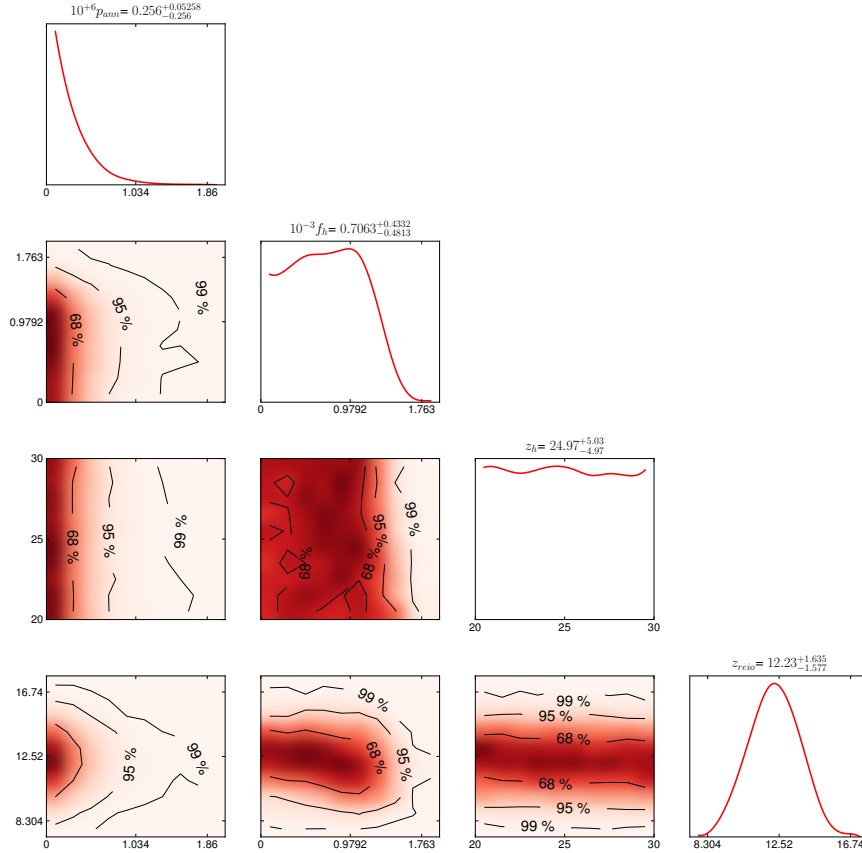
Figure 4.13 – Assuming a ΛCDM model with free effective neutrino number, dark matter annihilation (background and halos) and single-step reionization from stars, marginalized probability distribution of the annihilation parameters p_{ann}, f_{h}, z_{h} and z_{reio} given WMAP7 and SPT data, a prior $20 \leq z_{\mathrm{h}} \leq 30$ and an upper bound on the IGM temperature.

Our results are summarized in the last column of Table 4.1 and in the triangle plot of figure 4.13. The upper bound on f_{h} is reduced by one order of magnitude due to the IGM temperature constrain: the 95%CL upper limit on f_{h} decreases from $f_{\mathrm{h}}^{\mathrm{max}} = 25600\,\mathrm{m^3/s/kg}$ to $1400\,\mathrm{m^3/s/kg}$. This leads to a stronger bound on p_{ann}:

$$p_{\mathrm{ann}}(z=600) < 0.05 \times 10^{-6} \left[\frac{p_{\mathrm{ann}}(600)}{0.5 p_{\mathrm{ann}}(0)} \frac{61^3}{(1+z_{\mathrm{F}})^3} \frac{10^4}{f_{\mathrm{NFW}}(c_{\mathrm{h}})} \right] \mathrm{m^3/s/kg} \;\; (95\%\mathrm{C.L.}) \;\; (4.40)$$

Assuming that the factor between brackets is equal to one, this bound is almost twenty times stronger than the one inferred from annihilation in the smooth component only.

The heating effect of DM annihilation may also enhance the kinetic Sunyaev-Zel'dovich effect [129], leave a signature in secondary CMB anisotropies, and provide a further test

of this model [92]. We do not study this aspect in our work.

4.5 Conclusion and Outlook

We studied different possible contributions of annihilating Dark Matter to the thermal history of the universe. We confirmed previous results that the annihilation of the background DM distribution has non-trivial effects on the CMB, leading to the constraint

$$p_{\mathrm{ann}}(z \sim 600) < 0.91 \times 10^{-6} \mathrm{m}^3/\mathrm{s}/\mathrm{kg} \qquad (\mathrm{WMAP7 + SPT, \ 95\% C.L}), \qquad (4.41)$$

with a negligible impact of the variations of $p_{\mathrm{ann}}(z)$ in the range $100 < z < 2500$ suggested by a realistic study of DM annihilation channels.

We also showed that DM annihilation in halos could explain entirely the reionization of the universe from the point of view of CMB observations. In addition, if the constraints $x_{\mathrm{HI}}(6) \geq 10^{-3}$, $x_{\mathrm{HI}}(5.5) \leq 10^{-4}$ inferred from the Gunn-Peterson effect hold, and if we assume that reionization from stars takes place abruptly in one step, then a mixed model with DM annihilation in halos and star formation at $z \simeq 6.5$ could explain simultaneously CMB observations and the above bounds. However, these models tend to reheat the IGM well above the typical temperatures indicated by Lyman-α observations, unless our modeling of the matter temperature evolution at low redshift is incorrect.

Our most important conclusion is that constraints on DM annihilation in halos tend to be stronger than those from the smooth background distribution of DM, especially if we include a realistic upper bound on the matter temperature at low redhsift. Assuming Press-Schechter theory and NFW profiles, we see from eq. (4.40) that for $f_{\mathrm{NFW}}(c_{\mathrm{h}}) = 10^3$, $z_{\mathrm{F}} = 60$ and $[p_{\mathrm{ann}}(600)/p_{\mathrm{ann}}(0)] = 5$, the constraint coming from halos and from the smooth background are comparable. If in reality halos are more concentrated than in this simple model, then constraints on p_{ann} from annihilation in halos superseed those from annihilation in the background. We summarize our constraints on p_{ann} and their implications for the DM mass and cross-section in figure 4.14. A WIMP with standard thermal cross-section $\langle \sigma v \rangle \simeq 3 \times 10^{-26} \, \mathrm{cm}^3/\mathrm{s}$ is constrained by annihilations in the smooth background to have a mass larger than $18 \times f(z = 600) \, \mathrm{GeV}/c^2$ (95% C. L.). According to our simple model for DM annihilation in halos, the bound increases to about $100[\frac{f_{\mathrm{NFW}}}{10^4}]f(0) \, \mathrm{GeV}/c^2$ in order to avoid reionizing the universe too early (or even $1700[\frac{f_{\mathrm{NFW}}}{10^4}]f(0) \, \mathrm{GeV}/c^2$ when including IGM temperature bounds).

This work contains a systematic analysis of DM annihilation in halos, where values of unknown parameters (including those describing structure formation) are freely varied and fitted to the data. Several authors have previously investigated the effect of DM
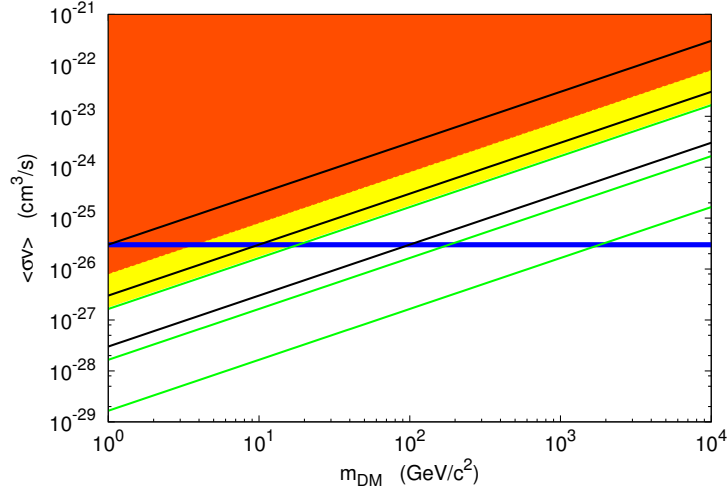
Figure 4.14 – Summary of our bounds on p_{ann} translated into constraints for the DM annihilation thermal cross-section $\langle \sigma v \rangle$ and mass m_{DM}. Points in the shaded regions are above the 95% preferred region for $p_{ann}(z = 600)$, considering only annihilation in the smooth DM background, and assuming either $f(z = 600) = 0.2$ (dark shade) or $f(z = 600) = 0.9$ (light shade): these two extreme assumptions cover the plausible range for $f(z = 600)$ in the case of WIMP annihilation, see [87]. The three black lines correspond to the CMB bounds inferred from DM annihilation in halos, assuming $f_{NFW}(c_h) = 10^3$ (top), 10^4 (middle) or 10^5 (bottom), and taking in all three cases $z_F = 60$ and $f(z \simeq 0) = 0.1$ (or in other words, $f(z = 600) = 0.5$ and $[p_{ann}(600)/p_{ann}(0)] = 5$). When a realistic upper bound on the matter temperature at low redshift is taken into account, the bounds move to the green lines. The horizontal lines shows the standard WIMP thermal cross-section.

annihilation in halos, for particular models with fixed parameter values. The authors of [84, 85, 91] reached the conclusion that annihilation in halos is usually inefficient. Indeed, they choose some DM density profiles corresponding roughly to $f_{NFW} = 100$ or 400. We found that halo bounds become stronger than smooth background bounds only for $f_{NFW} > 4200$. Hence our results are not contradicting these previous works.

Many aspects of this analysis could be improved. For example, we neglected Helium throughout the whole discussion. The effect of Helium has been studied by Galli et al. [89] (neglecting halo effects) and does not change the result significantly. The energy fraction going into ionization χ_i and Lyman-α excitation χ_α was also approximated, motivated by a common sense argument by Chen and Kamionkowski [93]. However, the exact behavior of these quantities have a negligible effect on the CMB. The average DM density during non-linear structure formation has been approximated with a basic Press-Schechter model and NFW profiles. We could have imposed priors on the parameters of this model inferred from N-body simulations, or tried different profiles (Einasto profile, etc.), or a more realistic differential mass function [118]. Instead of the Press-Schechter model, we could

have accounted for halo formation using the excursion set formalism [130]. One could try to model the matter temperature evolution at low redshift more accurately, taking into account matter inhomogeneities and the complicated thermodynamical evolution of the IGM (including, for instance, line cooling or Bremsstrahlung effects). However, all these refinements are probably unnecessary at the moment, given the large error bars on the optical depth inferred from CMB observations.

Throughout this work, we assumed that DM annihilates. A similar study can be performed in the case of decaying dark matter [93, 95, 96, 97]. In that case, the energy injection rate varies like $\bar{\rho}_{\mathrm{DM}}$ (instead of $\bar{\rho}_{\mathrm{DM}}^2$), i.e. like $(1+z)^3$. Hence, the effect of DM decay in the smooth DM background is not very different from the effect of DM annihilation in halos, studied in section 4.4. Note however that for a wide range of masses, constraints on the DM lifetime inferred from current CMB observations are not as strong as those inferred from cosmic rays [131, 132].

In a few months from now, results from the Planck satellite data may lead to a significant improvement of these bounds, and bring complementary information on the DM mass and cross-section (or lifetime) with respect to direct and other indirect DM search.

5 Decaying Dark Matter

Foreword

In chapter 4, we focused in particular on a stable DM component, and only studied the potential impact of its annihilation. In this chapter, we instead investigate the eventual decay of DM. As a first remark, it is important to understand that there is still some amount of model dependence in the work presented here. Indeed, we assumed that the decay product of theses particles were relativistic – an assumption that could be relaxed in a future work. We also supposed that they were sterile, as they would otherwise reheat the plasma, and refer to the work presented in the previous chapter. It nonetheless already covers a large fraction of the models, where the decay products are much lighter than the DM particle. Note that it is an effect present in any case, although it might be subdominant in some scenarios.

We mention in the paper the case of the majoron particle (that can act as both a DM candidate and an explanation for the neutrino masses), but it is worth noting that it is possible to have such decaying particles within the SUSY framework. Although such decays would be forbidden by R-parity, one could easily imagine this symmetry to be slightly broken, allowing the LSP to decay into SM particles. An additional advantage from having R-parity violating SUSY would be to provide an alternative to sphalerons for generating the baryon asymmetry of the universe [133].

By implementing the equations of motion of this decaying DM in the synchronous gauge, comoving with a standard DM component, there was one potential caveat: the definition of the gauge normally imposes to the velocity divergence of DM to vanish. With two DM components, it could be problematic to decide which one to fix. We show in section 5.2.2 that it actually causes no problem, and is rigorously defined – the result was cross-checked with coding the equations in Newtonian gauge as well. In any case, this result was not used in the paper because we studied only the case where DM is entirely decaying.

The final bound, obtained by doing a complete parameter extraction using Planck likelihoods, WMAP polarization, LSS data from WiggleZ and the BAO measurement from BOSS, is of the order of $200\,\mathrm{Gyr}$ for a DM particle decaying into relativistic species. Although being largely model-independent, it can be translated to direct implications for some models. The impact on the majoron case is discussed in the conclusion, but the impact on R-parity violating SUSY models is not easily quantified. Indeed, by allowing R-parity violation, the size of the SUSY parameter space increases greatly – essentially by 45 additional Yukawa couplings, and the possibility for a different LSP than the usual neutralino [134]. Nonetheless, with such a signature, neutralino LSP would be favored, and the loose constraint of $\tau_{\mathrm{LSP}} > 1\,\mathrm{s}$ coming from the primordial abundance of light nuclei is severely tightened.

Finally, it has to be noted that if the decay products are SM neutrinos, much tighter constraints exist on the lifetime of DM particles with a mass in the range of $1\,\mathrm{GeV}$ to a few TeV, coming from gamma-ray flux [135]. This, however, leaves a window of possible SUSY candidates unconstrained, as well as lighter DM candidates.

Strongest model-independent bound on the lifetime of Dark Matter

Benjamin Audren, Julien Lesgourgues, Gianpiero Mangano, Pasquale Dario Serpico, and Thomas Tram

Abstract: Dark Matter is essential for structure formation in the late Universe so it must be stable on cosmological time scales. But how stable exactly? Only assuming decays into relativistic particles, we report an otherwise model independent bound on the lifetime of Dark Matter using current cosmological data. Since these decays affect only the low-ℓ multipoles of the CMB, the Dark Matter lifetime is expected to correlate with the tensor-to-scalar ratio r as well as curvature Ω_k. We consider two models, including r and $r + \Omega_k$ respectively, versus data from Planck, WMAP, WiggleZ and Baryon Acoustic Oscillations, with or without the BICEP2 data (if interpreted in terms of primordial gravitational waves). This results in a lower bound on the lifetime of CDM given by $160 \, \mathrm{Gyr}$ (without BICEP2) or $200 \, \mathrm{Gyr}$ (with BICEP2) at 95% confidence level.

5.1 Introduction

5.1.1 Stability and particle physics

Although the existence of *dark matter* (DM) is well established by a large number of observations in cosmology and astrophysics, we have presently very few clues on its particle physics nature. This is mostly due to the purely gravitational origin of the evidence collected so far, which does not provide any handle for particle identification. While a number of strategies are ongoing to constrain or detect different classes of models, it is worth remarking that already some of the most basic DM properties can help shedding light on its nature. One such example is provided by the high stability that this species must possess. If one thinks of the Standard Model (SM) of particle physics, most of its particles are unstable: exact stability is in fact the exception and must be enforced by some exact symmetry, such as the unbroken QED gauge symmetry for the electron or Lorentz symmetry for the lightest neutrino. Much more frequent are examples of meta-stability due to some approximate symmetries, such as for the heavier neutrino states, for the ones often found in nuclear physics (including the neutron decay) due to mass quasi-degeneracies, and, possibly, for the proton itself if the accidental baryon number symmetry is broken at some very high energy scale as in Grand Unified gauge theories. In fact, this kind of considerations provides a useful guideline in DM model building, see e.g. [136].

Loosely speaking, one knows that the DM lifetime should be at least comparable to the

lifetime of the universe, otherwise it could not fulfil its role in structure formation and astrophysical observations. However, inferring from that phenomenological condition an infinite lifetime is a strong prejudice dictated by simplicity, but with very little empirical or theoretical justification. For example, for typical WIMP candidates one often *assumes* a discrete Z_2 symmetry under which the SM particles and DM have opposite charge, but it is easily conceivable that this symmetry is broken at a more fundamental level, with the only requirement that the lifetime of the DM particle is sufficiently long. Stringent bounds on the lifetime τ of WIMP DM candidates with electroweak scale masses come, for example, from the diffuse gamma ray flux , at the level of $\tau \gg 10^{26}$ s, see for instance [132]. Hence, allowed timescales for the decay should be longer than a billion times the lifetime of the universe, which would exclude any plausible effect on gravitational structures.

5.1.2 Gravitational effects

The drawback of these considerations is their model-dependence. In particular, the bounds depend on the nature and energy distribution of the by-products of the decay. Interestingly, however, looser but way more general and robust constraints can be obtained again from purely gravitational considerations. The key property that allows one to constrain the DM lifetime gravitationally is that in the decay process, a non-relativistic (usually cold) DM component is replaced by a combination of radiation and of massive particles, which in turn have a finite velocity dispersion. This alters notably the growth of structures. More specifically, if significant DM decay takes place, the background evolution of the universe can show departure from the standard case and affect several cosmological observables (e.g. the size of the sound horizon at recombination). At the perturbation level, one also expects an enhancement of the Late Integrated Sachs-Wolfe (LISW) effect, beyond the one due to the cosmological constant, as shown in [94] and described in section 5.3 below.

5.1.3 Previous works

In the past decade, several studies have derived constraints on the DM lifetime using cosmological data, starting from the study of decaying hot neutrino DM in [137]. The case of decaying cold DM was first analysed by Ichiki et al. [94], who found a 95% C.L. bound of 52 Gyr using WMAP-1yr temperature C_ℓ data, and assuming decay into fully relativistic species. Ref. [138] developed the formalism to describe the cosmological effects of an unstable relic and its relativistic decay products, both at the background and perturbation levels. Since then, the bounds have been refined in two ways. First, more data sets on CMB temperature/polarization and on large scale structures have been included in the analysis. For example, by including WMAP-5yr, Type Ia supernova data, Lyman$-\alpha$ forest, large scale structure and weak lensing observations, Ref. [139] obtained a bound of 100 Gyr (and also updated or corrected previous bounds from [140, 141, 142]).

Second, some more general bounds have been obtained by allowing the daughter particles to be massive and thus non-relativistic or only mildly relativistic, see for instance [143, 144, 145, 146, 147]. Most recently, a detailed formulation of the problem, both in presence of massless or massive decay products, has been given in [148]. In this reference, it has been additionally shown that the impact of σ_8 constraints are also important, and that a possible tension between the value of σ_8 inferred from Planck SZ cluster data and the one extrapolated from CMB temperature data could be resolved by assuming $\tau \sim 200\,\mathrm{Gyr}$ and relativistic daughter particles. However, this estimate did not account for parameter degeneracies, and relied on the assumption that Planck SZ cluster results are not affected by systematic errors.

5.1.4 Scope and outline of this paper

In this paper, we aim at updating cosmological bounds on the DM lifetime with a proper statistical analysis, accounting for degeneracies and correlations with other cosmological parameters, as well as estimating the *cosmological model dependence* of the bound thus obtained. In particular, we will check for degeneracies between decaying DM and spatial curvature, since both can have somewhat similar effects on the CMB. We also consider the impact of including or not BICEP2 results [15] on B-mode polarisation interpreted in terms of r.

In the following, we limit ourselves to the case of relativistic decay products, leaving the case of non-relativistic species for future investigation. Note that this case is nonetheless representative of several DM candidates, for which the decay products are either massless, or at least well inside the relativistic regime. This is usually the case, provided that the produced particles have a much smaller mass than the decaying DM matter particle, and that the decay happens reasonably late. The decay products could consist either in non-standard particles, or in standard model neutrinos produced with typical momenta much larger than their mass. A notable case of such a DM candidate is represented by the majoron J, with mass in the keV range [149, 140, 141, 150, 151]. In the simplest *see-saw*-like models, the leading decay channel is in two relativistic neutrinos. The majoron lifetime is then inversely proportional to the square of standard active neutrino masses m_ν,

$$\tau_J = \frac{16\pi}{m_J} \frac{v^2}{m_\nu^2} \ . \tag{5.1}$$

Here m_J is the Majoron mass, and v the lepton number breaking scale [152]. Bounds on τ_J can be used to constrain the value of v as function of the standard neutrino mass scale. Note that while the results of our study apply also to heavier DM candidates producing energetic neutrinos, these scenarios are better constrained using e.g. limits on the neutrino flux in the Milky Way, leading to stronger bounds (exceeding 10^6 Gyr, see for instance [135]) than what is found by using cosmological data only. On the other

hand, the constraints discussed here are basically the only limits applying to dark matter decaying into unspecified, non-standard forms of *dark radiation.*

This paper is structured as follows. In Section 5.2 we recall the formalism describing a cosmological scenario with a decaying DM candidate, both for the background and perturbation evolution. Note that we present perturbation equations both in the synchronous gauge (the only case treated in the previous literature) and in Newtonian gauge, which allowed us to double-check the numerical results we obtained. We then describe their implementation in the public numerical code CLASS[1] [23, 24]. Section 5.3 contains a short description of data sets used in the analysis and our results, and in Section 5.4 we conclude and give our outlooks.

5.2 Equations and implementation

5.2.1 Background equations

The background density of the decaying cold DM (dcdm) and of the produced decay radiation (dr) is governed by the two equations

$$\rho_{\mathrm{dcdm}}' = -3\frac{a'}{a}\rho_{\mathrm{dcdm}} - a\,\Gamma_{\mathrm{dcdm}}\,\rho_{\mathrm{dcdm}}\;, \tag{5.2}$$

$$\rho_{\mathrm{dr}}' = -4\frac{a'}{a}\rho_{\mathrm{dr}} + a\,\Gamma_{\mathrm{dcdm}}\,\rho_{\mathrm{dcdm}}\;, \tag{5.3}$$

where Γ_{dcdm} is the decay rate defined with respect to proper time, and primes denote derivatives with respect to conformal time. In the language of CLASS, ρ_{dr} and ρ_{dcdm} fall into the category of {B}-variables since they must be evolved alongside the scale factor[2]. Choosing the fractional energy density in decaying DM plus decay radiation today, $\Omega_{\mathrm{dcdm}} + \Omega_{\mathrm{dr}}$, CLASS then finds the corresponding initial condition by using a shooting method. However, since the initial scale factor is set dynamically by the code, we must formulate our initial condition such that it is independent of a in the infinite past. Hence, the target of the shooting method is to find the correct value of the DM energy in a typical comoving volume, $E_{\mathrm{ini}} \equiv a_{\mathrm{ini}}^3\,\rho_{\mathrm{dcdm}}(a_{\mathrm{ini}})$. At the same time, we fix the initial condition for the density of decay radiation using the asymptotic solution of Eqs. (5.2, 5.3) for a going to zero.

---

[1] www.class-code.net
[2] www.cern.ch/lesgourg/class-tour/lecture1.pdf

5.2.2 Perturbation equations in synchronous gauge

At the level of scalar perturbations, the transfer of energy between the dcdm and dr species is encoded into the continuity and Euler equations of the type

$$T^{\mu 0}_{\mathrm{dcdm};\mu} = -C \ , \qquad T^{\mu 0}_{\mathrm{dr}\ ;\mu} = C \ , \tag{5.4}$$

$$\partial_i T^{\mu i}_{\mathrm{dcdm};\mu} = -D \ , \qquad \partial_i T^{\mu i}_{\mathrm{dr}\ ;\mu} = D \ . \tag{5.5}$$

The coupling terms C, D accounting for the decay of non-relativistic particles take a trivial form in the synchronous gauge comoving with the decaying species dcdm, i.e. in the gauge such that the metric perturbations δg_{00}, δg_{i0} and the velocity divergence θ_{dcdm} vanish. In this gauge, denoted by the index (s), $C^{(s)}$ is given by the product of the conformal decay rate, the dcdm particle rest mass and the local value of the number density of these particles. Expanding this quantity in background and perturbations, one gets

$$C^{(s)} = a\, \Gamma_{\mathrm{dcdm}}\, \rho_{\mathrm{dcdm}} \left(1 + \delta_{\mathrm{dcdm}}\right) \ . \tag{5.6}$$

In the same gauge, the decays do not create any additional flux divergence, and $D^{(s)} = 0$. Note that assuming similar expressions for C and D in other gauges would lead to wrong results. The Euler equation derived from (5.5) for dcdm in the synchronous gauge (s) then reads

$$\theta^{(s)}_{\mathrm{dcdm}}{}' = -\frac{a'}{a}\, \theta^{(s)}_{\mathrm{dcdm}} = 0 \ . \tag{5.7}$$

Given adiabatic initial conditions there is no reason for ordinary DM (cdm) and dcdm not to be aligned at early times. Hence, one can fully specify the synchronous gauge by choosing an initial equal-time hypersurface such that $\theta_{\mathrm{dcdm}} = \theta_{\mathrm{cdm}} = 0$. It follows that they will remain zero at any time and we conclude that the synchronous gauge comoving with cold DM is simultaneously comoving with dcdm. Therefore, one can refer to a single synchronous gauge (s), in which the Euler equations for both cdm and dcdm can be omitted.

5.2.3 Perturbation equations in Newtonian gauge

Since the CLASS code is written in both synchronous and Newtonian gauge, we wish to derive the full set of equations in both gauges, while the previous literature only presented synchronous equations. Implementing both gauges allows for a useful consistency check, since one must recover the same observables in the two gauges. After writing the continuity and Euler equations in the synchronous gauge, we gauge-transform them using Eqs. (27a-27b) of [19], which take a slightly more complicated form in presence of a

	Synchronous	Newtonian
$\mathfrak{m}_{\text{cont}}$	$\dot{h}/2$	$-3\dot{\phi}$
$\mathfrak{m}_{\psi}$	0	ψ
$\mathfrak{m}_{\text{shear}}$	$(\dot{h} + 6\dot{\eta})/2$	0

Table 5.1 – Metric source terms for scalar perturbations in synchronous and Newtonian gauge.

decay rate:

$$\delta_{\text{dcdm}}^{(s)} = \delta_{\text{dcdm}}^{(n)} + \left(3\frac{a'}{a} + a\,\Gamma_{\text{dcdm}}\right)\alpha \ , \tag{5.8}$$

$$\delta_{\text{dr}}^{(s)} = \delta_{\text{dr}}^{(n)} + \left(4\frac{a'}{a} - a\,\Gamma_{\text{dcdm}}\frac{\rho_{\text{dcdm}}}{\rho_{\text{dr}}}\right)\alpha \ , \tag{5.9}$$

$$\theta_{\text{dr}}^{(s)} = \theta_{\text{dr}}^{(n)} - k^2\alpha = 0 \ , \tag{5.10}$$

with k the wavenumber, $\alpha \equiv (h' + 6\eta')/2k^2$ and where we address the reader to [19] for the (by now standard) notation of the different potentials. The final set of equations in *both* gauges can be written as

$$\delta_{\text{dcdm}}' = -\theta_{\text{dcdm}} - \mathfrak{m}_{\text{cont}} - a\,\Gamma_{\text{dcdm}}\mathfrak{m}_{\psi} \ , \tag{5.11}$$

$$\theta_{\text{dcdm}}' = -\frac{a'}{a}\,\theta_{\text{dcdm}} + k^2\mathfrak{m}_{\psi} \ , \tag{5.12}$$

$$\delta_{\text{dr}}' = -\frac{4}{3}\left(\theta_{\text{dcdm}} + \mathfrak{m}_{\text{cont}}\right) + a\,\Gamma_{\text{dcdm}}\frac{\rho_{\text{dcdm}}}{\rho_{\text{dr}}}\left(\delta_{\text{dcdm}} - \delta_{\text{dr}} + \mathfrak{m}_{\psi}\right) \ , \tag{5.13}$$

$$\theta_{\text{dr}}' = \frac{k^2}{4}\delta_{\text{dr}} - k^2\sigma_{\text{dr}} + k^2\mathfrak{m}_{\psi} - a\,\Gamma_{\text{dcdm}}\frac{3\rho_{\text{dcdm}}}{4\rho_{\text{dr}}}\left(\frac{4}{3}\theta_{\text{dr}} - \theta_{\text{dcdm}}\right) \ , \tag{5.14}$$

where the metric source terms $\mathfrak{m}_{\text{cont}}$ and $\mathfrak{m}_{\psi}$ are given in Table 5.1.

5.2.4   Boltzmann hierarchy for decay radiation

The full perturbations of the decay radiation distribution function can be written in different ways. We adopt here the same set of equations as in [138], in which the perturbations of the (integrated) phase-space distribution function are defined as

$$F_{\text{dr}} \equiv \frac{\int dq q^3 f_{\text{dr}}^0 \Psi_{\text{dr}}}{\int dq q^3 f_{\text{dr}}^0} r_{\text{dr}} \ , \tag{5.15}$$

with r_{dr} defined as

$$r_{\text{dr}} \equiv \frac{\rho_{\text{dr}} a^4}{\rho_{\text{cr},0}} \ , \tag{5.16}$$

where the the critical energy density today, $\rho_{\mathrm{cr},0}$, has been introduced to make r_{dr} dimensionless. The derivative of r_{dr} is given by

$$r_{\mathrm{dr}}' = a\,\Gamma_{\mathrm{dcdm}}\rho_{\mathrm{dcdm}}/\rho_{\mathrm{dr}}\ , \tag{5.17}$$

so that r_{dr} is constant in absence of a source. The point of introducing such a factor in the definition of F_{dr} is to cancel the time-dependence F_{dr} due to the background distribution function f_{dr}^0 in the denominator of equation (5.15). This simplifies the Boltzmann hierarchy for the Legendre multipoles $F_{\mathrm{dr},\ell}$, which obey the following equations

$$F_{\mathrm{dr},0}' = -kF_{\mathrm{dr},1} - \frac{4}{3}r_{\mathrm{dr}}\mathfrak{m}_{\mathrm{cont}} + r_{\mathrm{dr}}'\left(\delta_{\mathrm{dcdm}} + \mathfrak{m}_\psi\right)\ , \tag{5.18}$$

$$F_{\mathrm{dr},1}' = \frac{k}{3}F_{\mathrm{dr},0} - \frac{2k}{3}F_{\mathrm{dr},2} + \frac{4k}{3}r_{\mathrm{dr}}\mathfrak{m}_\psi + \frac{r_{\mathrm{dr}}'}{k}\theta_{\mathrm{dcdm}}\ , \tag{5.19}$$

$$F_{\mathrm{dr},2}' = \frac{2k}{5}F_{\mathrm{dr},1} - \frac{3k}{5}F_{\mathrm{dr},3} + \frac{8}{15}r_{\mathrm{dr}}\mathfrak{m}_{\mathrm{shear}}\ , \tag{5.20}$$

$$F_{\mathrm{dr},\ell}' = \frac{k}{2\ell+1}\left(\ell F_{\mathrm{dr},\ell-1} - (\ell+1)F_{\mathrm{dr},\ell+1}\right),\quad \ell > 2\ . \tag{5.21}$$

The expression for $\mathfrak{m}_{\mathrm{shear}}$ can be found in Table 5.1. For the sake of simplicity, we have reported these equations in a spatially flat universe, but for our analysis we implemented the equations in a general curved FLRW model, following [20]. The Boltzmann hierarchy is truncated at some $\ell_{\max}$ following the prescription of [19] generalised to spatial curvature [20].

5.3 Comparison with data

5.3.1 Observable effects

When discussing the effect of a given parameter on the CMB describing some new physics, one should specify which other parameters are kept fixed. The best choice is the one allowing to cancel all trivial effects, in order to isolate the distinct residual effect associated to the new physics.

Here the focus is on the effect of the DM decay rate Γ_{dcdm}. If we were varying Γ_{dcdm} while keeping the DM density fixed *today* (either the physical density $\omega_{\mathrm{dcdm}} = \Omega_{\mathrm{dcdm}}h^2$ or fractional density Ω_{dcdm}), the code would automatically adjust initial conditions in the early universe. The direct effect of Γ_{dcdm} on the perturbations would then be mixed with that of changing the early cosmological evolution, and in particular the redshift of equality.

Hence, a better choice is to fix all initial conditions, so that varying Γ_{dcdm} only affects the late cosmological evolution. In order to do this easily, we implemented an alternative parametrisation in CLASS. Instead of providing $\omega_{\mathrm{dcdm+dr}}$ or $\Omega_{\mathrm{dcdm+dr}}$ as input and letting

the code compute the initial dcdm density, the user can choose to pass the initial density of decaying DM (in dimensionless units, as $\Omega_{\text{dcdm}}^{\text{ini}} \equiv (\rho_{\text{dcdm}}^{\text{ini}} a^3/\rho_{\text{cr},0})$ or $\omega_{\text{dcdm}}^{\text{ini}} \equiv \Omega_{\text{dcdm}}^{\text{ini}} h^2)$, and the code will find the correct density today. Note however, that this procedure also involves a shooting method in order to satisfy the closure equation $\sum_i \Omega_i = 1 - \Omega_k$. With this approach, we preserve the full cosmological evolution at least until photon decoupling, since for realistic values of Γ_{dcdm} allowed by observations, the DM decay is only significant at late time, long after photon decoupling. In particular, the effects of Γ_{dcdm} on the CMB are the following:

i) a change in the angular diameter distance to decoupling, shifting the whole CMB spectra in multipole space;

ii) a late Integrated Sachs-Wolfe (ISW) effect, since a modification of the homogeneous and perturbed density of DM at late times affects the evolution of metric fluctuations through the Poisson equation;

iii) a different amount of CMB lensing, affecting the contrast between maxima and minima in the lensed CMB spectra.

To check (ii), we plot in Figure 5.1 the unlensed temperature spectrum of models with Γ_{dcdm} set either to 0 or $20\,\text{km s}^{-1}\text{Mpc}^{-1}$ [3]. To keep the early cosmological evolution fixed, we stick to constant values of the density parameters $(\omega_{\text{dcdm}}^{\text{ini}}, \omega_{\text{b}})$, of primordial spectrum parameters (A_s, n_s) and of the reionization optical depth τ_{reio}. Of course, for $\Gamma_{\text{dcdm}} = 0$, the dcdm species is equivalent to standard cold DM with a current density $\omega_{\text{cdm}} = \omega_{\text{dcdm}}^{\text{ini}}$. We need to fix one more background parameter in order to fully specify the late cosmological evolution. Possible choices allowed by CLASS include h, or the angular scale of the sound horizon at decoupling, $\theta_s = r_s(t_{\text{dec}})/d_s(t_{\text{dec}})$. We choose to stick to a constant value of θ_s, in order to eliminate the effect (i) described above, and observe only (ii). We see indeed in Figure 5.1 that with such a choice, the spectra of the stable and decaying DM models overlap everywhere except at small multipoles. To check that this is indeed due to a different late ISW effect, we show in Figure 5.2 the decomposition of the total spectrum in individual contribution, for the stable model and a dcdm model in which the decay rate was pushed to $100\,\text{km s}^{-1}\text{Mpc}^{-1}$.

Since the dominant effect of decaying DM is a modification of the small-ℓ part of the CMB temperature spectrum, in the rest of the analysis, it will be relevant to investigate degeneracies between Γ_{dcdm} and other parameters affecting mainly the large-angle CMB spectra, like the spatial curvature parameter Ω_k or the tensor-to-scalar ratio r (defined throughout this paper at the pivot scale $k_* = 0.05/\text{Mpc}$). We show examples of such models in Figure 5.1, from which it is not obvious that very small variations of Γ_{dcdm}, Ω_k and r can be distinguished, given the cosmic variance uncertainty on low ℓ's. It is useful to plot the matter power spectrum $P(k)$ of the same models, to see whether CMB lensing or direct measurements of $P(k)$ can help to reduce the degeneracy. This is done in Figure 5.3. We see that all the parameters discussed here have a different effect on

---

[3]It is useful to bear in mind the conversion factor $1\,\text{km s}^{-1}\text{Mpc}^{-1} = 1.02 \times 10^{-3}\text{Gyr}^{-1}$.
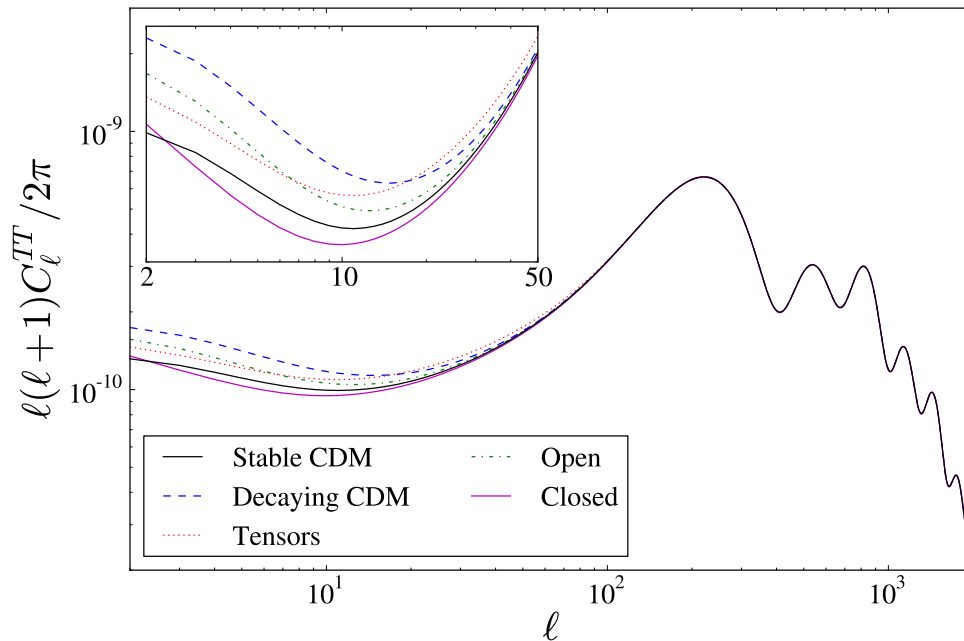
Figure 5.1 – CMB temperature power spectrum for a variety of models, all with the same parameters $\{100\,\theta_s, \omega_{\mathrm{dcdm}}^{\mathrm{ini}}, \omega_{\mathrm{b}}, \ln(10^{10}A_s), n_s, \tau_{\mathrm{reio}}\} = \{1.04119, 0.12038, 0.022032, 3.0980, 0.9619, 0.0925\}$ taken from the Planck+WP best fit [11]. For all models except the "Decaying CDM" one, the decay rate Γ_{dcdm} is set to zero, implying that the "dcdm" species is equivalent to standard cold DM with a present density $\omega_{\mathrm{cdm}} = \omega_{\mathrm{dcdm}}^{\mathrm{ini}} = 0.12038$. The "Decaying CDM" model has $\Gamma_{\mathrm{dcdm}} = 20\,\mathrm{km\ s^{-1}Mpc^{-1}}$, the "Tensors" model has $r = 0.2$, and the "Open" ("Closed") models have $\Omega_k = 0.02$ (-0.2). The main differences occur at low multiples and comes from either different late ISW contributions or non-zero tensor fluctuations.

$P(k)$. Playing with tensor modes leaves the matter power spectrum invariant, since it is related to scalar perturbations only. Varying Γ_{dcdm} changes $P(k)$ slightly for several reasons:

- the different background evolution of ρ_{dcdm} leads to an overall vertical shift of the spectrum;
- the different values of h needed to get the same θ_s changes the ratio of the Hubble scale at equality and today, hence shifting the spectrum horizontally;
- on top of these shifting effects, the different evolution of δ_{dcdm} is such that dcdm has a reduced linear growth factor, affecting the actual shape of the matter power spectrum.

When introducing the curvature parameter, one gets a combination of the first two effects only. Moreover, variations of Γ_{dcdm} and Ω_k leading to an effect in the CMB of the same
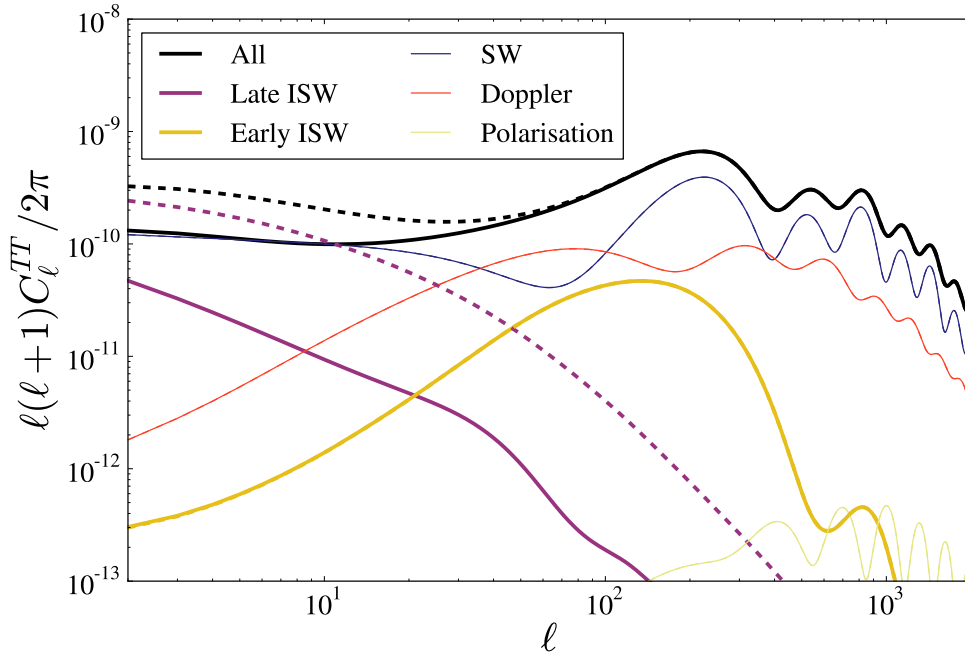
Figure 5.2 – The single contributions to the CMB temperature spectrum (Sachs-Wolfe, early and late Integrated Sachs-Wolfe, Doppler and polarisation-induced) for a stable model (solid) and a dcdm model (dashed) with $\Gamma_{\text{dcdm}} = 100$ km/s/Mpc. The value of other parameters is set as in Figure 5.1. We see that only the late ISW effect is sensitive to the decay rate (for other contributions, solid and dashed lines are indistinguishable).

amplitude give effects on the $P(k)$ with very different amplitudes. This comparison shows that, at least in principle, CMB lensing effects and direct constraints on $P(k)$ may help to break degeneracies, and to measure Γ_{dcdm} independently of Ω_k and r. This can only be confirmed by a global fit to current observations.

5.3.2 The data

The parameter extraction is done using a Metropolis Hastings algorithm, with a Cholesky decomposition to better handle the large number of nuisance parameters [46]. We investigate two combinations of experiments which we denote by A and B. Both share the Planck likelihoods, consisting of the low-ℓ, high-ℓ, lensing reconstruction and low-ℓ WMAP polarisation, as well as the WiggleZ data [153], and the BOSS measurement of the Baryon Acoustic Oscillation scale at $z = 0.57$ [154]. The set B adds the BICEP2 public likelihood code [15]. We used the publicly available Monte Python[4] code [1] for the analysis.

---

[4]https://github.com/baudren/montepython_public
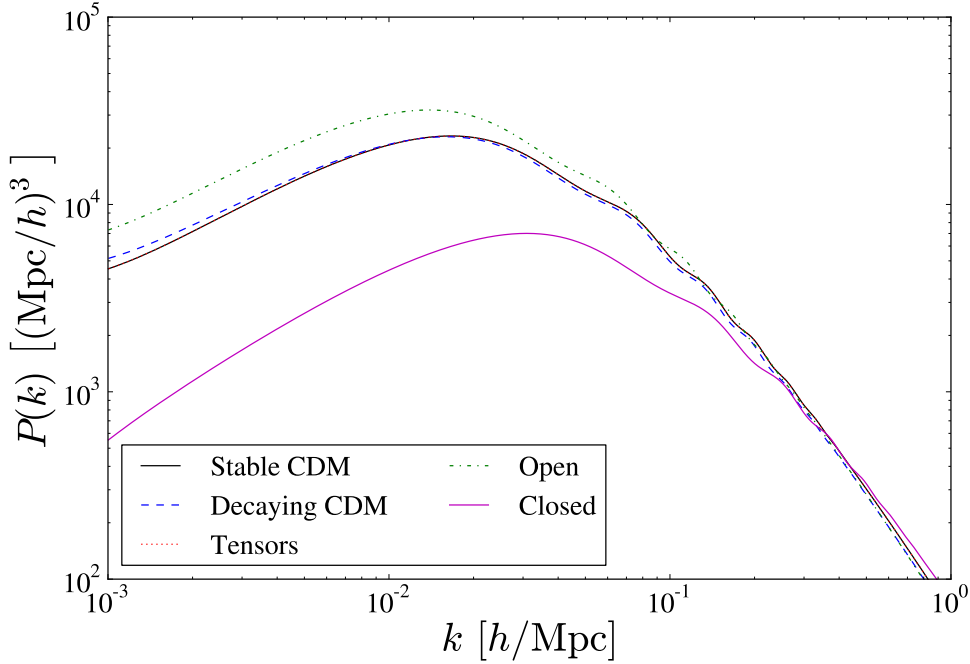
Figure 5.3 – Matter power spectrum $P(k)$ (computed in the Newtonian gauge) for the same models considered in Figure 5.1. The black curve (Stable CDM) is hidden behind the red one (Tensors).

We performed the analysis selecting flat priors for the following set of parameters

$$\{\omega_b, H_0, A_s, n_s, \tau_{\text{reio}}, \omega_{\text{dcdm+dr}}, \Gamma_{\text{dcdm}}, r, \Omega_k\} \ ,$$

in addition to the other nuisance parameters for the Planck likelihood, omitted here for brevity. The first five cosmological parameters stand respectively for the baryon density, the Hubble parameter, the amplitude at $k_* = 0.05/\text{Mpc}$ and tilt of the initial curvature power spectrum, and the optical depth to reionisation. The next parameter $\omega_{\text{dcdm+dr}}$ denote the physical density of decaying dark matter plus its decay product today (in practise, $\omega_{\text{dcdm+dr}}$ is extremely close to ω_{dcdm} up to typically 4%). Finally, the last two parameters are the dcdm decay rate and the tensor-to-scalar ratio, also measured at the pivot scale $k_* = 0.05/\text{Mpc}$. In some of our runs, we vary the curvature parameter $\Omega_k = 1 - \Omega_{\text{tot}}$.

The tensor tilt n_t is set to satisfy the self-consistency condition from inflation, *i.e* $n_t = -r/8(2 - r/8 - n_s)$, whereas the tensor running α_t is neglected. For the neutrino sector, for simplicity, we performed the same assumption as in [11] (two relativistic neutrinos and one with a mass of 0.06 eV).

5.3.3 Results

The results are summarized in table 5.2 and figs. 5.4 and 5.5.

Model	ΛCDM + $\{\Gamma_{\text{dcdm}}, r\}$		ΛCDM + $\{\Gamma_{\text{dcdm}}, r, \Omega_k\}$	
Data	A	B	A	B
$100\,\omega_{\text{b}}$	$2.231^{+0.025}_{-0.024}$	$2.226^{+0.024}_{-0.024}$	$2.247^{+0.028}_{-0.030}$	$2.247^{+0.028}_{-0.029}$
H_0 [km/s/Mpc]	$68.89^{+0.62}_{-0.61}$	$68.92^{+0.61}_{-0.62}$	$68.21^{+0.79}_{-0.79}$	$68.07^{+0.83}_{-0.80}$
$10^9 A_s$	$2.145^{+0.044}_{-0.050}$	$2.143^{+0.044}_{-0.047}$	$2.157^{+0.046}_{-0.054}$	$2.156^{+0.045}_{-0.052}$
n_s	$0.9643^{+0.0055}_{-0.0056}$	$0.9666^{+0.0055}_{-0.0056}$	$0.9705^{+0.0071}_{-0.0077}$	$0.9742^{+0.0072}_{-0.0076}$
τ_{reio}	$0.082^{+0.012}_{-0.011}$	$0.082^{+0.011}_{-0.011}$	$0.08676^{+0.012}_{-0.013}$	$0.08792^{+0.011}_{-0.013}$
$\omega_{\text{dcdm+dr}}$	$0.1142^{+0.0016}_{-0.0014}$	$0.1142^{+0.0017}_{-0.0014}$	$0.1117^{+0.0026}_{-0.0023}$	$0.1113^{+0.0025}_{-0.0023}$
Γ_{dcdm} [km s^{-1}Mpc^{-1}]	< 5.9	< 5.0	< 6.0	< 4.9
r	< 0.13	$0.164^{+0.032}_{-0.040}$	$0.05273^{+0.012}_{-0.053}$	$0.1713^{+0.033}_{-0.039}$
$10^2\Omega_k$	$-$	$-$	$-0.3517^{+0.28}_{-0.26}$	$-0.4405^{+0.30}_{-0.27}$
τ_{dcdm} [Gyr]	> 160	> 200	> 160	> 200

Table 5.2 – Marginalised Bayesian credible intervals for the cosmological parameters of the models considered in our analysis. We quote either mean values and 68% confidence levels or 95% upper/lower bounds. The last lines show the results for the derived parameter $\tau_{\text{dcdm}} = 1/\Gamma_{\text{dcdm}}$ representing the dcdm lifetime (assuming a flat prior on the rate Γ_{dcdm}, and not on the lifetime).

For the ΛCDM + $\{\Gamma_{\text{dcdm}}, r\}$ model, we find that the best-fit model has a negligible decay rate. Using the A dataset, the upper bound is $\Gamma_{\text{dcdm}} < 5.9\,\text{km s}^{-1}\text{Mpc}^{-1}$ (95% CL). The decay rate is not significantly correlated with any other cosmological parameter, except $\omega_{\text{dcdm+dr}}$ and r, as can be seen in Figure 5.4. Indeed, the data prefer a certain amount of DM at early times, corresponding to the correct redshift of equality. Hence models with a large decay rate have a smaller DM density today, explaining the negative correlation between Γ_{dcdm} and $\omega_{\text{dcdm+dr}}$. There is also a correlation between Γ_{dcdm} and r: both parameters can enhance the small-l CMB temperature spectrum, so larger values of r lead to a stronger bound on Γ_{dcdm}. Still, since r is peaked in zero (as usual using Planck data), we know that the bound on Γ_{dcdm} that we would obtain under the assumption $r = 0$ would be very similar to what we get here.

For the same model and the B dataset, the bounds on the tensor-to-scalar ratio moves close to $r \simeq 0.17$ at $k_* = 0.05/\text{Mpc}$ (slightly lower than in the ΛCDM + r model, because

bound on the lepton number breaking scale v

$$v > 4.4 \cdot 10^8 \, \frac{m_\nu}{\text{eV}} \left(\frac{m_J}{\text{keV}} \right)^{1/2} \, \text{GeV} \,.$$ (5.22)

This is just an example of how a strong constraint on DM stability can provide relevant information on its yet unknown nature and constrain models of new non-standard interactions. Finally, we would like to remark that these bounds are expected to become even stronger in the near future. Indeed, a key role in their improvement will be played by future weak lensing surveys, which will also help in reducing degeneracies with massive neutrinos, see e.g. [155, 156].

Acknowledgements

6 Neutrino Masses Forecast

Foreword

This chapter deals with a different observable entirely: the clustering of the Large Scale Structures (LSS). There are already several available datasets that measured some simple statistical properties of the galaxy distribution in our observable universe (the Baryon Oscillation Spectroscopic Survey, BOSS, for instance), but many more are being planned. One of the most promising ones is the EUCLID mission, that has recently been approved by the European Space Agency to be launched in 2020.

The satellite will actually contain several probes, as it will try to shed some new lights on many fundamental questions at once. We focused in this paper in the potential predictive power of EUCLID concerning the total neutrino mass, and we therefore looked at the spectroscopic redshift survey, and the cosmic shear survey (or weak lensing). Obviously, with the launch being still far away, the final sensitivity of these two measurements is not yet definitive, but we followed the design documents of the experiment at the time of publication.

Another important thing to notice is that, evidently, there is no data yet - and considering this, any Bayesian analysis seems fruitless. Nonetheless, it is possible to proceed with a fiducial analysis.[1] The principle is rather simple to understand: before performing the analysis, a model is chosen, along with values for its parameters. In our case, this would be the standard model, plus three degenerate massive neutrinos with a given total mass, with all the parameters set at the best-fit of Planck measurement, and a non-zero m_ν chosen arbitrarily.

Once this reference values are chosen (the *fiducial cosmology*), a fake observation is generated, with these data points stored, alongside the expected error bars of the measurement. This step is a simplification, because it assumes that the central value

---

[1]Not to be understood in the sense of Fiducial statistic, as opposed to Bayesian or frequentist.

measured in each wave-number bin is the exact theoretical prediction. However, since the experimental error is also taken into account, this should not bias the result. In any case, once this fake measurement has been recorded, a standard Metropolis-Hastings analysis can be performed, which will give the posterior distribution of the parameters of the model.

As was explained in section 1.6.2, the posterior distribution is the *a posteriori* information on the parameters *given the data*. Since in this case, the data was chosen by hand, it may appear to be a useless quantity to compute. It is important to realize indeed that the central value recovered by the analysis is a trivial information, as it corresponds to the input. Nevertheless, the width of the posterior distribution is an interesting piece of information in itself - with the caveat that it will depend on the fiducial model chosen (for instance, a high neutrino mass will present a deep, characteristic dent in the matter power spectrum, which would be more precisely captured by the experiment than the weaker effect coming from a smaller total mass).

In the case of neutrino mass, though, it is an important exercise to play. Indeed, the total mass m_ν is bounded, both from above and below - respectively by observations of the CMB (the Planck mission gave an exclusion of $m_\nu < 0.23$ eV [11], by combining their high-ℓ and low-ℓ measurements, with WMAP polarization, SPT and ACT data, along with the BAO observations) and neutrino flavor oscillation ($0.056(0.095)$ eV $< m_\nu$ for normal (inverted) hierarchy [32]). This gives a relatively limited range in which the neutrinos may be hiding, rendering the fiducial study very significant. The arbitrary choice for the fiducial value of the total neutrino mass is therefore restricted to this range, and the exact value will have therefore a smaller impact on the analysis. It seems thus nearly certain from the start that a future LSS experiment should finally be able to close the gap and find a non-zero preferred value.

There is however a significant problem standing in the way of reconstructing the neutrino mass from observations, no matter how good they become. So far, in the previous chapters, we more or less carefully avoided to talk about the non-linear evolution of perturbations. By studying the CMB, even with the effect of lensing, we only tackled mostly linear evolution. But structure formation is a strongly non-linear effect, with density variations of forty four orders of magnitude (see section 1.3). It is therefore crucial to understand these non-linearities in order to extract properly all the information contained in LSS surveys.

To follow completely non-linear equations, the brute-force approach embodied by the N-body simulation is certainly the most straightforward, albeit not necessarily the most practical. It consists in following the evolution of individual particles, representing themselves an ensemble of particles, by solving numerically the full equations for the species represented, *i.e.* eqs. (1.19) and (1.20). This approach presents several problems:[2]

---

[2]Although recent developments [157] indicate a possible way forward

1) the simultaneous simulation of cold dark matter, baryon and neutrinos is particularly tricky since they each have very discrepant behaviours, and *2)* it is very expensive numerically to run, of the order of a few days on one CPU.

Concerning the first problem, if the simulation would only contain CDM, it would be rather straightforward. But if it also needs to take into account baryonic effects – notably pressure, reheating by supernovae explosions, star formation – the situation is much more complicated. It has been so far done in a rather empirical way for baryons. Neutrinos are even more difficult to handle because of their large peculiar velocity: because of their relatively small mass, they travel much faster than the rest of the particles, crossing the volume of the simulation several times over the timespan of one simulation step [158]. There are currently some codes able to handle the situation, but it obviously slows down the simulation.

In any case, the second problem is even more concerning. A direct method to solve these equations for N particles would be of order $\mathcal{O}(N^2)$, because for each particle, you need to compute the influence of all the $N-1$ other particles. By using instead a Tree-Particle Mesh (Tree-PM) method, one can bring down the computing time scaling to a $\mathcal{O}(N \log(N))$. The simulation is then divided in cells, where inside, the direct method is used, but from outside, it is only the average gravitational effect that is taken into account. Nonetheless, the typical running times are of the order of days: as explained in section 1.6.3, such a long execution time is incompatible with parameter extraction, where several hundreds of thousands of points are sometimes needed. This is why most studies have been so far limiting the range at which they use the data from LSS to low wavenumbers, typically of the order of $k \simeq 0.1 \, \mathrm{h/Mpc}$ at redshift 0, to stay within the linear regime as much as possible. While keeping only low wavenumbers eases the analysis, it also means that much of the information collected by the experiment will be discarded. Ideally, one would like to find a fast way of computing a theoretical prediction for at least the mildly non-linear scales (up to $k \simeq 0.3 \, \mathrm{h/Mpc}$), in order to use more of the available data.

In this paper, we thus used a refined HALOFIT[3] method [39] that includes the effect of massive neutrinos. It predicts the power spectrum of matter, with a certain uncertainty. What is crucial to realize, however, is that on the mildly non-linear scales, this theoretical uncertainty is actually bigger than the observational one. The situation, therefore, is much different than the usual one in cosmology, with a sharp prediction from the model and a rather vague measurement. Consequently, we had to develop a new way to handle the theoretical uncertainty in the modelling of the experiment. As expected from the discrepancy between uncertain theory and precise data, and despite being very optimistic in the expected accuracy of the theoretical prediction, extending the range of used wavenumber values does not significantly improve the constraint on the total neutrino mass, as can be seen in tables 6.1 and 6.2. Nevertheless, the sensitivity is enough to

---

[3]It is a fitting formula that was calibrated on N-body simulations [159]

almost ensure a detection of a non-zero total mass from EUCLID. This will never be as good as a direct detection of the mass of a single neutrino, since the process used here is rather indirect, but it will be an important milestone for neutrino physics nonetheless.

Neutrino masses and cosmological parameters from a Euclid-like survey: Markov Chain Monte Carlo forecasts including theoretical errors

Benjamin Audren, Julien Lesgourgues, Simeon Bird, Martin G. Haehnelt, Matteo Viel

Abstract: We present forecasts for the accuracy of determining the parameters of a minimal cosmological model and the total neutrino mass based on combined mock data for a future Euclid-like galaxy survey and Planck. We consider two different galaxy surveys: a spectroscopic redshift survey and a cosmic shear survey. We make use of the Monte Carlo Markov Chains (MCMC) technique and assume two sets of theoretical errors. The first error is meant to account for uncertainties in the modelling of the effect of neutrinos on the non-linear galaxy power spectrum and we assume this error to be fully correlated in Fourier space. The second error is meant to parametrize the overall residual uncertainties in modelling the non-linear galaxy power spectrum at small scales, and is conservatively assumed to be uncorrelated and to increase with the ratio of a given scale to the scale of non-linearity. It hence increases with wavenumber and decreases with redshift. With these two assumptions for the errors and assuming further conservatively that the uncorrelated error rises above 2% at k = 0.4 h/Mpc and z = 0.5, we find that a future Euclid-like cosmic shear/galaxy survey achieves a 1-σ error on $M(\nu)$ close to 32 meV/25 meV, sufficient for detecting the total neutrino mass with good significance. If the residual uncorrelated errors indeed rises rapidly towards smaller scales in the non-linear regime as we have assumed here then the data on non-linear scales does not increase the sensitivity to the total neutrino mass. Assuming instead a ten times smaller theoretical error with the same scale dependence, the error on the total neutrino mass decreases moderately from $\sigma(M(\nu)) = 18$ meV to 14 meV when mildly non-linear scales with 0.1 h/Mpc $< k <$ 0.6 h/Mpc are included in the analysis of the galaxy survey data.

6.1 Motivations

Several ambitious ground-based and space-based galaxy surveys have been planned for the next decade (e.g. SKA[4], LSST[5]), or are about to take place (e.g. DES[6]). One of the most ambitious approved missions, the *Euclid*[7] satellite [160], is expected to be launched by ESA in 2019. It will combine a galaxy redshift survey with weak lensing observations, measuring the matter power spectrum and the growth of structure with unprecedented

---

[4] http://www.skatelescope.org/
[5] http://www.lsst.org/lsst/
[6] http://www.darkenergysurvey.org/
[7] http://www.euclid-ec.org

accuracy. This will offer a unique opportunity to improve measurements of cosmological parameters, including the neutrino mass, known to slow down structure formation on intermediate and small scales[32], as well as constraints on dark energy and modified gravity models.

Recent constraints on the total neutrino mass appear to have converged on an upper limit of about 0.3 eV at the 95% confidence level (e.g. [161, 162, 163, 164, 165, 166, 167]), with the notable exception of Lyman$-\alpha$ forest data, which gives an even lower bound of 0.17eV [168]. These constraints rely on a combination of data from Cosmic Microwave Background (CMB) experiments such as WMAP, Baryonic Acoustic Oscillations (BAOs), SuperNovae (SN) distance moduli, galaxy clustering and cosmic shear (especially from the SDSS[8] and CFHTLS[9] surveys). Data sets provided by Large Scale Structure (LSS) are particularly important, since they are able to probe scales and redshifts affected by neutrino free streaming both in the linear and non-linear regimes. Neutrino oscillation experiments provide a lower bound of 0.05eV on the total neutrino mass, meaning that the allowed range is now significantly squeezed by cosmological data, and well within reach of future planned surveys.

Several forecasts have already been published on the sensitivity of *Euclid* to cosmological parameters, with a focus on dark energy, modified gravity, the neutrino mass, or other extensions of the minimal ΛCDM model (see e.g. [169, 170, 171, 172, 173, 174, 175, 176, 177]). However reliable forecasts are difficult to obtain; interpreting *Euclid* data on small (non-linear) scales will require a more accurate modeling of systematic effects than is currently achievable. This is true for both non-linear corrections to the matter power spectrum, and for effects specific to each survey. In the case of the galaxy redshift survey, for instance, redshift space distortions and scale-dependent bias. In the case of the cosmic shear survey, noise bias in shape measurements [178]. Some authors have pointed out that without considerable progress in modeling these effects, the sensitivity to cosmological parameters might degrade considerably (see e.g. [176]).[10]

Current forecasts tend either to incorporate only linear scales and neglect these systematics, or to include a small range of mildly non-linear scales and model systematics by including nuisance parameters which are then marginalized over. Introducing such nuisance parameters (for instance, in order to describe redshift-space distortions) still assumes that we can predict the shape of these effects, and reduce them to a simple family of curves. Hence, this approach is not the most conservative.

On top of this, many forecasts are affected by a methodology issue: apart from two recent works [177, 180], they are based on a Fisher matrix technique, which assumes that the posterior distribution is a multivariate gaussian of the parameters, and whose results

---

[8]http://www.sdss.org/
[9]http://www.cfht.hawaii.edu/Science/CFHLS/
[10]A study [179] made after the publication of this paper shows also that combining the two different experiments improve significantly the constraining power than either alone.

depend on the step chosen in the calculation of numerical derivatives of the spectrum with respect to the parameters (see e.g. [180, 181]). It is possible to choose the step size in a careful and consistent way, but the chosen steps are not always mentionned explicitely.

The present forecast has three objectives:

- First, we wish to use a reliable forecast method for the sensitivity of a *Euclid*-like survey to ΛCDM parameters and to the total neutrino mass, based not on Fisher matrices, but on a parameter extraction from mock data with Markov Chain Monte Carlo (MCMC). This goal has also been achieved very recently by [177], although with a different approach for modeling the galaxy redshift survey. To our knowledge, the present analysis is the first MCMC forecast of a *Euclid*-like galaxy redshift survey using as an observable the power spectrum $P(k)$ in wavenumber space.
- Second, we wish to incorporate non-linear corrections using the most accurate available fitting formula accounting for neutrino mass effects, namely the version of HALOFIT [159] presented in Ref. [39]. This formula has been obtained by fitting to a suite of N-body simulations which incorporate neutrinos as free-streaming dark matter particles, using the code first presented in Ref. [182]. The error in this formula specific to the neutrino mass was estimated by Ref. [39] to be Gaussian, with squared variance

$$\alpha(k, z) \equiv \frac{\Delta P(k, z)}{P(k, z)} = \frac{\ln[1 + k/k_\sigma(z)]}{1 + \ln[1 + k/k_\sigma(z)]} \, f_\nu \,, \tag{6.1}$$

where $f_\nu = \omega_\nu/\omega_m$ and $k_\sigma(z)$ is the non-linear wavenumber as defined and computed in HALOFIT. We include this in the likelihood as a fully correlated error, as described in detail in Appendix C.1, associated to a unique nuisance parameter.

- In order to obtain conservative results while keeping the analysis simple, we will combine this correlated error with a second uncorrelated error. This second uncorrelated error is assumed to account for extra uncertainties in our approximate modeling of non-linear corrections, redshift space distortions, scale-dependent bias and other systematic effects. By assuming an uncorrelated error on each data point, we remain more conservative than if we marginalized over a small set of nuisance parameters representing several types of fully correlated errors. Throughout this work, we assumed for convenience that the relative theoretical error on the power spectrum was given by Eq. (6.1), with f_ν replaced by a constant factor, by default 0.05. This error grows smoothly from zero on linear scales up to 5% on deeply non-linear scales. For a concordance cosmology and at redshift $z = 0.5$, it reaches 1% near $k = 0.1 \, h\mathrm{Mpc}^{-1}$ and 2.3% around $k = 0.6 \, h\mathrm{Mpc}^{-1}$. This choice matches roughly the estimate of HALOFIT errors in Figure 16 of Ref [183]. We assume that ten years from now, this will provide a reasonable description of the total uncertainty

127

coming from all systematic effects in each of the two surveys[11]. Occasionally, we will consider the effect of dividing the magnitude of the error by two or ten, to evaluate the effect of better control of non-linear systematics. We emphasise that the exact form of the uncorrelated error is obviously just an educated guess and that a different k-dependence will *e.g.* influence the assessment of how useful pushing to smaller scales will be. Of course, introducing a fully uncorrelated error (or alternatively, form filling functions as in [184]) is very conservative in that it assumes that no modeling of systematics is accurate enough. In several years from now, it might become realistic to model most systematics with several types of correlated errors, and to reduce the residual uncorrelated theoretical error to a smaller level than assumed in this work.

6.2 Galaxy redshift survey

Throughout this paper, our fiducial model is chosen to be a flat ΛCDM model with three degenerate massive neutrino species. The fiducial parameter values are taken to be $\omega_b = 0.02258$, $\omega_c = 0.1109$, $A_s = 2.43 \times 10^{-9}$ (pivot scale $k_* = 0.05 \, h\mathrm{Mpc}^{-1}$), $n_s = 0.963$, $h = 0.710$, $z_\mathrm{reio} = 10.3$, $m_\nu = 0.07$ eV (so $M_\nu = 0.21$ eV). For the power spectrum of the mock data, we could take directly the fiducial power spectrum, or generate a random spectrum realization corresponding to the same model. As illustrated in [181], the two options lead to the same forecast errors, so for simplicity we assume an observed power spectrum equal to the theoretical power spectrum of the fiducial model.

We fit the mock and *Euclid*-like spectra using the MCMC code MONTEPYTHON [1]. MONTEPYTHON uses the Metropolis-Hastings algorithm like COSMOMC [58], but is interfaced with CLASS [23, 24] instead of CAMB [114], is written in `python`, and has extra functionality; it will soon be released publicly, including the *Euclid*-like likelihood codes used in this work.

Technical details of the assumed likelihood and our analysis are presented in Appendix C.1. Let us summarize here the essential points. As in most of the recent Fisher-matrix-based forecasts, we assume that the reduced data is described by a set of observable power spectra $P^\mathrm{obs}(k_\mathrm{ref}, \mu, z)$, related to the familiar non-linear matter power spectrum $P_{NL}(k, z)$ in a non-trivial way in order to take into account redshift space distortions, linear light-to-mass bias, spectroscopic redshift errors and the Alcock-Paczynsky effect (see C.1.1). Of course, this modeling is imperfect: for this reason we introduce a theoretical error. For instance, we do not take into account galactic feedback [185], assuming that this contamination can be predicted by simulations up to the level of our residual theoretical error function. The arguments k_ref and μ of the observable power spectrum stand respectively for the observed wavenumber assuming the fiducial

---

[11]This description is obviously more optimistic for the galaxy survey, due to the extra complications generated by bias and redshift-space distortions.
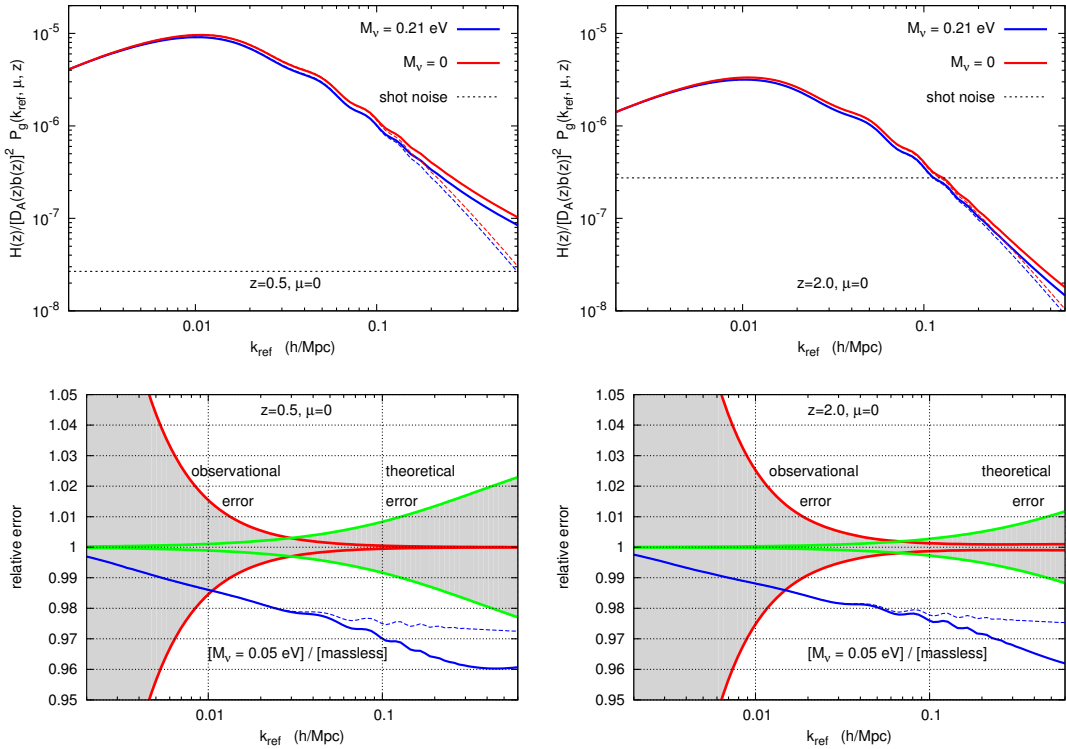
Figure 6.1 – Observable spectrum (top) and relative error on this spectrum (bottom), for the first redshift bin (left) and last redshift bin (right) of a *Euclid*-like galaxy redshift survey. The quantity displayed in the top is the galaxy power spectrum $P_g(k_{\rm ref}, \mu, z)$ as a function of the fiducial wavenumber $k_{\rm ref}$, for fixed redshift and perpendicularly to the line of sight ($\mu = 0$), rescaled by the inverse squared bias $b(z)^{-2}$ and by a factor $H(z)/D_A(z)^2$: it is therefore a dimensionless quantity. The upper plots show a comparison between a model with massless neutrinos and our fiducial model ($M_\nu = 3m_\nu = 0.21$ eV). Solid lines are derived from the non-linear matter power spectrum using the updated HALOFIT version of ref. [39], while dashed lines are derived from the linear power spectrum. The lower plots show the part of the relative error coming from observational or theoretical errors only (cosmic variance is included in the observational error). In these plots, the individual 1-σ error on each data point has been rescaled by the square root of the number of points, in such a way that the edges of the error bands correspond to a shift between theory and observation leading to $\Delta\chi^2 = 1$, when only the observational or theoretical error is incorporated in the likelihood expression. In these lower plots, we also show for comparison the ratio between a massless model and a model with the minimum total mass allowed by neutrino experiments, $M_\nu = 0.05$ eV.

cosmology, and the cosine of the angle between the observed wavevector and the line of sight. We assume sixteen redshift bins with mean redshift ranging from 0.5 to 2, and bin widths of $\Delta z = 0.1$. For a fixed theoretical model, each observed value of $P^{\rm obs}$ in a bin centered on the point $(k_{\rm ref}, \mu, z)$ follows, to a good approximation, a Gaussian

distribution with variance

$$\left(\Delta P^{\mathrm{obs}}\right)^2 = \frac{2(2\pi)^2}{k_{\mathrm{ref}}^3 V_{\mathrm{survey}} d\mu [dk_{\mathrm{ref}}/k_{\mathrm{ref}}]} \left(P^{\mathrm{th}} + 1/n_g\right)^2 \ , \tag{6.2}$$

where $d\mu$ is the size of the bins in μ space, and $[dk_{\mathrm{ref}}/k_{\mathrm{ref}}]$ the size of the logarithmic bins in wavenumber space (see C.1.2). The characteristics of the survey are encoded in V_{survey}, the survey volume, and n_g, the comoving number density of galaxies accounting for shot noise (see C.1.3). Hence, if for *every* observed data point the theory and the observation differed by this amount, the effective χ^2 would increase with respect to its minimum value by the number of data points, namely

$$N = B\frac{2}{d\mu} \frac{\ln(k_{\max}/k_{\min})}{[dk_{\mathrm{ref}}/k_{\mathrm{ref}}]} \ , \tag{6.3}$$

where B is the number of redshift bins.

To illustrate this error, in figure 6.1, we show the relative error bar on the observed spectrum in the first and last redshift bin, assuming no additional theoretical error. For the purpose of comparing with the theoretical error introduced below, we do not show as usual the error corresponding to a one-sigma deviation for each given data point; we divided each error by $\sqrt{N}$, in such a way that the edge of the error band corresponds to a deviation between the observed and theoretical spectrum leading to $\Delta\chi^2 = 1$. Note that the displayed quantity $\pm\Delta P^{\mathrm{obs}}/(P^{\mathrm{obs}}\sqrt{N})$ does not depend on the width of the bins in $(k_{\mathrm{ref}}, \mu, z)$ space, but only on P^{th}, V_{survey} and n_g.

We incorporate the theoretical error in the likelihood in the way described in section C.1.4. In few words, this error is normalized in such a way that a shift between theory and observations by a relative amount α (the quantity defined in eq. (6.1)) leads to an increase of the χ^2 by one. This is achieved simply by adding a term $N(\alpha P^{\mathrm{th}})^2$ to the total error variance. Figure 6.1 shows the relative theoretical error on the observed spectrum, normalized in such a way that the edge of the error band corresponds to a deviation between the observed and theoretical spectrum leading to $\Delta\chi^2 = 1$ when the observational error is switched off. These edges are directly given by $\pm\alpha$.

We see in this figure that our assumption for α leads to an error of 1% at $k = 0.1h\mathrm{Mpc}^{-1}$ and 2.5% at $k = 0.6h\mathrm{Mpc}^{-1}$ for the first redshift bin centered on $z = 0.5$. For the last redshift bin in the galaxy survey, centered on $z = 2$, non-linear corrections appear on smaller scales, and the error is only 1% at $k = 0.6h\mathrm{Mpc}^{-1}$.

We performed several forecasts for a combination of *Planck* data and a *Euclid*-like galaxy redshift survey data. It should be stressed that the characteristics of *Euclid* are not yet finalized. Our choice for V_{survey} and $n_g(\bar{z})$, detailed in C.1.3, should be taken as indicative only. For *Planck*, we follow the method presented in [181] and do not include lensing extraction. For the experimental *Planck* sensitivity, we use the numbers presented in the

k_{max} (h/Mpc)	un. err.	co. err.	$10^4\omega_b$	$10^4\omega_c$	$10^3 n_s$	$10^{11} A_s$	$10^3 h$	z_{reio}	$3m_\nu = M_\nu$ (meV)
0.1	−	−	1.2	6.2	2.8	3.0	4.1	0.38	18
0.1	1/10	−	1.2	6.9	2.8	3.1	4.5	0.39	18
0.1	1/2	−	1.3	9.5	3.2	3.5	6.1	0.39	23
0.1	●	−	1.3	11	3.4	3.6	6.7	0.40	25
0.1	●	●	1.3	11	3.4	3.6	6.7	0.40	25
0.6	−	−	0.86	2.1	0.37	1.2	0.40	0.23	5.9
0.6	1/10	−	1.1	4.8	2.5	2.7	3.0	0.37	14
0.6	1/2	−	1.2	8.6	3.2	3.4	5.7	0.39	22
0.6	●	−	1.3	10	3.4	3.6	6.7	0.39	25
0.6	●	●	1.3	10	3.4	3.6	6.7	0.39	25

Table 6.1 – Marginalized 1-σ error for each model parameter, in a fit of *Planck + Euclid*-like galaxy survey data. The different lines correspond to different choices of k_{max}, to the inclusion or not of the global uncorrelated theoretical error (un. err.), divided by ten (1/10), by two (1/2), or full (●), to that of the specific neutrino-related correlated error (co. err.), and to the use of the non-linear or linear power spectrum. The models with correlated error have one more nuisance parameter e_ν not shown here, with unit 1-σ error.

Planck Bluebook[12]. This is a rather conservative model since the sensitivities are based on 14 months of observations instead of 30.

The differences between our forecasts reside in the maximum wavenumber, equal to $k_{max} = 0.1$ or $0.6\,h\mathrm{Mpc}^{-1}$, and in various prescription for the theoretical error: no error at all, the uncorrelated error described above and in C.1.4 (divided by ten, by two, or full), or additionally the correlated error accounting for neutrino-mass-related effects (described in C.1.5). Since we are using an increasing theoretical error on non-linear scales, we expect the amount of information contained in the data to saturate above some value of k_{max}: this is the reason we can consider such a high value as $0.6\,h\mathrm{Mpc}^{-1}$. We did not try even higher values, first because our result would not change, and second because our forecast would become unrealistic: deep in the non-linear regime, the Gaussian assumption for the likelihood breaks down.

Our results are presented in Table 6.1. Parameters like ω_b and z_{reio} are well determined by CMB data, and their forecast error depends very mildly on our different assumptions. For other parameters, the redshift survey plays a crucial role in removing parameter degeneracies. In that case, even with $k_{max} = 0.1\,h\mathrm{Mpc}^{-1}$, including the uncorrelated theoretical error makes a difference: the parameter sensitivity degrades by up to 70% for h. The 68% neutrino mass error bar degrades by 40%, from $\sigma(M_\nu) = 0.018$ eV to

---

[12]http://www.rssd.esa.int/SA/PLANCK/docs/Bluebook-ESA-SCI(2005)1_V2.pdf, page 4, Table 1.1 (using only the best three HFI channels: 100, 143 and 217 GHz).

$\sigma(M_\nu) = 0.025$ eV.

Assuming only this uncorrelated error, the cases $k_{\max}$=0.1 hMpc^{-1} and $k_{\max}$=0.6 hMpc^{-1} give almost the same results. Hence, our assumption for the theoretical error magnitude is such that most of the information is contained on linear scales. Thanks to realistic (or at least conservative) assumptions for the theoretical error, the results of our forecast are nearly independent of the cut-off $k_{\max}$. Without a theoretical error, increasing $k_{\max}$ to $0.6\,h$Mpc^{-1} would lead to a spectacular (but totally unrealistic) decrease of the error bars, with $\sigma(M_\nu) = 0.0059$ eV.

If we are more optimistic and half the uncorrelated error, the error bars decrease marginally, as can be seen in the Table (lines starting with "1/2"). The error on the neutrino mass only decrease by $\sim 10\%$. Assuming no error at all implies that the spectrum can be predicted up to the 0.1% level or better on small scales. In comparison, assuming a precision of one percent is not very different from assuming two percent. With the halved error, the sensitivity to the neutrino mass increases from $\sigma(M_\nu) = 0.023$eV to $\sigma(M_\nu) = 0.022$eV when including data in the range from 0.1 to $0.6\,h$Mpc^{-1}.

Finally, in a very optimistic forecast with an error ten times smaller, we start to see how extra information can be extracted from non-linear scales; the error decreases from $\sigma(M_\nu) = 0.018$ eV to $\sigma(M_\nu) = 0.014$ eV when pushing $k_{\max}$ from 0.1 to $0.6\,h$Mpc^{-1}.

The inclusion of an additional correlated error accounting for neutrino-mass-related systematics has a negligible impact on our results. In our forecast, the uncorrelated and correlated part of the error have similar amplitudes and the same shape; however the uncorrelated error allows much more freedom and thus leads significantly more conservative results: this explains why the correlated error has a comparatively small effect. It should be stressed that our results depend not only on the assumed error amplitude at a given scale and redshift, but also on the wavenumber dependence of the error function α. Different assumptions, with a steeper or smoother step in the error function around the scale of non-linearity, would lead to different forecasts. In particular, as already mentioned the actual benefit from pushing to smaller, non-linear scales depends on the assumed k-dependence of the residual uncorrelated theoretical error.

For the case with $k_{\max} = 0.6\,h$Mpc^{-1} and no neutrino-related correlated error, we show the one and two-dimensional posterior probability on cosmological parameters in figure 6.2. We see several pronounced parameter degeneracies. For instance, the neutrino mass is very correlated with ω_c and h. This suggests that further progress could be made by including extra data sets, such as direct measurements of the Hubble parameter, the cluster mass function, supernovae luminosity, 21-cm anisotropies, and so on.

The results in Table 5 of [172] and Table 2.1 of [186] agree very well with our prediction in the case with no non-linear scales and no theoretical error included. A similar sensitivity
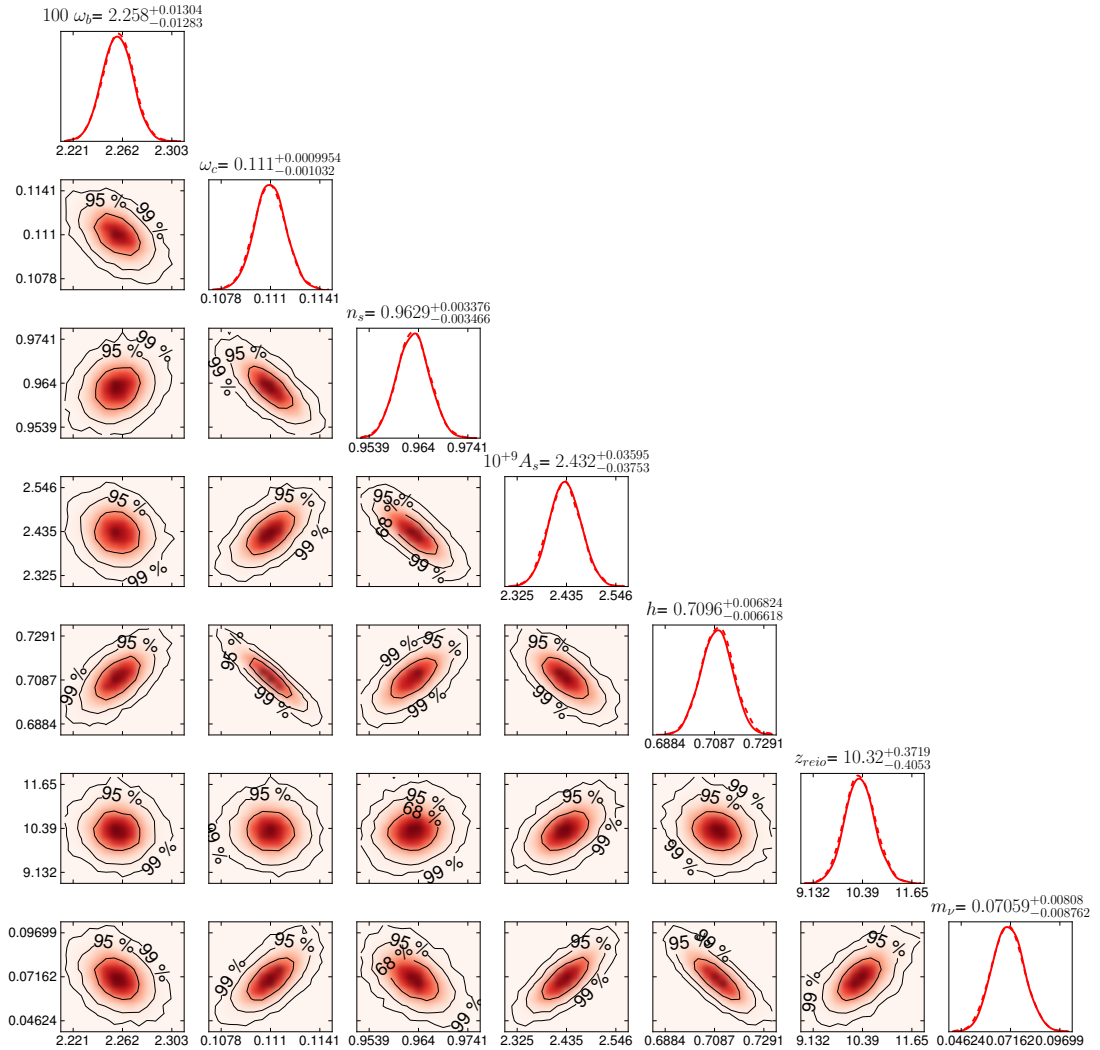
Figure 6.2 – Marginalized posteriors and two-dimensional probability contours in a fit of *Planck* plus a *Euclid*-like galaxy survey mock data, with $k_{\max} = 0.6\,h\mathrm{Mpc}^{-1}$ and a global uncorrelated theoretical error (second line starting from the bottom in Table 6.1).

was found by [177] for a Euclid-like photometric redshift survey, referred to as "cg" in their Table 2. However, this reference presents other results based on even more conservative assumptions than ours. We assumed that the bias function for each redshift bin could be determined in advance (up to corrections on non-linear scales contained in our global theoretical error). This assumption has also been made in most recent forecasts, since both N-body simulations and higher-order statistics in the real data allow the prediction of the redshift-dependent bias of a given population of galaxies, at least on linear scales. Were this approach found to be unreliable, it would be necessary to marginalize over the linear bias in each redshift bin, $b(z_i)$. Ref. [177] did such a marginalization in the runs

called "cgb" and "cgbl", with no prior at all on each $b(z_i)$. They found roughly the same error bar on ω_c and h than in our forecast with theoretical error, but a much larger error on the neutrino mass. However, it seems unlikely that at the time when *Euclid* data will be analyzed, no information at all will be available on the linear bias of the observed population of galaxies. Finally, [175] finds more pessimistic results when studying the case of a Euclid-like photometric cluster catalogue.

6.3   Cosmic shear survey

For the case of a *Euclid*-like cosmic shear survey, we stick to the same fiducial model and methodology as in the previous section. The likelihood is now a function of the observed lensing power spectrum $C_l^{\text{obs}\, ij}$ in harmonic space and for each pair ij of redshift bins, taking into account photometric redshift errors and shot noise (for details, see C.2.1 and C.2.2). We assume experimental sensitivities summarized in C.2.3, and cut the observations in five redshift bins covering the range $0 < z < 3.5$ (although a negligible amount of galaxies contribute between 3 and 3.5). We do not take into account intrinsic alignment, assuming that this contamination can be removed up to the level of our residual theoretical error function [187, 188].

As explained in detail in C.2.4, there is a small technical difference between the likelihood of the galaxy survey and the shear survey in the way we incorporate the uncorrelated theoretical error. For the galaxy survey, the theoretical error was encoded as an extra contribution to the total error variance. This can be justified mathematically by marginalizing over one nuisance parameter for each data point. The shape of the galaxy survey likelihood allows for an analytical minimization over each nuisance parameter, in such a way that nuisance parameters do not appear explicitly in the final likelihood. We found that no such scheme is accurate enough in the case of the (chi-square type) shear likelihood. Hence our likelihood routine performs an explicit minimization over one nuisance parameter per data point. For simplicity, we assume that the error is uncorrelated between different values of l, but not between different bins for a given l: this assumption could be relaxed, at the expense of increasing the computing time.

We fixed $l_{\text{max}} = 2000$, since beyond this value both the shot noise term and the theoretical error are large, as shown in figure 6.3. This figure also shows the relative error on the observed spectrum in the first and last redshift bins, coming either from observational errors (including cosmic variance) or from the theoretical error, and using exactly the same conventions as in the previous section: the edges of each of the two error bands correspond to a shift between the theory and the observation leading to $\Delta\chi^2 = 1$ when either the observational or the theoretical error are included in the likelihood. The lowest redshift bin incorporates small non-linear scales: this explains why at $l = 2000$, the theoretical error reaches 3.5%.
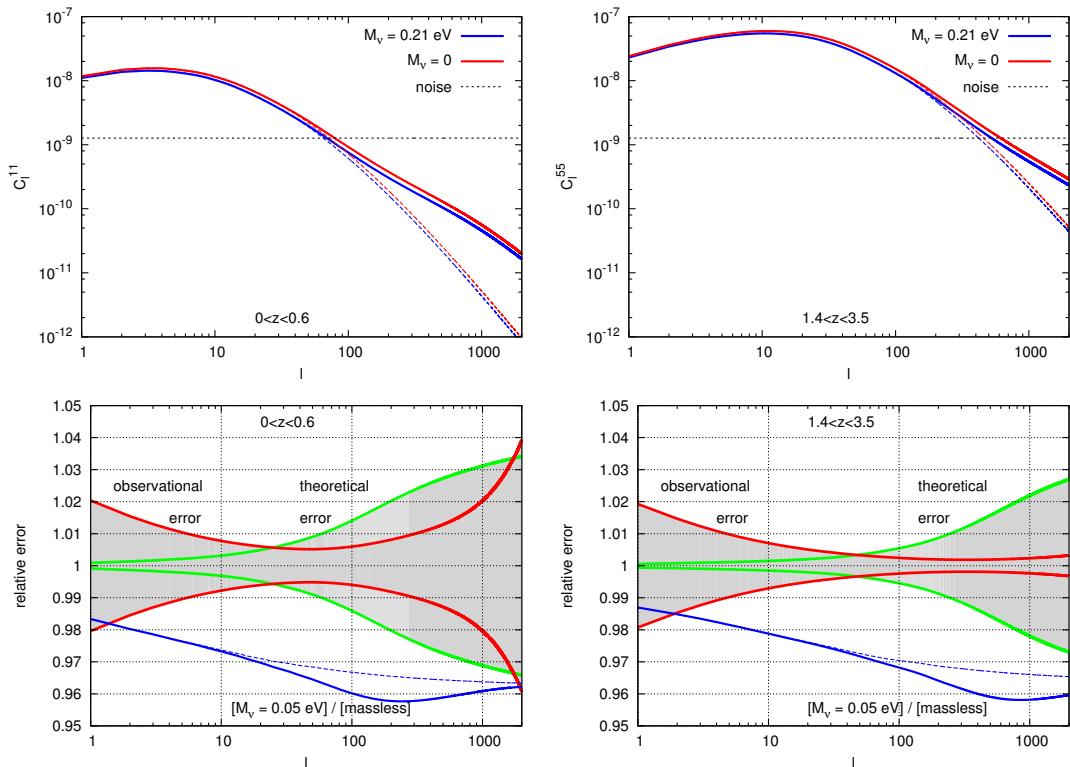
Figure 6.3 – Observable cosmic shear power spectrum (top) and its relative error (bottom) for the first redshift bin (left) and last redshift bin (right) of a *Euclid*-like shear survey. The quantity displayed above is the lensing auto-correlation spectrum C_l^{ii} (dimensionless). The upper plots show the comparison of a model with massless neutrinos to our fiducial model ($M_\nu = 3m_\nu = 0.21$ eV). Solid lines are derived from the non-linear matter power spectrum using the recent update of HALOFIT [39], while dashed lines are derived from the linear power spectrum. The lower plots show the part of the relative error coming from observational or theoretical errors only (cosmic variance is included in the observational error). In these plots, the individual 1-σ error on each data point has been rescaled by the square root of the number of points, in such a way that the edges of the error bands correspond to a shift between theory and observation leading to $\Delta\chi^2 = 1$, when only the observational or theoretical error is incorporated in the likelihood expression. In these lower plots, we also show for comparison the ratio between a massless model and a model with the minimum total mass allowed by neutrino experiments, $M_\nu = 0.05$ eV.

Our results are presented in Table 6.2 for three cases: no theoretical error, uncorrelated error only (described in C.2.4), or additional neutrino-related correlated error (described in C.2.5). The impact of the uncorrelated error is again important, but not as pronounced as in the galaxy power spectrum case, because on small scales the precision of the shear survey is limited by a significant shot noise contribution. The neutrino mass error degrades only from $\sigma(M_\nu) = 0.026$ eV to 0.028 eV. For the shear survey we did not perform runs with a twice or ten times smaller error: the result for $\sigma(M_\nu)$ would simply

un. err.	co. err.	$10^4\omega_b$	$10^4\omega_c$	$10^3 n_s$	$10^{11} A_s$	$10^3 h$	$10 z_{\text{reio}}$	$3m_\nu = M_\nu$ (meV)
–	–	1.1	3.9	2.4	2.8	4.0	3.7	26
●	–	1.2	6.3	2.7	2.9	5.2	3.8	28
●	●	1.2	6.6	2.7	3.0	5.3	3.9	32

Table 6.2 – Marginalized 1-σ error for each model parameter, in a fit to *Planck + Euclid*-like shear survey data. The different lines correspond to the inclusion or not of the global uncorrelated theoretical error (un. err.), and of the specific neutrino-related correlated error (co. err.). Our preferred prediction is given on the last line, and is very close to that of the second line.

lie between those two numbers. The impact of the neutrino-related error is small but further degrades the sensitivity to $\sigma(M_\nu) = 0.032$ eV. While in the absence of theoretical error the galaxy survey seems more sensitive to the neutrino mass, the performance of the two methods are roughly identical once the same theoretical error ansatz is included.

The triangle plot of figure 6.4 shows that the parameter degeneracies are very similar for the two cases of the galaxy survey and shear survey. Nevertheless, [177] showed that combining the two data sets (with a proper cross-correlation matrix) leads to sensitivity improvements. It would be interesting to test this conclusion in presence of theoretical errors.

Our results are consistent with those of [169], although a direct comparison is difficult, since these authors include several extra parameters (w_0, w_a, r, α_s) in their forecast. The predictions of [177] (case "cs" in their Table 2) lie between our results with and without theoretical errors. This is consistent since on the one hand, these authors use more optimistic survey characteristics (d, $\langle\gamma_{rms}^2\rangle$, σ_{ph}), and on the other hand, we are including much larger values of l (which is legitimate if our theoretical error is realistic).

6.4   Conclusions

We have presented forecasts of cosmological parameters by using, in combination with *Planck* data, two *Euclid*-like mock future data sets: a galaxy spectroscopic redshift survey and a cosmic shear survey. We focused our attention on constraints that can be achieved on the total neutrino mass by using the data in the linear and non-linear regimes.

In order to do this conservatively we adopt the following improvements with respect to similar works performed recently in the literature: *i*) we make use of Markov Chain Monte Carlo rather than the Fisher Matrix, which results in more reliable error bars, as well as considering degeneracies between parameters. Ultimately, we found that the posterior probability is very close to a multivariate Gaussian for the model considered. However, a
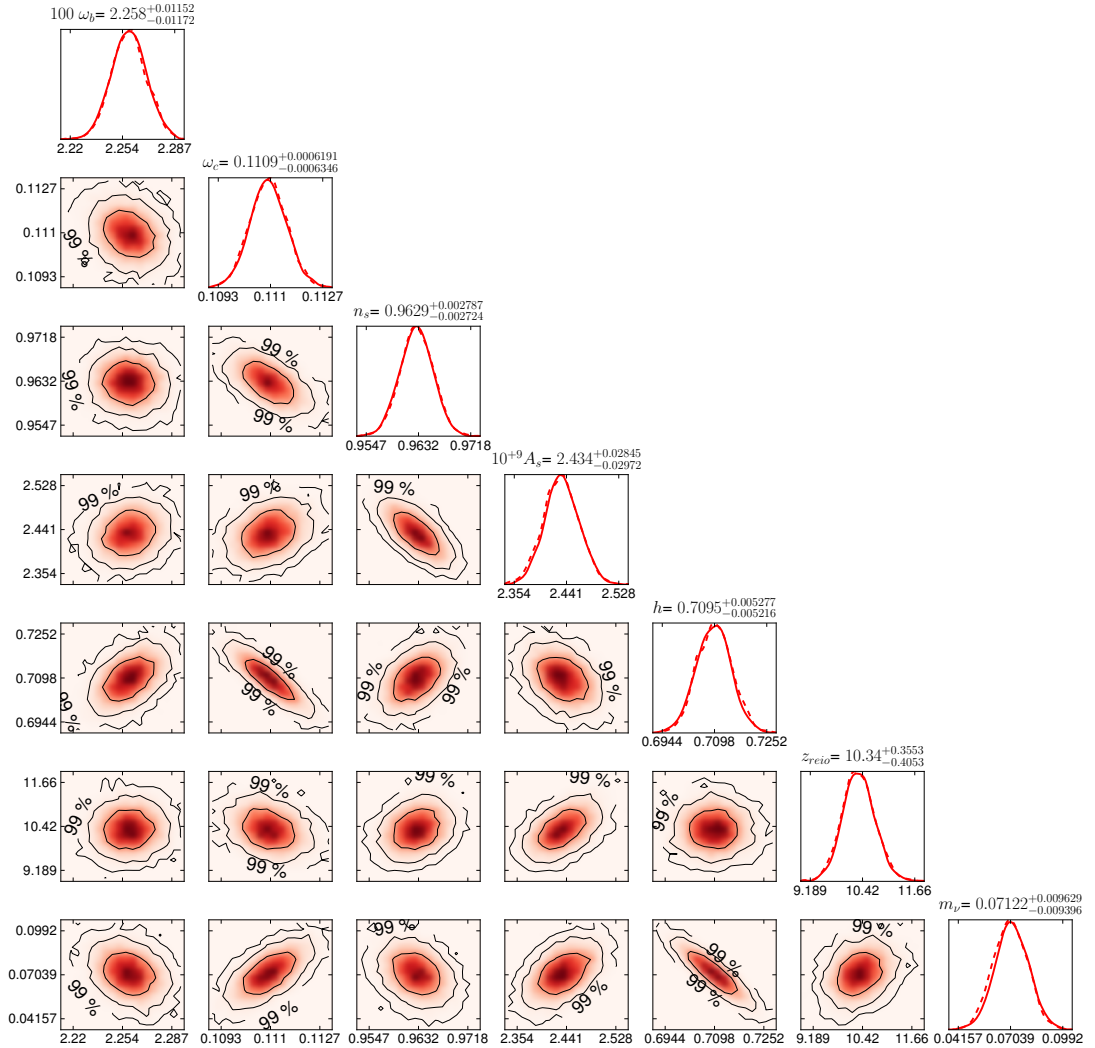
Figure 6.4 – Marginalized posteriors and two-dimensional probability contours in a fit of *Planck + Euclid*-like shear survey data, with a global uncorrelated error of 5% on non-linear scales (second model in Table 6.2).

Fisher matrix approach could not have confirmed this, and would not have been explicitly independent of the stepsize in the numerical derivatives. *ii*) we rely on a modification of HALOFIT that accounts for massive neutrinos, and predicts the non-linear matter power spectrum to small scales, based on the results of N-body and hydro simulations. *iii*) we conservatively consider errors both on the non-linear observable power at small scales and on the neutrino induced suppression, and explictly show how to implement these errors in the likelihood calculation.

It is instructive to see that with the shape assumed for the uncorrelated theoretical

error, and a conservative assumption on its amplitude (leading to a 2% error at $k_{\mathrm{max}} = 0.4\,h/\mathrm{Mpc}$ and $z = 0.5$), the sensitivity to cosmological parameter is still satisfactory. The error bar on the total neutrino mass, of the order of 32 meV (cosmic shear) or 25 meV (redshift survey), would still allow for a two sigma detection of the total neutrino mass in the minimal normal hierarchy scenario[13]. However, with this amplitude and k-dependence of the theoretical error, essentially all the information comes from linear scales. The next interesting question is to check how much the uncorrelated error should be controlled in order to start being sensitive to mildly non-linear scales. Assuming a twice smaller error does not change the parameter sensitivity by a significant amount. Extracting significant information from non-linear scales requires an error ten times smaller, at the level of 0.2%. Here the error on the neutrino mass decreased from $\sigma(M_\nu) = 18$ meV to 14 meV when adding scales with $0.1 < k < 0.6\,h/\mathrm{Mpc}$ to the analysis. This shows that it would be extremely useful to be able to predict the observable power spectrum of a given cosmological model up to a residual uncorrelated error of the order of 0.1% (resp. 0.2%) at $k \sim 0.1\,h/\mathrm{Mpc}$ (resp. $k \sim 0.4\,h/\mathrm{Mpc}$) and $z = 0.5$. This will be a major challenge for theoretical and numerical cosmology in the next decade.

---

[13]For a more precise statement, one should study the dependence of the error on the fiducial mass. We did not perform such an analysis because the HALOFIT version that we are using is valid for three degenerate masses, which is only consistent with assuming a large fiducial. The results of [189, 172] suggest that the error would be slightly larger when assuming a smaller value of the total fiducial mass close to 0.1 eV or 0.05 eV.

7 Plaidoyer for Software Development

7.1 Introduction

As opposed to Numerics, which has earned its rank among other scientific fields of study, Software Development has still an outlier place in Physics. Open source, version control and testing are words that are not usually associated with the software created or used in publications - with the massive exception of the field of Particle Physics, and the ROOT software, used to analyse data coming from the Large Hadron Collider. The common practice is rather the opposite, with most of the time not even a link to the code. However, a vast majority of results in today's Cosmology are heavily dependent on numerical methods and complex softwares, ranging from algebraic computations using Mathematica, differential equations solved with Boltzmann codes, or N-body simulations. Obviously, an algebraic result can be checked manually, and a numerical result can be verified in a simple limiting case. But one needs to trust the output of a code even on a case where there is no simple verification – otherwise it simply is not a sane foundation for a rigorous work.

This peculiar position is further enhanced by the fact that, by mostly using the online resource arXiv to exchange papers in our field, our scientific community is adhering to these very concepts of open source, version control and testing for our papers. All our research papers are always accessible, readable by anyone, and their history is preserved, too, as you can select a specific revision of the paper. Moreover, we consider this as granted, and fundamental to the communication of scientific knowledge: no one would claim any result, any theory, without presenting a clear argumentation, alongside the main lines of the computation, for everyone to read and convince oneself that it is correct. Naturally, we also strongly rely on peer-review to accept a result from a paper, but we do not rely on this step only. Without access to the source material, no result is considered valid.

How can we follow these important concepts on one aspect of our work, and so blatantly

ignore them in another? Perhaps the confusion lies in the view of available software by the community: it is not sufficiently clear for everyone that any complex code has bugs. These are mostly avoidable given enough time, and proper development practice. In science, as in the corporate world, the first item is severely constrained, albeit for different reasons. Without applying basic principles from software development, we are bound to using severely bugged code. The consequences of this may seem inconsequential, but are as embarrassing as publishing a paper with a faulty algebraic computation. I would even argue that they can be worse than this, especially if the code is never made public. Indeed, given time, the scrutiny of the community will eventually reveal typos and errors in a paper's computation. But when the code is hidden from view, except by duplicating independently the code, there is no way for the community to identify a problem.

I wanted to highlight through this small discussion a few of these best practice that, if followed, would help increasing the trust of the entire community in every branch of knowledge that would follow them. All these recommendations of course will look strange for a physicist not trained in developing, as they are mostly considered as an absolute waste of time. However, no one would consider shunning experimentalists for maintaining a lab-book, calibrating their machine regularly, or testing it against simple samples. Should the software developed for scientific research avoid to aim for the same amount of rigor? Can we accept a series of paper on an untested and undisclosed complicated software?

More than this, scientists will also criticise open-source because it gives the feeling of losing the benefit of their own effort. After having worked tremendously to produce a complex code, implementing a complicated algorithm, why would they want to release it publicly so that everyone can perform the same work, without effort? What would sharing the code bring them back?

7.2 Version Control

The first stepping stone for a proper development hygiene is to set up a system for version control. At its core, this simple tool allows the developer to revert to an older version of the code at anytime. Many softwares provide this functionality, falling in two broad classes: centralized and distributed. Distributed version control systems, such as *git*, or *mercurial*, offer two additional functionalities compared to centralized ones: it is possible to work on the code without being connected to a centralized server, and every copy on every machine will contain the entire history of development.

This last feature easily reminds us of the strategy of a biological virus. It maximizes its chances of never losing its identity – its DNA – by duplicating the entire information at every possible occasion. From every single entity of the virus, the biological code survives.

The analogy is not perfect, since the DNA is prone to errors in copying, resulting in an altered code - a situation that we want to avoid at any cost in our case. However, it brings the point that this distributed system is very robust against a disk failure of any sort. Where a centralized version control scheme requires a careful back-up of the main server, the security of the decentralized system is enforce by its usage. Note however that the decentralized system also has a central repository where the official version is read from. This can be on a server, and will serve as the intermediate between the different revision on the separate machines.

In a very rough sense, scientists already use a mild system of distributed version control when collaborating on papers, through a remote repository, which is locally shared by all collaborators - via proprietary tools such as Dropbox, for instance. This allows everyone to edit the same file without sending it by email at each iteration, which is of course a tremendous boost in productivity. It also provides some basic control over the versions of the file, allowing one to revert to previous state of the text.

When developing a piece of scientific software, on the other hand, one needs additional features, which are only present in more complex version control systems. The two first items are equally well implemented by both groups of version control softwares, whereas the last two are the strong arguments in favor of the distributed ones.

i. **A clear history of all the features implemented**: as a code grows in complexity, new features are added to the source code. Considering the changing nature of science, these features were not necessarily foreseen, and so the code might need some extra reworking to accommodate for it. When debugging, being able to revert to a previous version where a specific feature was absent is of crucial importance.

ii. **A good branching system**: oftentimes, we need the code to perform separate tasks for two different projects: it is a daily reality in any collaboration. Without an efficient branching system, the only way around this issue is to create an entire copy of the source code in a separate folder, and modify this version. But as the original code expands, or fixes bug, the task of keeping updated this separate folder becomes unmaintainable, and leads to the abandon of the code. The inverse task – merging a separate branch into the main code – should also be an easy step.

iii. **Being able to work at the same time on the same code**: as every computer possesses the entire source code, it is possible to work at the same time on the file, committing changes. The merging will be made when pushing to the central repository, and should be painless, even when the same file was modified by two parties.

iv. **Being able to work at any time on the code**: another very important aspect of this system is the ability to develop meaningfully even offline. With a centralized system where modification of the main code is only possible with internet access, any length of developing offline will lead to commits containing many separate changes, reducing the clarity of the development history.

These points come for free when using such a system, and by themselves offer a sufficient justification to adopt it. But there is an added benefit that is even more desirable. With such a system, it becomes trivial to merge changes from a scientist who is not a part of the developing team.

It is of such a frequent occurrence that patches for scientific code are found on researchers' web-page, only accessible through advertisement in a publication, or by word of mouth. This state is highly undesirable, but is a direct consequence of the difficulty to implement such a change for the owners of the original code. Without a good version control tool, it is delicate to incorporate the changes made at a certain stage in the code's history.

An obvious, clear disadvantage of using a version-control system instead of none at all is the time it takes to use it. It requires a significant amount of time, at first, to master the commands needed for a daily usage. Arguably, this is more a one-time investment, because using the system becomes very automatic after a while.

7.3   Testing

This step is probably the most overlooked component of proper software development. Arguably, it is also the least straightforward to adopt, and use practically. However, by the very nature of scientific programming, it is a corner stone of any important software. Indeed, agile development is crucial in research, as we have to adapt to a moving target at all time. A new experiment can crush an interesting development for the code, or on the contrary, favor a model that the code was not designed to handle in the first place.

Following this constantly shifting target while continuing to support older functionalities is specifically what testing can allow us to do. Testing, in its stricter sense, is to make sure the program that was created behaves in the way it was designed to be. Said like that, it also sounds like a tautology – surely, if it was designed to do this, the author of the code checked that it indeed performed the task? But precisely, because of the constant changes that are applied to the source code, an old functionality, that was working before, might suddenly not work anymore. The problem is very prominent in duck-typed language,[1] such as Python, but it does not mean that non duck-typed languages are free of these issues – they are simply more subtle to find.

It is very easy to give an example of this problem. Imagine a Python function that was dealing with an array of integers. At the time of writing, the array was small, and thus a simple list was used. But as the code evolved, the list was found to be very intensely used, and was therefore changed into a numerical array (Numpy). The original function

---

[1] One of the design principle behind some high-level languages. Instead of typing every variable before its first use, as an integer, float, or array for instance, the type is determined by the methods of the object. Hence, if a part of the code receives an object that quacks and has feathers, it is assumed to be a duck, even though it might not be of the class Duck. This allows a more flexible approach to coding.

will work as intended if it only replaced numbers in the list, but if it inserted numbers inside the list, or appended the list, then the functionality will break.

An example in non-duck-typed language is even easier to understand for a scientist. The inclusion of a new set of parameters in the code can force the author to change some default precision values. This might, in turn, affect another part of the computation, which could break with these new settings. As long the old model is not computed again, this issue will remain undetected.

Such examples can be arbitrarily easy or hard to notice. It all depends on the frequency of use of each part of the code. And it is in this precise domain that testing becomes crucial. It is indeed possible in high-level languages such as Python, Ruby or `C#`, to specify in the header of a function a basic set of input and their corresponding expected output. In the first example given, one would have then tested the behaviour of the function given a certain list in input, and expecting a certain return statement.

By regularly running this set of little code snippets, with the help of robust testing frameworks, one can ensure that at least some basic functionality is being maintained as the code evolves. But, as is evident from the example, this way of testing does not ensure that the code, as a whole, still works. Indeed, the small test of the function used lists, and not a numerical array. In order to also prevent these type of errors, it is crucial to globally test the behaviour of the code by running entire modules in a situation as close as possible from its real use.[2]

There are also tools, such as the *nosetests* framework for Python, that facilitates this process. Every test is then designed with a set-up and a tear-down phase, were quantities are initialised to reproduce a given scenario. Then, a series of question is asked to the code, or to a submodule, which should behave as expected. It is also possible to make sure that the code would fail given a nonsensical input, in order to assess the correct behaviour of the error messaging system.

As explained at the beginning of the section, writing such tests can be hard. If the code is usually running for days on a cluster, how is it possible to test for any possible outcome? Of course, the more the users of the code, the easier it is to find out bugs. And it is tempting to believe that it is sufficient to fix bugs as they appear. But it is considerably more useful to fix them once and for all by testing that they are not there anymore. With the help of these automated testing tools, it is possible to launch all these tests with a simple one-liner, just before committing a change to the repository, for instance.

The clear drawback of such a system, just as for version-control, is that it requires time to setup properly, and also time to test regularly. All this time could be devoted to add another feature in the code, or work on a more scientific topic. Contrarily to

---

[2]It would also work to test the function for all possible misuse case, but this would quickly blow out of proportions, and will never be as fool-proof as proper global testing.

version-control, however, it is a constant fight against bugs and missing functionalities, which requires constant dedication. In addition to continuously writing new tests as functionalities are added, the previous ones have to be checked for problems.

7.4 Open-source

If the advice proposed in sections 7.2 and 7.3 are followed, one would think that this last step, making the code open to everyone, is not necessary. It might seem that if all good practice are respected in the privacy of development, there is no additional need to show the code to everyone. There are however three major advantages for doing this, that I will try to highlight here.

Firstly, having a version controlled code is not nearly enough in order to allow users to send modifications. Indeed, without having access to the current version of the code, but only a few releases, developing modifications and sending them to the author is still complicated. What if the code evolved so much during the modification that merging is bothersome? It is only through publicly showing the code as it evolves that a true communication can take place between the author and the users.

Obviously, this can be seen as incompatible with the competitive nature of scientific research. How can the authors of the code be sure not to be "scooped" when they publish the source code of the computation before the release? This issue can be solved efficiently, by simply putting the source code online after the release of the first paper. This will never prevent people from using the code and publishing more papers using the code after that, but this is precisely a scientific goal: to bring the field forward and allow people to research on topics that were previously inaccessible. It is also possible to develop new features in a parallel branch, not available online with the main code, until a new paper using it is published. At that moment, that development branch gets merged into the main code, and everyone can use it.

A second clear advantage of open sourcing the code is to reduce the chances of a code going to waste if abandoned by the original author. By sharing it openly, it encourages people to get involved in the development, which makes it more certain to find someone with enough knowledge of the code to continue the effort. With a private code, no matter how well written, it is an extremely time-consuming task to try and understand its inner working, and therefore unmaintained codes like that are more often than not completely abandoned, and a new code is created in its place to replace it.

Another strong justification for this approach might be the tougher to understand for someone that never shared any code: it is what might be referred to as *public pressure*. It is the exact same mechanism that makes you feel uncomfortable with guests if your house is not clean enough: it is deeply embarrassing to share badly written code. The simple

knowledge that someone will look at these lines trying to understand what happens usually triggers a reaction from the author, that improves the overall quality, legibility and functionality of the code.

As a last remark, it is important to realize that open sourcing the code does not imply losing the control over it. With the help of licensing, the author is still acknowledged as the creator of the code, and decides what to implement. Copies of the code can be made, that will be managed by other users, but a trace will be kept of the original author, such that proper credits and citations can be given. But more than this, by allowing people to participate in the code evolution, through proper use of version control and testing, the level of quality that can then be reached beats any attempt by a single developer.

7.5 Concluding remarks

What has been briefly discussed here might look like an idealized version of what scientific programming should look like. Given unlimited time and resources, everyone can program like this - the issue is always with the time and effort. Having to learn all these habits of programming takes time, thinking properly ahead of coding is also complicated, and retracts from the time that should be devoted to research.

Another point that was not mentioned previously because of its evidence, but which also detracts from research, is writing good documentation. With the help of modern tools, like Sphinx or Doxygen, it is possible to have the documentation extracted automatically from the source code and presented as a website, simplifying considerably the reading experience. It nonetheless requires a careful and constant updating of the documentation, as the code evolves. It is obviously nice to have a clear documentation for oneself, but again, the public pressure makes scientists more likely to keep maintaining it.

By not following these guidelines, our community tends to waste a considerable amount of energy. Continuously, a lot of effort is spent to reproduce existing codes that fell into disuse, and do not possess an intelligible enough documentation to be recovered. When the code in question requires two days of work, it is not an issue. But when it represents months, or years, it becomes a dramatic waste of time.

A major step in trying to follow these advice would be to start using a modern, high-level language as the outside shell of the code. A language such as Python provides, as mentioned already, efficient automatic tools for documentation and testing, and brings a clarity to the structure that is hard to reach with any low-level language. It also integrates robust libraries doing many low-level operations, such as file access, saving the developer the effort to redevelop everything. But using such a high-level language does not save the scientists the time needed to develop properly – it simply makes it easier.

It seems therefore obvious to me that a research laboratory could increase its global

productivity by hiring a professional software developer. As a person already trained in these fields, the developer could construct the code from the science goals and numerical precision desired from the scientific collaborator – therefore saving the scientists from wading through complicated programming concepts and lose focus. Most importantly, an enormous amount of time could be saved by avoiding to lose the energy of a post-doc or student that would prefer, reasonably, to focus on writing good papers instead of good code. The latter takes time, and is not currently rewarded nearly as much as it could be, leading to poorly constructed and commented code, that soon fall into disuse. It should therefore be self-evident that a numerical laboratory needs a software developer as much as an experimental laboratory needs a technician.

It is probable that the highest obstacle to overcome would be the initial reticence of scientists to the usefulness of testing, and in general proper development practice. There is hope in this direction nonetheless, as only a few demonstrations of bug finding from automated testing is usually enough to convince people.

What we could do also, as a community, to reinforce the importance of these points would be to take inspiration in the field of collider particle physics, where these standards are held and applied daily. We should remember that without them, no trustworthy result would have come out of the LHC experiment.

8 | Conclusions

In this manuscript, we presented several analyses covering a broad range of topics in cosmology. The guiding principle that links them together is the will to refine our understanding of the Standard Model of cosmology in order to meaningfully interpret the results from current and upcoming experiments.

Chapters 2 and 3 focused on disassembling the early and late parts of the model, and understanding them separately. Indeed, the SM incorporates assumptions about very varied stages, as discussed in sections 1.2 and 1.3. Most notably, our knowledge about the late universe, the formation of structure, reionization, is much less precise than our knowledge about the initial amplitude of fluctuations, or the abundance of matter and radiation. These chapters therefore focus primarily on preventing the uncertainty from the late universe to spoil our knowledge about the early universe. We showed how any evidence for an extra relativistic degree of freedom is removed when analysing the data in the agnostic way, described in chapter 2. In a second step, the goal was centered on utilizing this model-independent knowledge to probe the uncertainty associated to one background effect: the late-time homogeneous accelerated expansion of the universe. We then demonstrated that the already weak tension between Planck data and BAO measurements can not be interpreted as a failure of the cosmological constant Λ to explain the present-day accelerated expansion of the universe.

In chapters 4 and 5, the focus was instead on the properties of dark matter, another relatively unknown part of the Standard Model. As mentioned in the introduction, the range of potential DM candidates is extremely large, and therefore the possible effects on cosmology are very varied. In chapter 4, we dealt with DM particles able to annihilate and produce SM particles that would in turn reionize the Inter-Galactic Medium. In this setup, bounds on the decay of these particles coming from gamma-ray data are extremely stringent, and exclude any observable cosmological effect. We therefore concentrated on annihilation, finding out that a simple model with reionization coming both from stars and DM annihilation would fit both CMB data and work with the Gunn-Peterson

effect, but reheat the IGM too much. By taking a prior on the IGM temperature, we set competitive bounds on the DM annihilation cross-section. In chapter 5, we instead investigated a completely model-independent setup: the gravitational effect of relativistic products of DM decay. If the decay products are not sterile, then other constraints will be stronger, but our analysis also stands in the case of sterile products. We found that the life-time of such a species should be above $160\,\mathrm{GeV}$ at 95% confidence level.

Finally, chapter 6 tackled the question of the neutrino mass sensitivity of a future experiment, EUCLID. We introduced a systematic and realistic way to take into account the uncertainty of our theoretical predictions – a crucial issue as observations of large scale structures will reach a much sharper precision than we presently have. With this framework, and using the current expected sensitivity of EUCLID, we demonstrated that a significant detection of a non-zero total neutrino mass is an almost guaranteed result of the experiment. However, we showed that almost no additional information will be possibly extracted from the mildly non-linear scales, due to the poor theoretical precision. A joint effort from the CDM non-linear power spectrum, bias and redshift-space distortions is in order to start using the coming wealth of data efficiently.

The other main theme in these five papers is the usage of MONTE PYTHON, a Monte-Carlo code that I developed in order to perform cosmological parameter extraction. Designed to work with the Boltzmann solver CLASS from the beginning, it was developed from the ground up with many goals in mind, as presented in appendix A. Opening the source code to the general public, via the code sharing platform Github[1] allowed me to increase its visibility and improve its efficiency as the user-base grew over time. It was also a time-consuming activity to maintain, as discussed at length in chapter 7. Recently, a lot of effort was dedicated to improving the quality of both codes, through the usage of automatic documentation tools, giving workshops on the codes, and most importantly implementing a robust automated-testing environment. This last item, especially for CLASS, significantly increased the robustness and trustability of the code – key factors for public codes to be used in scientific publications, from individual research groups to collaborations.

---

[1]https://github.com

9 Outlook

Cosmology only recently entered an era of precision experiments. After having measured with definitive precision the temperature anisotropies[1], Planck will now leave place for other measurements. The E-mode polarization anisotropies have already been measured by WMAP, but will be further refined with Planck and possible future experiment, such as PRISM. The B-mode is a currently hot topic, with the recent detection claim from the BICEP collaboration [15]. Hopefully, upcoming information from Planck should settle the debate, and determine whether or not primordial B-modes have really been observed. If it were true, the SM would need to add a non-zero tensor-to-scalar ratio r to its list of parameters – showing once more how young this field is.

On the side of LSS, two exciting experiments will soon bring a lot of data. On the one hand, Euclid will deploy a series of cosmological probes that should map with unprecedented accuracy our universe up to a redshift of 2. We discussed in chapter 6 about the two main ones, the galaxy power spectrum and the weak-lensing survey, but there will also be a galaxy cluster count probe, and galaxy cluster power spectrum computation. Theoretically, the information coming from these two other probes should further refine the precision on cosmological parameters thanks to their complementarity (for a detailed example concerning dark energy, see [190])

On the other hand, experiments probing LSS at large redshift (2 to 4) through the Ly-α forest [191] will also soon be available, from the BOSS collaboration. Having several measurements of the matter power spectrum will shed light on many topics, such as the nature of dark energy through the measure of the growth factor.

As emphasized in chapter 6, the prediction of non-linearities has a long way to go before possibly being used in a parameter extraction. There was a recent regain in the activity of the field through the discovery of several new techniques [31, 47, 48], but no agreement is reached yet. It would be interesting to follow these developments, and perform a

---

[1]The error bars in Planck are mostly dominated by cosmic variance

systematic comparison between them and a suite of N-body simulations. Indeed, until now, this sort of comparison has never been performed, leading to accidental agreement with particular sets of parameters, as was pointed out originally in [192]. In practice, this would require the source code of each of these methods to be part of the public domain, or to set up a close collaboration with the original authors, in order to merge them with CLASS. This is a long term project of our group.

On the side of N-body simulations, recent progress has been made, in the form of a code able for the first time to follow simultaneously the time evolution of baryons and CDM [157]. This is certainly an interesting development, and should increase our knowledge about bias by giving the community reliable and precise benchmarks.

Finally, the hunt for dark matter is a tough and ongoing process, with four simultaneous directions of research – collider searches, cosmological effects, indirect detection and direct detection. The recent hint of a signal as an X-ray emission in nearby galaxies is not confirmed, and needs further observation. Moreover, it is not the first time that such a signal excited the dark matter community. It provides nonetheless an interesting research direction, as current particle physics experiments are not designed to look in this keV mass range.

A Advantages of Monte Python

The results of this paper were obtained with the new parameter inference code Monte Python, that we release publicly together with this article. Currently, Monte Python is interfaced with the Boltzmann code class, and explores parameter space with the Metropolis-Hastings algorithm, just like CosmoMC[1] (note however that interfacing it with other codes and switching to other exploration algorithms would be easy, thanks to the modular architecture of the code). Hence, the difference with CosmoMC [58] does not reside in a radically different strategy, but in several details aiming at making the user's life easy. It is not our goal to describe here all the features implemented in Monte Python: for that, we refer the reader to the documentation distributed with the code. We only present here a brief summary of the main specificities of Monte Python.

Language and compilation. As suggested by its name, Monte Python is a Monte Carlo code written in Python. This high-level language allows to code with a very concise style, and the implementation of e.g. new likelihoods requires very few lines. Python is also ideal for wrapping other codes from different languages: Monte Python needs to call class, written in C, and the WMAP likelihood code, written in Fortran 90. Python codes do not require a compilation step, which further simplify the installation on many different machines.

Modularity. A parameter inference code is based on distinct blocks: a likelihood exploration algorithm, an interface with a code computing theoretical predictions (in our case, a Boltzmann code solving the cosmological background and perturbation evolution), and an interface with each experimental likelihood. In Monte Python, all three blocks are clearly split in distinct modules. This would make it easy, e.g., to interface Monte Python with camb [114] instead of class, or to switch from the in-build Metropolis-Hastings algorithm to another method, e.g. a nested sampling algorithm.
The design choice of the code has been to write these modules as different classes, in the

---

[1]In this paper we refer to the version of CosmoMC available at the time of submitting, i.e. the version of October 2012.

sense of C++, whenever it served a purpose. For instance, all likelihoods are defined as separated classes. This allows basic properties inheritance that simplify the writing of new likelihoods, as well as offering an easy and intuitive way of comparing two runs

Memory keeping and safe running. Each given run, i.e. each given combination of a set of parameters to vary, a set of likelihoods to fit, and a version of the Boltzmann code, is associated to a given directory where the chains are written (e.g. it could be a directory called `chains/wmap_spt/lcdm`). All information about the run is logged automatically in this directory, in a file `log.param`, at the time when the first chain is started. This file contains the parameter names, ranges and priors, the list of extra parameters, the version of the Boltzmann code, the version and the characteristics of each data likelihood, etc. Hence the user will always remember the details of a previous run. If a later run is send to this folder with a different input file, the code will refuse to start

No need to edit the code when adding parameters. The name of cosmological parameters is never defined in Monte Python. The code only knows that in the input file, it will read a list of parameter names (e.g. `omega_b`, `z_reio`, etc.) and pass this list to the cosmology code together with some values. The cosmology code (in our case, CLASS) will read these names and values as if they were written in an input file. If one of the names is not understood by the cosmology code, the run stops. The advantage is that the user can immediately write in the input file any name understood by CLASS, without needing to edit Monte Python.

Playing with covariance matrices. When chains are analyzed, the covariance matrix is stored together with parameter names. When this matrix is passed as input at the beginning of the new run, these names are read. The code will then do automatically all the necessary matrix manipulation steps needed to get all possible information from this matrix if the list of parameter has changed: this includes parameter reordering and rescaling, getting rid of parameters in the matrix not used in the new runs, and adding to the matrix some diagonal elements corresponding to new parameters. All the steps are printed on screen for the user to make sure the proper matrix is used.

Friendly plotting. The chains produced by Monte Python are exactly in the same format as those produced by CosmoMC: the user is free to analyze them with `GetDist` or with a customized code. However Monte Python incorporates its own analysis module, that produce output files and one or two dimensional plots in PDF format (including the usual "triangle plot"). Information on the parameter best-fit, mean, minimal credible intervals, convergence, etc., are then written in three output files with different presentation: a text file with horizontal ordering of the parameters, a text file with vertical ordering, and a latex file producing a latex table. In the plots, the code will convert parameter names to latex format automatically (at least in the simplest cases)

in order to write nice labels. The code stores in the directory of the run only a few PDF files (by default, only two; more if the user asks for individual parameter plots).

Convenient use of mock data. The released version of Monte Python includes simplified likelihood codes mimicking the sensitivity of *Planck*, of a *Euclid*-like galaxy redshift survey, and of a *Euclid*-like cosmic shear survey. The users can take inspiration from these modules to build other mock data likelihoods. They have been developed in such way that dealing with mock data is easy and fully automatized. The first time that a run is launched, Monte Python will find that the mock data file does not exist, and will create one using the fiducial model parameters passed in input. In the next runs, the power spectra of the fiducial model will be used as an ordinary data set. This approach is similar to the one developed in the code FuturCMB[2] [181] compatible with CosmoMC, except that the same steps needed to be performed manually.

---

[2]http://lpsc.in2p3.fr/perotto/

B Modifications in HYREC

In HYREC, the evolution equation are written in function of time for x_e and of $\ln a$ for T_M. In addition, the units are CGS+eV for temperatures, except in the two functions describing the temperature evolution, where we have Kelvin. So, the equations are

$$
H\frac{dx_e}{d\ln a} = \frac{1}{H}\left[C\left(-n_H x_e^2\alpha_B + \beta_B(1-x_e)e^{-\frac{E_{21}}{T_r}}\right)\right.
$$
$$
\left. + \rho_c^2 c^2 \Omega_{DM}^2 \frac{1-x_e}{3n_H}(1+z)^6 p_{ann}(z)\left(\frac{1}{E_i} + \frac{1-C}{E_\alpha}\right)\right], \tag{B.1}
$$

$$
\frac{dT_M}{d\ln a} = -2T_M + \frac{1}{H}\left[\frac{8\sigma_T a_r T_r^4}{3m_e c}\frac{x_e}{1+x_e+f_{He}}(T_r - T_M)\right.
$$
$$
\left. + \frac{2}{3k_b}\frac{1+2x_e}{3n_H}\frac{1}{1+x_e+f_{He}}\rho_c^2 c^2\Omega_{DM}^2(1+z)^6 p_{ann}(z)\right]. \tag{B.2}
$$

These equations are equivalent with the ones in RECFAST, but the C-factor is now defined as:

$$
C = \frac{\frac{3}{4}R_{Ly\alpha} + \frac{1}{4}\Lambda_{2s,1s}}{\beta_B + \frac{3}{4}R_{Ly\alpha} + \frac{1}{4}\Lambda_{1s,2s}}, \tag{B.3}
$$

with the two-photon rate $\Lambda_{2s,1s} = 8.22458$ s^{-1} and the escape rate of Lyman-α photons $R_{Ly\alpha} = \frac{8\pi H}{3n_H(1-x_e)\lambda_{Ly\alpha}^3}$.

Quasi steady-state equation

In HYREC, we can find a function describing the temperature evolution in the quasi steady-state approximation. In general, as seen above, the equation for the temperature in the presence of annihilating Dark Matter is

$$
\frac{dT_M}{d\ln a} = -2T_M + \gamma(T_r - T_M) + \left.\frac{dT_M}{d\ln a}\right|_{DM}. \tag{B.4}
$$

Appendix B. Modifications in HYREC

The quasi steady-state approximation consists of considering the case when the second term in equation (B.4) is bigger than the other two, i.e. when $\gamma \gg 1$. In this situation, $T_\mathrm{M} \approx T_r$ and $\frac{dT_\mathrm{M}}{d\ln a} \approx -T_\mathrm{M}$, thus

$$T_\mathrm{M} \approx \frac{T_r}{1 + \gamma^{-1}} + \gamma^{-1} \left.\frac{dT_\mathrm{M}}{d\ln a}\right|_\mathrm{DM}. \tag{B.5}$$

The different modes of HYREC

The above evolution equation for x_e is used when HYREC runs in the modes `peebles` or `recfast`. For the `EMLA` mode, there exist two different C-factors, namely C_{2s} and C_{2p}

$$C_{2s} = \frac{\Lambda_{2s1s} + R_{2s \to 2p} \frac{R_{Ly\alpha}}{\Gamma_{2p}}}{\Gamma_{2s} - R_{2s \to 2p} \frac{R_{2p \to 2s}}{\Gamma_{2p}}}, \tag{B.6}$$

$$C_{2p} = \frac{R_{Ly\alpha} + R_{2p \to 2s} \frac{\Lambda_{2s1s}}{\Gamma_{2s}}}{\Gamma_{2p} - R_{2p \to 2s} \frac{R_{2s \to 2p}}{\Gamma_{2s}}}. \tag{B.7}$$

The inverse life times are defined by:

$$\Gamma_{2s} = B_{2s} + R_{2s \to 2p} + \Lambda_{2s,1s}, \tag{B.8}$$

$$\Gamma_{2p} = B_{2p} + R_{2p \to 2s} + R_{Ly\alpha}, \tag{B.9}$$

where B_i are the ionization coefficient and $R_{i \to j}$ the transition coefficients. We can take $R_{2s \to 2p} = 3R_{2p \to 2s}$ since there are 3 times more states in 2p than in 2s.
C_{2s} (C_{2p}) represents the probability that a hydrogen atom initially in the 2s (2p) state reaches the ground sate before being ionized. The Lyman-α line is the excitation from 1s to 2p. So the new factor in equation (B.1) should be[1] $C = C_{2p}$. Exactly the same approach is used for the `full` mode of HYREC.

---

[1] We used C_{2p} assuming that excitations were mostly $1s \to 2p$, as would be the case if DM annihilations lead to additional Ly-α photons. If excitations are instead collisional, this treatment is not formally valid; however, this would represent a correction to a process that is already subdominant and we need not worry about such subtleties here.

C Neutrino Forecast

C.1 Galaxy redshift survey implementation

C.1.1 Observed spectrum

Let P^{obs} be the observed/mock/fiducial power spectrum, and P^{th} the spectrum that one would expect to see given the theoretical model. Each of these quantities relates to the galaxy spectrum P_g and finally to the total non-linear matter spectrum P_{NL} by taking into account redshift distortion effects, spectroscopic redshift errors and light-to-mass bias. A good approximation of such a relation is given by (see e.g. [174, 173]):

$$P^{\mathrm{th/obs}}(k_{ref\perp}, k_{ref\parallel}, z) = \frac{D_A(z)^2_{\mathrm{ref}} H(z)}{D_A(z)^2 H(z)_{\mathrm{ref}}} P_g^{\mathrm{th/obs}}(k_{ref\perp}, k_{ref\parallel}, z) \ , \tag{C.1}$$

$$P_g^{\mathrm{th/obs}}(k_{ref\perp}, k_{ref\parallel}, z) = b(z)^2 \left[1 + \beta(z,k) \frac{k^2_{ref\parallel}}{k^2_{ref\perp} + k^2_{ref\parallel}} \right]^2 P_{NL}^{\mathrm{th/obs}}(k, z) e^{-k^2 \mu^2 \sigma_r^2} \ , \tag{C.2}$$

with the definitions

$$\beta(k,z) \equiv b(z)^{-1} \frac{d\ln[P_{NL}^{\mathrm{th/obs}}(k,z)]^{1/2}}{d\ln a} = \frac{1}{2b(z)} \frac{d\ln P_{\mathrm{NL}}^{\mathrm{th/obs}}(k,z)}{d\ln a} \ , \tag{C.3}$$

$$k_{\mathrm{ref}\perp} = k_\perp H(z)_{\mathrm{ref}}/H(z), \quad k_{\mathrm{ref}\parallel} = k_\parallel H(z)_{\mathrm{ref}}/H(z), \tag{C.4}$$

$$\mu \equiv \hat{k}_{\mathrm{ref}}.\hat{r} = k_{\mathrm{ref}\parallel}/k_{\mathrm{ref}}, \tag{C.5}$$

$$k^2 = \left(\frac{(1-\mu^2)D_A(z)^2_{\mathrm{ref}}}{D_A(z)^2} + \frac{\mu^2 H(z)^2}{H(z)^2_{\mathrm{ref}}} \right) k^2_{\mathrm{ref}} \ . \tag{C.6}$$

Here $b(z)$ is the bias, assumed to be scale-independent in the range of scales of interest, a is the scale factor, $H(z)$ is the Hubble parameter, $D_A(z)$ the angular diameter distance, and $\beta(z,k)$ accounts approximately for redshift space distortions. So we can treat k as a

function of the arguments $(k_{\mathrm{ref}}, \mu, z)$ and write

$$
\begin{aligned}
P^{\mathrm{th/obs}}(k_{\mathrm{ref}}, \mu, z) = {} & \frac{D_A(z)^2_{\mathrm{ref}} H(z)}{D_A(z)^2 H(z)_{\mathrm{ref}}} b(z)^2 \left[1 + \beta(z, k(k_{\mathrm{ref}}, \mu, z)) \mu^2 \right]^2 \times \\
& P^{\mathrm{th/obs}}_{\mathrm{NL}}(k(k_{\mathrm{ref}}, \mu, z), z) e^{-k(k_{\mathrm{ref}}, \mu, z)^2 \mu^2 \sigma_r^2}
\end{aligned}
\tag{C.7}
$$

C.1.2 Likelihood

For a narrow redshift bin b centered on $\bar{z}$, the likelihood reads

$$
\mathcal{L}_b = \mathcal{N}_b \exp\left[-\frac{1}{2} \int_{k_{\min} < k_{\mathrm{ref}} < k_{\max}} \frac{d^3 \vec{k}_{\mathrm{ref}}}{(2\pi)^3} V_{\mathrm{eff}}(k_{\mathrm{ref}}, \mu, \bar{z}) \frac{(P^{\mathrm{obs}}(k_{\mathrm{ref}}, \mu, \bar{z}) - P^{\mathrm{th}}(k_{\mathrm{ref}}, \mu, \bar{z}))^2}{2(P^{\mathrm{th}}(k_{\mathrm{ref}}, \mu, \bar{z}))^2} \right]
\tag{C.8}
$$

$$
= \mathcal{N}_b \exp\left[-\frac{1}{2} \int_{-1}^{1} d\mu \int_{k_{\min}}^{k_{\max}} \frac{k_{\mathrm{ref}}^2 dk_{\mathrm{ref}}}{(2\pi)^2} V_{\mathrm{eff}}(k_{\mathrm{ref}}, \mu, \bar{z}) \frac{(P^{\mathrm{obs}}(k_{\mathrm{ref}}, \mu, \bar{z}) - P^{\mathrm{th}}(k_{\mathrm{ref}}, \mu, \bar{z}))^2}{2(P^{\mathrm{th}}(k_{\mathrm{ref}}, \mu, \bar{z}))^2} \right] ,
\tag{C.9}
$$

with an effective survey volume given by

$$
V_{\mathrm{eff}}(k_{\mathrm{ref}}, \mu, \bar{z}) = V_{\mathrm{survey}}(\bar{z}) \left[\frac{n_g(\bar{z}) P_g^{\mathrm{th}}(k_{\mathrm{ref}}, \mu, \bar{z})}{1 + n_g(\bar{z}) P_g^{\mathrm{th}}(k_{\mathrm{ref}}, \mu, \bar{z})} \right]^2 .
\tag{C.10}
$$

Later, we will specify the sensitivity of the survey, parameterized by V_{survey}, n_g, σ_r, $k_{\min}$ and $k_{\max}$. We skip here the derivation of the Fisher matrix, obtained by differentiating the above formula twice with respect to the cosmological parameters on which P^{th} depends, and evaluating this derivative at the maximum likelihood point. We checked that this calculation gives exactly the formula commonly used in the literature (see e.g. [174, 173]). For the purpose of the discussion in the next section (and also of the numerical implementation), we wish to write explicitly the discrete limit of the integrals. We discretize μ in a set of equally spaced values μ_i, and $l \equiv \ln k$ in a set of equally spaced values $l_j = \ln k_{\mathrm{ref}j}$. The step sizes are denoted $\Delta\mu$ and Δl respectively. We then expand the integral as a sum, and for simplicity we omit the factors $1/2$ that should weight the boundary terms of each of the two integrals. We introduce the short-cut notations:

$$
N_{ij} \equiv \Delta\mu \Delta l \frac{k_{\mathrm{ref}j}^3 V_{\mathrm{eff}}(k_{\mathrm{ref}j}, \mu_i, z)}{(2\pi^2)},
\tag{C.11}
$$

$$
P_{ij}^{\mathrm{obs/th}} \equiv P^{\mathrm{obs/th}}(k_{\mathrm{ref}j}, \mu_i, z),
\tag{C.12}
$$

and we get

$$
-2 \ln \mathcal{L}_b = \sum_{i,j} \frac{\left(P_{ij}^{\mathrm{obs}} - P_{ij}^{\mathrm{th}} \right)^2}{2(P_{ij}^{\mathrm{th}})^2 / N_{ij}} .
\tag{C.13}
$$

This expression is easy to understand from first principles. Let us consider a single variable δ obeying a Gaussian distribution centered on zero and with variance $\langle \delta^2 \rangle = P$. If we observe N independent realization δ_n of the variable δ, we can build an estimator of the variance P of δ,

$$E = \frac{1}{N} \sum_n \delta_n^2. \tag{C.14}$$

The variance of this estimator can be computed by noticing that each δ_n^2 follows a χ^2 distribution of order one, for which the mean is P and the variance $2P^2$. So the sum $\sum_n \delta_n^2$ has a variance $2NP^2$. Finally E has a variance $(2NP^2)/N^2 = 2P^2/N$. Moreover, E is nearly Gaussian if N is large, as a consequence of the central limit theorem. So the probability of the data E given the theory P is a Gaussian of mean P and of variance $2P^2/N$. In other words,

$$-2\ln \mathcal{L}(E|P) = \frac{(E - P)^2}{2P^2/N} \; . \tag{C.15}$$

The previous likelihood follows this form for each discrete term. Indeed each term corresponds to the likelihood of the estimator of the power spectrum in a thin shell in Fourier space. The number of independent measurements, i.e. of independent wavenumbers in each shell, is given by N_{ij}. The role of E and P is played respectively by P_{ij}^{obs} and P_{ij}^{th}. Such a likelihood was first derived in pioneering papers like [193, 194].

C.1.3 Survey specifications and implementation details

We computed this likelihood for values of $V_{\mathrm{survey}}(\bar{z})$, $n_g(\bar{z})$, $\sigma_r(\bar{z})$ inspired from currently plausible *Euclid* specifications, which are likely to change over the next years. We divide the observations into sixteen redshift bins of width $\Delta z = 0.1$, ranging from $\bar{z} = 0.5$ to $\bar{z} = 2.0$. For each bin, we assumed:

- a volume per bin $V_{\mathrm{survey}}(\bar{z}) = 4\pi f_{\mathrm{sky}}[r(\bar{z})]^2 (1 + \bar{z})^{-3} \frac{\partial r(z)}{\partial z} \Delta z$, where $r(z)$ is the comoving distance up to a comoving object with redshift z, with the explicit assumption that $a_0 = 1$:

$$r(z) = \int_0^z \frac{dz'}{H(z')} \; . \tag{C.16}$$

  We assume a sky coverage $f_{\mathrm{sky}} = 0.375$.
- a galaxy number density per comoving volume $n_g(\bar{z})$, related to the number of galaxies per square degree $d_g(\bar{z})$ through

$$n_g(\bar{z}) = \frac{d_g(\bar{z}) \times 41\,253\,\mathrm{deg}^2}{4\pi[r(\bar{z})]^2 \frac{\partial r(z)}{\partial z} \Delta z} \; . \tag{C.17}$$

For $d_g(\bar{z})$, we start from the number presented in Table 2 of [195] for the case of a limiting flux of $3 \times 10^{-16} \mathrm{erg\,s^{-1}cm^{-2}}$. Following the recommendation of that paper, we divide these numbers by 1.37 in order to get conservative predictions. Finally, we multiply them by an efficiency factor $\epsilon = 0.25$ (standing for the redshift success rate). For instance, for the first redshift bin, this gives $d_g(\bar{z}) = 9376/1.37 \times 0.25 = 1710 \mathrm{\,deg^{-2}}$.

- a spectroscopic redshift error $\sigma_r = \frac{\partial r(z)}{\partial z}\sigma_z$ with $\sigma_z = 0.001(1+z)$.
- a scale-independent linear bias $b(\bar{z})$. The choice of $b(\bar{z})$ values affects the final result less crucially than that of $d_g(\bar{z})$. We could adopt the predictions of [196] inferred from N-body simulations, but for simplicity, our forecast is performed under the approximation $b(\bar{z}) = \sqrt{1+\bar{z}}$. So, we assume in this forecast that the linear bias will be accurately measured or predicted for each bin, and that deviations from this prediction (coming from the non-linear evolution) will be known up to the level described by the theoretical error function.
- $k_{\min}$ can be chosen arbitrarily close to zero without changing the results.
- we tested two values of $k_{\max}$: 0.1 and $0.6 \, h\mathrm{Mpc}^{-1}$.

C.1.4 Accounting for a global uncorrelated theoretical error

To present a realistic forecast, one should model all the systematic effects not accounted for by the previous likelihood formula, such as: theoretical errors in the calculation of the linear and non-linear power spectrum, scale-dependence of the bias on small scales, residual shot noise in galaxy counts beyond the contribution already included in the definition of V_{eff}, residual errors in the modeling of redshift space distortion beyond the above scheme. On top of these corrections, one may have to take into account the fact that the likelihood is not Gaussian on strongly non-linear scales. In this paper, we limit ourselves to mildly non-linear scales $k \leq k_{\max} = 0.6 h\mathrm{Mpc}^{-1}$, and assume that non-Gaussianity effects are sub-dominant to the previously mentioned systematics. We also neglect to marginalize over residual shot noise in each redshift bin, because Ref. [174, 173] found that this has a negligible impact.

Understanding these various systematics is a major challenge for the future, which should be addressed with better simulations and analytical modeling. Here we want to keep the analysis simple, and model these systematic errors in a simple way, by adding to the spectrum an uncorrelated theoretical error function. By uncorrelated we mean that the errors made at different scales are independent from each other, which is the most conservative possible assumption. In this case, we can introduce an independent Gaussian-distributed nuisance parameter ϵ_{ij} of variance 1 for each data point, and marginalize

over it – or rather, to a very good approximation, minimize over it:

$$-2\ln\mathcal{L}_b = \sum_{i,j} \min_{-\infty < \epsilon_{ij} < +\infty} \frac{\left[P_{ij}^{\mathrm{obs}} - \left(P_{ij}^{\mathrm{th}} + \epsilon_{ij}R_{ij}^{1/2}\right)\right]^2}{2\left(P_{ij}^{\mathrm{th}} + \epsilon_{ij}R_{ij}^{1/2}\right)^2/N_{ij}} + \epsilon_{ij}^2, \tag{C.18}$$

where R_{ij} is the theoretical error variance of P_{ij} for a bin in (μ, k_{ref}) space centered on $(\mu_i, k_{\mathrm{ref}\,j})$. As long as the theoretical error is assumed to be small, it is also a valid approximation to neglect the ϵ_{ij}-dependence of the denominator, in order to find a simple analytic solution for ϵ_{ij}, which, injected back in eq. (C.18), gives

$$-2\ln\mathcal{L}_b = \sum_{i,j} \frac{\left(P_{ij}^{\mathrm{obs}} - P_{ij}^{\mathrm{th}}\right)^2}{2(P_{ij}^{\mathrm{th}})^2/N_{ij} + R_{ij}}. \tag{C.19}$$

In other words, the theoretical error variance simply adds up to the noise variance.

Note that we explicitly checked that it is legitimate to neglect the ϵ_{ij}-dependence of the likelihood denominator when minimizing over ϵ_{ij}. We also coded the full likelihood with explicit minimization over each ϵ_{ij}, and found the same results up to very good accuracy.

We choose a numerical value of R_{ij} motivated mainly by the current level of precision of the HALOFIT algorithm. We assume a relative error on the non-linear power spectrum of the form

$$\alpha(k,z) \equiv \frac{\Delta P_{\mathrm{NL}}^{\mathrm{th}}(k,z)}{P_{\mathrm{NL}}^{\mathrm{th}}(k,z)} = \frac{\ln[1 + k/k_\sigma(z)]}{1 + \ln[1 + k/k_\sigma(z)]}\, 0.05\;, \tag{C.20}$$

where $k_\sigma(z)$ is the scale of non-linearity computed by HALOFIT. This function increases from zero to 5% around the scale of non-linearity. Using the function $k(k_{\mathrm{ref}}, \mu, \bar{z})$, this error can easily be propagated to the theoretical observable spectrum

$$\alpha(k_{\mathrm{ref}}, \mu, \bar{z}) \equiv \alpha(k(k_{\mathrm{ref}}, \mu, \bar{z}), \bar{z}) = \frac{\Delta P^{\mathrm{th}}(k_{\mathrm{ref}}, \mu, \bar{z})}{P^{\mathrm{th}}(k_{\mathrm{ref}}, \mu, \bar{z})}\;. \tag{C.21}$$

In terms of the discretized observable spectrum, the error reads

$$\alpha_{ij} = \alpha(k_{\mathrm{ref}\,j}, \mu_i, \bar{z})\;. \tag{C.22}$$

The error variance R_{ij} should be proportional to the power spectrum variance $(\alpha_{ij}P_{ij}^{\mathrm{th}})^2$. We also assume that the error makes a constant contribution to each logarithmic interval in the space where observations are performed, i.e. is of the form

$$R_{ij} \propto (\alpha_{ij}P_{ij}^{\mathrm{th}})^2 \frac{k_{\mathrm{ref}\,j}}{d\mu\; dk_{\mathrm{ref}}}\;. \tag{C.23}$$

We normalize the error variance R_{ij} in such a way that a one-sigma theoretical error in

each data point results in increasing the effective χ^2 by one unit, namely,

$$R_{ij} = \left[2B \left(\ln \frac{k_{\max}}{k_{\min}} \right) \right] (\alpha_{ij} P_{ij}^{\text{th}})^2 \frac{k_{\text{ref}j}}{d\mu \; dk_{\text{ref}}} \; , \tag{C.24}$$

where B is the number of bins. The role of the normalization factor between squared brackets will become clear below. The likelihood becomes (using eq. (C.19) and going back to the continuous limit)

$$\mathcal{L} = \Pi_b \, \mathcal{N}_b \exp \left[-\frac{1}{2} \int_{-1}^{1} \frac{d\mu}{2} \int_{k_{\min}}^{k_{\max}} \frac{dk_{\text{ref}}}{k_{\text{ref}}} \frac{(P^{\text{obs}} - P^{\text{th}})^2}{(P^{\text{th}})^2 \left\{ \frac{(2\pi)^2}{k_{\text{ref}}^3 V_{\text{eff}}} + \alpha^2 B \ln \frac{k_{\max}}{k_{\min}} \right\}} \right] \; , \tag{C.25}$$

where we omitted the argument $(k_{\text{ref}}, \mu, \bar{z}_b)$ of the functions P^{th}, P^{obs}, V_{eff} and α. If one assumes that the observed and theoretical spectra differ by αP^{th} for each (k, μ, z), and that in the denominator the theoretical error dominates over the observational one ($V_{\text{eff}} = \infty$), then

$$\mathcal{L} = \Pi_b \, \mathcal{N}_b \exp \left[-\frac{1}{2} \int_{-1}^{1} \frac{d\mu}{2} \int_{k_{\min}}^{k_{\max}} \frac{dk_{\text{ref}}}{k_{\text{ref}}} \frac{1}{B \ln \frac{k_{\max}}{k_{\min}}} \right] = (\Pi_b \mathcal{N}_b) \exp \left[-\frac{1}{2} \right] \; , \tag{C.26}$$

which corresponds to a shift by $\Delta\chi^2_{\text{eff}} = 1$ with respect to the maximum likelihood $\mathcal{L} = \Pi_b \mathcal{N}_b$.

If we had assumed the error to be fully correlated, instead of increasing the denominator of the likelihood, we would have replaced P^{th} by $P^{\text{th}}(1 + \epsilon\alpha)$, multiplied the likelihood by $\sqrt{1/2\pi} \exp[-\epsilon^2/2]$, and marginalized/minimized over ϵ. Then, the assumption $P^{\text{obs}} = P^{\text{th}}(1 + \alpha)$ would correspond to an optimal choice $\epsilon = 1$ in the large V_{eff} limit, and would also lead to a shift in $\Delta\chi^2_{\text{eff}}$ by one unit with respect to the assumption $P^{\text{obs}} = P^{\text{th}}$. In our case, we obtain the same shifting while assuming statistically independent errors for each data point.

Finally, the likelihood can be simplified to

$$\mathcal{L} = \Pi_b \mathcal{N}_b \exp \left[-\frac{1}{2} \int_{-1}^{1} \frac{d\mu}{2} \int_{k_{\min}}^{k_{\max}} \frac{dk_{\text{ref}}}{k_{\text{ref}}} \frac{\left(\frac{H_{\text{ref}}}{D_{A\text{ref}}^2} P_g^{\text{obs}} - \frac{H}{D_A^2} P_g^{\text{th}} \right)^2}{\frac{(2\pi)^2}{k_{\text{ref}}^3 V_{\text{survey}}} \left(\frac{H}{D_A^2} P_g^{\text{th}} + \frac{H}{D_A^2} \frac{1}{n_g} \right)^2 + \left(\alpha \frac{H}{D_A^2} P_g^{\text{th}} \right)^2 B \ln \frac{k_{\max}}{k_{\min}}} \right] \; , \tag{C.27}$$

where we omitted the argument $\bar{z}_b$ in the functions V_{survey}, D_A, H and n_g. This is exactly the relation implemented in our code.

C.1.5 Accounting for an extra neutrino-related error

The impact of massive neutrinos on non-linear corrections to the power spectrum has been investigated in [39]. By comparing with N-body simulations including neutrino particles, the authors of [39] re-calibrated HALOFIT, with a new neutrino mass dependent correction. This fitting procedure is of course not perfect and adds a systematic error growing with the neutrino mass. It was found that the leading error can be described with a correction

$$P_{NL}(k) = P_{NL}^{\text{halofit}}(k)(1 + e_\nu \sigma_\nu(k, z)), \qquad \sigma_\nu(k, z) = \frac{\ln[1 + k/k_\sigma(z)]}{1 + \ln[1 + k/k_\sigma(z)]} f_\nu \quad \text{(C.28)}$$

with $f_\nu \equiv \omega_\nu/\omega_m$, and e_ν is an unknown correction of unit variance, that we will treat as a Gaussian nuisance parameter. Hence our final definition of the likelihood accounting for both types of error reads

$$\mathcal{L} = \mathcal{N} \exp\left[-\frac{1}{2} \int_{-1}^{1} \frac{d\mu}{2} \int_{k_{\min}}^{k_{\max}} \frac{dk_{\text{ref}}}{k_{\text{ref}}} \frac{(P^{\text{obs}} - [P^{\text{th}}(1 + e_\nu \sigma_\nu)])^2}{[P^{\text{th}}(1 + e_\nu \sigma_\nu)]^2 \left[\frac{(2\pi)^2}{k_{\text{ref}}^3 V_{\text{eff}}} + \alpha^2 B \ln \frac{k_{\max}}{k_{\min}} \right]} \right]$$

$$\times \frac{1}{\sqrt{2\pi}} \exp\left[-\frac{1}{2} e_\nu^2 \right] , \tag{C.29}$$

where we omitted the argument $(k_{\text{ref}}, \mu, \bar{z})$ of the functions P^{obs}, P^{th}, σ_ν, α_ν and V_{eff}. Note that the correction proportional to e_ν should not be added to P^{obs} since we are assuming for simplicity that the fiducial value of e_ν in the mock data is zero.

C.2 Cosmic shear survey implementation

C.2.1 Observed spectrum

As in e.g. [174, 173], we define the likelihood of the shear auto or cross-correlation power spectrum (in the Limber approximation) in bins i and j:

$$C_l^{ij} = H_0^4 \int_0^\infty \frac{dz}{H(z)} W_i(z) W_j(z) P_{\text{NL}}\left(k = \frac{l}{r(z)}, z \right) . \tag{C.30}$$

Here, $W_i(z)$ is the window function of the i'th bin. It can be evaluated as a function of the radial distribution of galaxies in each redshift bin, $D_i(z)$, obtained by convolving the full radial distribution $D(z)$ with the photometric redshift uncertainty function $\mathcal{P}(z, z_{\text{ph}})$,

multiplied the top-hat window function of each bin:

$$W_i(z) = \frac{3}{2}\Omega_m(1+z)F_i(z) \tag{C.31}$$

$$F_i(z) = \int_0^\infty \frac{n_i(z_s)(r(z_s) - r(z))}{r(z_s)}dz_s \tag{C.32}$$

$$n_i(z) = \frac{D_i(z)}{\int_0^\infty D_i(z')dz'} \tag{C.33}$$

$$D_i(z) = \int_{z_i^{\mathrm{min}}}^{z_i^{\mathrm{max}}} \mathcal{P}(z, z_{\mathrm{ph}}) D(z_{\mathrm{ph}}) dz_{\mathrm{ph}} \,. \tag{C.34}$$

The radial distribution $D(z)$ can be arbitrarily normalized, since $n_i(z)$ is anyway normalized to one. We will assume that the photometric redshift uncertainty function is normalized to $\int_0^\infty \mathcal{P}(z, z_{\mathrm{ph}})dz_{\mathrm{ph}} = 1$, but a different normalization would not impact the final result for the same reason as for $D(z)$. The noise spectrum contaminating the measurement of C_l^{ij} is given by the diagonal matrix in ij space:

$$N_l^{ij} = \delta_{ij}\langle\gamma_{rms}^2\rangle n_i^{-1} \,, \tag{C.35}$$

where $\langle\gamma_{rms}^2\rangle^{1/2}$ is the root mean square intrinsic shear (like in the forecasts of the Euclid Red Book [160], we assume that this quantity is equal to 0.30), and n_i is the number of galaxies per steradian in the i'th bin, given by

$$n_i = 3600 \, d \, (180/\pi)^2 \hat{n}_i \,, \tag{C.36}$$

where d is the full number of galaxies per square arcminute in all bins, and $\hat{n}_i$ is the fraction of galaxies in the i'th bin, given by:

$$\hat{n}_i = \frac{\int_{z_i^{min}}^{z_i^{max}} D(z)}{\int_0^\infty D(z)} \,. \tag{C.37}$$

We used the survey specifications for $D(z)$, $\mathcal{P}(z)$, d and f_{sky} detailed in Appendix C.2.3.

Using $dz/dr = H$, we can write the same integrals in a different way (used in other papers and in our code):

$$C_l^{ij} = \frac{9}{16}\Omega_m^2 H_0^4 \int_0^\infty dr \, r^{-2} g_i(r) \, g_j(r) \, P\left(k = \frac{l}{r}, z(r)\right) \tag{C.38}$$

with

$$g_i(r) = 2r(1 + z(r)) \int_0^\infty dr_s \frac{\eta_i(r_s)(r_s - r)}{r_s} \tag{C.39}$$

$$\eta_i(r) = H(r)n_i(z(r)) \tag{C.40}$$

and $n_i(z)$ is the same as before.

C.2.2 Likelihood

Let's assume some theoretical spectra $C_l^{\text{th}\,ij}$ (here, the spectra of each model that we want to fit to the data, exploring the space of free cosmological parameters), and some observed spectra $\tilde{C}_l^{\text{obs}\,ij}$. The matrix $\tilde{\mathbf{C}}_l^{\text{obs}}$ of element $\tilde{C}_l^{\text{obs}\,ij}$ is called the data covariance matrix. It can be inferred from the observed multipoles $a_{lm}^{\text{obs}\,i}$, which are Gaussian distributed with a variance independent of m in an ideal full-sky experiment, so that

$$\tilde{C}_l^{\text{obs}\,ij} = (2l+1)^{-1} \sum_{m=-l}^{l} [a_{lm}^{\text{obs}\,i*} a_{lm}^{\text{obs}\,j}] \ . \tag{C.41}$$

For a parameter forecast, instead of the covariance matrix of mock data, we can use some fiducial spectra corrected by the noise spectra of the experiment at hand:

$$\tilde{C}_l^{\text{obs}\,ij} = C_l^{\text{fiducial}\,ij} + N_l^{ij} \ . \tag{C.42}$$

This data covariance matrix should be compared with the theoretical covariance matrix defined as

$$\tilde{C}_l^{\text{th}\,ij} = C_l^{\text{th}\,ij} + N_l^{ij} \ . \tag{C.43}$$

We define the determinant of these $N \times N$ symmetric matrices:

$$d_l^{\text{th}} = \det\left(\tilde{C}_l^{\text{th}\,ij}\right) \tag{C.44}$$

$$d_l^{\text{obs}} = \det\left(\tilde{C}_l^{\text{obs}\,ij}\right) \ . \tag{C.45}$$

The determinants are homogeneous polynomials of order N in the spectra, e.g. for $N = 2$:

$$d_l^{\text{th}} = \tilde{C}_l^{\text{th}\,11} \tilde{C}_l^{\text{th}\,22} - (\tilde{C}_l^{\text{th}\,12})^2 \ . \tag{C.46}$$

The quantity d_l^{mix} can be built starting from d_l^{th}, and replacing one after each other the theoretical spectra $\tilde{C}_l^{\text{th}\,ij}$ by the corresponding $\tilde{C}_l^{\text{obs}\,ij}$, e.g. for $N = 2$:

$$d_l^{\text{mix}} = \tilde{C}_l^{\text{obs}\,11} \tilde{C}_l^{\text{th}\,22} + \tilde{C}_l^{\text{th}\,11} \tilde{C}_l^{\text{obs}\,22} - 2\,\tilde{C}_l^{\text{th}\,12} \tilde{C}_l^{\text{obs}\,12} \ . \tag{C.47}$$

So, d_l^{mix} is always linear in the $\tilde{C}_l^{\text{obs}\,ij}$'s. By construction, when $\tilde{C}_l^{\text{th}\,ij} = \tilde{C}_l^{\text{obs}\,ij}$, one has $d_l^{mix} = N d_l^{\text{th}} = N d_l^{\text{obs}}$. Since in an ideal full-sky experiment, the different multipoles are uncorrelated in (l, m) space, the likelihood of the observed spectra given the theoretical

spectra is as simple as:

$$\mathcal{L} = \mathcal{N} \, \Pi_{lm} \left\{ \frac{1}{(d_l^{\text{th}})^{1/2}} \exp\left[-\frac{1}{2} \mathbf{a}_{lm}^{\text{obs}\,\dagger} (\tilde{\mathbf{C}}_l^{\text{th}})^{-1} \mathbf{a}_{lm}^{\text{obs}} \right] \right\} \, , \tag{C.48}$$

where $\mathbf{a}_{lm}^{\text{obs}} = \left\{ a_{lm}^{\text{obs}\,\text{i}} \right\}$ is the N-dimensional vector of observed multipoles in each bin, $\tilde{\mathbf{C}}_l^{\text{th}}$ is the theoretical covariance matrix of element $C_l^{\text{th}\,\text{ij}}$ and $\mathcal{N}$ is a normalisation factor. After some simple algebra[1], the likelihood simplifies to

$$\mathcal{L} = \mathcal{N} \, \Pi_l \left\{ \frac{1}{(d_l^{\text{th}})^{1/2}} \exp\left[-\frac{(2l+1)}{2} \frac{d_l^{mix}}{d_l^{\text{th}}} \right] \right\} \, . \tag{C.49}$$

The effective chi square

$$\chi_{\text{eff}}^2 \equiv -2\ln \mathcal{L} = -2\ln \mathcal{N} + \sum_l (2l+1) \left(\frac{d_l^{mix}}{d_l^{\text{th}}} + \ln d_l^{\text{th}} \right) \, , \tag{C.50}$$

reaches its minimum for $\tilde{\mathbf{C}}_l^{obs} = \tilde{\mathbf{C}}_l^{th}$, corresponding to

$$\chi_{\text{eff}}^{2\,\text{min}} \equiv -2\ln \mathcal{L}_{\text{max}} = -2\ln \mathcal{N} + \sum_l (2l+1) \left(N + \ln d_l^{\text{obs}} \right) \, . \tag{C.51}$$

The χ^2 relative to the best-fit model is then equal to

$$\Delta\chi_{\text{eff}}^2 \equiv -2\ln \frac{\mathcal{L}}{\mathcal{L}_{\text{max}}} = \sum_l (2l+1) \left(\frac{d_l^{mix}}{d_l^{\text{th}}} + \ln \frac{d_l^{\text{th}}}{d_l^{\text{obs}}} - N \right) \, . \tag{C.52}$$

Finally, a first-order approximation to account for the limited sky coverage of a given experiment, consists of increasing the cosmic variance by a factor $f_{\text{sky}}^{-1/2}$, equivalent to postulating:

$$\Delta\chi_{\text{eff}}^2 \equiv \sum_l (2l+1) f_{\text{sky}} \left(\frac{d_l^{mix}}{d_l^{\text{th}}} + \ln \frac{d_l^{\text{th}}}{d_l^{\text{obs}}} - N \right) \, . \tag{C.53}$$

This is precisely the expression used in the code.

C.2.3   Survey specifications and implementation details

A given survey is specified by $D(z)$, $\mathcal{P}(z)$, d, and finally by the covered faction of the sky f_{sky}; it can then be decomposed in redshift bins according to some strategy defined by the user. For a *Euclid*-like experiment we use the same characteristics as in the Euclid

---

[1]in particular, using $A^{-1} = \text{adj}(A)/\det(A)$ where $\text{adj}(A)$ is the adjugate matrix of A, i.e. the transpose of the matrix of cofactors of A.

Red Book [160]:

$$
\begin{aligned}
D(z) &= z^2 \exp[-(z/z_0)^{1.5}] \quad \text{for} \quad z < z^{max} = 3.5 \\
&\quad \text{with mean redshift} \quad z_{\text{mean}} = 1.412 z_0 = 0.9 \\
\mathcal{P}(z, z_{\text{ph}}) &= \frac{1}{\sqrt{2\pi\sigma_{\text{ph}}^2}} \exp\left[-\frac{1}{2}\left(\frac{z - z_{\text{ph}}}{\sigma_{\text{ph}}}\right)^2\right] \\
&\quad \text{with} \quad \sigma_{\text{ph}} = 0.05(1 + z) \\
d &= 30\,\text{arcmn}^{-2} \\
f_{sky} &= 0.375 \ .
\end{aligned}
$$

$$(C.54)$$
$$(C.55)$$
$$(C.56)$$
$$(C.57)$$

We assume five bins, with the first bin starting at $z_1^{min} = 0$, the last one ending at $z_N^{max} = 3.5$, and bin edges $z_i^{min} = z_{i-1}^{max}$ chosen such that each bin contains the same number of galaxies, i.e. $\hat{n}_i = 1/N$.

C.2.4 Accounting for a global uncorrelated theoretical error

Like for the power spectrum likelihood, taking into account an uncorrelated error on each data point is equivalent to minimizing over a number $L \equiv (l_{\max} - l_{\min} + 1)$ of nuisance parameters ϵ_l:

$$
\Delta\chi_{\text{eff}}^2 \equiv \sum_{l=l_{\min}}^{l_{\max}} \min_{-\infty < \epsilon < +\infty} \left[(2l+1)f_{\text{sky}}\left(\frac{\tilde{d}_l^{mix}(\epsilon_l)}{\tilde{d}_l^{\text{th}}(\epsilon_l)} + \ln\frac{\tilde{d}_l^{\text{th}}(\epsilon_l)}{d_l^{\text{obs}}} - N\right) + \epsilon_l^2\right] \ . \quad (C.58)
$$

Here, $\tilde{d}_l^{\text{th}}(\epsilon_l)$ stands for the determinant of the theory covariance matrix shifted by the theoretical error covariance matrix R_l^{ij}:

$$
\tilde{d}_l^{\text{th}}(\epsilon_l) = \det(\tilde{C}_l^{\text{th}\,ij} + \epsilon_l R_l^{ij}). \quad (C.59)
$$

Similarly, $\tilde{d}_l^{\text{mix}}(\epsilon_l)$ stands for the sum of N terms, each one being the determinant of a matrix built from $\tilde{C}_l^{\text{th}\,ij} + \epsilon_l R_l^{ij}$, where one column has been replaced by the same column in the observed covariance matrix. Hence the quantity d_l^{mix} defined just above eq. (C.47) is identical to $\tilde{d}_l^{\text{mix}}(0)$.

Note that for simplicity, we consider here uncorrelated errors for each l, but not for each bin. This approach could easily be generalized to independent bin errors, at the expense of introducing more nuisance parameters.

In the case of the power spectrum likelihood, we could find an analytical approximation of the nuisance parameter value minimizing the effective χ^2. In the present case, we checked that simple approximate solutions are not accurate enough. We perform a numerical

minimization over each ϵ_l within the likelihood routine, using Newton's method.

We define our theoretical error covariance matrix R_l^{ij} in a similar way as for the power spectrum likelihood. We start from the power spectrum relative error function $\alpha(k, z)$ defined in eq.(C.20). The power spectrum error can be propagated to a covariance matrix error E_l^{ij}:

$$E_l^{ij} = \frac{9}{16}\Omega_m^2 H_0^4 \int_0^\infty dr\, r^{-2} g_i(r)\, g_j(r)\, \alpha\left(k = \frac{l}{r}, z(r)\right) P^{\text{th}}\left(k = \frac{l}{r}, z(r)\right) \ . \quad \text{(C.60)}$$

The theoretical error matrix R_l^{ij} should be proportional to E_l^{ij}. We normalize it to

$$R_l^{ij} = L^{1/2} E_l^{ij}, \quad \text{(C.61)}$$

in such a way that enforcing a one-sigma theoretical error for each l results in an increase of the χ^2 by one (as would be the case for a fully correlated theoretical error with the same amplitude). Then, if one assumes that for each l the observed spectra are equal to the theoretical ones shifted by a one-sigma theoretical error ($\tilde{C}_l^{\text{obs}} = \tilde{C}_l^{\text{th}} + E_l^{ij}$), the minimization gives (up to a very good approximation) $\epsilon_l = L^{-1/2}$, and

$$\Delta\chi_{\text{eff}}^2 = \sum_l \left[(2l + 1) f_{\text{sky}} \left(N + 0 - N \right) + L^{-1} \right] = 1. \quad \text{(C.62)}$$

C.2.5 Accounting for an extra neutrino-related error

Finally, we account for the correlated error modelling neutrino-related uncertainties by multiplying the theoretical power spectrum $P^{\text{th}}(k, z)$ by a factor $(1 + e_\nu \sigma_\nu(k, z))$, as in equation (C.28), as well as adding e_ν^2 to $\Delta\chi_{\text{eff}}^2$. The nuisance parameter e_ν is then marginalized over. Note that the factor $(1 + e_\nu \sigma_\nu(k, z))$ should not multiply the observed/fiducial spectrum, as long as we assume a fiducial value of e_ν equal to zero.

Bibliography

[1] B. Audren, J. Lesgourgues, K. Benabed, and S. Prunet, "Conservative Constraints on Early Cosmology: an illustration of the Monte Python cosmological parameter inference code," JCAP **1302** (2013) 001, `arXiv:1210.7183 [astro-ph.CO]`.

[2] B. Audren, "Separate Constraints on Early and Late Cosmology," `arXiv:1312.5696 [astro-ph.CO]`.

[3] G. Giesen, J. Lesgourgues, B. Audren, and Y. Ali-Haimoud, "CMB photons shedding light on dark matter," JCAP **1212** (2012) 008, `arXiv:1209.0247 [astro-ph.CO]`.

[4] B. Audren, J. Lesgourgues, G. Mangano, P. D. Serpico, and T. Tram, "Strongest model-independent bound on the lifetime of Dark Matter," `arXiv:1407.2418 [astro-ph.CO]`.

[5] B. Audren, J. Lesgourgues, S. Bird, M. G. Haehnelt, and M. Viel, "Neutrino masses and cosmological parameters from a Euclid-like survey: Markov Chain Monte Carlo forecasts including theoretical errors," JCAP **1301** (2013) 026, `arXiv:1210.2194 [astro-ph.CO]`.

[6] E. Hubble, "A Relation between Distance and Radial Velocity among Extra-Galactic Nebulae," Proceedings of the National Academy of Science **15** (Mar., 1929) 168–173.

[7] **Supernova Cosmology Project** Collaboration, S. Perlmutter et al., "Measurements of Omega and Lambda from 42 high redshift supernovae," Astrophys.J. **517** (1999) 565–586, `arXiv:astro-ph/9812133 [astro-ph]`.

[8] **Supernova Search Team** Collaboration, A. G. Riess et al., "Observational evidence from supernovae for an accelerating universe and a cosmological constant," Astron.J. **116** (1998) 1009–1038, `arXiv:astro-ph/9805201 [astro-ph]`.

[9] B. Audren, D. Blas, J. Lesgourgues, and S. Sibiryakov, "Cosmological constraints on Lorentz violating dark energy," JCAP **1308** (2013) 039, `arXiv:1305.0009 [astro-ph.CO]`.

[10] C. Blake, E. A. Kazin, F. Beutler, T. M. Davis, D. Parkinson, S. Brough, M. Colless, C. Contreras, W. Couch, S. Croom, D. Croton, M. J. Drinkwater, K. Forster, D. Gilbank, M. Gladders, K. Glazebrook, B. Jelliffe, R. J. Jurek, I.-H. Li, B. Madore, D. C. Martin, K. Pimbblet, G. B. Poole, M. Pracy, R. Sharp, E. Wisnioski, D. Woods, T. K. Wyder, and H. K. C. Yee, "The WiggleZ Dark Energy Survey: mapping the distance-redshift relation with baryon acoustic oscillations," Mon. Not. R. Astron. Soc. **418** (Dec., 2011) 1707–1724, arXiv:1108.2635 [astro-ph.CO].

[11] **Planck Collaboration** Collaboration, P. Ade et al., "Planck 2013 results. XVI. Cosmological parameters," arXiv:1303.5076 [astro-ph.CO].

[12] J. M. Bardeen, "Gauge Invariant Cosmological Perturbations," Phys.Rev. **D22** (1980) 1882–1905.

[13] T. H.-C. Lu, K. Ananda, C. Clarkson, and R. Maartens, "The cosmological background of vector modes," JCAP **0902** (2009) 023, arXiv:0812.1349 [astro-ph].

[14] J. García-Bellido, R. Durrer, E. Fenu, D. G. Figueroa, and M. Kunz, "The local B-polarization of the CMB: A very sensitive probe of cosmic defects," Physics Letters B **695** (Jan., 2011) 26–29, arXiv:1003.0299 [astro-ph.CO].

[15] **BICEP2 Collaboration** Collaboration, P. Ade et al., "Detection of B-Mode Polarization at Degree Angular Scales by BICEP2," Phys.Rev.Lett. **112** (2014) 241101, arXiv:1403.3985 [astro-ph.CO].

[16] R. Flauger, J. C. Hill, and D. N. Spergel, "Toward an Understanding of Foreground Emission in the BICEP2 Region," arXiv:1405.7351 [astro-ph.CO].

[17] B. Audren, D. G. Figueroa, and T. Tram, "A note of clarification: BICEP2 and Planck are not in tension," arXiv:1405.1390 [astro-ph.CO].

[18] J. Martin, C. Ringeval, R. Trotta, and V. Vennin, "Compatibility of Planck and BICEP2 in the Light of Inflation," arXiv:1405.7272 [astro-ph.CO].

[19] C.-P. Ma and E. Bertschinger, "Cosmological perturbation theory in the synchronous and conformal Newtonian gauges," Astrophys. J. **455** (1995) 7–25, arXiv:astro-ph/9506072.

[20] J. Lesgourgues and T. Tram, "Fast and accurate CMB computations in non-flat FLRW universes," arXiv:1312.2697 [astro-ph.CO].

[21] F. Bernardeau, S. Colombi, E. Gaztanaga, and R. Scoccimarro, "Large scale structure of the universe and cosmological perturbation theory," Phys.Rept. **367** (2002) 1–248, arXiv:astro-ph/0112551 [astro-ph].

[22] J. Lesgourgues and T. Tram, "The Cosmic Linear Anisotropy Solving System (CLASS) IV: efficient implementation of non-cold relics,"JCAP **9** (Sept., 2011) 32, `arXiv:1104.2935 [astro-ph.CO]`.

[23] J. Lesgourgues, "The Cosmic Linear Anisotropy Solving System (CLASS) I: Overview," `arXiv:1104.2932 [astro-ph.IM]`.

[24] D. Blas, J. Lesgourgues, and T. Tram, "The Cosmic Linear Anisotropy Solving System (CLASS) II: Approximation schemes," JCAP **1107** (2011) 034, `arXiv:1104.2933 [astro-ph.CO]`.

[25] **ATLAS Collaboration** Collaboration, G. Aad et al., "Observation of a new particle in the search for the Standard Model Higgs boson with the ATLAS detector at the LHC," Phys.Lett. **B716** (2012) 1–29, `arXiv:1207.7214 [hep-ex]`.

[26] **CMS Collaboration** Collaboration, S. Chatrchyan et al., "Observation of a new boson at a mass of 125 GeV with the CMS experiment at the LHC," Phys.Lett. **B716** (2012) 30–61, `arXiv:1207.7235 [hep-ex]`.

[27] F. Bezrukov, "The Higgs field as an inflaton," Class.Quant.Grav. **30** (2013) 214001, `arXiv:1307.0708 [hep-ph]`.

[28] A. Linde, "Inflationary Cosmology after Planck 2013," `arXiv:1402.0526 [hep-th]`.

[29] J. Rubio and M. Shaposhnikov, "Higgs-Dilaton Cosmology: Universality vs. Criticality," `arXiv:1406.5182 [hep-ph]`.

[30] W. Hu, "CMB temperature and polarization anisotropy fundamentals," Annals Phys. **303** (2003) 203–225, `arXiv:astro-ph/0210696 [astro-ph]`.

[31] D. Blas, M. Garny, and T. Konstandin, "On the non-linear scale of cosmological perturbation theory," JCAP **1309** (2013) 024, `arXiv:1304.1546 [astro-ph.CO]`.

[32] J. Lesgourgues and S. Pastor, "Massive neutrinos and cosmology," Phys.Rept. **429** (2006) 307–379, `arXiv:astro-ph/0603494 [astro-ph]`.

[33] M. Cirelli and A. Strumia, "Minimal Dark Matter: Model and results," New J.Phys. **11** (2009) 105005, `arXiv:0903.3381 [hep-ph]`.

[34] T. Asaka and M. Shaposhnikov, "The nuMSM, dark matter and baryon asymmetry of the universe," Phys.Lett. **B620** (2005) 17–26, `arXiv:hep-ph/0505013 [hep-ph]`.

[35] E. Bulbul, M. Markevitch, A. Foster, R. K. Smith, M. Loewenstein, et al.,
"Detection of An Unidentified Emission Line in the Stacked X-ray spectrum of
Galaxy Clusters," Astrophys.J. **789** (2014) 13, `arXiv:1402.2301`
`[astro-ph.CO]`.

[36] A. Boyarsky, O. Ruchayskiy, D. Iakubovskyi, and J. Franse, "An unidentified line
in X-ray spectra of the Andromeda galaxy and Perseus galaxy cluster,"
`arXiv:1402.4119 [astro-ph.CO]`.

[37] J. Jaeckel, J. Redondo, and A. Ringwald, "Signatures of a hidden cosmic
microwave background," Phys.Rev.Lett. **101** (2008) 131801, `arXiv:0804.4157`
`[astro-ph]`.

[38] S. Riemer-Sorensen, D. Parkinson, and T. M. Davis, "What is half a neutrino?
Reviewing cosmological constraints on neutrinos and dark radiation,"
`arXiv:1301.7102 [astro-ph.CO]`.

[39] S. Bird, M. Viel, and M. G. Haehnelt, "Massive Neutrinos and the Non-linear
Matter Power Spectrum," Mon.Not.Roy.Astron.Soc. **420** (2012) 2551–2561,
`arXiv:1109.4416 [astro-ph.CO]`.

[40] M. P. Hobson, Bayesian methods in cosmology. Cambridge University Press, 2010.

[41] R. E. Kass and A. E. Raftery, "Bayes factors," Journal of the american statistical
association **90** (1995) no. 430, 773–795.

[42] A. Lewis and S. Bridle, "Cosmological parameters from CMB and other data: A
Monte Carlo approach," Phys.Rev. **D66** (2002) 103511,
`arXiv:astro-ph/0205436 [astro-ph]`.

[43] A. Gelman, G. Roberts, and W. Gilks, "Efficient Metropolis jumping rules," in
Bayesian Statistics, J. M. Bernado et al., eds., vol. 5, p. 599. OUP, 1996.

[44] G. Robers, A. Gelman, and W. Gilks, "Weak convergence and optimal scaling or
random walk Metropolis algorithms," Annals of Applied Probability (1997)
110–120. http://www.jstor.org/view/10505164/di984007/98p0121o/0.

[45] F. Feroz, M. Hobson, and M. Bridges, "MultiNest: an efficient and robust
Bayesian inference tool for cosmology and particle physics,"
Mon.Not.Roy.Astron.Soc. **398** (2009) 1601–1614, `arXiv:0809.3437 [astro-ph]`.

[46] A. Lewis, "Efficient sampling of fast and slow cosmological parameters," Phys.Rev.
D87 (2013) 103529, `arXiv:1304.4473 [astro-ph.CO]`.

[47] J. J. M. Carrasco, S. Foreman, D. Green, and L. Senatore, "The Effective Field
Theory of Large Scale Structures at Two Loops," `arXiv:1310.0464`
`[astro-ph.CO]`.

172

[48] A. Manzotti, M. Peloso, M. Pietroni, M. Viel, and F. Villaescusa-Navarro, "A coarse grained perturbation theory for the Large Scale Structure, with cosmology and time independence in the UV," `arXiv:1407.1342 [astro-ph.CO]`.

[49] M. Biagetti, V. Desjacques, A. Kehagias, and A. Riotto, "Non-local halo bias with and without massive neutrinos," `arXiv:1405.1435 [astro-ph.CO]`.

[50] B. Audren and J. Lesgourgues, "Non-linear matter power spectrum from Time Renormalisation Group: efficient computation and comparison with one-loop," JCAP **1110** (2011) 037, `arXiv:1106.2607 [astro-ph.CO]`.

[51] M. Pietroni, "Flowing with Time: a New Approach to Nonlinear Cosmological Perturbations," JCAP **0810** (2008) 036, `arXiv:0806.0971 [astro-ph]`.

[52] **Wilkinson Microwave Anisotropy Probe** Collaboration, G. Hinshaw et al., "Nine-year Wilkinson Microwave Anisotropy Probe (WMAP) Observations: Cosmological Parameter Results,"APJS **208** (Oct., 2013) 19, `arXiv:1212.5226 [astro-ph.CO]`.

[53] **South Pole Telescope** Collaboration, B. A. Benson et al., "Cosmological Constraints from Sunyaev-Zel'dovich-selected Clusters with X-Ray Observations in the First 178 deg^2 of the South Pole Telescope Survey,"APJ **763** (Feb., 2013) 147, `arXiv:1112.5435 [astro-ph.CO]`.

[54] **Atacama Cosmology Telescope** Collaboration, J. L. Sievers et al., "The Atacama Cosmology Telescope: Cosmological parameters from three seasons of data," JCAP **1310** (2013) 060, `arXiv:1301.0824 [astro-ph.CO]`.

[55] F. L. Bezrukov, A. Magnin, and M. Shaposhnikov, "Standard Model Higgs boson mass from inflation," Phys.Lett. **B675** (2009) 88–92, `arXiv:0812.4950 [hep-ph]`.

[56] M. Vonlanthen, S. Rasanen, and R. Durrer, "Model-independent cosmological constraints from the CMB," JCAP **1008** (2010) 023, `arXiv:1003.0810 [astro-ph.CO]`.

[57] K. Story, C. Reichardt, Z. Hou, R. Keisler, K. Aird, et al., "A Measurement of the Cosmic Microwave Background Damping Tail from the 2500-square-degree SPT-SZ survey," Astrophys.J. **779** (2013) 86, `arXiv:1210.7231 [astro-ph.CO]`.

[58] A. Lewis and S. Bridle, "Cosmological parameters from CMB and other data: A Monte Carlo approach," Phys.Rev. **D66** (2002) 103511, `arXiv:astro-ph/0205436 [astro-ph]`.

[59] K. M. Smith, W. Hu, and M. Kaplinghat, "Cosmological Information from Lensed CMB Power Spectra," Phys.Rev. **D74** (2006) 123002, `arXiv:astro-ph/0607315 [astro-ph]`.

[60] **WMAP Collaboration** Collaboration, E. Komatsu et al., "Seven-Year Wilkinson Microwave Anisotropy Probe (WMAP) Observations: Cosmological Interpretation," Astrophys.J.Suppl. **192** (2011) 18, `arXiv:1001.4538` `[astro-ph.CO]`.

[61] C. Reichardt, L. Shaw, O. Zahn, K. Aird, B. Benson, et al., "A measurement of secondary cosmic microwave background anisotropies with two years of South Pole Telescope observations," Astrophys.J. **755** (2012) 70, `arXiv:1111.0932` `[astro-ph.CO]`.

[62] C. Howlett, A. Lewis, A. Hall, and A. Challinor, "CMB power spectrum parameter degeneracies in the era of precision cosmology," JCAP **1204** (2012) 027, `arXiv:1201.3654 [astro-ph.CO]`.

[63] J. Hamann, J. Lesgourgues, and G. Mangano, "Using BBN in cosmological parameter extraction from CMB: A Forecast for PLANCK," JCAP **0803** (2008) 004, `arXiv:0712.2826 [astro-ph]`.

[64] G. Mangano, G. Miele, S. Pastor, and M. Peloso, "A Precision calculation of the effective number of cosmological neutrinos," Phys.Lett. **B534** (2002) 8–16, `arXiv:astro-ph/0111408 [astro-ph]`.

[65] W. Hu and N. Sugiyama, "Small scale cosmological perturbations: An Analytic approach," Astrophys.J. **471** (1996) 542–570, `arXiv:astro-ph/9510117` `[astro-ph]`.

[66] S. Bashinsky and U. Seljak, "Neutrino perturbations in CMB anisotropy and matter clustering," Phys.Rev. **D69** (2004) 083002, `arXiv:astro-ph/0310198` `[astro-ph]`.

[67] R. Keisler, C. Reichardt, K. Aird, B. Benson, L. Bleem, et al., "A Measurement of the Damping Tail of the Cosmic Microwave Background Power Spectrum with the South Pole Telescope," Astrophys.J. **743** (2011) 28, `arXiv:1105.3182` `[astro-ph.CO]`.

[68] W. T. Hu, "Wandering in the Background: A CMB Explorer," `arXiv:astro-ph/9508126 [astro-ph]`.

[69] V. Marra, L. Amendola, I. Sawicki, and W. Valkenburg, "Cosmic variance and the measurement of the local Hubble parameter," Phys. Rev. Lett. 110, **241305** (2013) , `arXiv:1303.3121 [astro-ph.CO]`.

[70] **Planck Collaboration** Collaboration, P. Ade et al., "Planck intermediate results. XVI. Profile likelihoods for cosmological parameters," arXiv, 1311.1657 (2013) , `arXiv:1311.1657 [astro-ph.CO]`.

[71] L. Verde, P. Protopapas, and R. Jimenez, "Planck and the local Universe: quantifying the tension," `arXiv:1306.6766 [astro-ph.CO]`.

[72] D. Spergel, R. Flauger, and R. Hlozek, "Planck Data Reconsidered," `arXiv:1312.3313 [astro-ph.CO]`.

[73] A. G. Riess, L. Macri, S. Casertano, H. Lampeitl, H. C. Ferguson, et al., "A 3Telescope and Wide Field Camera 3," Astrophys.J. **730** (2011) 119, `arXiv:1103.2976 [astro-ph.CO]`.

[74] R. Amanullah, C. Lidman, D. Rubin, G. Aldering, P. Astier, et al., "Spectra and Light Curves of Six Type Ia Supernovae at 0.511 < z < 1.12 and the Union2 Compilation," Astrophys.J. **716** (2010) 712–738, `arXiv:1004.1711 [astro-ph.CO]`.

[75] F. Beutler, C. Blake, M. Colless, D. H. Jones, L. Staveley-Smith, et al., "The 6dF Galaxy Survey: Baryon Acoustic Oscillations and the Local Hubble Constant," Mon.Not.Roy.Astron.Soc. **416** (2011) 3017–3032, `arXiv:1106.3366 [astro-ph.CO]`.

[76] N. Padmanabhan, X. Xu, D. J. Eisenstein, R. Scalzo, A. J. Cuesta, et al., "A 2 per cent distance to z=0.35 by reconstructing baryon acoustic oscillations - I. Methods and application to the Sloan Digital Sky Survey," Mon.Not.Roy.Astron.Soc. **427** (2012) no. 3, 2132–2145, `arXiv:1202.0090 [astro-ph.CO]`.

[77] L. Anderson, E. Aubourg, S. Bailey, D. Bizyaev, M. Blanton, et al., "The clustering of galaxies in the SDSS-III Baryon Oscillation Spectroscopic Survey: Baryon Acoustic Oscillations in the Data Release 9 Spectroscopic Galaxy Sample," Mon.Not.Roy.Astron.Soc. **427** (2013) no. 4, 3435–3467, `arXiv:1203.6594 [astro-ph.CO]`.

[78] M. Tewes, F. Courbin, and G. Meylan, "COSMOGRAIL XI: Techniques for time delay measurement in presence of microlensing," `arXiv:1208.5598 [astro-ph.CO]`.

[79] S. Suyu, P. Marshall, M. Auger, S. Hilbert, R. Blandford, et al., "Dissecting the Gravitational Lens B1608+656. II. Precision Measurements of the Hubble Constant, Spatial Curvature, and the Dark Energy Equation of State," Astrophys.J. **711** (2010) 201–221, `arXiv:0910.2773 [astro-ph.CO]`.

[80] S. Suyu, M. Auger, S. Hilbert, P. Marshall, M. Tewes, et al., "Two accurate time-delay distances from strong lensing: Implications for cosmology," Astrophys.J. **766** (2013) 70, `arXiv:1208.6010 [astro-ph.CO]`.

[81] N. Padmanabhan and D. P. Finkbeiner, "Detecting dark matter annihilation with CMB polarization: Signatures and experimental prospects," Phys.Rev. **D72** (2005) 023508, `arXiv:astro-ph/0503486 [astro-ph]`.

[82] L. Zhang, X.-L. Chen, Y.-A. Lei, and Z.-G. Si, "The impacts of dark matter particle annihilation on recombination and the anisotropies of the cosmic microwave background," Phys.Rev. **D74** (2006) 103519, `arXiv:astro-ph/0603425 [astro-ph]`.

[83] A. Natarajan and D. J. Schwarz, "The effect of early dark matter halos on reionization," Phys.Rev. **D78** (2008) 103524, `arXiv:0805.3945 [astro-ph]`.

[84] A. V. Belikov and D. Hooper, "How Dark Matter Reionized The Universe," Phys.Rev. **D80** (2009) 035007, `arXiv:0904.1210 [hep-ph]`.

[85] M. Cirelli, F. Iocco, and P. Panci, "Constraints on Dark Matter annihilations from reionization and heating of the intergalactic gas," JCAP **0910** (2009) 009, `arXiv:0907.0719 [astro-ph.CO]`.

[86] S. Galli, F. Iocco, G. Bertone, and A. Melchiorri, "CMB constraints on Dark Matter models with large annihilation cross-section," Phys.Rev. **D80** (2009) 023505, `arXiv:0905.0003 [astro-ph.CO]`.

[87] T. R. Slatyer, N. Padmanabhan, and D. P. Finkbeiner, "CMB Constraints on WIMP Annihilation: Energy Absorption During the Recombination Epoch," Phys.Rev. **D80** (2009) 043526, `arXiv:0906.1197 [astro-ph.CO]`.

[88] A. Natarajan and D. J. Schwarz, "Distinguishing standard reionization from dark matter models," Phys.Rev. **D81** (2010) 123510, `arXiv:1002.4405 [astro-ph.CO]`.

[89] S. Galli, F. Iocco, G. Bertone, and A. Melchiorri, "Updated CMB constraints on Dark Matter annihilation cross-sections," Phys.Rev. **D84** (2011) 027302, `arXiv:1106.1528 [astro-ph.CO]`.

[90] D. P. Finkbeiner, S. Galli, T. Lin, and T. R. Slatyer, "Searching for Dark Matter in the CMB: A Compact Parameterization of Energy Injection from New Physics," Phys.Rev. **D85** (2012) 043522, `arXiv:1109.6322 [astro-ph.CO]`.

[91] G. Hutsi, J. Chluba, A. Hektor, and M. Raidal, "WMAP7 and future CMB constraints on annihilating dark matter: implications on GeV-scale WIMPs," Astron.Astrophys. **535** (2011) A26, `arXiv:1103.2766 [astro-ph.CO]`.

[92] A. Natarajan, "A closer look at CMB constraints on WIMP dark matter," Phys.Rev. **D85** (2012) 083517, `arXiv:1201.3939 [astro-ph.CO]`. Typo corrected in Eq.4, replaced to reflect the published version.

[93] X.-L. Chen and M. Kamionkowski, "Particle decays during the cosmic dark ages," Phys.Rev. **D70** (2004) 043502, `arXiv:astro-ph/0310473 [astro-ph]`.

[94] K. Ichiki, M. Oguri, and K. Takahashi, "WMAP constraints on decaying cold dark matter," Phys.Rev.Lett. **93** (2004) 071302, `arXiv:astro-ph/0403164 [astro-ph]`.

[95] L. Zhang, X. Chen, M. Kamionkowski, Z.-g. Si, and Z. Zheng, "Constraints on radiative dark-matter decay from the cosmic microwave background," Phys.Rev. **D76** (2007) 061301, `arXiv:0704.2444 [astro-ph]`.

[96] S. Kasuya and M. Kawasaki, "Early reionization by decaying particles in light of three year WMAP data," JCAP **0702** (2007) 010, `arXiv:astro-ph/0608283 [astro-ph]`.

[97] S. Yeung, M. Chan, and M.-C. Chu, "Cosmic Microwave Background constraints of decaying dark matter particle properties," Astrophys.J. **755** (2012) 108, `arXiv:1206.4114 [astro-ph.CO]`.

[98] P. Peebles, "Recombination of the Primeval Plasma," Astrophys.J. **153** (1968) 1.

[99] Y. Zeldovich, V. Kurt, and R. Sunyaev, "Recombination of hydrogen in the hot model of the universe," J.Exp.Theor.Phys. **28** (1969) 146.

[100] S. Seager, D. D. Sasselov, and D. Scott, "A new calculation of the recombination epoch," Astrophys.J. **523** (1999) L1–L5, `arXiv:astro-ph/9909275 [astro-ph]`.

[101] Y. Ali-Haimoud and C. M. Hirata, "HyRec: A fast and highly accurate primordial hydrogen and helium recombination code," Phys.Rev. **D83** (2011) 043513, `arXiv:1011.3758 [astro-ph.CO]`.

[102] D. Grin and C. M. Hirata, "Cosmological hydrogen recombination: The effect of extremely high-n states," Phys.Rev. **D81** (2010) 083005, `arXiv:0911.1359 [astro-ph.CO]`.

[103] J. Chluba, G. Vasil, and L. Dursi, "Recombinations to the Rydberg States of Hydrogen and Their Effect During the Cosmological Recombination Epoch," `arXiv:1003.4928 [astro-ph.CO]`.

[104] Y. Ali-Haimoud and C. M. Hirata, "Ultrafast effective multi-level atom method for primordial hydrogen recombination," Phys.Rev. **D82** (2010) 063521, `arXiv:1006.1355 [astro-ph.CO]`.

[105] M. Burgin, "Reduced multilevel atom method for calculating cosmological recombination kinetics," Bulletin of the Lebedev Physics Institute **37** (2010) no. 9, 280–283. http://dx.doi.org/10.3103/S1068335610090058.

[106] E. E. Kholupenko and A. Ivanchik, "Two-Photon 2s – 1s Transitions during Recombination of Hydrogen in the Universe," Astron.Lett. **32** (2006) 795–803, `arXiv:astro-ph/0611395 [astro-ph]`.

[107] J. Chluba and R. Sunyaev, "Cosmological hydrogen recombination: Ly-n line feedback and continuum escape," Astron.Astrophys. (2007) , arXiv:astro-ph/0702531 [astro-ph].

[108] C. M. Hirata, "Two-photon transitions in primordial hydrogen recombination," Phys.Rev. **D78** (2008) 023001, arXiv:0803.0808 [astro-ph].

[109] C. M. Hirata and J. Forbes, "Lyman-alpha transfer in primordial hydrogen recombination," Phys.Rev. **D80** (2009) 023001, arXiv:0903.4925 [astro-ph.CO].

[110] P. Peebles, S. Seager, and W. Hu, "Delayed recombination," Astrophys.J. **539** (2000) L1–L4, arXiv:astro-ph/0004389 [astro-ph].

[111] J. Shull and M. van Steenberg, "The ionization equilibrium of astrophysically abundant elements," Astrophys.J.Suppl. **48** (1982) 95–107.

[112] G. Huetsi, A. Hektor, and M. Raidal, "Constraints on leptonically annihilating Dark Matter from reionization and extragalactic gamma background," Astron.Astrophys. **505** (2009) 999–1005, arXiv:0906.4550 [astro-ph.CO].

[113] D. Scott and A. Moss, "Matter temperature after cosmological recombination," arXiv:0902.3438 [astro-ph.CO].

[114] A. Lewis, A. Challinor, and A. Lasenby, "Efficient computation of CMB anisotropies in closed FRW models," Astrophys.J. **538** (2000) 473–476, arXiv:astro-ph/9911177 [astro-ph].

[115] J. F. Navarro, C. S. Frenk, and S. D. White, "The Structure of cold dark matter halos," Astrophys.J. **462** (1996) 563–575, arXiv:astro-ph/9508025 [astro-ph].

[116] W. H. Press and P. Schechter, "Formation of galaxies and clusters of galaxies by selfsimilar gravitational condensation," Astrophys.J. **187** (1974) 425–438.

[117] Z. Lukic, K. Heitmann, S. Habib, S. Bashinsky, and P. M. Ricker, "The Halo Mass Function: High Redshift Evolution and Universality," Astrophys.J. **671** (2007) 1160–1181, arXiv:astro-ph/0702360 [ASTRO-PH].

[118] R. K. Sheth and G. Tormen, "Large scale bias and the peak background split," Mon.Not.Roy.Astron.Soc. **308** (1999) 119, arXiv:astro-ph/9901122 [astro-ph].

[119] D. Pequignot, P. Petitjean, and C. Boisson, "Total and effective radiative recombination coefficients,"Astron.Astrophys. **251** (Nov., 1991) 680–688.

[120] J. E. Gunn and B. A. Peterson, "On the Density of Neutral Hydrogen in Intergalactic Space," Astrophys.J. **142** (1965) 1633.

[121] X.-H. Fan, C. Carilli, and B. G. Keating, "Observational constraints on cosmic reionization," Ann.Rev.Astron.Astrophys. **44** (2006) 415–462, `arXiv:astro-ph/0602375 [astro-ph]`.

[122] J. Caruana, A. J. Bunker, S. M. Wilkins, E. R. Stanway, M. Lacy, et al., "No Evidence for Lyman-alpha Emission in Spectroscopy of z > 7 Candidate Galaxies," `arXiv:1208.5987 [astro-ph.CO]`.

[123] G. D. Becker, M. Rauch, and W. L. Sargent, "The Evolution of Optical Depth in the Ly-alpha Forest: Evidence Against Reionization at z 6," Astrophys.J. **662** (2007) 72–93, `arXiv:astro-ph/0607633 [astro-ph]`.

[124] I. D. McGreer, A. Mesinger, and X. Fan, "The first (nearly) model-independent constraint on the neutral hydrogen fraction at z 5–6," `arXiv:1101.3314 [astro-ph.CO]`.

[125] R. Cen, "The Universe was reionized twice," Astrophys.J. **591** (2003) 12–37, `arXiv:astro-ph/0210473 [astro-ph]`.

[126] J. S. B. Wyithe and A. Loeb, "Reionization of hydrogen and helium by early stars and quasars," Astrophys.J. **586** (2003) 693–708, `arXiv:astro-ph/0209056 [astro-ph]`.

[127] S. H. Hansen and Z. Haiman, "Do we need stars to reionize the universe at high redshifts? Early reionization by decaying heavy sterile neutrinos," Astrophys.J. **600** (2004) 26–31, `arXiv:astro-ph/0305126 [astro-ph]`.

[128] J. Schaye, T. Theuns, M. Rauch, G. Efstathiou, and W. L. Sargent, "The Thermal history of the intergalactic medium," Mon.Not.Roy.Astron.Soc. **318** (2000) 817, `arXiv:astro-ph/9912432 [astro-ph]`.

[129] R. Sunyaev and Y. Zeldovich, "The Observations of relic radiation as a test of the nature of X-Ray radiation from the clusters of galaxies," Comments Astrophys. Space Phys. **4** (1972) 173–178.

[130] M. Maggiore and A. Riotto, "The Halo Mass Function from Excursion Set Theory. I. Gaussian fluctuations with non-Markovian dependence on the smoothing scale," Astrophys.J. **711** (2010) 907–927, `arXiv:0903.1249 [astro-ph.CO]`.

[131] N. F. Bell, A. J. Galea, and K. Petraki, "Lifetime Constraints for Late Dark Matter Decay," Phys.Rev. **D82** (2010) 023514, `arXiv:1004.1008 [astro-ph.HE]`.

[132] M. Cirelli, E. Moulin, P. Panci, P. D. Serpico, and A. Viana, "Gamma ray constraints on Decaying Dark Matter," Phys.Rev. **D86** (2012) 083506, `arXiv:1205.5283 [astro-ph.CO]`.

[133] H. K. Dreiner, "An Introduction to explicit R-parity violation," Adv.Ser.Direct.High Energy Phys. **21** (2010) 565–583, arXiv:hep-ph/9707435 [hep-ph].

[134] R. Barbier, C. Berat, M. Besancon, M. Chemtob, A. Deandrea, et al., "R-parity violating supersymmetry," Phys.Rept. **420** (2005) 1–202, arXiv:hep-ph/0406039 [hep-ph].

[135] S. Palomares-Ruiz, "Model-Independent Bound on the Dark Matter Lifetime," Phys.Lett. **B665** (2008) 50–53, arXiv:0712.1937 [astro-ph].

[136] T. Hambye, "On the stability of particle dark matter," PoS **IDM2010** (2011) 098, arXiv:1012.4587 [hep-ph].

[137] J. A. Adams, S. Sarkar, and D. Sciama, "CMB anisotropy in the decaying neutrino cosmology," Mon.Not.Roy.Astron.Soc. **301** (1998) 210–214, arXiv:astro-ph/9805108 [astro-ph].

[138] M. Kaplinghat, R. E. Lopez, S. Dodelson, and R. J. Scherrer, "Improved treatment of cosmic microwave background fluctuations induced by a late decaying massive neutrino," Phys.Rev. **D60** (1999) 123508, arXiv:astro-ph/9907388 [astro-ph].

[139] S. De Lope Amigo, W. M.-Y. Cheung, Z. Huang, and S.-P. Ng, "Cosmological Constraints on Decaying Dark Matter," JCAP **0906** (2009) 005, arXiv:0812.4016 [hep-ph].

[140] M. Lattanzi and J. Valle, "Decaying warm dark matter and neutrino masses," Phys.Rev.Lett. **99** (2007) 121301, arXiv:0705.2406 [astro-ph].

[141] M. Lattanzi, "Decaying Majoron Dark Matter and Neutrino Masses," AIP Conf.Proc. **966** (2007) 163–169, arXiv:0802.3155 [astro-ph].

[142] Y. Gong and X. Chen, "Cosmological Constraints on Invisible Decay of Dark Matter," Phys.Rev. **D77** (2008) 103511, arXiv:0802.2296 [astro-ph].

[143] A. H. Peter, "Mapping the allowed parameter space for decaying dark matter models," Phys.Rev. **D81** (2010) 083511, arXiv:1001.3870 [astro-ph.CO].

[144] A. H. Peter and A. J. Benson, "Dark-matter decays and Milky Way satellite galaxies," Phys.Rev. **D82** (2010) 123521, arXiv:1009.1912 [astro-ph.GA].

[145] R. Huo, "Constraining Decaying Dark Matter," Phys.Lett. **B701** (2011) 530–534, arXiv:1104.4094 [hep-ph].

[146] S. Aoyama, K. Ichiki, D. Nitta, and N. Sugiyama, "Formulation and constraints on decaying dark matter with finite mass daughter particles," JCAP **1109** (2011) 025, arXiv:1106.1984 [astro-ph.CO].

[147] M.-Y. Wang, R. A. C. Croft, A. H. G. Peter, A. R. Zentner, and C. W. Purcell, "Lyman-alpha Forest Constraints on Decaying Dark Matter," arXiv:1309.7354 [astro-ph.CO].

[148] S. Aoyama, T. Sekiguchi, K. Ichiki, and N. Sugiyama, "Evolution of perturbations and cosmological constraints in decaying dark matter models with arbitrary decay mass products," arXiv:1402.2972 [astro-ph.CO].

[149] V. Berezinsky and J. Valle, "The KeV majoron as a dark matter particle," Phys.Lett. **B318** (1993) 360–366, arXiv:hep-ph/9309214 [hep-ph].

[150] F. Bazzocchi, M. Lattanzi, S. Riemer-Sorensen, and J. W. Valle, "X-ray photons from late-decaying majoron dark matter," JCAP **0808** (2008) 013, arXiv:0805.2372 [astro-ph].

[151] M. Lattanzi, S. Riemer-Sorensen, M. Tortola, and J. W. F. Valle, "Updated CMB, X- and gamma-ray constraints on majoron dark matter," Phys.Rev. **D88** (2013) 063528, arXiv:1303.4685 [astro-ph.HE].

[152] J. Schechter and J. Valle, "Neutrino Masses in SU(2) x U(1) Theories," Phys.Rev. **D22** (1980) 2227.

[153] D. Parkinson, S. Riemer-Sorensen, C. Blake, G. B. Poole, T. M. Davis, et al., "The WiggleZ Dark Energy Survey: Final data release and cosmological results," Phys.Rev. **D86** (2012) 103518, arXiv:1210.2130 [astro-ph.CO].

[154] **BOSS Collaboration** Collaboration, L. Anderson et al., "The clustering of galaxies in the SDSS-III Baryon Oscillation Spectroscopic Survey: Baryon Acoustic Oscillations in the Data Release 10 and 11 galaxy samples," arXiv:1312.4877 [astro-ph.CO].

[155] M.-Y. Wang and A. R. Zentner, "Weak Gravitational Lensing as a Method to Constrain Unstable Dark Matter," Phys.Rev. **D82** (2010) 123507, arXiv:1011.2774 [astro-ph.CO].

[156] M.-Y. Wang and A. R. Zentner, "Effects of Unstable Dark Matter on Large-Scale Structure and Constraints from Future Surveys," Phys.Rev. **D85** (2012) 043514, arXiv:1201.2426 [astro-ph.CO].

[157] M. Vogelsberger, S. Genel, V. Springel, P. Torrey, D. Sijacki, et al., "Introducing the Illustris Project: Simulating the coevolution of dark and visible matter in the Universe," arXiv:1405.2921 [astro-ph.CO].

[158] F. Villaescusa-Navarro, F. Marulli, M. Viel, E. Branchini, E. Castorina, et al., "Cosmology with massive neutrinos I: towards a realistic modeling of the relation between matter, haloes and galaxies," JCAP **1403** (2014) 011, arXiv:1311.0866 [astro-ph.CO].

[159] **Virgo Consortium** Collaboration, R. Smith et al., "Stable clustering, the halo model and nonlinear cosmological power spectra," Mon.Not.Roy.Astron.Soc. **341** (2003) 1311, arXiv:astro-ph/0207664 [astro-ph].

[160] R. Laureijs, J. Amiaux, S. Arduini, J.-L. Augueres, J. Brinchmann, et al., "Euclid Definition Study Report," arXiv:1110.3193 [astro-ph.CO].

[161] A. Mantz, S. W. Allen, and D. Rapetti, "The observed growth of massive galaxy clusters - IV. Robust constraints on neutrino properties,"Mon. Not. R. Astron. Soc. **406** (Aug., 2010) 1805–1814, arXiv:0911.1788 [astro-ph.CO].

[162] B. A. Reid, L. Verde, R. Jimenez, and O. Mena, "Robust neutrino constraints by combining low redshift observations with the CMB,"JCAP **1** (Jan., 2010) 3, arXiv:0910.0008 [astro-ph.CO].

[163] S. A. Thomas, F. B. Abdalla, and O. Lahav, "Upper Bound of 0.28 eV on Neutrino Masses from the Largest Photometric Redshift Survey,"Physical Review Letters **105** (July, 2010) 031301, arXiv:0911.5291 [astro-ph.CO].

[164] S. Saito, M. Takada, and A. Taruya, "Neutrino mass constraint from the Sloan Digital Sky Survey power spectrum of luminous red galaxies and perturbation theory,"Physical Review D **83** (Feb., 2011) 043529, arXiv:1006.4845 [astro-ph.CO].

[165] M. E. C. Swanson, W. J. Percival, and O. Lahav, "Cosmology at the frontier of neutrino physics," in American Institute of Physics Conference Series, J. Kouneiher, C. Barbachoux, T. Masson, and D. Vey, eds., vol. 1446 of American Institute of Physics Conference Series, pp. 286–297. June, 2012.

[166] S. Riemer-Sorensen, C. Blake, D. Parkinson, T. M. Davis, S. Brough, et al., "The WiggleZ Dark Energy Survey: Cosmological neutrino mass constraint from blue high-redshift galaxies," Phys.Rev. **D85** (2012) 081101, arXiv:1112.4940 [astro-ph.CO].

[167] J.-Q. Xia, B. R. Granett, M. Viel, S. Bird, L. Guzzo, et al., "Constraints on Massive Neutrinos from the CFHTLS Angular Power Spectrum," JCAP **1206** (2012) 010, arXiv:1203.5105 [astro-ph.CO].

[168] U. Seljak, A. Slosar, and P. McDonald, "Cosmological parameters from combining the Lyman-α forest with CMB, galaxy clustering and SN constraints,"JCAP **10** (Oct., 2006) 14, arXiv:astro-ph/0604335.

[169] T. Kitching, A. Heavens, L. Verde, P. Serra, and A. Melchiorri, "Finding Evidence for Massive Neutrinos using 3D Weak Lensing," Phys.Rev. **D77** (2008) 103008, arXiv:0801.4565 [astro-ph].

[170] I. Debono, A. Rassat, A. Refregier, A. Amara, and T. Kitching, "Weak lensing forecasts for dark energy, neutrinos and initial conditions," `arXiv:0911.3448 [astro-ph.CO]`.

[171] Y. Wang, W. Percival, A. Cimatti, P. Mukherjee, L. Guzzo, et al., "Designing a space-based galaxy redshift survey to probe dark energy," Mon.Not.Roy.Astron.Soc. **409** (2010) 737, `arXiv:1006.3517 [astro-ph.CO]`.

[172] C. Carbone, L. Verde, Y. Wang, and A. Cimatti, "Neutrino constraints from future nearly all-sky spectroscopic galaxy surveys," JCAP **1103** (2011) 030, `arXiv:1012.2868 [astro-ph.CO]`.

[173] L. Amendola, V. Pettorino, C. Quercellini, and A. Vollmer, "Testing coupled dark energy with next-generation large-scale observations," Phys.Rev. **D85** (2012) 103008, `arXiv:1111.1404 [astro-ph.CO]`.

[174] A. B. Belloso, J. Garcia-Bellido, and D. Sapone, "A parametrization of the growth index of matter perturbations in various Dark Energy models and observational prospects using a Euclid-like survey," JCAP **1110** (2011) 010, `arXiv:1105.4825 [astro-ph.CO]`.

[175] C. Carbone, C. Fedeli, L. Moscardini, and A. Cimatti, "Measuring the neutrino mass from future wide galaxy cluster catalogues," JCAP **1203** (2012) 023, `arXiv:1112.4810 [astro-ph.CO]`.

[176] A. P. Hearin, A. R. Zentner, and Z. Ma, "General Requirements on Matter Power Spectrum Predictions for Cosmology with Weak Lensing Tomography," JCAP **1204** (2012) 034, `arXiv:1111.0052 [astro-ph.CO]`.

[177] J. Hamann, S. Hannestad, and Y. Y. Wong, "Measuring neutrino masses with a future galaxy survey," `arXiv:1209.1043 [astro-ph.CO]`.

[178] A. Refregier, T. Kacprzak, A. Amara, S. Bridle, and B. Rowe, "Noise bias in weak lensing shape measurements," `arXiv:1203.5050 [astro-ph.CO]`.

[179] D. Kirk, O. Lahav, S. Bridle, S. Jouvel, F. B. Abdalla, et al., "Optimising Spectroscopic and Photometric Galaxy Surveys: Same-sky Benefits for Dark Energy and Modified Gravity," `arXiv:1307.8062 [astro-ph.CO]`.

[180] L. Wolz, M. Kilbinger, J. Weller, and T. Giannantonio, "On the Validity of Cosmological Fisher Matrix Forecasts," `arXiv:1205.3984 [astro-ph.CO]`.

[181] L. Perotto, J. Lesgourgues, S. Hannestad, H. Tu, and Y. Y. Wong, "Probing cosmological parameters with the CMB: Forecasts from full Monte Carlo simulations," JCAP **0610** (2006) 013, `arXiv:astro-ph/0606227 [astro-ph]`.

[182] M. Viel, M. G. Haehnelt, and V. Springel, "The effect of neutrinos on the matter distribution as probed by the intergalactic medium," JCAP **6** (June, 2010) 15, `arXiv:1003.2422 [astro-ph.CO]`.

[183] K. Heitmann, M. White, C. Wagner, S. Habib, and D. Higdon, "The Coyote Universe I: Precision Determination of the Nonlinear Matter Power Spectrum," Astrophys.J. **715** (2010) 104–121, `arXiv:0812.1052 [astro-ph]`.

[184] T. Kitching, A. Amara, F. Abdalla, B. Joachimi, and A. Refregier, "Cosmological Systematics Beyond Nuisance Parameters : Form Filling Functions," `arXiv:0812.1966 [astro-ph]`.

[185] E. Semboloni, H. Hoekstra, J. Schaye, M. P. van Daalen, and I. J. McCarthy, "Quantifying the effect of baryon physics on weak lensing tomography," `arXiv:1105.1075 [astro-ph.CO]`.

[186] **Euclid Theory Working Group** Collaboration, L. Amendola et al., "Cosmology and fundamental physics with the Euclid satellite," `arXiv:1206.1225 [astro-ph.CO]`.

[187] J. Blazek, R. Mandelbaum, U. Seljak, and R. Nakajima, "Separating intrinsic alignment and galaxy-galaxy lensing," JCAP **1205** (2012) 041, `arXiv:1204.2264 [astro-ph.CO]`.

[188] D. Kirk, A. Rassat, O. Host, and S. Bridle, "The Cosmological Impact of Intrinsic Alignment Model Choice for Cosmic Shear," `arXiv:1112.4752 [astro-ph.CO]`.

[189] J. Lesgourgues, S. Pastor, and L. Perotto, "Probing neutrino masses with future galaxy redshift surveys," Phys.Rev. **D70** (2004) 045016, `arXiv:hep-ph/0403296 [hep-ph]`.

[190] T. Basse, O. E. Bjaelde, J. Hamann, S. Hannestad, and Y. Y. Wong, "Dark energy properties from large future galaxy surveys," JCAP **1405** (2014) 021, `arXiv:1304.2321 [astro-ph.CO]`.

[191] D. H. Weinberg, R. Dave, N. Katz, and J. A. Kollmeier, "The Lyman - alpha forest as a cosmological tool," AIP Conf.Proc. **666** (2003) 157–169, `arXiv:astro-ph/0301186 [astro-ph]`.

[192] J. Carlson, M. White, and N. Padmanabhan, "A critical look at cosmological perturbation theory techniques," Phys.Rev. **D80** (2009) 043531, `arXiv:0905.0479 [astro-ph.CO]`.

[193] H. A. Feldman, N. Kaiser, and J. A. Peacock, "Power spectrum analysis of three-dimensional redshift surveys," Astrophys.J. **426** (1994) 23–37, `arXiv:astro-ph/9304022 [astro-ph]`.

[194] M. Tegmark, "Measuring cosmological parameters with galaxy surveys," Phys.Rev.Lett. **79** (1997) 3806–3809, `arXiv:astro-ph/9706198 [astro-ph]`.

[195] J. Geach, A. Cimatti, W. Percival, Y. Wang, L. Guzzo, et al., "Empirical H-alpha emitter count predictions for dark energy surveys," `arXiv:0911.0686 [astro-ph.CO]`.

[196] A. Orsi, C. Baugh, C. Lacey, A. Cimatti, Y. Wang, et al., "Probing dark energy with future redshift surveys: A comparison of emission line and broad band selection in the near infrared," `arXiv:0911.0669 [astro-ph.CO]`.

Benjamin AUDREN
Born on the 12th of Sep. 1987
✉ Avenue de Préfaully, 25C
1022 CHAVANNES-PRÈS-RENENS (SUISSE)
☎ (+0041) (0)78.928.09.49.
✉ benjamin.audren@gmail.com

Experience with Scientific Python

Programs: ▲ MONTE PYTHON,[1] an **open-source** cosmological parameter inference program, with a user-base of around 50 scientists in laboratories worldwide.
▲ Implemented **automated testing** inside the C code CLASS.[2]

Teaching: ▲ Week-long schools in laboratories to present MONTE PYTHON,[3] in Mexico City, Munich, Geneva, London, Tokyo, Barcelona. The lectures included an introduction to Python, version control and testing best practice.
▲ Co-teacher of a Doctoral level course of Python for beginners.

Formation: Course on advanced scientific usage of Python by Valentin Haenel, on **agile programing, test-driven development and unit-testing**.

Skills

▶ **Basic IT skills:** Linux and Mac, C, Python, Java, html, bash scripting.

▶ **Advanced IT skills:** cluster computing, automated testing, version control, open-source development.

▶ **Communication:** talks in major international conferences (EPS-HEP Grenoble and Stockholm, Cosmo in Cambridge), 4 years of teaching assistant.

▶ **Team Work:** 6 peer-reviewed and published articles written in small international collaborations [1, 2, 3, 4, 5, 7].

▶ **Personal Initiative:** 1 single-authored peer-reviewed article [6], PhD deputee for two Doctoral School committee during 2 years.

▶ **Languages:** French (mother tongue), English (proficient), German (intermediate), Swedish and Spanish (beginner level).

▶ **Other interests:** aïkido, piano.

---

[1] https://github.com/baudren/montepython_public
[2] https://github.com/lesgourg/class_public
[3] http://lesgourg.web.cern.ch/lesgourg/class-tour/class-tour.html

187

Education

2010– now: PhD in theoretical cosmology at EPFL (École Polytechnique Fédérale de Lausanne) with Prof Julien Lesgourgues.

2008–2010: Master 2 *Sciences de la Matière*, Physics, at the ÉNSL (École Normale Supérieure de Lyon). Spring semester of 2008 at Uppsala's University (Sweden) in Erasmus exchange, with a strong focus on Astrophysics.

2007–2008: Bachelor *Sciences de la Matière*, Physics, at the ÉNSL :*Très Bien* grade (16.1/20), equivalent to 1st class honours. Internship in an experimental biophysics laboratory in Lyon.

2005–2007: Two years of *classes préparatoires* in Montpellier.

Publications

[1] B. Audren and J. Lesgourgues, "Non-linear matter power spectrum from Time Renormalisation Group: efficient computation and comparison with one-loop," JCAP **1110** (2011) 037 http://arxiv.org/abs/1106.2607.

[2] G. Giesen, J. Lesgourgues, B. Audren and Y. Ali-Haimoud, "CMB photons shedding light on dark matter," JCAP **1212** (2012) 008, http://arxiv.org/abs/1209.0247

[3] B. Audren, J. Lesgourgues, S. Bird, M. G. Haehnelt and M. Viel, "Neutrino masses and cosmological parameters from a Euclid-like survey: Markov Chain Monte Carlo forecasts including theoretical errors," JCAP **1301** (2013) 026, http://arxiv.org/abs/1210.2194

[4] B. Audren, J. Lesgourgues, K. Benabed and S. Prunet, "Conservative Constraints on Early Cosmology: an illustration of the Monte Python cosmological parameter inference code," JCAP **1302** (2013) 001, http://arxiv.org/abs/1210.7183

[5] B. Audren, D. Blas, J. Lesgourgues and S. Sibiryakov, "Cosmological constraints on Lorentz violating dark energy," JCAP **1308** (2013) 039, http://arxiv.org/abs/1305.0009

[6] B. Audren, "Separate constraints on early and late cosmology," http://arxiv.org/abs/1312.5696.

[7] B. Audren, J. Lesgourgues, G. Mangano, P. D. Serpico and T. Tram, "Strongest model-independent bound on the lifetime of Dark Matter," https://arxiv.org/abs/1407.2418.

188